Imre Takács

EXPERIMENTS

IN

ACTIVATED SLUDGE
MODELLING

Do one thing every day that scares you.

Eleanor Roosevelt

to Anne

Promoter   Prof. P.A. Vanrolleghem (Ghent University)

Ph.D. Review Committee: Dr. Damien Batstone (University of Queensland)
                             Prof. Ulf Jeppsson (Lund University)
                             Prof. László Somlyódy (Budapest University of Technology)
                             Prof. Henri Spanjers (Ghent University)

Other jury members: Prof. Willy Verstraete (Ghent University, Chairman)
                             Prof. Bernard De Baets (Ghent University)
                             Prof. Mark Verloo (Ghent University)

Dean: Prof. Herman van Langenhove
Rector: Prof. Paul Van Cauwenberge

ACKNOWLEDGEMENTS

Wolfgang Rauch. The chapters that contain elemental balancing are the result of cooperation with the wonderful Bernhard Wett and my tireless promoter, Peter Vanrolleghem. Peter also translated the summary to Dutch. Other translations were provided by Anne-Emmanuelle and Zhirong Hu. Lorenzo Benedetti and Ingmar Nopens helped with printing, one of the most tedious tasks in making a PhD happen. J.K. Rowling magically kept my sanity during the final formatting struggle. I wish to thank all.

I owe a special thank-you to the two Peters. One is Peter Vanrolleghem, my promoter at BioMath, a good friend and the fastest brain on earth. I don't know if others have noticed this, but it is great craniovascular exercise just to have a discussion about modelling with him. Peter had the vision for this work; saw me as a lost PhD student and had the patience and invested time (and heaps of it) to guide me towards this day.

The other Peter is the one and only Peter Dold. Peter wholeheartedly supported the idea with his time and professional advice, as well as by funding what is likely the best paid PhD student ever. I probably learnt more from Peter about wastewater process engineering (considering his influence in the past 26 years) than from anyone else on the planet.

I am grateful to the four dedicated reviewers (Damien, László, Ulf and HenRi) whose attention to content and detail significantly improved the quality of this thesis.

There are so many good people I have met and so many friends I have who in some way played a part in this work. They will not be listed by name here lest I fail the page limit on the PhD, but I am sure they all know they have their own special place in my heart.

I send special hugs to my parents who brought me up with love and an open mind, Judit and Miki, the greatest kids on Earth, their mother Erzsi, as well as the whole extended family.

And finally all my love goes to Anne-Emmanuelle (Happy Birthday, Anne!). Anne put up and even looked after a grumpy, and what at times surely must have seemed like a hopelessly confused PhD student.

<div align="right">

Imre Takács

Dundas, January 15, 2008

</div>

ADF   Adaptive Data Filter
ASDM   Activated Sludge - Digestion Model
ASF   Active Site Factor
ASM   Activated Sludge Model
BET   Brunauer, Emmett and Teller (Brunauer *et al.*, 1938) surface analysis method
BOD   Biological Oxygen Demand
BNR   Biological Nutrient Removal
CBIM   Continuity-Based Interfacing Method
COD   Chemical Oxygen Demand
DO   Dissolved Oxygen
DRE   Direct Respirogram Evaluation
DSA   Dynamic Sludge Age
DSRT   Dynamic Solids Residence Time
F/M   Food to Microorganism ratio
GPS   General Purpose Simulator
HAP   Hydroxy-apatite
HDP   Hydroxy-dicalcium-phosphate
HFO   Hydrous ferric oxide
IC   Inorganic Carbon
MLSS   Mixed Liquor Suspended Solids
MLVSS   Mixed Liquor Volatile Suspended Solids
OCR   Optical Character Recognition
ODE   Ordinary Differential Equation
OP   Orthophosphate
OUR   Oxygen Uptake Rate
PE   Population Equivalent
SEM   Scanning Electron Microscopy
SSI   Supersaturation Index
SRT   Solids Residence Time
SVI   Sludge Volume Index
TEFL   Total extended filament length
TEM   Transmission Electron Microscopy
TOD   Total Oxygen Demand
TSP   Total Soluble Phosphorus
UCT   University of Cape Town
VSS   Volatile Suspended Solids
WWTP   Wastewater Treatment Plant

Very few of the actual experiments and laboratory analyses of this work were performed by the author himself. The author was lucky to work with many dedicated, talented people in various research teams over the years. Most of the data collection, laboratory experiments and analyses (apart from some early research presented in Chapter 9) were done by other team members. My focus was usually to interpret and evaluate the data, conceiving and setting up models and performing simulations. In later years, while the author maintained the direct technical input as described in specific details below, he frequently provided technical and logistic management for the team. In general and without exception, the author made a significant contribution to the referenced papers that the chapters of this work are mostly based on and assembled and wrote this thesis.

Chapter 1 A Dynamic Model of the Clarification-Thickening Process

The author designed the dynamic simulators GPS and later GPS-X, and wrote all the process simulation code in ACSL for the biological and settling models used in this study. The author developed the concept for the double-exponential correction of the Vesilind settling function, and performed the optimization runs to fit model parameters to data from literature. The author developed the fast steady-state solver (a new numerical method) still in use in GPS-X which allows finding a solution to the ODE system without having to simulate it dynamically forward in time. Without this the study may not have been possible or practical. (The layered settler model as described in this chapter is not solvable using the usual Newton-Raphson search due to the "minimum of fluxes" expression used).

Chapter 2 Settling of Flocculent Suspensions in Secondary Clarifiers

The author helped formulate the problem (whether the settling velocity of effluent solids in a discrete settling regime can actually depend on their concentration) and provided technical assistance to the first author of the article in addressing this and developing the solution.

Chapter 3 Hindered and Compression Settling: Parameter Measurement and Modelling

The author provided experimental design and developed the functions that describe the "blanket height – time" relationship used to evaluate zone settling velocity tests. The author also developed the correction for the Vesilind settling function in an attempt to include compression in 1-D models independent of the number of layers. The author performed part of the model simulations necessary to fit the double exponential and

quadruple exponential model to experimentally observed data and summarized the results in the paper.

Chapter 4 Modelling of the Micromorphology of the Activated Sludge Floc: Low DO, Low F/M Bulking

The author developed and coded the floc model in ACSL, performed all simulations and the model evaluation, as well as summarizing the results.

Chapter 5 In Context: Modelling Phase Separation

The author wrote this chapter.

Chapter 6 Modelling pH in Wastewater

The author developed the solution to equilibrium equations in Maple and performed most of the simulations and evaluation in BioWin.

Chapter 7 Modelling Iron and Aluminium Precipitation Based on Equilibrium Chemistry

The author developed the sets of equilibrium equations necessary for the practical use of iron-phosphate - iron hydroxide precipitate model. The author performed simulations with the model in BioWin, as well as evaluating and summarizing the results.

Chapter 8 Chemical Phosphorus Removal: Processes, Modelling and Design

The author provided technical management to the team working on the project that resulted in a new model approach to chemical phosphorus removal. Experimental design, data evaluation, comparison of analytical and Tableau methods, conceptual model formulation, as well as synthesis and presentation of the results were part of the author's responsibility.

Chapter 9 Mathematical Model Suggested for the Powdered Activated Carbon Treatment (PACT) System

The author performed the batch and continuous experiments, operated and maintained the experimental setup, performed some of the laboratory analyses and directed the full-scale experiment on site. The author developed the model and ran batch and continuous simulations as well as the evaluation and summarizing the results.

Chapter 10 Direct Parameter Extraction from Respirograms for Wastewater and Biomass Characterization

The author contributed to the development of the concept, coded the direct respirogram evaluation method in ACSL, and performed the model and real respirogram evaluations.

Chapter 11 Sensitivity Analysis in Practice

The author developed this chapter.

Chapter 12 The Dynamic Solids Residence Time

The author developed the concept and participated in the development of the algebraic solution of the dynamic SRT equation. The author simulated the test cases with the exception of the data set from Austria. The author evaluated all results and wrote the chapter.

Chapter 13 Elemental Balances in Activated Sludge Modelling

The author developed the concept and equations necessary, performed the analysis and summarized the results.

Chapter 14 Elemental Balance Based Methodology to Establish Reaction Stoichiometry in Environmental Modelling

The author developed the concept and equations necessary, performed the analysis and summarized the results.

INTRODUCTION

The wastewater treatment plant is essentially a large and complex industrial factory. In large cities processing raw material (sewage) in the range of ten tons per second (one million tons per day) is not unusual. The product the plant manufactures is clean effluent, and the product quality depends, to a large degree, on proper process design and operation. The task of the process engineer is to conceive a system that takes maximum advantage of the potential that exists in the wastewater and in properly sized equipment. Such a plant will be easier and more economical to operate. Engineers use their experience, design knowledge and guidelines contained in books, manuals, handbooks and articles; and, in the past two decades, ever improving mathematical models for this purpose in their daily work.

Mathematical models are useful in many areas: they can rigorously frame a problem and further understanding in research, or can be used for easy storage and transfer of information (training or marketing). They are widely used as tools in design and operation, as well as control design of wastewater treatment plants. The technology that modelling in this field first considered in detail and with lasting success was the activated sludge process. Activated sludge is the base technology at most municipal wastewater treatment plants; it has proven to be a very stable process, capable to perform according to varied and sometimes extremely demanding objectives in removing suspended and soluble organics, nitrogen, phosphorus and many other contaminants from wastewater.

However capable activated sludge models are, they are just approximations and simplifications of reality. No matter how much additional process knowledge and complexity is built into them, the modeller or engineer at the wastewater treatment plant always runs into their limitations. Full-scale plants, even those where most of the work is performed by the traditional activated sludge process, contain many other complex, sometimes not well understood processes and interactions. Without proper understanding, design and operation of these "auxiliary" processes, the whole plant will not function optimally.

The author, early in his career and full with enthusiasm arrived to a treatment plant armed with a state-of-the-art activated sludge model that was perfectly capable to provide accurate predictions on sludge production, aeration requirements and effluent quality. However, the first question the operators wanted an answer for was related to sludge blanket behaviour and the loss of sludge (which obviously has a large influence on the key process variables), as well as process recovery time. In those days there was not even a settler model linked to the activated sludge reactors…

And so the quest started to incorporate additional elements into activated sludge models considering the full-scale plant environment, to extend their capability and validity field for

real-life engineering applications. Since there is a dynamic mass balance ("sludge shuffles", *quote from professor Andrews, in 1989*) between the settler and the reactors, without a dynamic settler model that contains some spatial resolution it is not possible to predict what fraction of the biomass is actually available in the reactors at any given time. The layered settler model with the Vesilind settling function does not provide realistic effluent solids estimation. The layered settler model "seemed" to work with ten layers ("why ten?" *question from professor Somlyódy, in 1991*). Exactly, why ten? Does a model, using the Vesilind function, exclusively based on zone settling velocity, account for compression settling?

Activated sludge models incorporate and make easily accessible knowledge that we as a profession have. Wastewater professionals are quite aware that reactors are not ideally mixed – and that diffusion limitation affects the microenvironment inside the activated sludge floc. But the reactors in our models are ideally mixed, homogenous. How does the actual gradient environment inside the activated sludge floc affect the balance between filaments and floc-formers, and can it be used to predict whether bulking sludge will or will not develop under any given operating conditions?

Attempts to answer these questions lead to modelling experiments that are summarized in Part One of the thesis – Physical processes.

All processes at the wastewater treatment plant occur in a polar solvent, water. Chemical processes, ionization of dissolved species, their dissociation and potential precipitation reactions form the fundamental basis and environment in which the biomass operates. pH influences plant performance directly unless it is within a narrow range. Biological reactions and chemical dosing can upset pH rapidly. In chemical phosphorus removal, iron or aluminium salt dosing does result in low effluent phosphate concentrations – but the dosage required to achieve a certain result seems to be quite variable, and effluent phosphate levels change in time, indicating that both complex equilibrium and kinetic processes may be at play.

Investigating pH, the chemistry and kinetics of phosphorus removal lead to the modelling experiments described in Part Two – Chemical processes.

Activated sludge models were initially developed for and deal with typical municipal wastewater. Accumulation of inert material, substrate degradation, biomass growth and decay occur in industrial plants as well. One technology industrial plants use in certain cases is powdered activated carbon dosage to their activated sludge reactors. How do adsorption/desorption, reactivation, and biokinetic adaptation in this environment affect effluent quality? One tool to answer some of these questions is respirometry. Well-developed respirograms contain detailed information about important wastewater fractions, their concentrations and degradation kinetics. Is there a way to evaluate those characteristic shapes and inflection points that an expert identifies so easily? Does sensitivity analysis give us practical information we would otherwise miss?

Questions, such as these above, promoted model-based experimentation described in Part Three – Biological processes.

Finally, there are questions and modelling experiments that just do not fit into any well-defined box or category. We can learn more about processes just by looking at them from a different perspective. The age of solids, the Solids Residence Time is one of the most

important process variables. But something is not right if halving the wastage rate makes our sludge age estimate increase instantly by several days. Moreover, models are based on mass balances. Elemental balancing is the ultimate in mass balancing – every type of atom, hydrogen, oxygen and others, need to be accounted for. Can this concept give us new insight into process behaviour, influent fractions and stoichiometry? Without expensive, new elemental measurements?

Several theoretical considerations in wastewater treatment modelling are investigated in Part Four - Theoretical aspects.

At this point a clarification of terminology is necessary. The process of creating a model goes through several well-defined steps starting from conceptualization (which variables and processes are important to capture the phenomenon to be described), model definition and implementation (coding), simulation (executing, calculating or "running the model) calibration (fitting model output to data by measuring and varying parameters) and verification (predicting a new set of data with a calibrated model). Specifically calibration is frequently meant the use of a numerical optimizer such as the Nelder-Mead, reduced gradient, genetic algorithm or other method to find the best combination of parameters that will match a given data set. In this thesis and in the work of the author calibration is used in a much wider sense than just a numerical optimization. There are two main reasons for this:

- Most of the work is design and not control oriented. In wastewater design, due to the inherent variation in many circumstances from influent to sampling representativity, having one measurement is frequently meaningless. The model will only be useful for design if it is able to replicate general trends. In other words, the data set to fit to is frequently not the result of one set of experiments, but the collective knowledge of the profession collected over many years.

- The best calibration is when there is no need to fit any parameters, because they can be directly measured in isolation. To do this completely is usually impossible, but the general objective is to measure and deduce as many parameters as possible outside the model, and use a numerical optimization technique only to fine-tune the remaining ones. This also means that the model has parameters with physical meaning, always preferred if possible.

This dissertation is somewhat unusual in that it does not focus on one particular topic in exquisite detail, as is normally expected after several years of PhD studies. Rather, the author considers several subjects that are all relevant to plant-wide, multidisciplinary modelling. Research results that were published in papers (in some cases a significant time ago) are presented in their original context or with minor revisions to improve clarity. Where it was necessary, context was added without a complete rewrite of the original concept. Also, it was not the objective to provide a complete literature re-review to each topic researched in the past.

PART ONE – PHYSICAL TREATMENT PROCESSES

(Phase separation)

1 A DYNAMIC MODEL OF THE CLARIFICATION-THICKENING PROCESS[1]

1.1 Introduction

The separation of solids from water by gravity sedimentation is one of the most important physical processes in a wastewater treatment plant. Solids-liquid separation is a vital component of every biological wastewater treatment system. In the primary clarifier, settleable organic matter is removed by gravity prior to reaching the biological reactor. By design, activated sludge plants transform soluble organic matter into biomass; the effective operation of the process requires that the biomass be removed from the liquid stream (in the secondary settler) prior to being discharged in the receiving waters. Part of the biomass is wasted, while a large fraction is returned to the biological reactor to maintain the appropriate substrate-to-biomass ratio.

Notwithstanding the importance of the solids-liquid separation process, few investigators have proposed a unified settling model designed to address the clarification and thickening functions of settlers. Accordingly, the purpose of this chapter is to suggest an alternate form of the settling velocity model, allowing for the development of a unified approach to dynamic modelling of the clarification and thickening functions of settlers.

1.2 The solid-liquid separation process

Depending on the nature and concentration of the solid particles, four types of settling characteristics are normally encountered in a wastewater treatment plant.

Discrete particle settling Associated with the removal of grit and sand particles, discrete particle settling is characterized by solids which settle as individual entities with little or no interaction with other particles.

Flocculent particle settling Typical of the type of settling found in primary clarifiers, and the middle layers of a secondary settler, flocculent particle settling is characterized by the flocculation of solid particles as they settle through the water column, according to the Kynch (1952) theory.

Hindered settling In a flocculent suspension inter-particle forces hinder the settling process. The mass of particles settles as a unit.

Compression settling "Settling" is achieved by compression of the mass of particles. Compression results from the weight of particles added to the system.

There are two distinct settling regimes that need to be addressed in a general phase separation model.

Clarification The theory of discrete particle settling has been rigorously addressed (Camp, 1945). Given the fact that the solids concentration in the upper layers of the clarifier is sufficiently low to result in discrete particles, one would think that this theory can readily be extended to the clarification component of primary and secondary settling basins. However, the problem does not lie with the settling velocity theory, but with the flocculent nature of these particles which affects the particle size distribution from one layer to another. Li and Ganczarczyk (1987) have found the settling velocity of activated sludge floc particles to be a linear function of their cross-sectional diameter. However, little effort has been made so far to predict the size distribution of the solids particles in the upper layers of a secondary clarifier as a function of the operational characteristics of the activated sludge process. Roth and Pinnow (1981) are among the few investigators that have examined the particle size distribution of secondary clarifier effluent from activated sludge plants. Consequently, a direct application of the discrete particle settling theory to the primary and secondary clarification functions is premature.

Most of the clarification models reported in the literature are based on a statistical analysis of full-scale plant data, relating the effluent suspended solids concentration to a number of process parameters, such as mixed-liquor suspended solids (MLSS), recycle flow rate, overflow rate, change in overflow rate, detention time, air flow rate in the biological reactor, etc. Chapman (1984) and Hill (1985) provide a good review of the more popular models.

Thickening As the concentration of solids increases, the mass of solids tends to settle as a unit. The settling velocity of the sludge blanket has been found to be a nonlinear function of the solids concentration. Hill (1985) provides a comprehensive review of the many settling velocity models applicable to the thickening function of the settler.

The solids handling capacity of a settler can be assessed by performing a limiting solids flux analysis (Keinath *et al.*, 1977). In a continuous flow settler, the downward solids flux is the sum of the gravity settling flux (J_s) and the solids flux due to the bulk movement of the liquid (J_{dn}), namely the underflow:

$$J = J_s + J_{dn} \tag{1.1}$$

$$J_j = X_j \cdot v_{s,j} + X_j \cdot v_u \tag{1.2}$$

where

J_j	= downward solids flux in layer j;
J_s	= gravity settling flux;
J_{dn}	= settling flux due to the bulk movement of the liquid;
X_j	= solids concentration in layer j;

$v_{s,j}$ = settling velocity of the solids in layer j;

v_u = underflow velocity.

Dick and Ewing (1967), Vesilind (1968) and Keinath *et al.* (1977) have described in detail the thickening theories under steady-state conditions.

1.3 Dynamics of the solids-liquid separation processes

Bryant (1972) was one of the first to develop a dynamic model of the activated sludge process, including solids-liquid separation models for both the primary and secondary settlers. Based on a variable thickness variable number of layers concept, Bryant developed a complex set of heuristics to govern the fate of the physical dimensions of a layer within the secondary clarifier (i.e. the layer's appearance and disappearance depending on its thickness). Bryant's model of the primary settler was not as sophisticated and was based on a sequence of five continuous flow stirred tank reactors (CFSTR), selected in such a way as to replicate the appropriate detention time for the system (e.g. 1.5-2.0 h in his case).

Busby (1973), Stenstrom (1976) and Hill (1985) have all made significant efforts to improve our understanding of the dynamics of the thickening process using the solids flux theory in a one-dimensional layered settler. While Bryant and Busby made use of a variable number of layers of time-varying thickness, Stenstrom and Hill used a fixed number of layers of constant thickness to describe the thickening function of settlers.

Vitasovic (1986, 1989) developed a more rigorous analysis of the dynamics of secondary settlers, that included consideration of the upward bulk movement of the liquid in the layers above the feed point. The approach, described briefly in the next section, is based on the work of Vitasovic (1986).

However, before focusing on the development of the model, it should be emphasized that all of the solids-liquid separator models referenced so far have failed to provide a unified framework to predict the suspended solids in the effluent of the clarifier. In all cases, authors have made use of statistically-based models to predict the effluent suspended solids. While this approach might seem logical, it fails to account for a rigorous solids balance in the settler. The problem can be particularly important as settlers reach failure.

1.4 Layered settler model

Vitasovic's (1986) model predicts the solids concentration profile in the settler by dividing the settler into a number of layers (10) of constant thickness as shown in Figure 1.1, and by performing a solids balance around each layer.

Vitasovic's model falls in the same class of one-dimensional models as those of Bryant (1972), Busby (1973), Stenstrom (1976) and Hill (1985). All of them, including the one presented in this chapter, are based on the following assumptions:

- incoming solids are distributed instantaneously and uniformly across the entire cross-sectional area of the clarifier layer; and
- only vertical flow is considered in the model.

Vitasovic's model does not include a clarification component. Consequently, effluent suspended solids are not predicted during normal operating conditions. However, when the settler's thickening and/or storage function fails, the model will predict large quantities of effluent suspended solids. Vitasovic (1986) arbitrarily defines the sludge blanket height as the height of the first layer with a solids concentration greater than 3000 mg/l.
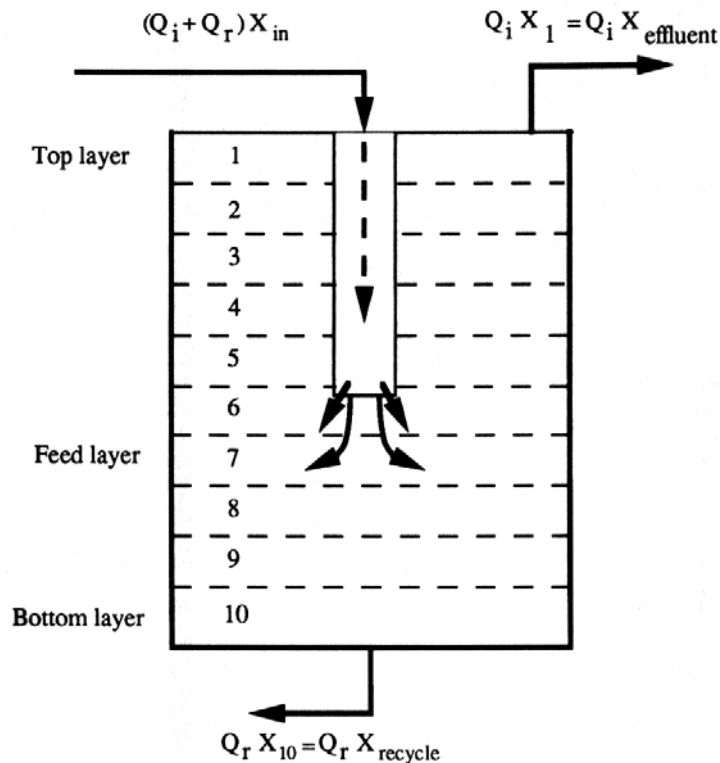
Figure 1.1. Layered settler model.

Five different groups of layers are present in the proposed model, depending on their position relative to the feed point. Table 1.1 summarizes the input and output of solids to each group of layers, while the solids balance around each type of layer is summarized in Figure 1.2.

Vitasovic's model is based on the traditional solids flux analysis, with the exception of the threshold concentration (X_t) designed to limit the downward flux of solids to that which can be handled by the layer below. For example, above the feed layer the flux out of layer "j" is restricted, if the concentration in layer "$j + 1$" is greater or equal than some threshold value (X_t), in which case the flux out of layer "j" is set equal to the min [$J_{(j)}$, $J_{(j+1)}$]. The specifics of the algorithm are summarized in Fig. 1.2.

The solids flux due to the bulk movement of the liquid is straightforward to assess, being equal to the product of the concentration (**X**) and the bulk velocity of the liquid (v_b), which can be upwards or downwards depending on the position of the layer with respect to the feed point.

The solids flux due to gravity settling of the solids particles is given as the product of the concentration (**X**) and the settling velocity of the solids particles (v_s). As indicated previously, several models have been suggested to describe the settling velocity of a mixed-liquor. One of the more widely accepted settling velocity model is that of Vesilind (1968):

26

$$v_s = v_0 \cdot e^{-nX} \qquad\qquad (1.3)$$

where

v_s	= settling velocity of the suspension;
v_0	= maximum settling velocity;
X	= solids concentration; and
n	= model parameter.

This model was used successfully by Hill (1985) and Vitasovic (1986).
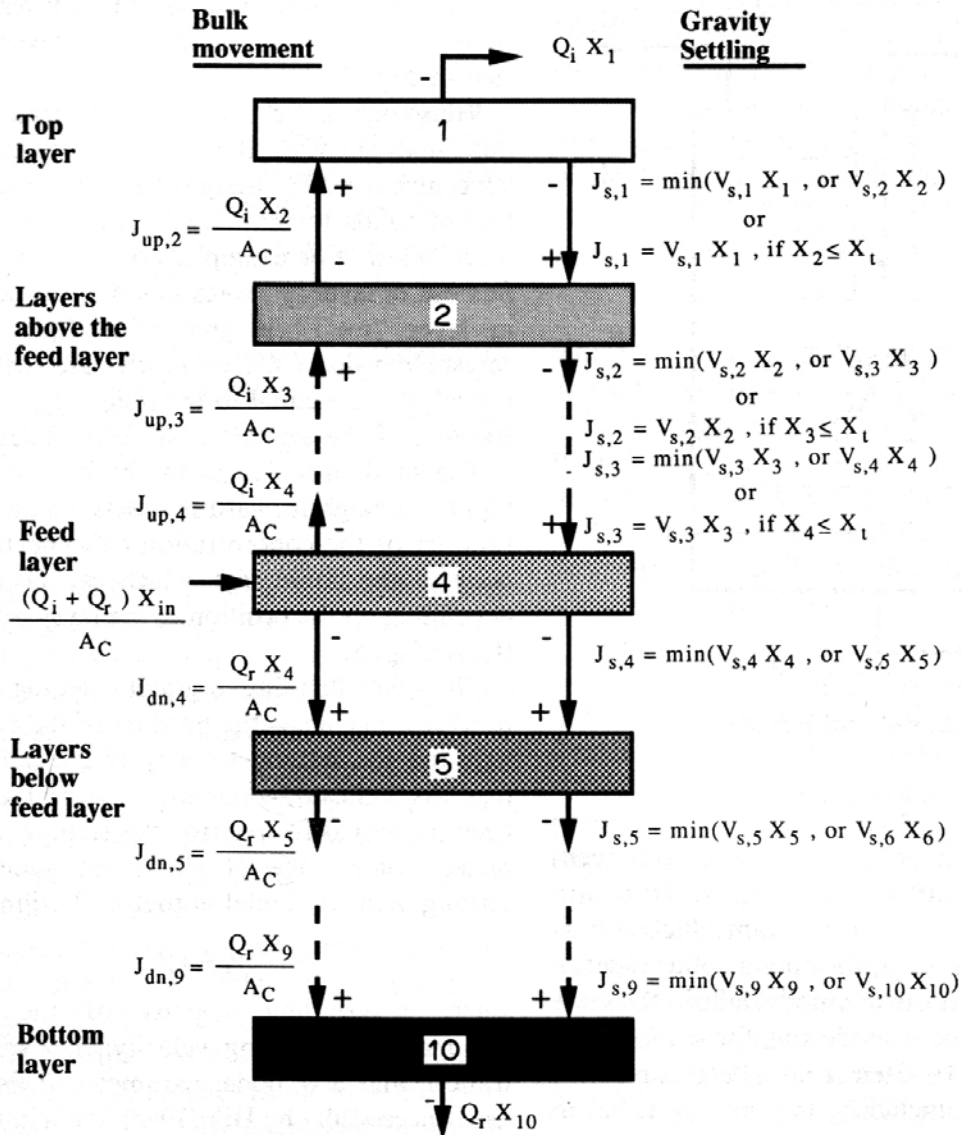
Figure 1.2. Solids balance across settler layers.

However, it should be recognized that Vesilind's settling velocity equation applies only to hindered settling conditions. As the solids concentration in the upper layers of the clarifier decreases below the hindered settling concentration, settling velocities predicted by Vesilind's equation will exceed the actual settling velocity of the floc particles as predicted by Li and Ganczarczyk (1987).

Table 1.1. Layered settler model: input-output summary

Layer	Input			Output	
	Feed	Settling	Bulk liquid flux	Settling	Bulk liquid flux
Top layer	-	-	Up	+	Up
Layers above feed point	-	+	Up	+	Up
Feed layer	+	+	-	+	Up-down
Layers below feed point	-	+	Down	+	Down
Bottom layer	-	+	Down	-	Down
Note : + phenomenon considered; – phenomenon not considered.					

In a well operating settler, the concentration of solids in the upper layers of a clarifier increases with depth. Because of the dynamic forces acting on the floc particles above the feed point, the particle size distribution of the floc particles changes from one layer to another. In their study on particle size distribution, Roth and Pinnow (1981) found that floc particles in the effluent of secondary clarifiers from activated sludge plants, followed a log-normal distribution. In Chapter 2, a relationship is derived between particle size distribution, described by the mean and variance of the log of the particle diameters, and their concentration. A similar expression was also derived for the average settling velocity of a flocculent suspension in the upper layers of a secondary clarifier. Finally, because of the operational constraints of a secondary clarifier, the authors have shown that the average settling velocity of solids in the upper layers of a secondary clarifier could be related to its concentration. Consider for example a layer in the upper portion of a secondary clarifier having a log-normal particle size distribution. As the overflow rate increases, particles with a higher settling velocity (i.e. larger particle diameter) will be fluidized and carried upward. Because particle size is bounded at zero, this will result in a larger mean and variance in the log of the particle diameters. Based on the relationship derived, the increase in overflow rate will result in a larger solids concentration, as would have normally been expected from an increase in overflow rate. However, an increase in the mean and variance of the log of the particle diameters will also result in an increase in the average settling velocity of the suspension as depicted in region II of Figure 1.3.

From a practical standpoint, the correlation between average settling velocity and solids concentration (region II, Figure 1.3) is valid for low solids concentration. A more detailed analysis of this relationship is presented in Chapter 2. As the solids concentration increases, a region exists (region III, Figure 1.3) where the average settling velocity of the suspension reaches a maximum upper limit. This corresponds to the transition zone between the low solids concentration region (region II) and hindered settling conditions (region IV). Ossenbruggen and McIntire (1990) have also suggested that a maximum practical settling velocity be used below the hindered settling concentration. Assuming maximum floc particle diameters of 1-2 mm in this concentration range would result in floc particle settling velocities in the range of 175-400 m/d (Li and Ganczarczyk, 1987).
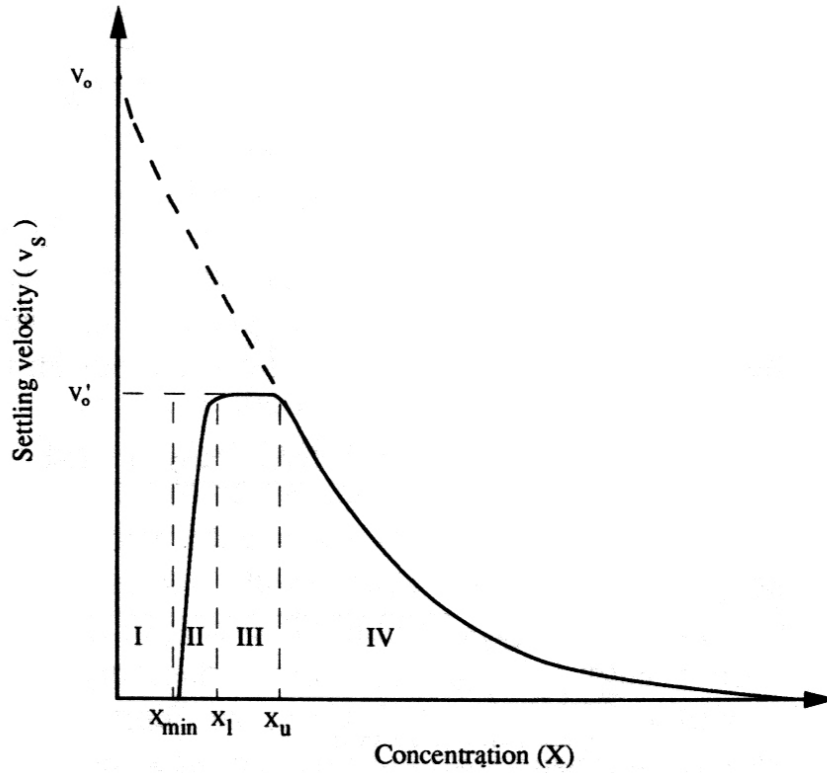
Figure 1.3. Settling velocity model.

Mathematically, the generalized settling velocity model can be represented as the sum of two exponential terms:

$$v_{sj} = v_0 e^{-r_h X_j^*} - v_0 e^{-r_p X_j^*} \qquad (1.4)$$

$$0 \le v_{sj} \le v'_0 \qquad (1.5)$$

where

v_{sj} = settling velocity of the solids particles in layer j (m/d);

v_0 = maximum settling velocity (m/d);

r_h = settling parameter characteristic of the hindered settling zone (m^3/g);

r_p = settling parameter characteristic of low solids concentration (m^3/g);

X_j^* = $X_j - X_{min}$

X_j = suspended solids concentration in layer j (g/m^3);

X_{min} = minimum attainable suspended solids concentration (g/m^3);

X_{min} = $f_{ns} X_{in}$

X_{in} = mixed-liquor suspended solids entering the settler (g/m^3);

f_{ns} = non-settleable fraction of X_{in} .

29

As depicted in Figure 1.3, v_{sj} reaches a maximum value of v'_0, in the range of $X_l - X_u$, where X_l and X_u represent the lower and upper concentrations of region III, respectively.

The first term ($v_0 e^{-r_h X_j^*}$) in equation (1.4) reflects the settling velocity of the large, well flocculating particles. On the other hand, the second term ($v_0 e^{-r_p X_j^*}$) of equation (1.4) is a velocity correction factor to account for the smaller, slowly settling particles.

Four regions are of interest in equation (1.4):

$X < X_{min}$ In this region, the settling velocity is set equal to zero, as the suspended solids concentration reaches the minimum attainable concentration.

$X_{min} < X < X_l$ In this region, the settling velocity is dominated by the slowly settling particles; in this case, Vs is the most sensitive to r_p.

$X_l < X < X_u$ In this concentration range (typically between 200-2000 g/m^3) the settling velocity is independent of concentration. Floc particles reach their maximum size resulting in an average settling velocity that is more or less independent of concentration.

$X > X_u$ In this region, the effect (correction factor) of the slowly settling particles is small in comparison to the total settling velocity. The settling velocity is most sensitive to r_h and the model effectively reduces to Vesilind's equation.

This settling velocity model was found to produce realistic estimates of the effluent and underflow suspended solids concentration under both steady-state and dynamic conditions.

1.5 Assessing model parameters

In this study, model parameters were assessed based on an analysis of field and pilot-scale experimental data. In all cases, SIMUSOLV (Steiner *et al.*, 1987), non-linear dynamic optimization package was used for model parameter identification.

Alternatively, model parameters of the proposed settling velocity model could be assessed through a combination of laboratory experiments and nonlinear optimization techniques (Kennedy, 1991). For example, f_{ns}, the minimum effluent suspended solids concentration, can readily be measured in a settling column analysis. An estimate of the maximum practical settling velocity, v_o', can be obtained by diluting the mixed liquor to 1-2 g/l, and measuring the settling velocity of the large individual floc particles. Vesilind's hindered settling velocity model parameters, v_o and r_h, can be measured through a series of column settling tests (Vesilind, 1968; Keinath *et al.*, 1977). Finally, r_p is best assessed using a non-linear optimization search technique, such as the one considered in this study.

1.6 Application of the model

Two examples will serve to illustrate the application of the settling velocity model. In the first example, the model will be applied to full-scale data collected by Pflanz (1969) assuming that steady-state conditions prevailed at the time of the experiments. In the second example,

dynamic data collected at pilot scale (Thompson, 1988) will be used to assess the potential of the model under transient conditions.

1.6.1 Pflanz full-scale data

Pflanz (1969) carried out experiments to determine the settling characteristics of sludges under different conditions. In one of his experiments at Celle, Germany, he provided solids profiles in a final settling tank with sufficient detail to calibrate the model presented earlier.

The high-rate activated sludge treatment plant received mainly domestic wastewater. Pflanz measured the suspended solids concentrations at seven points along the radius of the circular secondary settler and at ten points along its depth. For the purpose of this analysis, the two-dimensional suspended solids concentration data base was filtered and the data weighted with respect to the cross-sectional area of the clarifier prior to being reduced to one-dimensional solids profiles. A summary of the characteristics of the three experimental conditions conducted by Pflanz is presented in Table 1.2.

Table 1.2. Summary of the experimental conditions (Pflanz, 1969)

				Suspended solids concentration		Mass of SS	
	Flow rate	Residence time	Sludge return flow rate	Input	Recycle	Loading	Output
Experiment	(m^3/h)	(h)	(m^3/h)	(g/l)	(g/l)	(t/d)	(t/d)
Low load	360	5	300	5.62	12.87	89	92.8
Medium load	450	4	300	5.52	12.8	99.4	92.3
High load	600	3	300	5.10	14.72	110.2	106.2

The settler model was coded in ACSL (Advanced Continuous Simulation Language), a continuous simulation language developed by Mitchell & Gauthier (1986). Model parameters were estimated using SIMUSOLV, an integrated multi-functional parameter estimation and optimization package coupled to ACSL (Steiner *et al.*, 1987). SIMUSOLV was used to identify a consistent set of model parameters for each of the three data sets.

Results of the analysis are presented in Figure 1.4 (a-c), where the logarithm of the solids concentration is plotted as a function of depth. A logarithmic scale was chosen for the solids concentration to provide more detail at lower concentrations. Model parameters for each of the three events are shown in Table 1.3 while results of the simulation are presented in Table 1.4.

Based on the results of the analysis, it is apparent that the effluent suspended solids predictions are excellent - deviating from the recorded values by approx. 1% (i.e. a maximum of 0.1 g/m^3). In general, the underflow concentration is also very well simulated by the model. Deviations of 1.1, 13.8 and 18.2% from the observed underflow concentrations have been recorded for the low, medium and high load conditions, respectively. The largest

discrepancies between observed and simulated solids concentrations are found around the feed layer.

Table 1.3. Model parameters fitted to Pflanz full-scale data sets

Parameter	Low load	Medium load	High load
v'_0 (m/d)	214.2	370.0	172.8
v_0 (m/d)	150.2	142.9	112.1
r_p (m^3/g)	5.71×10^{-3}	2.86×10^{-3}	2.70×10^{-3}
r_h (m^3/g)	3.64×10^{-4}	3.78×10^{-4}	2.93×10^{-4}
f_{ns} (-)	1.23×10^{-3}	2.28×10^{-3}	2.59×10^{-3}
inp(6)	0.00	0.11	0.24
inp(7)	1.00	0.89	0.76
Note : inp(6) and inp(7) represent the fraction of the feed distributed to the sixth and seventh layers, respectively, with inp(6) = 1 - inp(7).			

However, in assessing the results of the simulation it should be emphasized that the details surrounding Pflanz's experiments and the accuracy of measurements were not available from the published reports. For example, in simulating the low, medium and high load conditions, steady-state conditions had to be assumed for each of the three events. It is easy to verify that this assumption is not strictly valid for the experiments, as the mass of solids entering the clarifier is larger than the mass of solids leaving the settler (i.e. 3-7 tonnes/d). Accordingly, for the medium and high load conditions, the model was forced to overpredict the underflow concentrations because this was necessary to reach steady-state. Notwithstanding this discrepancy, the model was able to replicate the general behaviour of the solids profile for all three experiments. In addition, the model was able to predict the depth of the sludge blanket measured by Pflanz.

While model parameters varied from one condition to another, the range of values is not unrealistically large given the limited data available and the natural variability in sludge settling characteristics.

1.6.2. Feed distribution to the clarifier

In his paper, Pflanz did not provide sufficient details about the physical characteristics of the settler to properly assess the feed distribution to the settler. However, an analysis of the concentration profiles reveals that the feed layer must have been above the eighth layer where zone settling conditions prevailed. Similarly, the feed layer had to be below the fifth layer because of the low solids concentration in and above the fifth layer. Accordingly, the sixth and seventh layers were considered as potential feed point layers. The feed distribution between layers is a function of the hydraulic regime. While the proposed model does not pretend to simulate the dynamics of feed point distribution, it does allow the flexibility to handle multiple feed layer conditions, to reflect more closely field conditions. Optimized results are shown in Table 1.3. As it turns out, most of the feed had to be distributed to layer 7. However, as the hydraulic load increased, a larger fraction of the feed had to be distributed

to layer 6. In fact, the choice of feed layer or the feed distribution is another calibration parameter and has not much to do with the physical configuration of the actual settler.
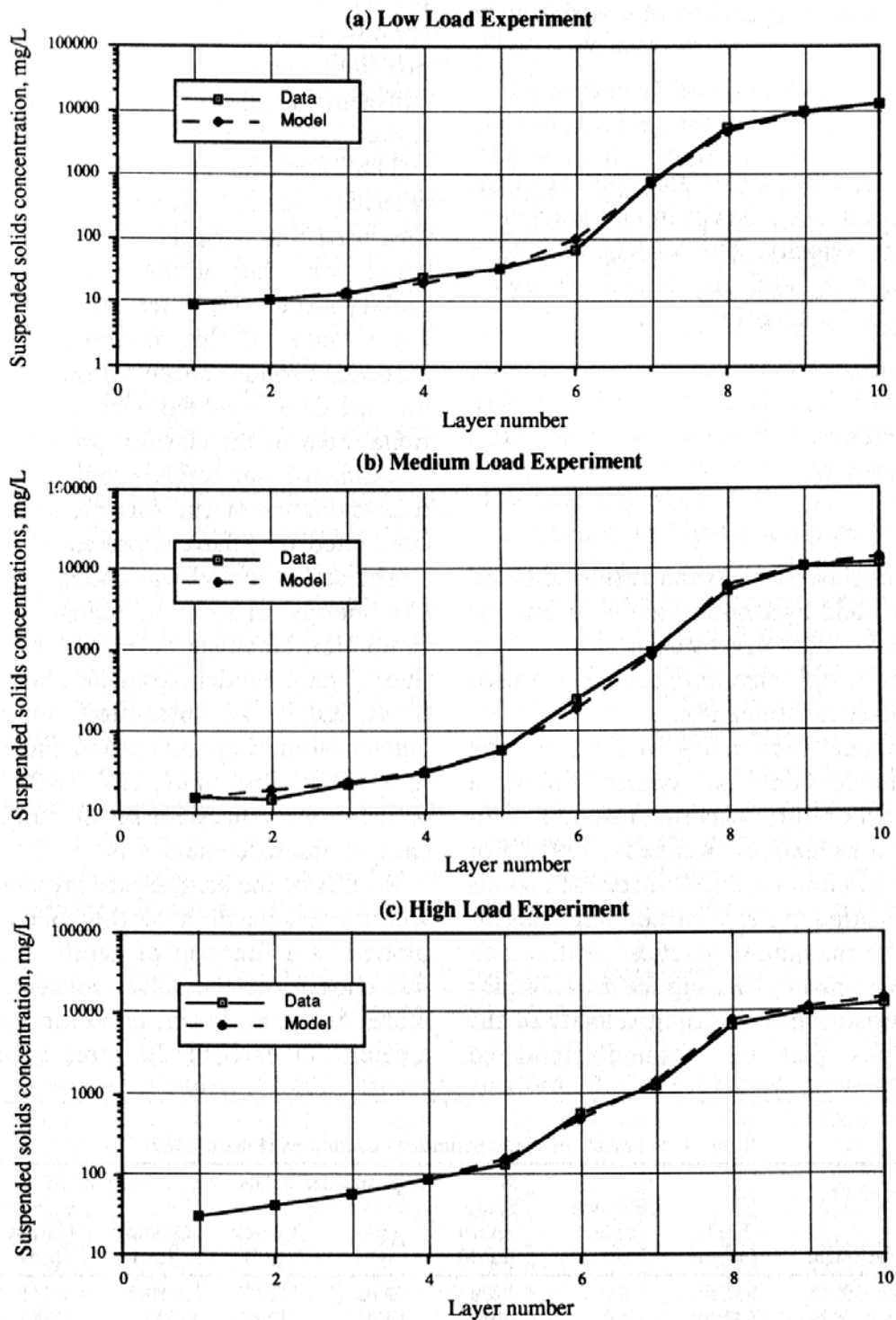
Figure 1.4. Observed and simulated concentration profiles

1.6.3. Pilot-scale experiments

Thompson (1988) investigated the benefits of step feed in reducing the impact of storm flows, using the 288 m^3/d pilot plant located at the Wastewater Technology Centre in Burlington

33

(Ontario, Canada). Using his data, efforts were made to calibrate the settling velocity model under dynamic conditions..

Table 1.4. Observed and simulated suspended solids concentrations (g/m^3)

Suspended solids concentration (g/m^3)								
Low load			Medium load			High load		
Layers	Observed	Simulated	%dif.	Observed	Simulated	%dif.	Observed	Simulated	%dif.
1	9.0	9.1	1.1	15.6	15.7	0.6	30.7	30.8	0.3
2	10.7	11.2	4.7	14.8	18.9	27.7	41.4	42.9	3.6
3	13.6	14.1	3.7	21.8	23.6	8.3	59.4	58.5	1.5
4	23.8	19.5	18.1	29.9	32.9	10.0	88.6	87.4	1.4
5	35.0	33.8	3.4	58.8	59.2	0.7	135.5	163.5	20.7
6	66.6	96.6	45.0	274.2	187.4	24.2	567.7	481.1	15.3
7	787.1	706.7	10.2	933.0	826.0	11.5	1273.6	1377.6	8.2
8	5280.8	4618.9	12.5	5263.6	6130.3	16.5	6999.4	8308.6	18.7
9	10021.5	9124.4	9.0	10481.9	10699.6	2.1	10613.5	11901	12.1
10	12487.2	12353.1	1.1	12100.1	13766.5	13.8	12893	15238.4	18.2

The pilot plant consists of three aeration tank-in-series followed by a final settler. Settled sewage entering the plant can be fed to any of the three reactors. The secondary settler has a sidewater depth of 2.7 m, while the overflow rate to the settler was set to 27.6 m/d. A constant recycle was used in the study. The characteristics of the plant are summarized in more detail by Thompson (1988).

A mathematical model of the pilot plant was constructed using a library of dynamic models developed by Patry and Takács (1990). The biological reactors were modelled using the IAWPRC Task Group model of the activated sludge process (ASM1). Details of the model are given elsewhere (Henze *et al*., 1987). The settler model described earlier was coupled to the activated sludge model providing a complete representation of the pilot plant.

No major calibration was needed for the activated sludge portion of the model; however parameters of the settling velocity model were adjusted to reflect more closely the actual behaviour of the secondary clarifier. The calibrated set of model parameters is:

$v_0 = 712.0 \, \text{m/d}$;
$v'_0 = 340.0 \, \text{m/d}$;
$r_h = 4.26 \times 10^{-4} \, \text{m}^3 / \text{g}$;
$r_p = 5.0 \times 10^{-3} \, \text{m}^3 / \text{g}$; and
$f_{ns} = 1.0 \times 10^{-4}$.

The model was verified against two sets of experiments:

(a) storm flow conditions without step feed; and
(b) storm flow conditions with step feed to the second reactor.

The analysis focused on the solids distribution within the settler, the sludge blanket height, and the effluent suspended solids.

Storm flow conditions without step feed. Results of the simulation under storm flow conditions without step feed are shown in Figure 1.5(a) and (b) and compared with the recorded observations. Storm flow conditions were simulated by an abrupt change in flow rate from 200 to 500 L/s, while the recycle flow rate was kept constant. This produced an increase in the sludge blanket height (H_S) and consequently a high effluent suspended solids value once the sludge blanket reached the weirs (Figure 1.5(b)).
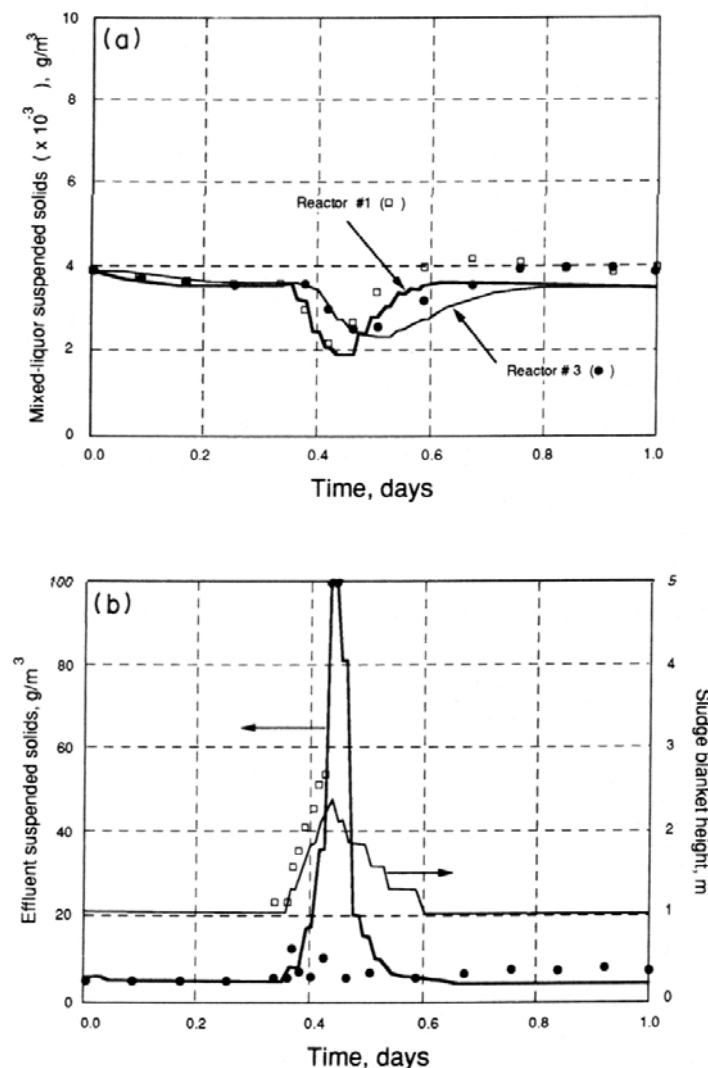
Figure 1.5. Storm flow without step feed ((a) MLSS, (b) blanket and effluent solids).

As observed by Thompson (1988), the effluent suspended solids concentration (ESS) is relatively independent of the sludge blanket height until the moment the blanket reaches the

weir level. The sludge blanket, as well as the effluent suspended solids concentration, returned to their normal levels once normal flow conditions were re-established. The solids concentration in the reactors was drastically reduced during storm flow. A 40% reduction in the MLSS concentration in each reactor was observed in the model (Figure 1.5(a)). This reduction is in close agreement with Thompson's results. The mixed liquor suspended solids, in the first and third reactors, are plotted in Figure 1.5(a). The decrease in the MLSS concentration is well simulated, however, the recovery is underestimated by the model. A possible explanation for this discrepancy lies in the fact that the mass of solids lost from the settler during storm flow is not known precisely. Accordingly, it is possible that the actual mass of solids washed out from the pilot plant could have been significantly smaller than that predicted by the model.
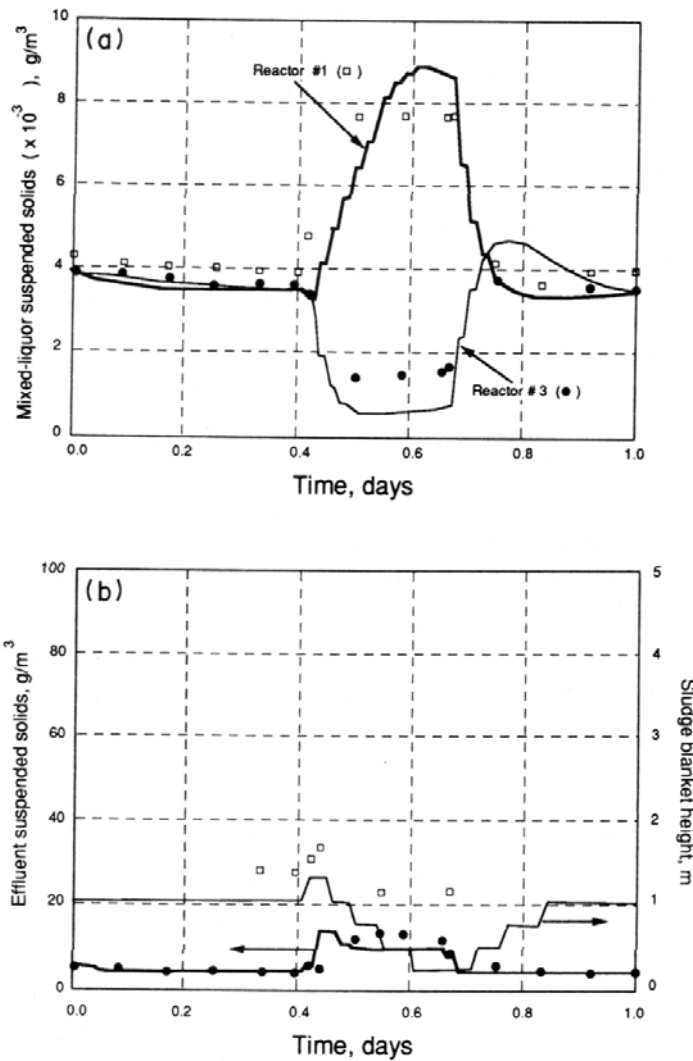
Figure 1.6. Storm flow with step feed to second reactor ((a) MLSS, (b) blanket and effluent solids).

Storm flow conditions with step feed to the second reactor. To prevent a significant loss of solids during storm flow conditions, Thompson (1988) experimented with a number of step feed control measures. In this particular set of experiments, the operational strategy was to step feed the settled sewage to the second reactor during storm flow conditions. The simulated and observed results are shown in Fig 1.6(a) and (b).

36

As shown in Figure 1.6(a), the first reactor was used to store the biomass during the storm, while solids from the third reactor were washed out, decreasing the solids loading to the settler. Initially, the height of the sludge blanket rose slightly, however this tendency was soon reversed (Figure 1.6(b)). Simulated and measured effluent suspended solids are in close agreement.

In general, the model was able to replicate fairly closely the trends in MLSS, effluent suspended solids, and sludge blanket height under a variety of dynamic events. The discrepancies between the observed and simulated results fall within the expected range of accuracy for such complex models. It should be noted that Thompson's experiments were not initially designed for dynamic modelling purposes. Accordingly, a full solids profile and balance were not available for this investigation.

1.7 Conclusions

A multi-layer general dynamic model of the clarification/thickening process is presented. Based on the solids flux concept and a mass balance around each layer of a one-dimensional settler, the model is designed to predict the solids profile along the settling column, including the effluent and underflow suspended solids. The model provides a unified framework for the simulation of the clarification and thickening processes under both steady-state and dynamic conditions. The model was applied to both pilot-scale and full-scale experimental data with very good results.

2 SETTLING OF FLOCCULENT SUSPENSIONS IN SECONDARY CLARIFIERS[2]

2.1 Introduction

Modelling of the settling velocity of floc particles in the upper layers of an activated sludge secondary clarifier represents one of the key processes in the development of an integrated clarification/thickening model. In Chapter 1, it is postulated that a relationship exists between the average settling velocity of a flocculent suspension in the upper layers of a secondary clarifier and the suspended solids concentration of that layer.

At first, this statement appears contradictory to our understanding of discrete particle settling. The settling velocity of discrete particles should be independent of their concentration as long as the particles do not interact. However, as will be demonstrated in this chapter, a relationship does exist between the average settling velocity of a suspension in the upper layers of a secondary clarifier and the suspended solids concentration of that layer. The point to remember is that we are dealing with a suspension of non-uniform particles with a certain particle size distribution, and during settling both the concentration and the particle size distribution are changing.

2.2 Settling of floc particles

Settling of floc particles depends on a number of factors, including:

- particle density, i.e., dry solids (ρ_s);
- particle porosity (ε);
- particle shape (S); and
- particle size (ϕ).

In the case of floc particles normally found in the upper layers of a secondary clarifier, the dry solids density (ρ_s) is more or less constant. In dealing with activated sludge floc particles, Smith and Coackley (1984) have reported a value of 1.4 g/ml, while Atkinson and Daoud (1976) have reported a dry solids density of 1.32 g/ml for *S. cerevisiae*. On the other hand, floc porosity ($\in$) defined by:

$$\in = \frac{\rho_s - \rho_f}{\rho_s - \rho_w}$$

(2.1)

---

[2] Originally published as Patry, G.G., Takács, I. (1992) Settling of Flocculent Suspensions in Secondary Clarifiers. Water Research, **26**, No 4., pp. 473-479.

increases with floc size. In Equation 2.1, ρ_f refers to the floc density (g/ml), and ρ_w refers to the density of the medium (water) (g/ml). However, beyond a floc size of 200 μm the floc porosity remains relatively constant (Li and Ganczarczyk, 1987). The following expression can be used to relate floc porosity to floc diameter (or characteristic length):

$$\in (\phi) = \gamma + \frac{\kappa}{\phi^{\theta}}$$

(2.2)

where γ, κ, and θ are fitted model parameters. Using Eqs. 2.1 and 2.2 one can derive the following expression between floc density and floc diameter:

$$\rho_f (\phi) = [\rho_s (1 - \gamma)]\gamma \rho_w + \kappa (\rho_s - \rho_w)\phi^{-\theta}$$

(2.3)

If we let $\rho_d (\phi)$ be the dry floc density, i.e., $\rho_d (\phi) = \rho_s [1 - \varepsilon(\phi)]$ then:

$$\rho_d (\phi) = \eta + \tau\phi^{-\theta}$$

(2.4)

where $\eta = \rho_s (1 - \gamma)$ and $\tau = -\kappa\rho_s$.

While the shape of floc particles plays a definite role in assessing the actual settling velocity of an individual floc particle, the assumption of an equivalent spherical floc particle does not detract from the generality of the development presented in the next section. Accordingly, for our purposes we will refer exclusively to spherical floc particles, realizing that the sphericity of floc particles depends on a number of morphological factors that fall beyond the development and objectives sought in this chapter.

Finally, particle floc size measured either in terms of the cross-sectional diameter or as a function of the longest floc dimension, plays an important role in the settling velocity of individual floc particles. For example, Li and Ganczarczyk (1987) have found that the settling velocity of individual floc particles could be given as:

$$v_s (\phi) = \alpha + \beta\phi$$

(2.5)

where $v_s (\phi)$ is the settling velocity of a floc particle of diameter ϕ, (mm/s); ϕ is the cross-sectional diameter of the floc particle (mm); and α and β are model parameters (0.35 min/s and 1.77 1/s, respectively).

2.3 Settling velocity of flocculent suspensions

2.3.1 Introduction

From a theoretical perspective it can easily be argued that the average settling velocity of discrete and/or flocculent suspensions is independent of the concentration of particles in the suspension. Consider for example, a mono-diameter suspension ($X = X_0$) where the particles are, on the average, 100 diameters apart from each other. It can be argued that one could

double the concentration ($X = 2X_0$) by introducing the same number of mono-diameter particles and still maintain an inter-particle spacing of approximately 80 diameters, thereby doubling the concentration with no change in the average settling velocity of the suspension. The same argument holds true for any particle size distribution where the increase in solids concentration is achieved without affecting the particle size distribution.

However, this is **not** the phenomenon that leads to variations in suspended solids concentrations in the upper layers of a final clarifier. The development that follows will illustrate that prevailing conditions in the upper layers of a clarifier are such that the average *settling velocity* of a suspension is a function of the suspended solids concentration of that suspension.

2.3.2 Settling velocity and particle size distribution

Consider a section of the upper layers of a secondary clarifier receiving mixed-liquor from an activated sludge plant. The concentration of particles of diameter ϕ is given:

$$X(\phi) = N(\phi)\rho_d(\phi)V_p(\phi) \tag{2.6}$$

where $X(\phi)$ is the concentration of particles of diameter ϕ (mg/L); $N(\phi)$ is the number of floc particles of diameter ϕ (No/L); $V_p(\phi)$ is the volume of a floc particle of diameter ϕ (mm^3); and ρ_d is the dry density for floc particles of diameter ϕ, (g/ml). Recall that the volume of a spherical floc particle of diameter ϕ is given by:

$$V_p(\phi) = \pi\phi^3/6 \tag{2.7}$$

Accordingly, the concentration of particles of diameter ϕ can be written as

$$X(\phi) = N(\phi)\rho_d(\phi)\frac{\pi}{6}\phi^3 \tag{2.8}$$

Roth and Pinnow (1981) are amongst the only investigators to have studied the characteristics of particle size distribution in the effluent of secondary clarifiers. Following a statistical analysis of the data, the authors suggest that the particle size distribution of solids found in the effluent of secondary clarifiers follows a lognormal distribution. In an attempt to develop a clearer understanding of the basic floc breakup mechanism, Parker *et al.* (1971, 1972) examined the size distribution of floc particles in the mixed liquor of an activated sludge system as a function of the energy supplied to the reactor. Parker found that mixed liquor floc sizes followed a bi-modal distribution with little or no particles in the 5-25 μm range (Figure 2.1). In contrast, the particle size distribution from the effluent of a secondary clarifier for the three cases reported by Roth and Pinnow (1981) are shown in Figure 2.2. Parker's floc size distribution is probably typical of the particle size distribution of floc particles entering a secondary clarifier (feed point distribution). However, because of the sweeping nature and high settling velocity of large floc particles, it is likely that the bi-modal distribution would not extend significantly upwards beyond the feed point.

If ϕ is lognormally distributed, then the probability density function (pdf) of ϕ, $f\phi$ is given by:

$$f(\phi) = \frac{1}{\sqrt{2\pi}\zeta\phi} \exp\left[-\frac{1}{2}\left(\frac{\ln\phi - \lambda}{\zeta}\right)^2\right] \tag{2.9}$$

where λ is the mean of the log of the particle diameter, i.e., $E[\ln\phi]$; and ζ is the standard deviation of the log of the particle diameter, i.e., $Var[\ln\phi]$. Accordingly, the probability that floc particles will be in the range of $[\phi_l, \phi_u]$ is given by:

$$\Pr[\phi_l \le \phi \le \phi_u] = \Phi\left[\frac{\ln\phi_u - \lambda}{\zeta}\right] - \Phi\left[\frac{\ln\phi_l - \lambda}{\zeta}\right] \tag{2.10}$$

where Φ represents the standardized cumulative normal probability distribution.

If we let N_0 be the total number of particles in a given layer, then the number of particles of diameter ϕ is given by:

$$N(\phi) = \frac{N_0}{\sqrt{2\pi}\zeta\phi} \exp\left[-\frac{1}{2}\left(\frac{\ln\phi - \lambda}{\zeta}\right)^2\right] \tag{2.11}$$

or

$$N[\phi_l \le \phi \le \phi_u] = N_0\left[\Phi\left[\frac{\ln\phi_u - \lambda}{\zeta}\right] - \Phi\left[\frac{\ln\phi_l - \lambda}{\zeta}\right]\right] \tag{2.12}$$

42
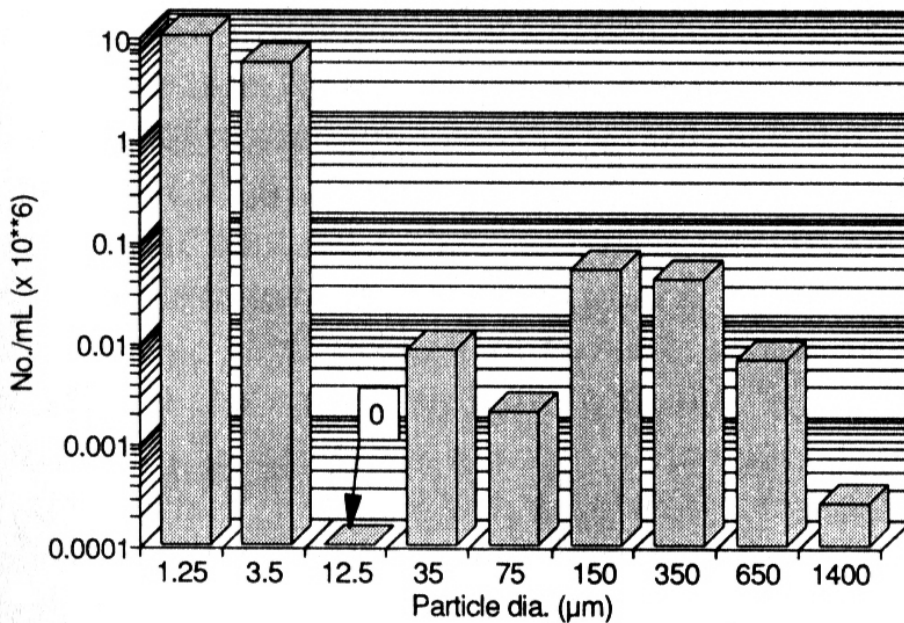
Figure 2.1. Particle size distribution in the mixed liquor of an activated sludge process (Parker *et al*., 1971).
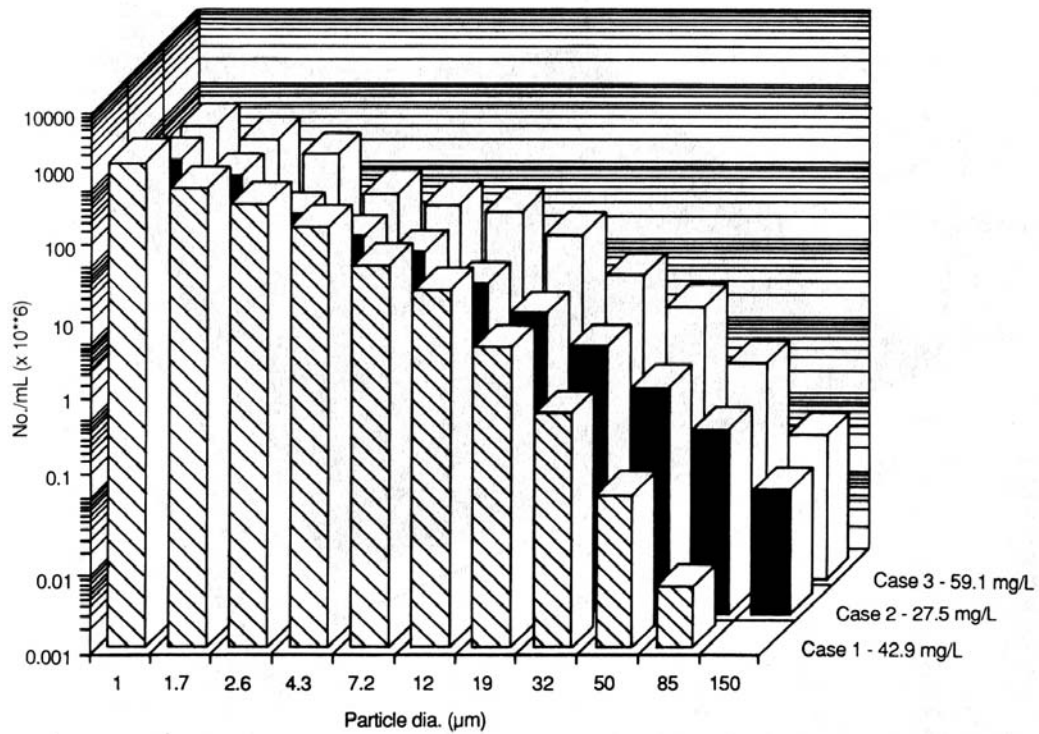
Figure 2.2. Effluent particle size distribution (Roth and Pinnow, 1981)

The particle concentration can then be written as:

$$X(\phi) = N_O \rho_d(\phi) V_p(\phi) f(\phi)$$

(2.13)

or

$$X(\phi) = N_0 \left(\eta + \tau\phi^{-\theta}\right) \frac{\pi}{6} \phi^3 \frac{1}{\sqrt{2\pi}\zeta\phi} \exp\left[-\frac{1}{2}\left(\frac{\ln\phi - \lambda}{\zeta}\right)^2\right]$$

(2.14)

If we let X be the solids concentration in the layer of interest then the suspended solids concentration is given by:

$$X = \int_0^\infty X(\phi) d\phi$$

(2.15)

$$X = N_0 \frac{\pi}{6} \int_0^\infty \left(\eta + \tau\phi^{-\theta}\right) \frac{\phi^3}{\sqrt{2\pi}\zeta\phi} \exp\left[-\frac{1}{2}\left(\frac{\ln\phi - \lambda}{\zeta}\right)^2\right] d\phi$$

(2.16)

The settling flux out of a given layer of the clarifier is:

43

$$\varphi = \int_0^\infty \upsilon_s(\phi) X(\phi) d\phi \tag{2.17}$$

Replacing the value of υ, ϕ and $X(\phi)$ from above yields:

$$\varphi = N_0 \frac{\pi}{6} \int_0^\infty \left(\eta + \tau\phi^{-\theta}\right)\left(\alpha + \beta\phi\right)\frac{\phi^3}{\sqrt{2\pi}\zeta\phi} \exp\left[-\frac{1}{2}\left(\frac{\ln\phi - \lambda}{\zeta}\right)^2\right]d\phi \tag{2.18}$$

Recall that the average settling velocity of the floc particles is given by:

$$\overline{\upsilon_s} = \frac{\varphi}{X} \tag{2.19}$$

or

$$\overline{\upsilon_s} = \frac{N_0 \dfrac{\pi}{6} \displaystyle\int_0^\infty \left(\eta + \tau\phi^{-\theta}\right)\left(\alpha + \beta\phi\right)\dfrac{\phi^3}{\sqrt{2\pi}\zeta\phi} \exp\left[-\dfrac{1}{2}\left(\dfrac{\ln\phi - \lambda}{\zeta}\right)^2\right]d\phi}{N_0 \dfrac{\pi}{6} \displaystyle\int_0^\infty \left(\eta + \tau\phi^{-\theta}\right)\dfrac{\phi^3}{\sqrt{2\pi}\zeta\phi} \exp\left[-\dfrac{1}{2}\left(\dfrac{\ln\phi - \lambda}{\zeta}\right)^2\right]d\phi} \tag{2.20}$$

The solution to this equation is given by:

$$\overline{\upsilon_s} = \alpha + \beta\frac{\eta e^{4\lambda + 16\zeta^2/2} + \tau e^{(4-\theta)\lambda + (4-\theta)^2 \zeta^2/2}}{\eta e^{3\lambda + 9\zeta^2/2} + \tau e^{(3-\theta)\lambda + (3-\theta)^2 \zeta^2/2}} \tag{2.21}$$

In effect:

$$\overline{\upsilon_s} = \alpha + \beta\overline{\phi} \tag{2.22}$$

where

$$\overline{\phi} = \frac{\eta e^{4\lambda + 16\zeta^2/2} + \tau e^{(4-\theta)\lambda + (4-\theta)^2 \zeta^2/2}}{\eta e^{3\lambda + 9\zeta^2/2} + \tau e^{(3-\theta)\lambda + (3-\theta)^2 \zeta^2/2}} \tag{2.23}$$

represents the effective diameter of the suspension of concentration X. Recall that α and β are settling velocity-diameter parameters, while η and τ are floc porosity-diameter model parameters. Equation 2.21 shows that $\overline{\upsilon_s}$ is a function of the mean of the log of the particle diameter λ as well as the standard deviation of the log of the particle diameter ζ. A plot of

$\overline{\upsilon}_s$ as a function of λ and ζ is provided in Figure 2.3 for a typical activated sludge suspension found in the upper layers of a secondary clarifier.
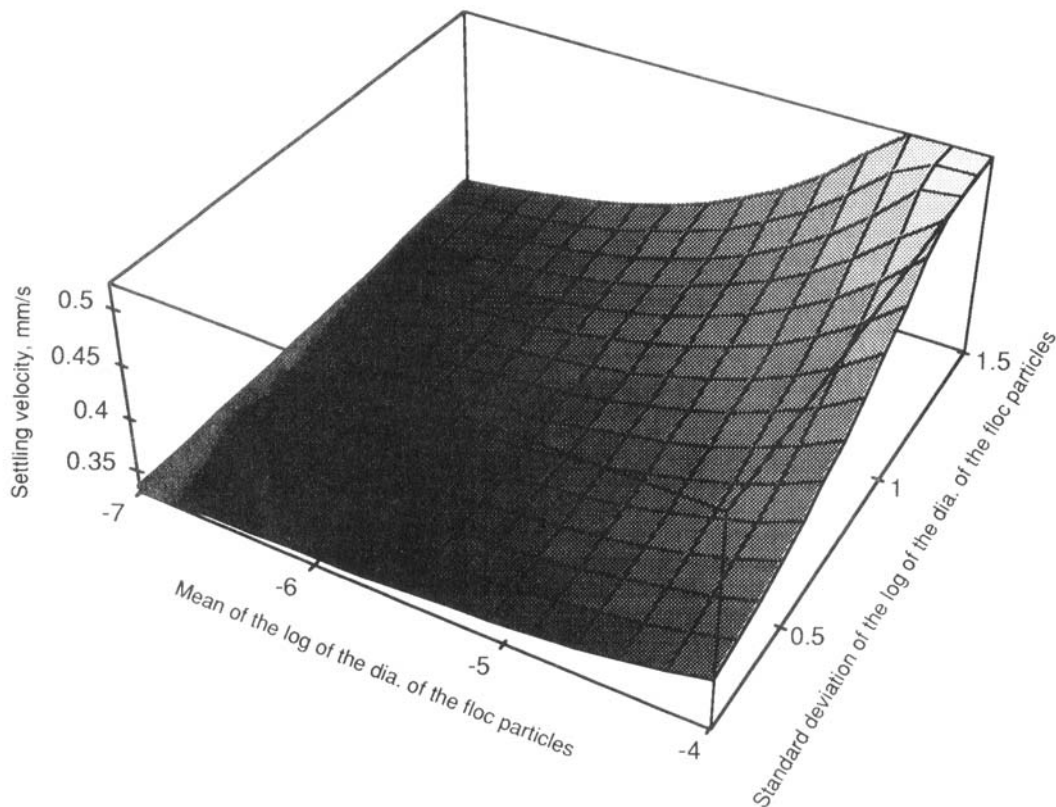
Figure 2.3. Average settling velocity as a function of particle size distribution.

2.3.3 Relationship Between Concentration and Particle Size Distribution

The point that will be made in this section is that, from a practical perspective, the solids concentration in the upper layers of a final clarifier is also related to λ and ζ.

Consider for example what happens to the particle size distribution under hydraulic disturbances. For the sake of discussion, let the overflow rate (i.e., upflow velocity) increase from Q to Q'. Under steady-state conditions, at an overflow rate of Q (m/h), the maximum floc particle size, ϕ_m, that will be carried upwards because of the upflow velocity of the liquid can be estimated using Stokes law (Aiba *et al.,* 1965). In effect, floc particles of diameter ϕ_m are at equilibrium between the gravitational and the upflow velocity forces. These floc particles will either break up and be carried into the effluent (or upper layers of the settler), or grow in size through flocculation and settle to a lower layer of the clarifier.

As the overflow rate increases from Q to Q', larger floc particles will be carried upwards, meaning that ϕ_m will increase to ϕ'_m. Because floc particle size is bounded at zero, an increase in overflow rate is likely to result in a larger mean particle size diameter of the flocculent suspension as larger floc particles will be carried upward, as well as in a larger variance in the particle diameters.

45

It is important to remember at this stage that because of the dependency of X on ϕ^3, the contribution to mass comes not from the large number of small diameter floc particles but from the smaller number of large diameter floc particles. This is illustrated in Table 2.1 using data from Roth and Pinnow (1981) for three samples taken from the secondary effluent of an activated sludge treatment plant. Cases 1-3 correspond to an effluent suspended solids concentration of 42.9, 27.5, and 59.1 mg/L, respectively. Finally, the introduction of large diameter particles in a suspension will not only affect λ but will have a definite impact on ζ. Accordingly, an increase in the overflow rate will shift the particle size distribution, resulting in larger values of both λ and ζ and a corresponding increase in the solids concentration.

Table 2.1. Mass and particle size distribution.

	CASE 1			CASE 2			CASE 3		
Average diameter μm	No/L 10^6	Cum. Mass	Cum. Particles	No/L 10^6	Cum. Mass	Cum. Particles	No/L 10^6	Cum. Mass	Cum. Particles
1	2000	0.031	0.506	750	0.02	0.48	750	0.01	0.41
1.7	900	0.099	0.734	500	0.08	0.80	500	0.04	0.69
2.6	600	0.243	0.886	150	0.13	0.89	300	0.07	0.85
4.3	300	0.440	0.962	80	0.20	0.95	100	0.11	0.91
7.2	95	0.616	0.986	50	0.33	0.98	70	0.18	0.94
12	45	0.847	0.997	20	0.46	0.99	60	0.34	0.97
19	8	0.949	0.999	8	0.60	0.99	30	0.54	0.99
32		0.989	0.999	3	0.75	1.00	9	0.72	0.99
50	0.1	0.998	0.999	0.85	0.85	1.00	3.5	0.88	1.00
85	0.0065	1.000	1.000	0.25	0.93	1'00	0.6	0.96	1.00
150				0.06	0.99	1.00	0.075	0.99	1.00
225				0.001	1.00	1.00	0.003	1.00	1.00

To illustrate this point further, consider a step change in overflow rate from 1 m/h to 1.5 m/h. For an overflow rate of 1 m/h the equivalent Stokes diameter as defined by Aiba *et al.* (1965) and Aiba and Nagatani (1971) is around ϕ_m =0.6 mm. When the overflow rate increases to 1.5 m/h, the equivalent Stokes diameter of the largest floc particle reaches $\phi_m' = 1.3$ mm. Because the solids concentration depends on the cube of the diameter of the floc particles, an increase in overflow rate will result, as expected, in an increase in suspended solids. While one could argue on the strict applicability of Stokes' law, the fact remains that a change in overflow rate will result in a change in the particle size distribution of the flocs being carried out in the effluent. As the overflow rate increases, the mean diameter will increase (as will the variance in the particle size), resulting in an increase in the suspended solids concentration.

The analytical expression relating the solids concentration to the particle size distribution is obtained by integrating Equation 2.16, i.e.,

$$X = N_0 \frac{\pi}{6} \left[\eta e^{3\lambda + 9\zeta^2/2} + \tau e^{(3-\theta)\lambda + (3-\theta)^2\zeta^2/2} \right] \tag{2.24}$$

A graph of the solids concentration as a function of the mean of the log of the particle diameter (λ) and their standard deviation (ζ) is shown in Figure 2.4. It can easily be seen from Equation 19 that the average settling velocity of floc particles ($\overline{\upsilon}_s$) depends on X. While this dependency is less obvious in Equation 2.21, the fact remains that the average settling velocity of floc particles depends on the particle size distribution within each layer, which in turn affects the solids concentration of that layer (Equation 2.24).
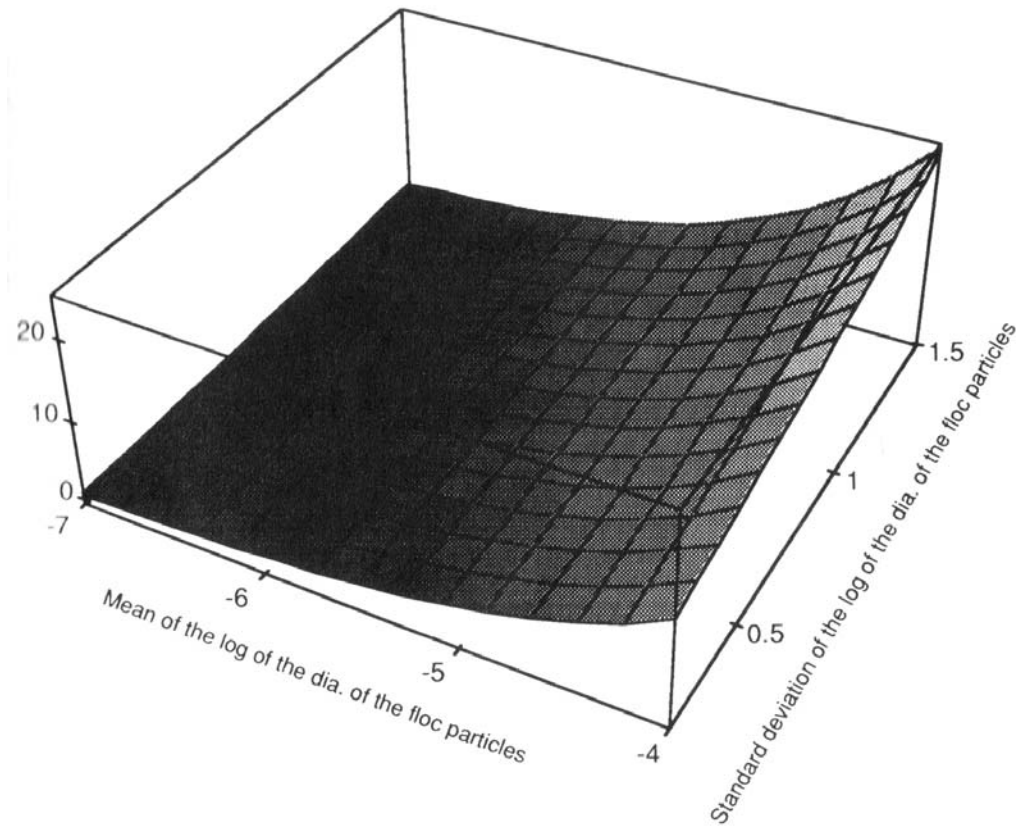
Figure 2.4. Solids concentration as a function of particle size distribution.

In fact, if the floc density (ρ_f) had been independent of particle diameter, it could easily have been shown that:

$$\overline{\upsilon}_s = \alpha + \psi X^{1/3} \tag{2.25}$$

where $\overline{\upsilon}_s = \beta \left(\dfrac{6}{N_0 \rho_d \pi} \right)^{1/3} e^{4\zeta^2/2}$.

However, this assumption would only be valid for floc particle size beyond 200 μm (Li and Ganczarczyk, 1987).

From the above, it is clear that a change in the particle size distribution that produces an increase in λ and ζ, will result in an increase in X, and a corresponding increase in $\bar{\upsilon}_s$. This observation is particularly obvious in Equation 2.25 under constant floc density.

The purpose of the previous exercise was to show that under normal operating conditions, the practical and operational constraints of a secondary clarifier lead to the conclusion that the average settling velocity of a flocculent suspension is correlated to the suspended solids concentration. Accordingly, in Chapter 1 it is proposed to extend Vesilind's settling velocity model for use in modelling the dynamics of the clarification/thickening processes.

As mentioned previously, the correlation between average settling velocity and solids concentration (region II, Figure 1.3) is valid for low solids concentration. As the solids concentration increases, a region exists (region III, Figure 1.3) where the average settling velocity of the suspension reaches a maximum upper limit. This corresponds to the transition zone between the low solids concentration region (region II) and hindered settling conditions (region IV). Ossenbruggen and McIntire (1990) have also suggested that a maximum practical settling velocity be used below the hindered settling concentration. Chapter 1 contains a discussion on how this model was used in modelling the dynamics of the clarification-thickening processes.

2.4 Conclusions

While it can be theoretically argued that the average settling velocity of discrete particles in the flocculent settling zone is independent of concentration, the practical and operational constraints of secondary clarifiers lead to the conclusion that the average settling velocity of flocculent suspensions is correlated to the suspended solids concentration. This is because the phenomenon that causes the change in the concentration of particles is not dilution, but settling. Settling, in addition to changing the concentration of particles in the upper layers of clarifiers, also changes the particle size distribution. The closer the layer is to the top of the clarifier, the lower the mean particle size is. Analytical expressions describing the concentration and average settling velocity of a suspension as a function of particle size distribution are presented. Finally, the relationship between particle size distribution and overflow rate is addressed.

3 HINDERED AND COMPRESSION SETTLING: PARAMETER MEASUREMENT AND MODELLING[3]

3.1 Introduction

Secondary settler design is frequently based on state-point analysis (Ekama *et al.*, 1997). This method relies on a settling velocity curve (settling velocity, v_s as a function of solids concentration, X), commonly described by the Vesilind function (Vesilind, 1968). The parameters of this function, v_0 and r_{hin}, can be established from the initial settling velocity of hindered settling tests performed at different concentrations on the same sludge. It is known that the configuration of the test vessel has an impact on the settling process and thus on the Vesilind parameters. Extensive experiments in test tanks of three different heights and surface areas were performed. The objective was to investigate the error that is made by inferring settling parameters from a bench-scale cylinder instead of the actual settling tank. The method of parameter extraction, with special attention to the required expert input and its influence on the results, was also investigated.

The same Vesilind settling velocity function is frequently used in 1-D dynamic settler models for process modelling purposes, as described in Chapter 1. The data collected was used to verify the hindered settling part of the model and develop an extension to account for compression settling.

3.2. Source of sludge and settling vessels

The activated sludge used in the settling experiments originates from a pilot-scale sequencing batch reactor (SBR) operating at the Environment Canada experimental hall. The reactor is fed with pretreated municipal sewage and operated around 10 day SRT year-round. The diluted SVI is consistently low (60 to 80 mL/g). Two series of approximately 10 batch settling tests were conducted over a MLSS concentration range of 1500 to 9500 mgTSS/L. For each initial concentration (X_0), the test was repeated in 4 different experimental setups: a) In the pilot scale SBR (2.5 m^3, 1.15 m deep); b) In a 3L graduated cylinder, equipped with a slow stirring mechanism operating at 1 rpm; c) In the same cylinder with the stirrer off; d) In a 1L graduated cylinder (unstirred). The objective was to study the effect of the characteristics of the vessel on the settling parameters, and to verify if bench settling tests can be representative of the full-scale process.

For the first test series (in short "Slow up"), the MLSS was slowly built up in the SBR by stopping wastage during 24 days. Once the MLSS concentration had reached 9.5 g/L, a second series (in short "Fast down") was conducted by successive dilutions with final effluent during 4 days.

3.3 Method of batch settling test

The batch settling tests were performed using material and expertise typically available at wastewater treatment plants (Rombardo *et al.*, 2005). After initial energetic mixing, the height of the liquid/sludge interface was monitored visually against graduation marks for 30 to 60 minutes on a transparent section of each vessel. More sophisticated equipment may provide a more consistent data set (Vanderhasselt and Vanrolleghem, 2000), but was not available at the time of the experiments.

3.4 Determination of the Vesilind settling parameters

For each test the recorded height of the interface was plotted against time. This yields a typical profile as shown in Figure 3.1 and 3.4 with three distinct phases: a) lag phase (residual turbulence), b) linear phase (hindered settling), c) compression phase.

The Vesilind function (Vesilind, 1968) was developed to describe the hindered settling process (linear phase) characterized by its slope v_s (m/d), the hindered settling velocity. Its parameters v_0 (m/d), the theoretical settling velocity at $X_0 = 0$, and r_{hin} (L/gTSS), the hindered settling parameter, were extracted from the data by three methods (1a, 1b and 2) with increasing level of automation.

Method #1: Fit to expert chosen linear section. The first approach consisted of visually delimiting the linear section of the curve by drawing a straight line through the data points, and dropping out points as they diverge at both ends. From here, two methods were used for parameter identification:

a) Each test was separately evaluated by fitting a linear function with a slope of v_s to the selected interface height data. The logarithm of the obtained v_s series was then plotted against X_0 and a linear function containing v_0 and r_{hin} was fitted to the data as shown in Figure 3.2. In both steps the objective function was the sum of squares which was minimized (using the Excel Solver). This is a practical implementation of the traditional method (Vesilind, 1968).

b) The slope (v_s) was expressed directly as a function of v_0 and r_{hin}. The square of errors between measured and calculated interface height of each test was added for all tests within one series to calculate one objective function. The values of v_0 and r_{hin} were optimized directly in one step by minimizing the combined sum of squares.

Method #2: Fit to whole curve without pre-selecting data points. The visual determination of the linear section of the settling curve can introduce bias as it depends on human subjectivity. A function was developed that allows the identification of v_s after fitting the whole curve. The function is of the form $h = f(p,t)$ where h is the height of the interface, t is time and p is a set of parameters including v_s. It was constructed starting from a linear expression fitting the hindered settling part of the experiment with a slope of v_s:

$$h = h'_{ini} - v_s * t \tag{3.1}$$

where h'$_{ini}$ is the intercept of the linear function at t = 0.

The effect of initial turbulence can be described as the slope of Eq. 3.1 changing from zero (or an apparent initial slope) to v_s (De Clercq, 2006). This is implemented using an exponential multiplier on the slope, which is 0 at t=0 and converges to 1:

$$h = h'_{ini} - v_s * \left(1 - e^{-\frac{1}{t_{turb}}t} \right) * t \tag{3.2}$$

where t_{turb} is an empirical concentration dependent turbulence time constant.

The phase of the experiment when compression settling starts to take over can be approximated by another exponential function to be added. The correcting function f_{compr} should start at a characteristic time, and slow the linear function until it stops at a final compressed height:

$$f_{compr} = if \left(t < t_{compr}, 0, e^{-r_{compr}\left(t - \frac{\ln\left(\frac{v_s}{r_{compr}}\right)}{r_{compr}} - t_{compr} \right)} + v_s \left(t - t_{compr} \right) - \frac{v_s}{r_{compr}} \right) \tag{3.3}$$

where t_{compr} is the time of compression onset and r_{compr} is a compression correction parameter. The resulting function is expressed as:

$$h = h'_{ini} - v_s * \left(1 - e^{-\frac{1}{t_{turb}}t} \right) * t + f_{compr} \tag{3.4}$$

Figure 3.1 shows the fit between data and Eq. 3.4 on one example. After the linear section of the test, the function first slightly overpredicts settling velocity (calculated height below the data points), and then underpredicts it (final interface height overpredicted). The residual error between this function and the data has the same characteristic shape as in Figure 3.1 for the whole concentration range (not shown), with increasing amplitude towards lower concentrations. This consistent residual interferes with the correct determination of the slope. The observed shape of residuals was used to develop a further correction l$_{corr}$ to Eq. 3.4, consisting of a double logistic function:

$$l_{corr} = \frac{h_1}{1 + e^{-p_1(t-t_1)}} - \frac{h_2 + h_1}{1 + e^{-p_2(t-t_2)}} \tag{3.5}$$

where h_1 is the maximum correction height on the first interface height deviation, h_2 is the correction on the final interface height deviation, p_1 and p_2 are logistic parameters (steepness factors), and t_1 and t_2 are characteristic times (for the time of maximum derivative correction). The final function is:

$$h = h_{ini}^{'} - v_s * \left(1 - e^{-\frac{1}{t_{turb}}t} \right) * t + f_{compr} + l_{corr} \tag{3.6}$$

Figure 3.1 shows the improved fit between the data and the corrected function. Eq. 3.6 contains 10 parameters, one of which (and the only concern) is v_s. The function was implemented in the Excel spreadsheet and its parameters were optimized with the solver to best fit the data on each settling test curve using the least squares method. At first the solver would find inappropriate slopes on occasion even when using good initial guesses. This was traced to the correction factors (Eqs 3.3 and 3.5) taking over the first term in Eq. 3.6 by starting to act too soon. It was mitigated by adding the following constraints on the time parameters in Eq. 3.6:

$$t_2 > t_1 > t_{compr} > t_{turb} * 3 \tag{3.7}$$

Once all v_s variables were extracted for a given series, the Vesilind parameters were identified with the same semi-log procedure as in method #1.a.
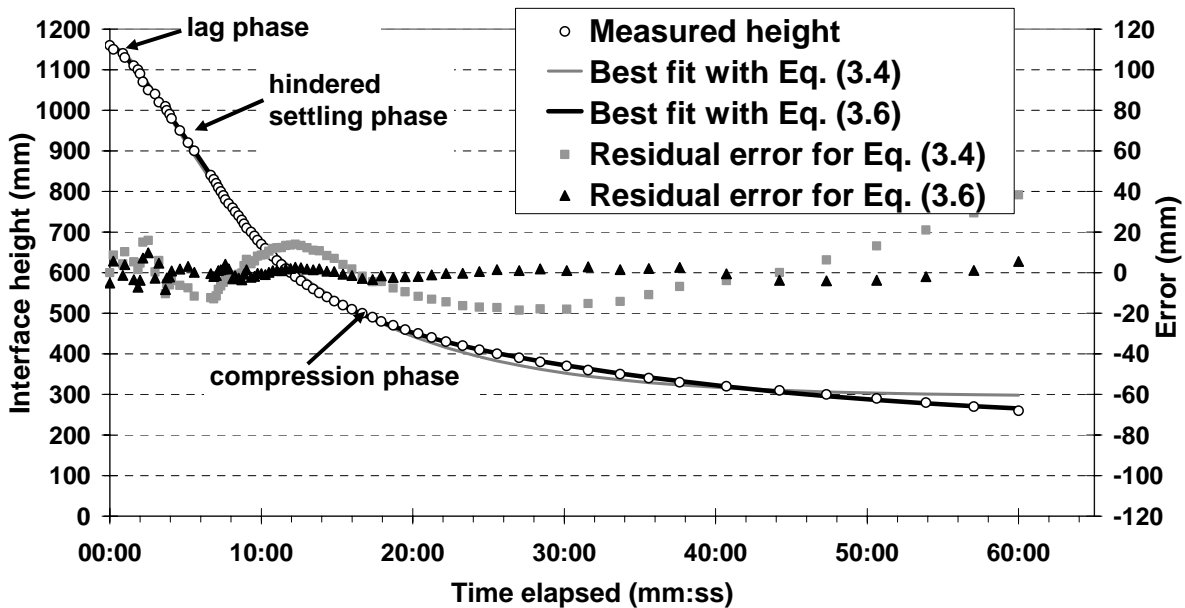
Figure 3.1. Fitted functions on the interface curve, and residual error (SBR, $X_0 = 3740$ mgTSS/L)

3.5. Results and discussion

3.5.1 Effect of settling vessel characteristics

The settling velocities (v_s) extracted by method #1.a are presented in Figure 3.2 for slow sludge build-up series and Figure 3.3 for fast dilution test series.

The alignment of the points shows that settling velocities are in agreement with the Vesilind model in the SBR reactor for the entire concentration range. The test concentrations were not high enough to encounter compression settling conditions during the initial zone settling phase. The results in the 3L stirred cylinder closely follow the results in the pilot plant tank. This is no longer true in the absence of stirring for initial concentrations beyond 4300 mg/L: the settling velocity is drastically slowed down in both unstirred bench cylinders. This is a known phenomenon that is attributed to elevated wall friction due to a higher ratio of inner surface area to volume. This ratio is 15 to 22 times higher in the bench cylinders than in the SBR pilot plant. Consequently, for the 2 unstirred vessels, only the points below 4300 mg/L were used for parameter extraction.
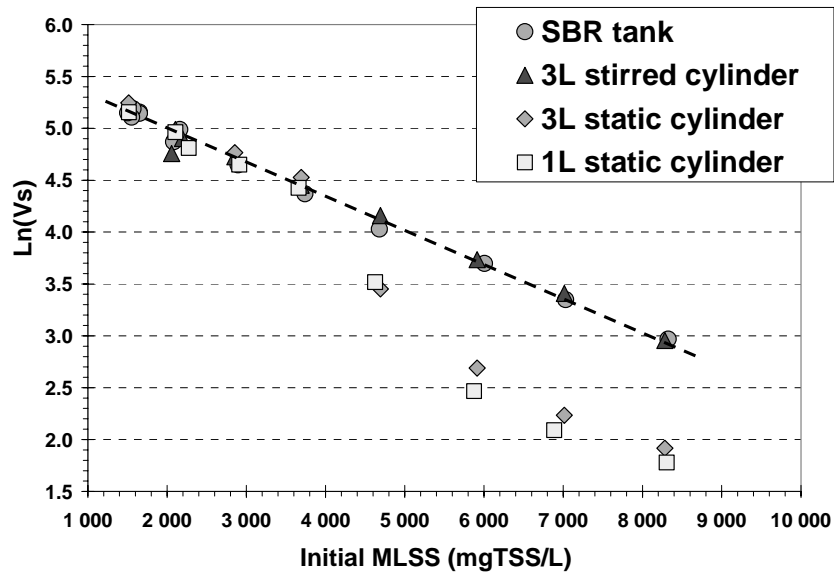
Figure 3.2. Hindered settling velocities versus initial MLSS concentration in the semi-logarithmic format for the slow sludge build-up series.
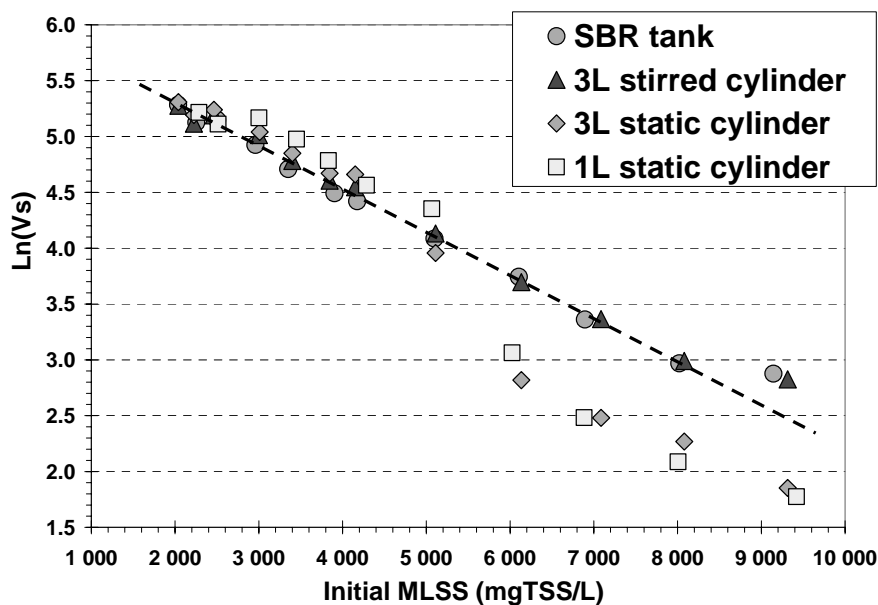
Figure 3.3. Hindered settling velocities versus initial MLSS concentration in the semi-logarithmic format for the fast dilution series

In conclusion, both series confirm that it is not as much the size of the cylinder, but rather the slow stirring that is the key factor in obtaining representative settling rate measurements at bench-scale at high MLSS concentrations.

3.5.2 Effect of parameter estimation method

Goodness of fit. Figure 3.4 shows that for all methods, the fit to the interface height curve is excellent at higher concentrations but less good at lower concentrations. This is mainly due to poorer data quality, especially below 2200 mg/L: the fast settling rates combined with poorly identifiable interface make it difficult for the human eye to deliver reliable readings.
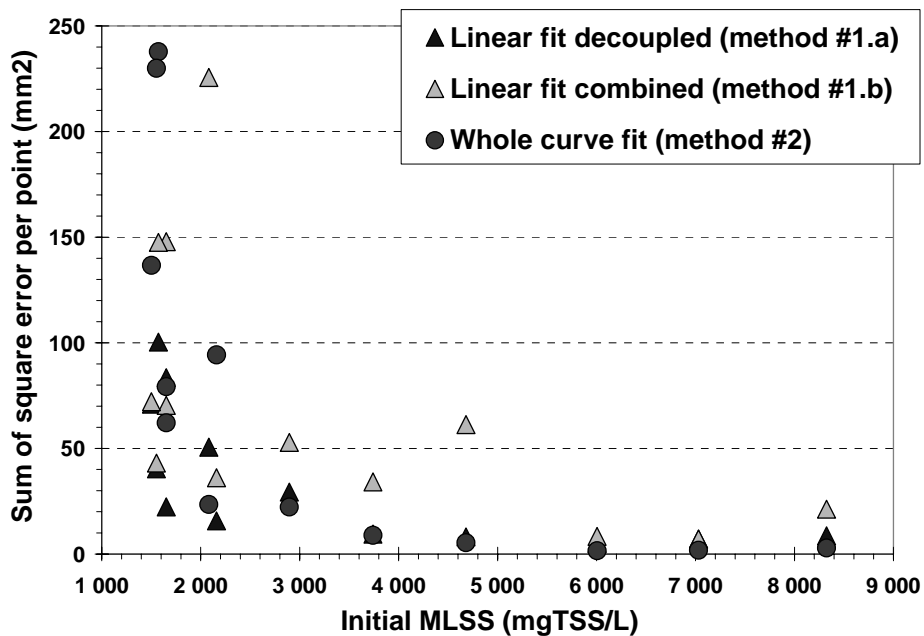
Figure 3.4. Relative sum of square error between fitted function and interface height data points for the three parameter estimation methods (SBR reactor, series "slow up")

The fitting method that requires the most human decisions (1.a) seems to be best able to reduce this scatter in this particular case. However the selection of the linear portion of the curve can have a significant impact on the v_s result especially at low concentrations. The "combined fitting method" (1.b) provides the highest error since it does not fit data points individually. The fit for the automated method #2 is shown for the whole concentration range in Figure 3.5. However it provides as good a fit as the expert method (#1.a) above 2200 mg/L. Below this concentration it yields similar results to 1.b. due to the scatter in measured data.

Comparison of estimated Vesilind parameters. Table 3.1 shows the final results of the parameter estimation. Overall the different methods give very similar results for a given vessel, with a maximum relative standard deviation of +/-5% (v_0 in the 3L static cylinder). This confirms indirectly that the two new methods (1.b and 2) are valid and applicable.
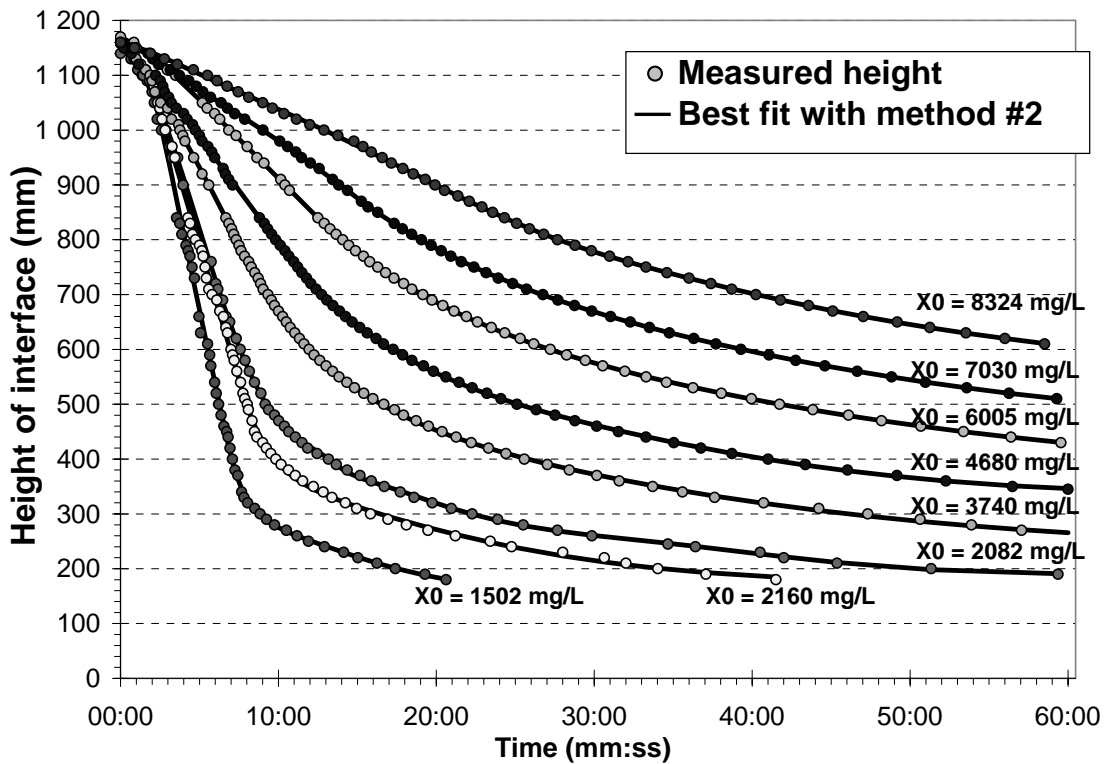
Figure 3.5. Measured and fitted interface height with method #2 (SBR, series "slow up")

The 4 vessels also yield similar results, with a maximum relative standard deviation of +/-8% (v_0 for method #1.b). It is confirmed that the bench vessel that represents the SBR reactor with the least error is the 3L stirred cylinder. However it is surprising that the 1L static cylinder gives almost as accurate results, if the tests beyond $X_0 = 4300$ mg/L are not used for Vesilind parameter estimation. This means that the 5 remaining points contain enough information to allow the identification of parameters. The case of the 3L static cylinder is marginal with only 3 relevant data points.

Table 3.1. Vesilind parameters estimated with the 3 methods (series "slow up")

Parameter identification method	Vessel											
	SBR reactor			3L stirred cylinder			3L static cylinder			1L static cylinder		
	# tests	v_0	r_{hin}	# tests	v_0	r_{hin}	# tests	v_0	r_{hin}	# tests	v_0	r_{hin}
	-	m/d	L/g	-	m/d	L/g	-	m/d	L/g	-	m/d	L/g
1.a	13	281	0.33	9	262	0.31	3	311	0.33	5	283	0.34
1.b	13	277	0.32	9	261	0.31	3	314	0.34	5	287	0.34
2	13	268	0.33	9	258	0.33	3	289	0.32	5	293	0.37

3.6 Use of settling parameters in one-dimensional (1-D) dynamic modelling

Clarifier capacity and critical loading are often estimated by two methods, both relying on the Vesilind hindered settling velocity function.

1. *State Point Analysis.* This method provides an easy graphical procedure to determine loading conditions in a clarifier. The method uses the Vesilind settling parameters to calculate settling velocity and solids flux that the clarifier can handle, depending on bulk flow conditions.

55

2. *1-D flux models.* One of the more frequently used models is described in Chapter 1. A slightly modified, simpler version is used in this chapter. The simplified description uses the same expression for all layers independent of feed layer position and threshold solids concentration. This simpler definition of the fluxes provides similar results to the original model:

$$v_{s,i} = \max\left(0, \min\left(v_{s,\max}, v_0\left(e^{-r_{hin}(X_i - X_{\min})} - e^{-r_{floc}(X_i - X_{\min})}\right)\right)\right) \tag{3.8}$$

$$J_{s,i} = \min\left(v_{s,i}X_i, v_{s,i+1}X_{i+1}\right) \tag{3.9}$$

where i is the layer number, J_s is the settling flux, $v_{s,\max}$, $X_{\min}$ and r_{floc} are double exponential settling parameters not affecting the discussion in this chapter.

This equation for the purpose of calculating the interface height reduces to the Vesilind settling function, but uses an additional "minimum of fluxes" operator to be able to predict a stable steady-state sludge blanket (Vitasovic, 1989). A feature of the double exponential model is that it uses the number of layers as a model parameter. The smaller the number of layers, the more numerical diffusion or "backmixing" occurs between layers, and this will have a smoothing effect on the gradients in the solids profile. Ideally the model results should become less and less dependent of the number of layers, as this number increases.

1-D flux models calculate a solids profile, and do not provide interface height (sludge blanket level) as an output. To calculate sludge blanket level, the following three steps were implemented: 1) A typical concentration at the sludge blanket interface (2000 mg/L) was chosen; 2) A continuous cubic spline function was fit to the concentrations in the middle position of the three adjacent layers; 3) The exact position in terms of tank depth where the concentration crossed the selected blanket concentration was extracted and defined as interface or blanket height. This approach shows a slight "waviness" in the calculated interface (Figure 3.6), due to the discrete number of layers, but gives a good indication of the approximate position of the simulated sludge blanket.

The settling experiment performed in the SBR "slow up" series at 3740 mg/L initial MLSS concentration was simulated using the double exponential model (Figure 3.6) with the Vesilind parameters extracted previously by method #2 (v_0 = 268 m/d, r_{hin}= 0.33 g/L).

The optimal number of layers providing best fit is nine in this case. The low number of layers allows an approximation of the effect of compression, which the Vesilind function does not contain. To illustrate this, the double exponential model was simulated with the same parameters using 100 layers (Figure 3.6). The interface height during the hindered settling phase is well matched, but during the following compression phase, the simulated and measured interfaces diverge.
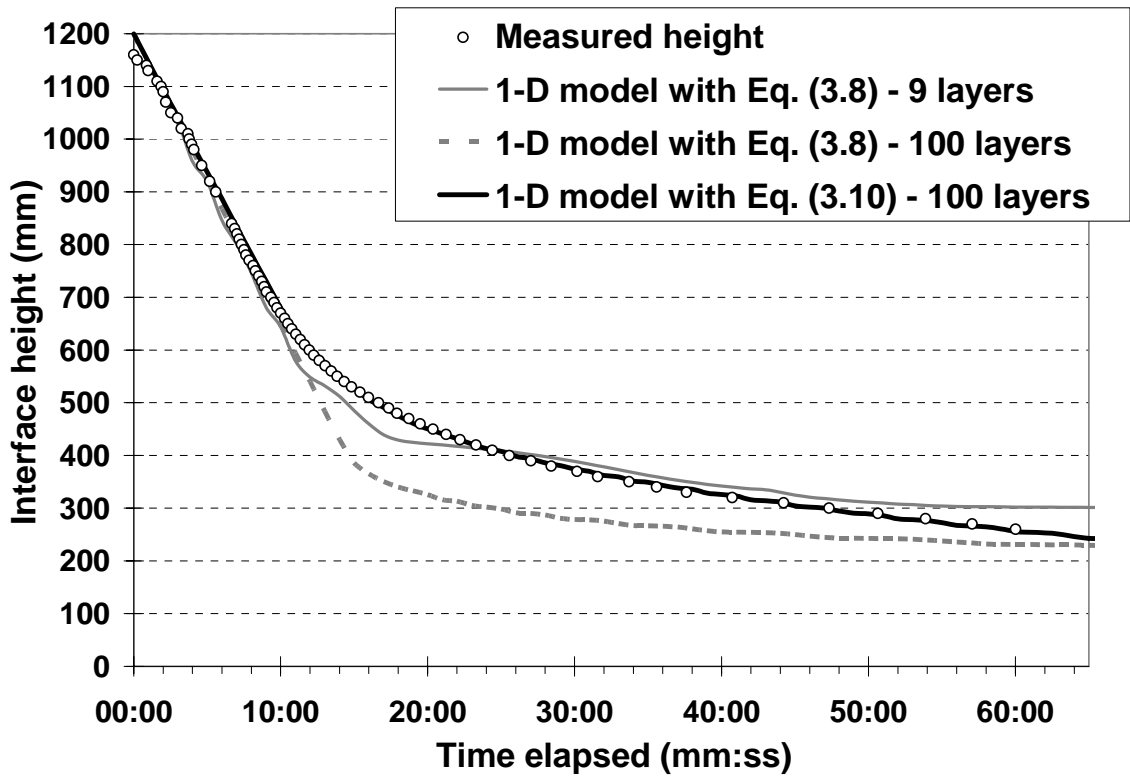
Figure 3.6. Measured and simulated interface height with the 1-D flux model (SBR, $X_0 = 3740$ mgTSS/L)

There are several attempts to account for compression settling in 1-D flux modelling (De Clercq, 2006; De Clercq *et al.*, 2008; Zhang *et al.*, 2006). In this work, it was noted that the residual error, if compression settling is simulated using the Vesilind function alone, is similar to the error correction provided by Eq. 3.5, for all experiments (not shown). Consequently, the same correction function form was applied to the Vesilind settling function according to Eq. 3.10:

$$v_{s,i} = \max\left(0, \min\left(v_{s,\max}, v_0\left(e^{-r_{hin}(X_i - X_{\min})} - e^{-r_{floc}(X_i - X_{\min})}\right) + \frac{v_{corr}}{1 + e^{-r_{corr1}(x - x_{corr1})}} - \frac{v_{corr} + v_{res}}{1 + e^{-r_{corr2}(x - x_{corr2})}}\right)\right) \quad (3.10)$$

where v_{corr} is the maximum velocity correction on the first deviation, v_{res} is the correction on the final compression velocity, r_{corr1} and r_{corr2} are logistic parameters (steepness factors) #1 and #2 respectively, and X_{corr1} and X_{corr2} are characteristic concentrations (for concentrations of maximum derivative correction).

This function slows down the settling velocity once compression settling starts to take effect (around the 11th minute in Figure 3.5), and predicts the final residual settling velocity. Simulation of the same experiment with the Vesilind function adjusted by the compression function (3.10) shows a good fit independent of the number of layers (as long as this layer number is sufficiently large). Parameters used were $v_{corr} = 20$ m/d; $v_{res} = 0.5$ m/d; $r_{corr1} = 3$L/g; $r_{corr2} = 0.5$ L/g; $X_{corr1} = 4000$ mg/L and $X_{corr2} = 8000$ mg/L. These values were determined by visual observation of the error between the uncorrected model and this specific data set. Simulation of more experiments is required in the future to investigate the general applicability of the correction terms.

3.7 Conclusions

High quality and extensive settling data sets were generated by careful observation of interface heights in a series of settling vessels. One of these was a large pilot scale reactor that is a valid surrogate of the full-scale process. It was verified that bench cylinders must be slowly stirred to be representative of full scale reactors beyond a certain MLSS concentration (4300 mg/L for this sludge). Data points collected below this concentration in unstirred cylinders may still allow proper determination of the Vesilind parameters, but with decreased confidence.

Three methods were used to determine Vesilind parameters and gave similar results. Compared to parameter estimation based on human choice, automating the extraction with a simple Excel routine has several advantages: lower impact of human bias, uniform procedure and reduced workload. However, the method is not fail-safe: human input is still required to define acceptable initial guesses that will allow the solver to find the appropriate solution. Whole-curve fitting requires simultaneous optimization of an increased number of parameters, compared to fitting limited to only the linear portion of the curve.

Using the extracted Vesilind parameters, 1-D flux models simulate the hindered settling phase of the test correctly, but the simulations deviate from the data in the compression phase. The usual approach is to use a small number of layers (8-30), which provides numerical "smoothing". Instead, a correction function is proposed, consisting of two logistic terms. The fit to several batch settling curves is excellent, but further batch and flow-through studies are required to verify that the function is generally valid and has stable parameters, as well as to develop an easy measurement/calibration method.

4 MODELLING OF THE MICROMORPHOLOGY OF THE ACTIVATED SLUDGE FLOC: LOW DO, LOW F/M BULKING[4]

4.1 Introduction

One of the most frequent process failure conditions in activated sludge, and the least predictable using mathematical models, is bulking. Some bulking events can be related to low DO or low F/M conditions. Filaments and floc-formers experience different environmental conditions depending on their position within the activated sludge floc.

In the process of biological wastewater treatment, electron acceptors and donors are subject to mass transfer limitations. Gradients around and inside the biofilm and activated sludge flocs are maintained by the balance between the substrate uptake (utilization rate) and diffusion of the compounds (renewal rate) from the bulk solution. The removal of electron donors (soluble substrates) and electron acceptors (such as oxygen and nitrate) from the proximity of the cells leads to the establishment of patchy microenvironment characterized by several dynamic gradients. The existence of such gradients in bacterial aggregates and in biofilms was recognized earlier by using microscopic staining techniques and by the development of advanced microelectrodes. Models for biofilm substrate kinetics and population dynamics were also developed in the past few years. A review can be found in Charaklis and Marshall (1990).

The importance of gradient-governed microenvironments was recognized by the application of immobilized cell bioreactors for biotechnological purposes. Gradient-governed microenvironments are present not only in immobilized cell and biofilm bioreactors but also in reactors containing suspended organisms forming aggregates. Theoretical considerations of diffusion limitation in connection with the shape and size of the bacterial aggregates and computer simulations in this area are in an early stage of development (Koch, 1990). In fact, most bacteria live in immobilized form, or in aggregates, not as single, suspended cells. Although this fact is widely accepted (Stolp, 1988), its consequences are hardly investigated.

The morphological clustering of activated sludge microorganisms has resulted in extensive monographs and reviews on the identification of filament types and assessment methods for their abundance, in relation to the settleability of the sludge (Jenkins *et al.*, 1984, Eikelboom and van Buijsen, 1981). Another research direction is devoted to the questions of population dynamics, with special emphasis on sludge bulking (Wanner and Grau, 1989). There is, however, an existing gap between the morphological classification and physiological groups or metabolic abilities of filaments. The developments of the past five decades indicate the

---

emergence of different theories of bulking, some of which are morphologically based, while others are more physiologically oriented. The objective of this chapter is to describe an initial attempt to merge the consequences of the morphological attributes with physiological (metabolic) characteristics of the activated sludge bacteria.

4.2 The activated sludge floc: microbiological background

Theories of bulking. More than half a century ago it was recognized that certain sludge settleability problems are due to excessive growth of filamentous organisms (Morgan and Beck, 1928). It was argued that the quality of the influent (i.e. composition rich in carbohydrates) was the cause of the population outburst of Sphaerotilus spp. Together with the widespread application of activated sludge systems, the understanding of the problem of bulking gained importance (Dreier, 1945). More recently, insight, especially in areas of microbiology, biochemistry and ecology, has deepened on the biological knowledge of activated sludge systems. The influence of process control elements (i.e. mixing regimes, reactor configurations, etc.) on the structure and species composition of activated sludge flocs has been investigated in many aspects. There are a number of bulking theories, but none of them is generally accepted as a single explanation for bulking. It is rather considered that different types of bulking exist as indicated by several national surveys on the presence of filamentous organisms in the activated sludge system (Eikelboom 1977; Tomlinson 1982; Wagner 1982; Blackbeard *et al.*, 1986, 1988). A variety of mechanisms playing a role in bulking was identified, including: metabolic pathways (preferential substrate utilization) (Chudoba, 1985), the effect of electron acceptor availability (Blackbeard *et al.*, 1988; Hao *et al.*, 1983; Lau *et al.*, 1984a), colloid properties and bioflocculation (Heukelekian, 1941), the effect of mixing regime (Kroiss and Ruider, 1977, Chambers, 1982), feeding pattern (Palm *et al.*, 1980).

In this modelling study the first two mechanisms were selected for investigation since they are both based on the same principle, mass diffusion limitation, which can be handled effectively mathematically. According to the proposed new approach, the structural properties and the different growth patterns can impose differences in population dynamics between the filament and floc-former groups, provided that environmental factors meet a predetermined set of conditions. In fact, these conditions will determine the onset conditions and the boundaries of bulking situations. In gradient governed microenvironments those bacteria with lower specific growth rate and half-saturation constants (typical to filaments) have a competitive advantage over the regular floc-formers having a higher specific growth rate and half-saturation constants. This well-known concept using the Monod saturation function is illustrated in Figure 4.1, where in the shaded low concentration range filaments can outgrow floc-formers. The non-randomly growing filaments grow towards the edge of the floc, where higher substrate concentration is available, while floc-formers exhibit non-oriented growth patterns and remain trapped in the core.

The settling characteristics of the flocs are influenced by the ratio of filaments to floc-formers. Too low a level of filaments results in "pin-point", very small flocs. Elevated levels of filaments, protruding from the floc, increase its Stokes radius and hinder settling. An optimum level exists where there are filaments present, enhancing the attachment and settling of pin-point flocs, but not in excessive numbers. A number of attempts have been made to establish a quantitative relationship between the sludge settling characteristics and the amount of filaments present per unit reactor volume (Sezgin *et al.*, 1978; Palm *et al.*, 1980; Lee *et al.*, 1983). These authors also point to the fact that micromorphological parameters, like total

extended filament length (TEFL), are only in very loose and ill-defined relationship with typical process control parameters (like Sludge Volume Index, SVI), making these latter parameters less than ideal for process control.

Growth rate

Floc-formers

Filaments

Substrate concentration
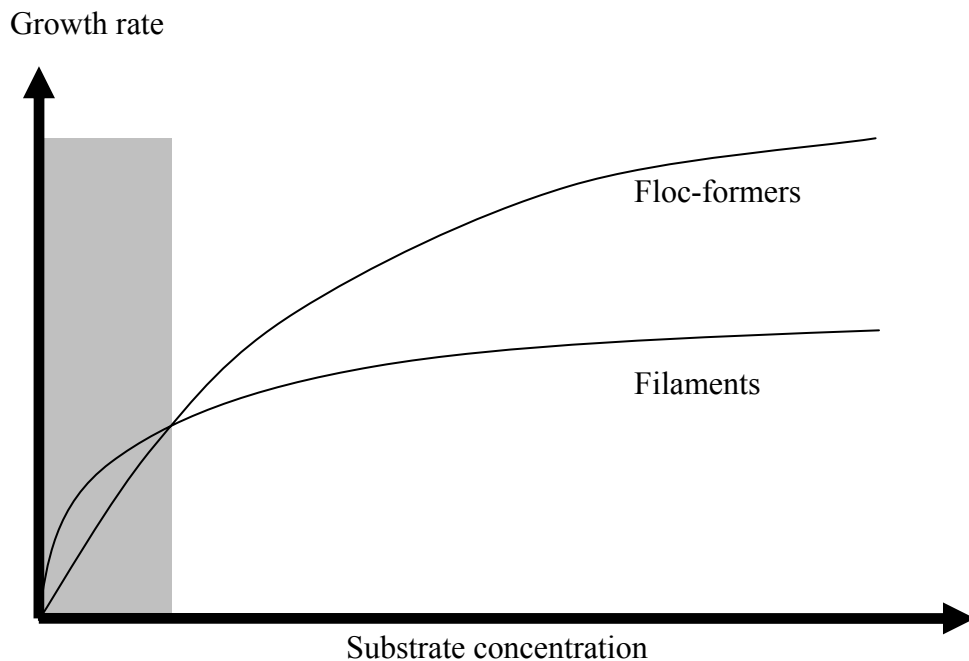
Figure 4.1. Filaments enjoy advantage at low concentrations

4.3 The activated sludge floc: a model for the microenvironment

Simulation of multispecies populations is an established method in mathematical models dealing with activated sludge dynamics (e.g. Dold, 1990; Wentzel, *et al.*, 1992). Bacterial growth dynamics and diffusion are both relatively well known and models do exist for the steady-state simulation of a floc with predetermined shape consisting of dual species composition (Lau *et al.*, 1984b). However, at the time of this study there was no research that has taken the oriented growth characteristics of the filaments and the micromorphology of the floc into account.

The intent of the authors was to simulate the patchy microenvironment of the activated sludge floc in as much detail as possible, including the unidirectional growth characteristics of filaments. Some simplifications were necessary in an effort to keep the mathematical model within reasonable limits. The Advanced Continuous Simulation Language (Mitchell and Gauthier Associates, 1987) was used for coding the dynamic model, and a SUN Sparc 1 workstation provided the platform for the simulations. Simulations usually took longer than real time to run (i.e. one day simulated time took longer than one day to simulate).

The activated sludge floc model developed in this study consisted of the following key elements:

Process model. Three types of bacteria (floc-formers, low DO and low F/M filaments) and soluble substrate as well as DO were calculated in the simulation model. Double-substrate (DO and organic substrate) limited Monod terms were used for bacterial growth and substrate utilization. Particulate substrate, hydrolysis, nitrogen and phosphorus forms were ignored in the model at this stage. Decay was handled on an individual cell basis (*see Aging*).

Diffusion. Diffusion of soluble substrate and dissolved oxygen was calculated based on Fick's Law (Fick, 1855, from the 19th century)). The perimeter of the simulated floc was directly in contact with the bulk liquid, which provided an infinite supply of the two soluble materials. Diffusion coefficients were obtained from Matson and Charaklis (1976). Typical values found inside the floc are lower than in clean water due to the porous structure and the effect of the extracellular polymers found in flocs. Diffusion coefficients used in the dynamic simulations were $0.1^{.}10^{-5}$ cm^2/s for soluble substrate (glucose) and $0.5^{.}10^{-5}$ cm^2/s for oxygen. The model could also be run without diffusion limitation (effectively infinite diffusivities).

Resolution. Some preliminary runs were done in order to determine the necessary and maintainable resolution level. Since the size of typical bacteria is in the order of micrometers, 1 μm resolution seemed to be a good starting point. When looking at the complexity of the floc at this level though, it turned out that an average 3-D floc with a diameter of about 100 μm would contain about five million state variables. Two steps were taken to reduce this complexity. First, the floc was assumed to be symmetrical in the third dimension and thus just one two-dimensional slice (the "computational plane") was simulated, secondly the final resolution selected was 2 by 2 μm. This results in a 50 by 50 grid, and 12500 state variables within one floc. Each element of the grid contained soluble substrate and dissolved oxygen, as governed by bacterial uptake and diffusion. In addition, the grid element was either empty, or contained a single bacterial cell of one type only.

Parameters. Model parameters used in the study are listed in Table 4.1.

Table 4.1. Model parameters

Parameters	Unit	Floc- formers	Low DO filaments	Low F/M filaments
Spec. max. growth rate	1/h	0.25	0.05	0.05
DO half-satu-ration	g/m^3	0.5	0.01	0.5
Substrate half-saturation	g/m^3	4.0	4.0	0.1
Yield	-	0.5	0.5	0.5

Propagation rules. When the "size" of the bacterial cell, due to growth, reached the full capacity of the grid element, the bacterial cell propagated, losing 25% of the mass which was placed in a neighbouring element. In case of the floc-formers, the direction of the propagation was supposed to be random, while the filaments "remembered" the first, randomly directed propagation step in the following cell divisions with a certain, high probability. It should be mentioned that there were only eight directions available for the propagating cells, corresponding to the eight neighbouring elements of a square. If the division took place in a cell completely surrounded by other cells, the next generation or "child" cell created an empty

location by displacing all the cells in the selected direction by one gridline. If an empty location was available around a floc-former bacteria, the "child" occupied that one. The result was a fairly compact floc growth in the simulations, since first all empty spaces were populated within the floc, then the growth continued by gradually increasing floc mass from the inside. There was no intention at this stage to try to simulate the real morphological arrangement of the activated sludge floc, other than the concentration gradients in the microenvironment.

Aging. The age of all individual cells (from the moment of propagation) was stored and used to determine when a cell would die. Since propagation reset the age of both the "parent" and the "child" cells to zero, the life expectancy of the bacterial cell (at least in the range of a few to few dozen hours used in the runs) did not seem to influence the course of the simulation. In the event of a decayed cell, since no hydrolysis was simulated in the model, the cell became an inert mass occupying one element of the grid.

Seeding. Initialization of the floc was done placing a small seed floc (10 by 10 grid elements) into the middle of the computational plane, distributing about 90% of the initial mass to floc-formers, and placing one filament of each type into the seed floc (as shown in the first frames of Fig 4.2 – 4.4.). For the soluble components, the initial concentrations were set to the bulk liquid concentration in all elements.

Simplifications. The process of diffusion is several orders of magnitude faster than bacterial propagation. To simplify the complexity of the numerical solution, only bacterial growth was simulated dynamically, and the concentration gradient for soluble substrate and dissolved oxygen was periodically updated assuming steady-state component distribution based on the uptake rate of the bacterial population at that time. Only batch runs were done with the simulated floc, following the development of the seed for one or two days typically, until it reached the perimeter of the computational plane. Continuous simulations would have required some algorithm mimicking floc breakup due to shearing forces and were not considered in this study. Consequently, bacterial mass proportions are only indicative of growth preferences and to some extent, initial conditions, and do not reflect real mass proportions within the activated sludge. Also, the computed floc structure based on the simplified geometrical propagation rules at this stage does not simulate the morphology, porosity and other physical characteristics of a real activated sludge floc.

4.4 Results and discussion

4.4.1 Simulated scenarios

Three scenarios were selected to investigate the behaviour of the model. In these, normal loading conditions were compared against DO-limited and substrate-limited situations (Table 4. 2).

In this study, the model was not calibrated to a particular data set and the concentrations of the soluble compounds were selected arbitrarily, based on typical values experienced at wastewater treatment plants. All three scenarios were run in two operating modes, with and without diffusion limitation, resulting in a total of six dynamic runs. A simple ideally mixed version of the process model was also developed and run under DO limited conditions. The results of this run were compared to the corresponding case in the floc model (low bulk DO, but no diffusion limitation). It was found that the two models (the simple ideally mixed model

and the full floc model without the diffusion component) produce effectively identical results for the propagation of cell masses of the individual bacteria types. This means that as expected, the floc model, consisting of 2500 fields reduces to a simple ideally mixed model (1 field), if diffusion is ignored.

Table 4.2. Simulated scenarios

Scenarios	Bulk substrate concentration	Bulk DO concentration
	mg COD/L	mg O_2/L
1. Normal conditions	20	1.5
2. Low DO conditions	20	0.2
3. Low F/M conditions	4	1.5

Two-dimensional DO and substrate concentration profiles were prepared during the runs for post-processing. A typical example of the dissolved oxygen profile with the bulk concentration being 1.5 mg/l is shown in Figure 4.2 (origin is bottom left corner of the computational plane, i.e. the floc).

This concentration profile was taken on a substrate-limited case where the oxygen uptake rate (OUR) is constrained by the available organics. It shows that dissolved oxygen concentrations can drop to very low levels in the core of the floc, even under normal operating conditions.
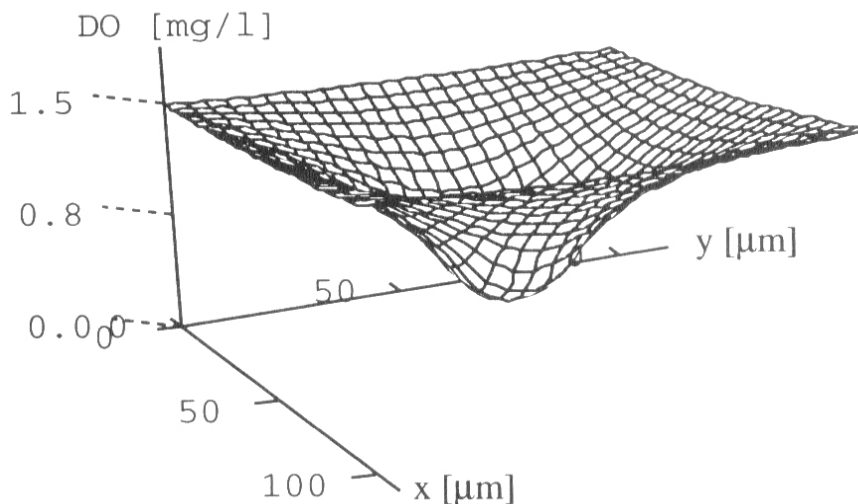
Figure 4.2. Simulated dissolved oxygen profile in a floc

Visual observation of the simulated flocs may provide further information with respect to roughness, total extended filament length, or other morphological characteristics which could be used as an output from the model. This avenue was not pursued at this stage though.

For illustration, Figure 4.3 shows the simulated development of a floc, under normal oxygen and substrate bulk concentration conditions. Lightly shaded areas indicate elements of the grid occupied by floc-formers, while darker spots in two tones represent the two types of filaments. Five stages of development were selected, from the seed on the left to the fully developed floc 19 hours later. The run in Figure 4.3 is a diffusion limited case, but visually

64

there is not much difference between this run and the three scenarios where diffusion was ignored, apart from the changing shape due to the random propagation direction used in the model.

Figure 4.3. Simulated development of a healthy floc

The excessive growth of filaments induced by low DO concentration (0.2 mg/l) in the bulk liquid is shown in Figure 4.4.

Figure 4.4. Simulated development of a floc in low DO environment

The age of this floc, due to the slower growth under DO limited conditions, is approximately two times larger than that of the previous one on Figure 4.3, i.e. about 40 hours. It has to be pointed out that when diffusion limitation was ignored, in spite of the low bulk DO concentration, the shape and other characteristics of the simulated floc were closer to the normal floc than this filamentous, "bulking" one.

Similarly, low bulk liquid substrate concentration, together with diffusion limitation resulted in excessive filament growth of the low F/M type, shown in Figure 4.5.

Figure 4.5. Simulated development of a floc in low F/M environment (the age of the floc on the right side is 31 hours)

The concentration of DO and substrate in the core of the floc was another variable used for evaluation of the runs. Typically the concentration of the components in the floc core decreased well below the half-saturation constant of the floc-formers, giving an advantage to the filaments in this region.

The most important indicator of the status of the floc was found to be the relative mass fraction of filaments (both the low DO and low F/M type, handled individually) in comparison to the mass of floc-formers, within one floc.

In Figure 4.6, results from the low DO scenario are plotted, both for the diffusion limited and the ideally mixed cases. In all the simulations when low DO and low F/M scenarios were simulated without diffusion limitation, the relative fraction of filaments stayed constant or decreased from the initial value. In contrast, when concentration gradients based on diffusion for the components were calculated, the model predicted excessive growth for the low DO filaments in the low DO environment, and similarly, high relative fraction of the low F/M ratio filaments in a substrate limited environment was observed.
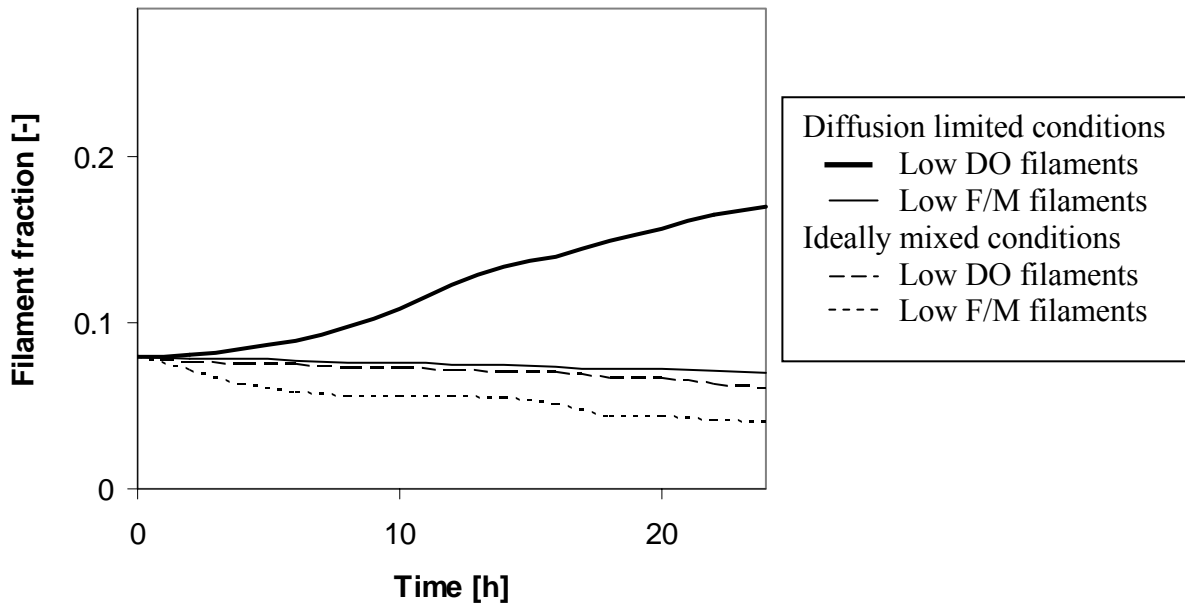
Figure 4.6. Filament mass fraction in development of a floc in low DO environment

4.4.2 Potential applications

The model, as demonstrated, is a valuable research tool which promotes studying the effect of gradient environments on filament development. After calibration, it could also be used to predict when an increased possibility for settling problems on a wastewater treatment plant exists. Running the model on a continuous basis using measured dissolved oxygen concentration in the aeration tank would enable the operators to easily check if there is a potential for excessive filament growth (low DO bulking) in the next few days. Prediction of low F/M bulking situations would require a sophisticated continuous OUR probe providing available substrate levels for the model. Alternatively, a calibrated plant model can be used to generate the required input data for the model.

4.4.3 Further research

Additional development of the model is required in several aspects. It is necessary to implement a more complex biokinetic model including the simulation of particulate substrate and hydrolysis. The actual concentration gradients in the real floc are more complex than the simple "bowl" shape suggested by this model. The main reason is that encapsulated particulate organic material will provide soluble food for the microorganisms from within the floc through hydrolysis. If a more complex model, such as the IAWQ Task Group's Activated Sludge Model No 1. (Henze *et al.*, 1987) can be implemented within a floc configuration, other potential applications become available, such as prediction of denitrification in the

aerobic zone of the aeration tank. Some effort should be directed towards identifying the necessary minimum resolution without compromising the predictive power of the model. Methodology to perform continuous simulations (floc breakup and flocculation) should also be developed. In this context, the environment of the floc would change periodically from that of the aeration tank to that of the sludge blanket, opening up new possibilities in predicting bulking conditions. Finally, more quantitative calibration of the simulated results to real plant situations would be beneficial.

4.5 Conclusions

With the development of hardware and software in the last few years it has become possible to tackle computational problems which are orders of magnitude more complex in mathematical terms than just a few years ago.

The model developed and illustrated in this chapter has a few simple geometrical propagation rules for different groups of bacteria, in addition to the usual, *albeit* simplified, biokinetic model component, and is capable of predicting excessive filament growth even when traditional, "ideally mixed" models fail to do so. Simulation of the micromorphology of the floc including directional growth of filaments may provide an insight into processes happening on the microscale of the activated sludge floc, as well as having the potential to act as an "early warning system" to detect certain conditions conducive to bulking. Simulation of the activated floc structure on this scale may lead to better understanding and the establishment of a closer relationship between widely used process parameters, such as influent conditions, plant operation, and the settling characteristics of the activated sludge.

5 IN CONTEXT: MODELLING PHASE SEPARATION

5.1 One-dimensional flux settler models

The so-called "double-exponential model" has become widely used and cited in the past 15 years. In 2006 the paper (Takács *et al.*, 1991), written by this author, Gilles Patry and Daniel Nolasco, was chosen by Water Research as one of the ten most ground-breaking papers in the 40-year publication history of the journal. The model is essentially a one-dimensional settler model as described by Vitasovic (1986), with a modified Vesilind function to predict low settling velocities at low suspended solids concentrations (Chapter 1). When low concentrations occur, floc particles are small and settle slowly (Chapter 2). This relationship was not clear before the publication of the paper (Patry and Takács, 1992) that forms the basis of Chapter 2. The double-exponential model in Takács *et al.* (1991) was not accepted in the first review because it uses a correlation between settling velocity and concentration of discrete particles, which is contrary to Stokes law. Convincing ourselves, the reviewers and the editors about the soundness of the approach required the development presented in Chapter 2.

The authors did not explicitly state that the model as set out initially in the paper (Takács *et al.*, 1991) works only with a low number (8-15) of layers. The low level of discretization, in an indirect way, accounts for the effect of compression not included in the flux theory (Chapter 3).

There is a large amount of literature that relates to various modifications and/or criticism of one-dimensional settler models in general and the double-exponential model in particular. A full review of this topic was not the objective of the author. Significant new developments include more thorough and consistent mathematics applied to clarifier modelling (Jeppsson, 1996, Jeppsson and Diehl, 1996), the theory of flocculation has been reviewed and addressed (Nopens *et al.*, 2007), as well as Computational Fluid Dynamic (CFD) models that are being developed (Ekama *et al.*, 1997, De Clercq, 2003). In spite of the fast pace of research and the results from all these developments, simple one-dimensional settler models (with the explicit objective of process modelling) are still widely used in practice. The following discussion considers why one-dimensional models are still in use when more detailed and mechanistic 2- and 3-D CFD models are available.

At this point a clear distinction between the two most important objectives of settler modelling must be made. A settler model can be used for:

1. Enhancing the simulation of the process performance of the activated sludge system or the whole plant. This task is almost exclusively performed by 1-D flux models. CFD

models are too complex, require too much input detail and are too slow to be linked with full plant process simulation at this time.

2. Detailed design of the settler geometry and mechanical structures. 1-D models are not suitable for this purpose, two or three dimensional CFD representations are required.

1-D models are fundamentally empirical models. Even the flux "theory", which is only one (although key) element of the 1-D clarifier model, is based on the empirical observation that zone settling velocity correlates to sludge concentration. 1-D models are fast, simple to understand, implement and operate, and provide an estimation of sludge mass exchange between the reactors and the settler, as well as effluent and return solids predictions linked with activated sludge models. They can be used to evaluate the effect of reactions (such as denitrification, P release, etc.) in sludge blankets. 1-D models do not distinguish between circular and rectangular tanks, and cannot simulate detailed structures, baffles, etc. (for those tasks a CFD model is required)

The main benefit of a 1-D empirical model is its simplicity. In general, it is not understood that these models do deal with the three different settling regimes. These are approximated and implemented in the following ways:

1. Discrete settling – through the double exponential extension of the Vesilind function (and several other similar empirical approaches). The principle of the extension is to slow down the Vesilind settling velocity at low concentrations. The Vesilind relationship is valid only above 1-2 g/L solids concentration, but not below. The justification to link discrete settling velocity to concentration is through the particle size distribution – in the top part of the clarifier, where settling is slow, particles are small (Chapter 2). The objective of this element of the model is to predict effluent solids. The model calculates effluent solids indirectly as a function of the three following effects:
   a. hydraulic loading
   b. solids loading
   c. proximity of sludge blanket
2. Zone (hindered) settling – according to flux theory and the Vesilind zone settling velocity function. This is the rate limiting critical step, determining how much solids get to the bottom of the settling tank.
3. Compression settling.
   a. The 1-D representation (used in the double exponential model) takes compression into account using the "minimum of fluxes" approach and a small number of layers (typically 8-15, in many implementations 10). In this method, the smaller of two fluxes is used in each layer, the one that can be "accepted" based on the current solids concentration present in the layer, or the one that can be delivered by the layer above based on its own solids concentration. The number of layers is essentially a model parameter providing a completely empirical numerical smoothing of the solids profile.
   b. Another approach used is to implement a backmixing or numerical diffusion process acting between layers (Hamilton *et al*., 1992). In this approach, the backmixing or diffusion constant is the model parameter, just as empirical as using the number of layers as a model parameter (although the diffusion parameter can be a non-integer number).
   c. Several other attempts include compression settling with correction functions to the Vesilind function (e.g. Chapter 3). Using this method the model solution

becomes independent of layer number and does not need backmixing (however there are several new parameters).

Without the modifications in a), b) or c), a 1-D settler model based on flux theory cannot predict a stable steady-state sludge blanket.

There is research that attempts to base discrete settling (by Parker, Nopens and others) and compression settling (by Kinnear, De Clercq and others) on more mechanistic principles, such as flocculation, compressibility, permeability. These attempts are not used widely in process modelling practice, even though they are more fundamentally based and take into account physical characteristics, such as viscosity, compressibility, pore volume, etc. The mathematics in these models is quite complex, and at this time it is not clear whether a final model structure has been agreed upon and if the 1-D implementation negates the advantages of the more theoretical basis (i.e. should they be in 2-D CFD models).

The choice of feed layer and distributing the feed into several layers allows further flexibility for model calibration and can be considered as another "model parameter". The closer the feed layer is to the top of the clarifier, the more sensitive the effluent solids predictions are for loading changes. The feed layer(s) can be directly linked to hydraulic loading with an empirical routine and this enables the one-dimensional model to predict gross loss of solids (for example at high inlet flow rate the feed can be distributed into the sludge blanket).

The one-dimensional representation can be implemented for settling tanks with sloping bottoms or sides (deep clarifiers, blanket filtration), and will produce better results than in their original pure 1-D representation, where the area of all layers is the same. The double-exponential model with its flexible, empirical settling velocity function, using a different set of parameters and low number of layers also approximates primary settler performance well (Gernaey *et al.*, 2001), and it has been used for thickeners. The investigation of these process units, however was not the objective of the author.

In summary, 1-D models play and will keep playing an important role in process simulation, while CFD models play an important role in detailed clarifier design, just as empirical sludge production rules are still used today even though complex mechanistic ASM models are available.

5.2 Individual-based modelling

The floc model based on Takács and Fleit (1995) presented in Chapter 4 may be one of the first examples of a modelling approach that has several variations and is known under different names: Individual Based Modelling (IBM), Agent Based Modelling (ABM), Population Balance Modelling (PBM), or Particle Based/Segregated/Distributed Modelling. This technique is now in use in various areas, such as fermentation, biotechnology, biofilms and biogeochemistry. Examples include Nopens *et al.* (2001), Gujer (2002), Picioreanu *et al.* (2004), Schuler (2006), Hellweger (2007) and others.

PART TWO – CHEMICAL TREATMENT PROCESSES

6 MODELLING pH IN WASTEWATER[5]

6.1 Introduction

The objective of this chapter is to describe a general numerical approach that can calculate pH in the complex solutions occurring throughout the different process units in the wastewater treatment plant. It has been recognized from the early stages of wastewater process modelling that pH is an important factor in simulating the performance of biological wastewater treatment processes, including activated sludge and anaerobic digestion. The pH impacts the species distribution of the weak acid systems (carbonate, ammonia, phosphate, acetate, propionate, etc.) present in the process. This in turn dictates the rate of many of the biological and physico-chemical phenomena occurring at the treatment plant, for example, (1) biological activity, that can be severely limited outside an optimal pH range, (2) chemical precipitation reactions when metal salts, such as alum or ferric chloride, are added for chemical P removal, (3) spontaneous precipitation of magnesium and calcium phosphates (struvite, HDP, HAP), and (4) stripping of ammonia at high pH and CO_2 gas/liquid mass transfer. It is difficult to accurately model pH in wastewater because the underlying components and reactions are so fast and complex. The traditional approach in activated sludge models has been to track alkalinity changes instead, and use that as a pseudo indicator of potential pH instability problems.
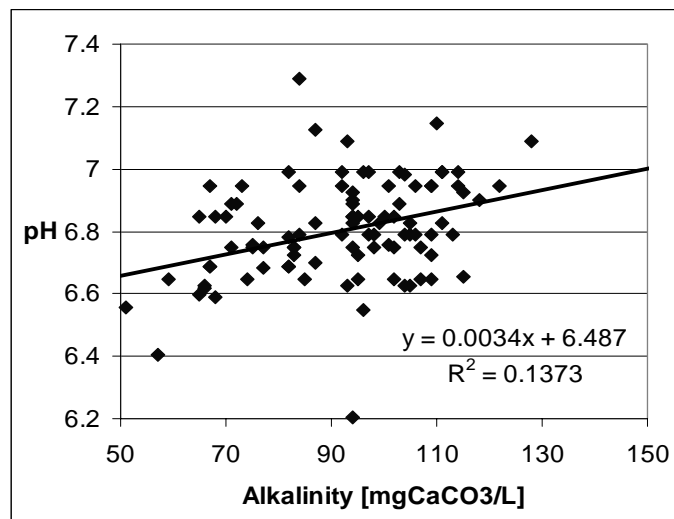
Figure 6.1. Alkalinity is not a good indicator of pH.

---

[5] Based on Takács I., Fairlamb M., Dold P.L., Bye C., Jones R. and Murthy S. (2004) pH in wastewater treatment plant modelling. In: Proceedings 4th IWA World Water Conference. Marrakech, Morocco, September 19-24 2004.

However, using alkalinity as an indicator of pH stability has several disadvantages. In systems with significant volatile fatty acid concentrations, such as acid fermenters or digesters, or in systems where significant gas transfer may occur, the predicted alkalinity may not be a good indicator of steady pH conditions. Analysis of a two year dataset from the DCWASA plant (Washington, DC) showed that the relationship between pH and alkalinity was very weak (Figure 6.1). As an example, two extreme solutions are shown:

1. High pH, low alkalinity solution. A solution of 0.7 mmol/L $NaHCO_3$ and 0.3 mmol/L of NaOH, closed to the atmosphere, has pH = 10 and alkalinity = 1 mmol/L. (Net Cations = 1 mmol/L, IC = 0.7 mmol/L (consequently HCO_3^- = 0.48 mmol/L, CO_3^{2-} = 0.22 mmol/L).

2. Low pH, high alkalinity solution. A solution with 10 mmol/L of $NaHCO_3$ and 118.3 mmol/L of H_2CO_3, closed to the atmosphere, has pH = 5 and alkalinity = 10 mmol/L (Net Cations = 10 mmol/L, IC = 228.3 mmol/L (HCO_3^- = 10mmol/L)).

Alkalinity can only be used to provide a single-sided inhibition function (i.e. when alkalinity is low), whereas pH can be used to calculate a two-sided inhibition function (both at low and high pH). This allows biological inhibition to be modelled at both low and high pH. Finally, alkalinity offers no means for modelling physico-chemical phenomena, such as chemical precipitation.

Calculation of the pH must consider the concentrations of strong acids and bases, the dissociation states of the weak acid, carbonate and phosphate systems, chemical precipitation reactions, and potential stripping of components involved in the acid-base systems, such as ammonia and carbon dioxide. All of these processes can be described using a kinetic approach (Musvoto *et al.*, 1997, 2000), but the rates of many of the reactions involved typically are four to twenty orders of magnitude larger than typical biological rates. As a result, calculation of the pH using a kinetic-based model will significantly reduce simulation speed. Hellinga *et al.* (1999) point out the need for pH calculation, and Batstone *et al.* (2002) describe a mixed kinetic/equilibrium based approach specifically for anaerobic digestion. However, there is a need for a method that is general enough to apply for all the major environments in the wastewater treatment plant. The formulation of the pH model used in this chapter is applicable across a wide range of biological treatment process models, i.e. the ASM-series for activated sludge (Henze *et al.*, 2000), ADM1 for anaerobic digesters (Batstone *et al.*, 2002), sidestreams (Wett *et al.*, 2007) and other models. The model has been verified on a number of laboratory scale systems which are described in this chapter.

6.2 Approach to modelling pH in solutions

The proposed approach for modelling pH is to divide the processes of interest into two groups, "equilibrium" processes and "kinetic" processes, based on their characteristics. Processes that fall into the "equilibrium" group are those whose rates are very fast. The rates must be fast enough so that we may consider them to be always essentially "at equilibrium". For the reactions in the equilibrium group, the reactants and products do not require separate state variables since the equilibrium method determines the current "state". For these, the total component concentration (e.g. total ammonia, $NH_4^+ + NH_3$) is a state variable. The remaining processes can then be placed in the "kinetic" group; that is processes with slower rate constants. For reactions in this group, state variables are required for both the reactants and the products of the reaction. This approach has the advantage of removing the very "fast" rate processes and low species concentrations from the kinetic system so simulation performance is not affected. Additionally the use of the equilibrium expressions results in a smaller number

of state variables to consider since the species distributions are controlled by the equilibrium expressions.

The first step in using this approach is to select the processes that may be considered using the "equilibrium" method. In this study, these were, (1) the carbonate system, (2) the phosphate – metal (ferric or aluminium ion) system, (3) the ionization of ammonia, (4) the volatile fatty acids (acetate and propionate), and (5) dissociation of water. These species were selected since the rates at which they ionize are typically extremely rapid. Assuming that the strong acids and bases (and the calcium and magnesium not bound in precipitates) are fully dissociated and noting the electro-neutrality requirement, the set of equations describing the equilibrium state can be solved. This involves the simultaneous solution of the following equations:

1. The dissociation expressions (one equation for each ion species in each of the systems);
2. Component material balances for each system (i.e. the total species concentration is the sum of ionized and unionized species for one particular component);
3. The equation for ionic strength and the Davies equation (a simplification of the extended Debye-Hückel law) to provide an estimate of each of the activity coefficients. Activity coefficients are used to assess the impact of ionic strength on species dissociations (Loewenthal and Marais, 1976);
4. The charge balance equation (electro-neutrality requirement).

The simultaneous solution of these equations allows determination of pH, ionic strength, and individual ion species concentrations. The ion species concentrations can then be used in kinetic expressions, such as gas transfer equations and chemical precipitation reactions, while the pH can be used to calculate biological inhibition.

As described in Chapter 7, a general term for metal species (Fe^{3+} or Al^{3+}) was included in the charge balance to allow for equilibrium-based modelling of chemical phosphorus removal. Another two state variables (Other anions, Other cations) were also added to account for additional anions and cations not explicitly considered (i.e. Na^+, K^+, Cl^-, SO_4^{2-}, etc.). These variables also allow for addition of strong acids and bases to the system. In addition to usual influent characteristics (ammonia, phosphate, magnesium, etc.), pH and alkalinity are used to calculate the net amount of influent anions and CO_2. There is only one specific set of these two concentrations that satisfies the given pH and alkalinity requirement. The liquid phase saturation concentrations used in the gas transfer equations were calculated with Henry's law from the gas phase concentration of the component (Perry and Green, 1985).

6.3 Model description

The pH model is based on the following elements:

1. Equilibrium modelling of the phosphate, carbonate, ammonium, volatile fatty acid systems and typical strong ions in wastewater (Mg^{2+}, Ca^{2+}, NO_3^-, etc.).
2. Incorporation of activity coefficients based on the ionic strength of the solution.
3. Gas-liquid transfer of ammonia and carbon dioxide.
4. Biological activity affecting compounds included in the model (e.g. CO_2 and many others)

Equilibrium expressions for the acid-base systems included in the model are shown in Table 6.1. These equilibria represent the predominant acid-base systems occurring in wastewater treatment systems.

Table 6.1. Acid-base equilibrium expressions included in the general pH model

System	Equilibrium Expression	Equilibrium Constant @20°C
Water	$\left(H^+\right)\left(OH^-\right) = K_w$	6.867×10^{-15}
Carbonic acid	$\dfrac{\left(H^+\right)\left(HCO_3^-\right)}{\left(H_2CO_3^*\right)} = K_{iCO_31}$	4.14×10^{-7}
Carbonic acid	$\dfrac{\left(H^+\right)\left(CO_3^{2-}\right)}{\left(HCO_3^-\right)} = K_{iCO_32}$	4.201×10^{-11}
Acetic acid	$\dfrac{\left(H^+\right)\left(CH_3COO^-\right)}{\left(CH_3COOH\right)} = K_{iAc}$	1.754×10^{-5}
Propionic acid	$\dfrac{\left(H^+\right)\left(CH_3CH_2COO^-\right)}{\left(CH_3CH_2COOH\right)} = K_{iPr}$	1.318×10^{-5}
Phosphoric acid	$\dfrac{\left(H^+\right)\left(H_2PO_4^-\right)}{\left(H_3PO_4\right)} = K_{iPO_41}$	7.452×10^{-3}
Phosphoric acid	$\dfrac{\left(H^+\right)\left(HPO_4^{2-}\right)}{\left(H_2PO_4^-\right)} = K_{iPO_42}$	6.103×10^{-8}
Phosphoric acid	$\dfrac{\left(H^+\right)\left(PO_4^{3-}\right)}{\left(HPO_4^{2-}\right)} = K_{iPO_43}$	9.484×10^{-13}
Ammonium	$\dfrac{\left(H^+\right)\left(NH_3\right)}{\left(NH_4^+\right)} = K_{iNH_3}$	3.966×10^{-10} *

*temperature dependency used: $K_{i,NH3} = 10^{-(2835.8/T - 0.6322 + 0.00123*T)}$ where T is temperature in Kelvin (Musvoto *et al.*, 2000).

All of the equilibrium expressions in Table 6.1 are expressed in terms of active concentrations rather than molar concentrations. The interaction of ions in solution causes a deviation from ideal behaviour whereby the activity of the ions in equilibrium reactions is less than expected from the molar concentrations. To account for this behaviour, the molar concentration of the ions, $[X_i]$, is reduced by a factor known as the activity coefficient f_i. The reduced ionic concentration is called the active concentration (X_i), as determined by the following expression:

$$(X_i) = f_i [X_i] \qquad (6.1)$$

where

(X_i)	=	active concentration of X_i
$[X_i]$	=	molar concentration of ion X_i
f_i	=	activity coefficient of ion X_i

Activity coefficients are estimated in the general pH model using the Davies equation, which is a simplification of the extended Debye-Hückel law. The activity coefficient (f_i) for each ion i in solution is determined as follows (Loewenthal and Marais, 1976):

$$\log f_i = -0.5 \cdot Z_i^2 \cdot \left(\frac{\sqrt{\mu}}{1 + \sqrt{\mu}} - 0.2\mu \right) \tag{6.2}$$

where
Z_i = ionic charge of ion X_i
μ = ionic strength of solution

Note that because the deviation from ideal solution behaviour is caused by electrostatic attraction between ions, the activity coefficient of a neutral species in solution (i.e. $H_2CO_3^*$) is one (1).

The expression for ionic strength is as follows:

$$\mu = 0.5 \sum_{i=1}^{n} [X_i] Z_i^2 \tag{6.3}$$

where

n = the number of ionic species in solution

Since the overall charge of the solution must be neutral, the sum of the concentrations of the positively charged ions in solution must equal the sum of the negatively charged ion concentrations. This charge balance relationship is expressed for the pH model as follows:

$$
\begin{aligned}
&[H^+] + [NH_4^+] + 2[Mg^{2+}] + 2[Ca^{2+}] + [Cations^+] + V_{Me}[Me] \\
&= [OH^-] + [H_2PO_4^-] + 2[HPO_4^{2-}] + \\
&3[PO_4^{3-}] + [HCO_3^-] + 2[CO_3^{2-}] + \\
&[CH_3COO^-] + [CH_3CH_2COO^-] + \\
&[NO_3^-] + [Anions^-]
\end{aligned} \tag{6.4}
$$

In addition to the ionic species shown in Table 6.1, there are a number of other ions likely to occur in significant concentrations in wastewater treatment systems, and these have been included in the charge balance. Calcium (Ca^{2+}) and Magnesium (Mg^{2+}) will be present in the natural source waters. Although inclusion of chemical phosphorus removal is not necessary in all systems modelled, a general term for metal species (Me) with charge v_{Me} has been added to the charge balance to allow for chemical phosphorus removal. General variables have also been added for other cations ($Cations^+$) and other anions ($Anions^-$) to account for additional species not included separately (i.e. K^+, Na^+, SO_4^{2-}, Cl^-, etc.). These variables also allow for addition of strong acids and bases (see the examples below).

Material balances are written for each of the total species concentrations in the charge balance. For example, a material balance for total dissolved inorganic carbon in a reaction vessel is written as follows:

$$\frac{dM_{CO2t,L}}{dt} = Q_{L,i}S_{CO2t,i} - Q_{L,o}S_{CO2t,o} - (CO_{2,Stripping}) + (\text{Net Reaction}) \tag{6.5}$$

where

subscript i	=	influent
subscript o	=	effluent
$M_{CO2t,L}$	=	mass of dissolved total inorganic carbon
S_{CO2t}	=	total dissolved inorganic carbon concentration
Q_L	=	liquid flow rate
Net Reaction	=	biological reaction rate

$$CO_{2\,Stripping} = -k_{L,CO2} \cdot A_{GT} \cdot (S_{CO2,sat} - [H_2CO_3^*]) \cdot V_L \tag{6.6}$$

where

V_L	=	liquid volume
k_L	=	liquid phase mass transfer coefficient
A_{GT}	=	specific interfacial area for gas transfer
$S_{CO2\,sat}$	=	saturation concentration for dissolved CO_2
$[H_2CO_3^*]$	=	undissociated carbonic acid concentration

The "Net Production by Reaction" term accounts for biological generation (e.g. from oxidation of organics by heteretrophs) and consumption (e.g. by autotrophs). The saturation concentration (S_{CO2sat}) in the "Gas Stripping" term is calculated from a Henry's law relationship at the system temperature and pressure. A simplification of the model assumes that the gas phase concentration of the component is constant (i.e. atmospheric concentration for CO_2, in spite of its ever increasing value, and zero for ammonia), and therefore the saturation concentration of the dissolved component is constant for a given temperature. However, for many systems (e.g. anaerobic digesters), a material balance is also required for the gas phase. For the carbon dioxide component, the gas phase material balance is written as follows:

$$\frac{dM_{CO2,G}}{dt} = Q_{G,i}G_{CO2,i} - Q_{G,o}G_{CO2,o} + (CO_2 Stripping) \tag{6.7}$$

where

$M_{CO2,G}$	=	mass of CO_2 in the gas phase
Q_G	=	gas flow rate
G_{CO2}	=	gas phase carbon dioxide concentration

Similar material balances (gas and liquid phase) are required for the total ammonia concentration. For the other ionic species in solution (i.e. volatile acids, phosphate, etc.), there is no stripping and thus material balances for these components are written only for the liquid phase.

To simulate the pH response of a system, the following stepwise procedure is followed:

1. Material balances are iteratively solved to find a steady state, or used to compute the derivatives for the next time step in a dynamic simulation. This determines the total species concentrations.
2. An initial estimate of pH and ionic strength (μ) is obtained (typically from the last solution of the system state).
3. Equations (6.3) and (6.4) are solved simultaneously for a new pH and μ using an iterative non-linear equation solver, such as the Newton-Raphson method.

6.4 Model discussion

6.4.1 Alkalinity and species ionization

Figure 6.2 shows a logarithmic-concentration versus pH diagram for the carbonate system. This diagram was generated with the pH model by simulating a system with a total dissolved inorganic carbon concentration of 10 mmol/L, and successively adding an increasing amount of anions to the system to change the pH. The model determines alkalinity by noting that at the H_2CO_3* equivalence point $[H^+] = [HCO_3^-]$. This additional equation can then be used to solve the carbonate equilibrium explicitly to determine the $[HCO_3^-]$ concentration (and consequently the pH). From this the charge balance can be used to calculate the amount of strong acid that would be required to move the solution to the H_2CO_3* equivalence point. As a result, the impact of all of the ionic species included in the general pH model is considered in the calculation of alkalinity. Note that the alkalinity is not *explicitly* related to the stoichiometry of the biological processes in the system when estimated with the pH model. Instead, it is related to concentrations of ionic species at the current system state.
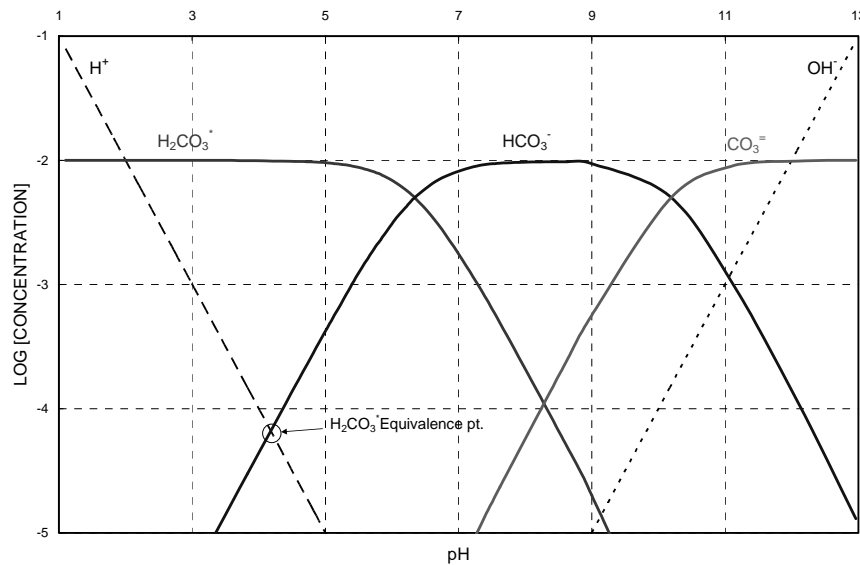
Figure 6.2. Logarithmic concentration versus pH diagram for the carbonate system as generated by the general pH model.

6.4.2 Simulation of a nitrification rate test with high pH

The pH model was tested for a domestic wastewater system by simulating a batch "High F/M" nitrification rate test (Melcer *et al.*, 2002). In the experiment, 75 mL of nitrifying mixed

liquor with a total suspended solids concentration of 2080 mg/L was added to secondary effluent for a combined total volume of 3 L. The test was spiked with ammonium chloride to achieve an initial total ammonia-N concentration of 120 mg/L. At the start of the test 1.0 g of $NaHCO_3$ was added, and 1.0 g was added three more times over the course of the test. The liquid was mixed with a magnetic stir bar and aerated continuously with an aquarium air pump and a ceramic aeration stone. Samples were extracted intermittently for analysis of NO_3-N, NO_2-N, and total ammonia-N. The pH was measured continuously throughout the test.

Similar nitrification rate tests had been conducted with intermittent aeration controlled by a dissolved oxygen controller. One of the objectives of this test was to determine the impact of continuous aeration on the response.

Figure 6.3 shows the simulated and measured nitrogen response. Two cases are shown for the simulated ammonia response. In the first case, the k_L for ammonia stripping was set equal to zero. In this case, the decrease in the ammonia concentration is due primarily to nitrification. In the second case, the k_L was set to 0.05 m/d. In this case, the simulation results closely followed the measured ammonia concentration, indicating that significant ammonia stripping was occurring during the test.

Figure 6.4 is a plot of the simulated and measured pH. The initial response indicates a rapid increase in the pH due to the stripping of dissolved carbon dioxide. The pH throughout the test is significantly higher than previous tests conducted with intermittent aeration.
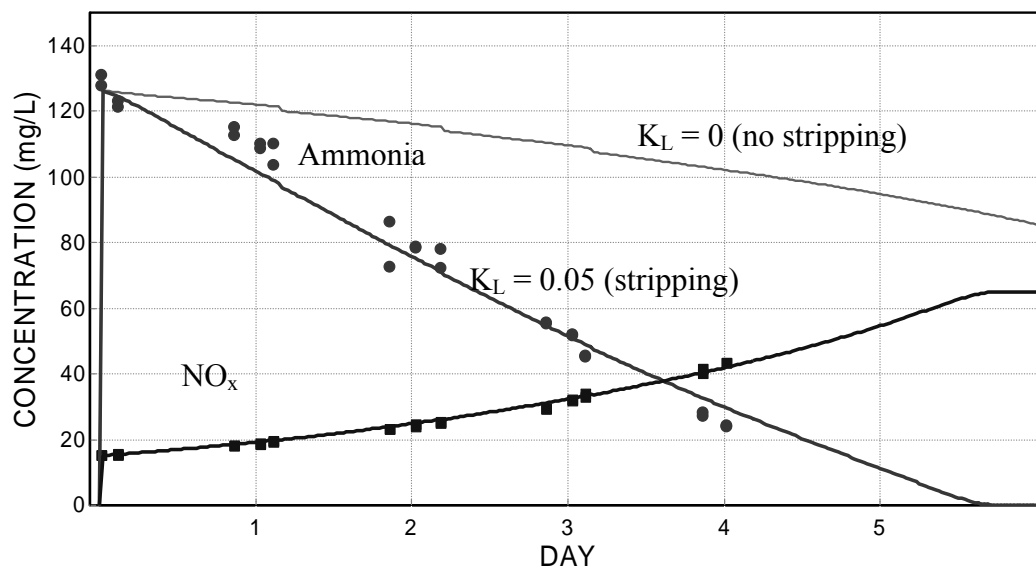
Figure 6.3. Simulated and measured nitrogen response during the batch "High F/M" nitrification rate test.

To understand the response in this experiment, it is informative to examine the logarithmic-concentration versus pH diagram for ammonia shown in Figure 6.5. The pH region of the experiment is shown on the diagram, and it is clear that a significant amount of the ammonia is in the unionized NH_3 form. Because this is the form that is stripped, the higher pH in this experiment resulted in significant ammonia stripping.

82
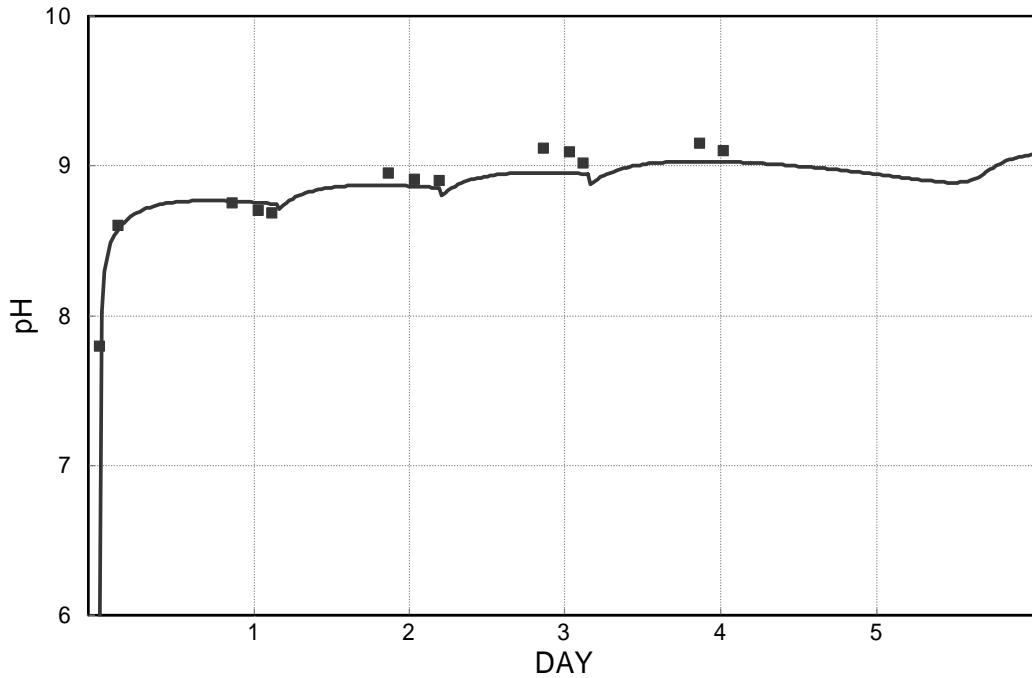
Figure 6.4. Simulated and observed pH response during the batch "High F/M" nitrification rate test.
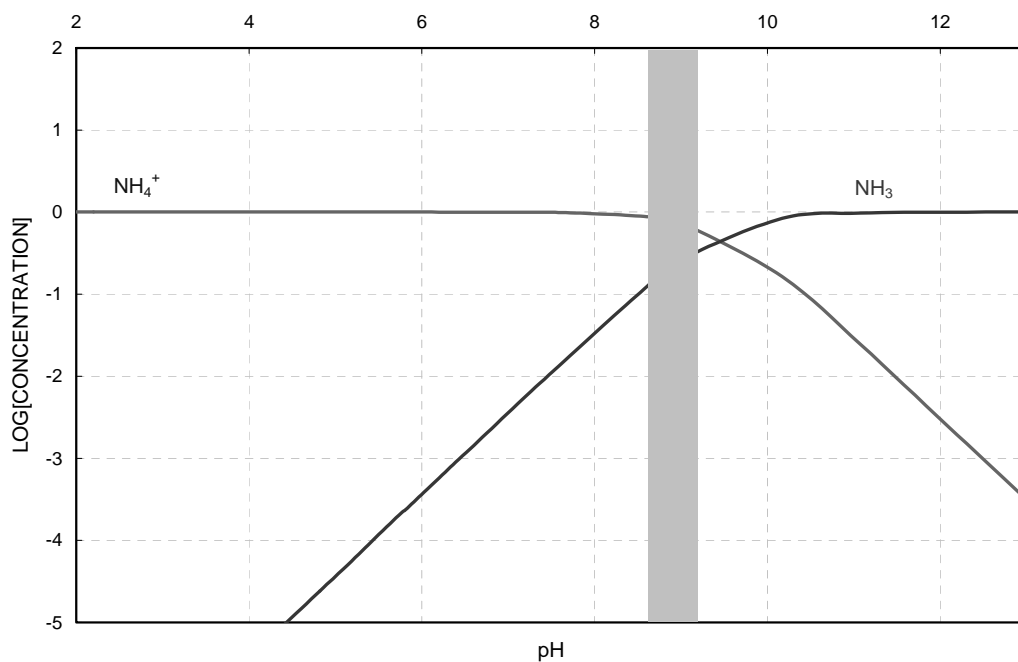
Figure 6.5. Logarithmic concentration versus pH diagram for ammonia as generated by the general pH model. The pH range during the test is shown by the shaded band.

Figure 6.6 shows the simulated alkalinity during the experiment; the saw tooth shape clearly indicates the consumption and intermittent addition of alkalinity. It should also be noted that for the duration of the experiment the alkalinity was maintained above 5 mmol/L. In considering the impact of low pH on biological activity Henze *et al.* (1987) suggest that "if total alkalinity falls below about 50 g/m^3 as calcium carbonate (CaCO$_3$) (1 mole total

alkalinity/m^3), then the pH may become unstable". For this reason many models use alkalinity as an indicator of stable pH, however, at high pH the alkalinity provides little information as to the impact that pH may have on biological activity.
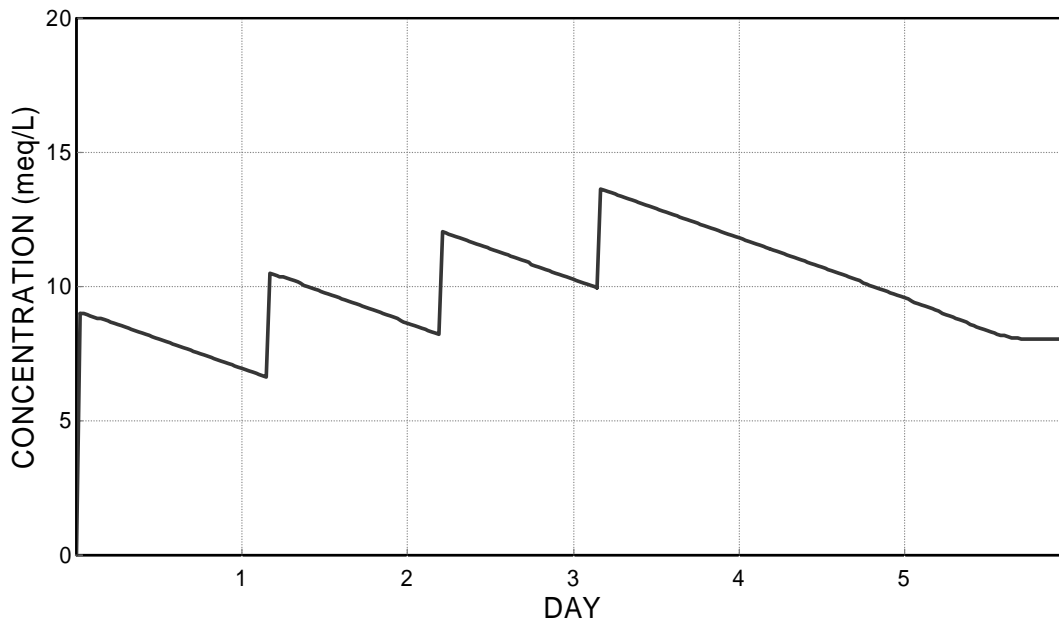
Figure 6.6. Batch test simulated alkalinity.

Figure 6.7 shows the observed nitrogen response and the simulated nitrogen response for two cases. In the first case, the experiment was simulated using a pH inhibition function both on low and high pH (Batstone *et al.*, 2002) on biological activity, while in the second case the simulation was performed without considering inhibition. It is evident that the simulation which considers pH inhibition at high pH provides a more accurate estimate of the observed experimental response. The nitrification rate used for both simulations was 0.9 1/d which was independently measured by Jones *et al.* (2003) for the same sludge.

6.4.3 High F/M experiment at circumneutral pH levels

Another experiment was conducted to measure nitrifier growth rate in an activated sludge sample from the Dundas Wastewater Treatment Plant (WWTP) in Ontario, Canada on June 4-8, 2001 (Melcer *et al.*, 2002). In the high F/M bioassay, a relatively low concentration of nitrifying mixed liquor is spiked with ammonia, and the increase in nitrite and nitrate concentration with time is monitored for a period of approximately 4 days. High F/M tests were conducted in pairs in mixed, aerated, 4 L glass beakers operated at a liquid volume of 3 L. A sample of mixed liquor to be used as a seed source was collected from the Dundas WWTP. The mixed liquor seed was diluted with secondary effluent to achieve an initial seed concentration in the test of 30 to 35 mg VSS/L. At the start of the experiment effluent, seed sludge and reagents were added to each reactor. The reagents were ammonium chloride and 1 g of sodium bicarbonate (for additional alkalinity).
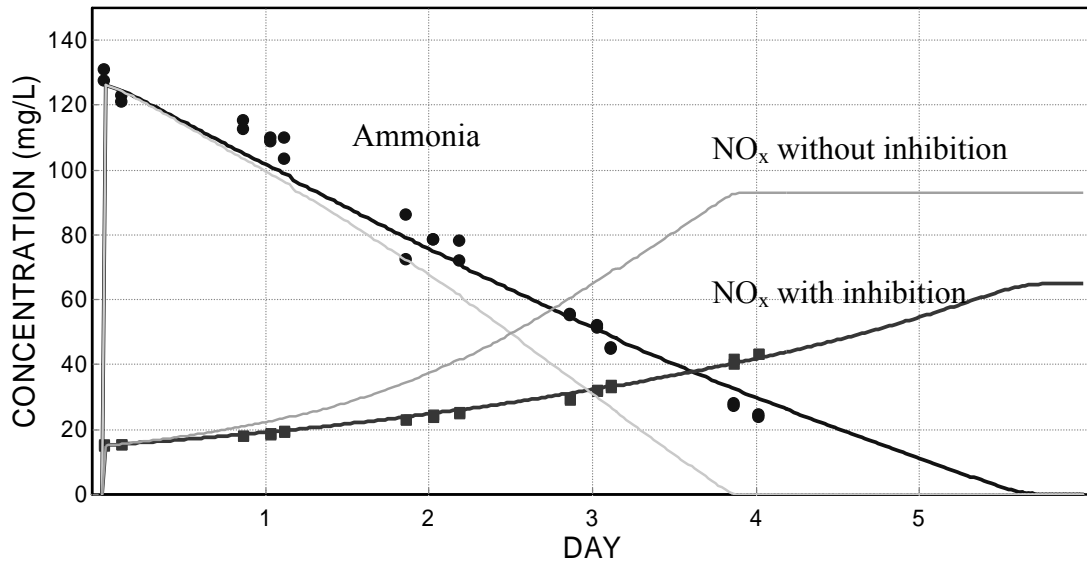
Figure 6.7. Effect of pH inhibition on predicted nitrification rate.

The amount of ammonium chloride added was calculated to achieve an initial ammonia concentration of about 120 mg N/L. The reactor was mixed for the duration of the experiment. The pH was monitored continuously throughout the experiment. Samples were extracted intermittently for analysis of NO_3-N, NO_2-N, and total ammonia-N. Additional alkalinity in the form of sodium bicarbonate was added whenever the pH dropped to approximately 7.5. Aeration in the reactor was controlled by a dissolved oxygen (DO) controller, which cycled aquarium pumps on and off to maintain the DO concentration between 4 and 6 mg/L. An example of a high F/M test result is shown in Figure 6.8. A non-linear least squares regression routine was applied to fit the equation expressing the nitrate production rate to the measured NO_x-N data. The resulting nitrifier growth rate was used for the simulations of this experiment.

Figure 6.8 shows the simulated and measured pH responses during the experiment. The four periods of sharp pH increase are due to bicarbonate dosage that was used to maintain the pH. It is apparent from the pH response that the dosed bicarbonate was consumed more quickly as the experiment progressed due to accelerating nitrification. The data points show the extremes of pH variation caused by the on-off aeration. Aeration was typically turned on for 1.0 to 1.5 minutes and caused CO_2 to be stripped, which resulted in an increase of pH during this short period of time. The on-off aeration was not modelled, since the exact aeration times were not recorded. An average DO concentration setpoint of 5 mg/L was used in the simulation, which resulted in a slowly increasing average airflow rate as the biological activity increased.

85
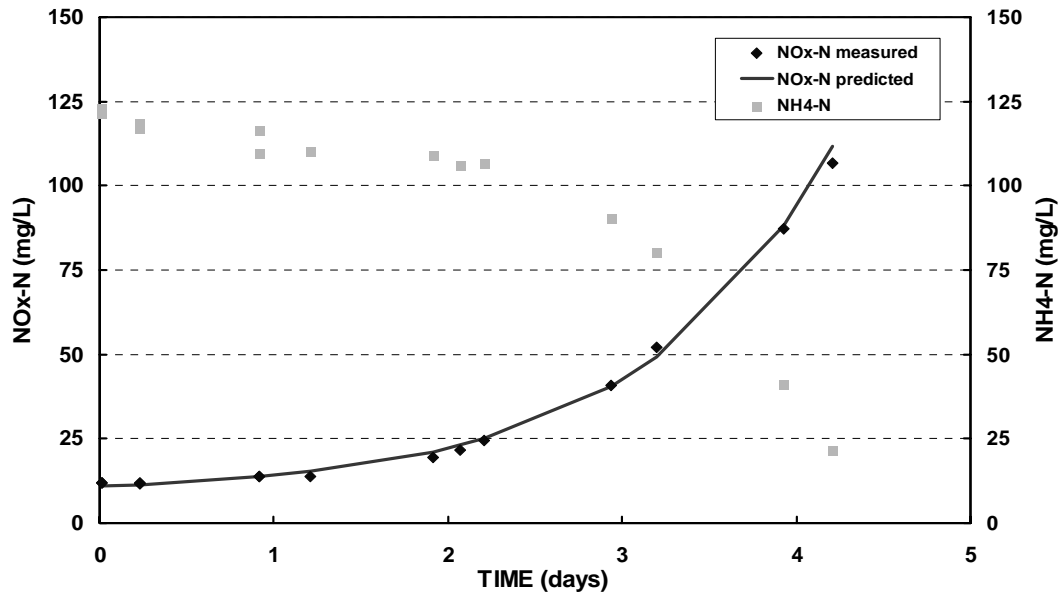
Figure 6.8. NO$_x$ and ammonia responses in High F/M test. The nitrifier growth rate is determined by fitting the nitrate production rate model (solid line) to the NO$_x$-N data.
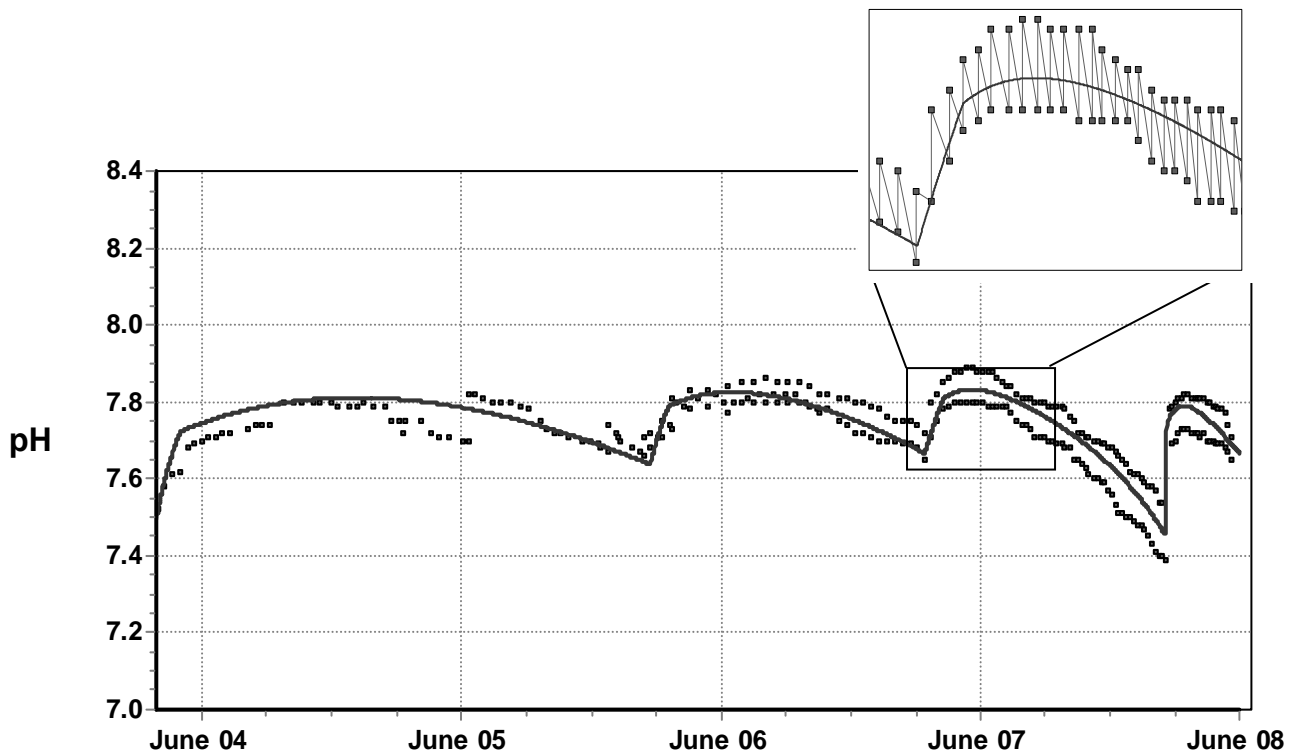
Figure 6.9. pH in a high F/M experiment (solid line - model). The insert shows pH increasing and decreasing due to intermittent aeration, and the data points represent the extremes.

The model accurately predicts the trend and the absolute value of the pH, usually within 0.1 pH units. The model provided good estimates of all other important process variables.

6.4.4 Enhanced culture bench scale BNR systems

Wentzel *et al*. (1989) operated several enhanced culture (acetate-fed) bench scale systems under steady-state conditions at a number of solids residence times (SRTs). The authors monitored the pH and measured the concentrations of PO_4^-, NH_3, NO_3^- in each of the anaerobic, anoxic and aerobic reactors during these experiments.

Four of these systems were simulated using the combined biokinetic (ASDM) – pH model (Dold *et al*., 2007). The model predicts all process variables accurately with the same parameter set. There is a good agreement between measured and simulated nutrient profiles, shown for orthophosphate in Figure 6.10. The development of a BNR model was the original aim of the experiment.
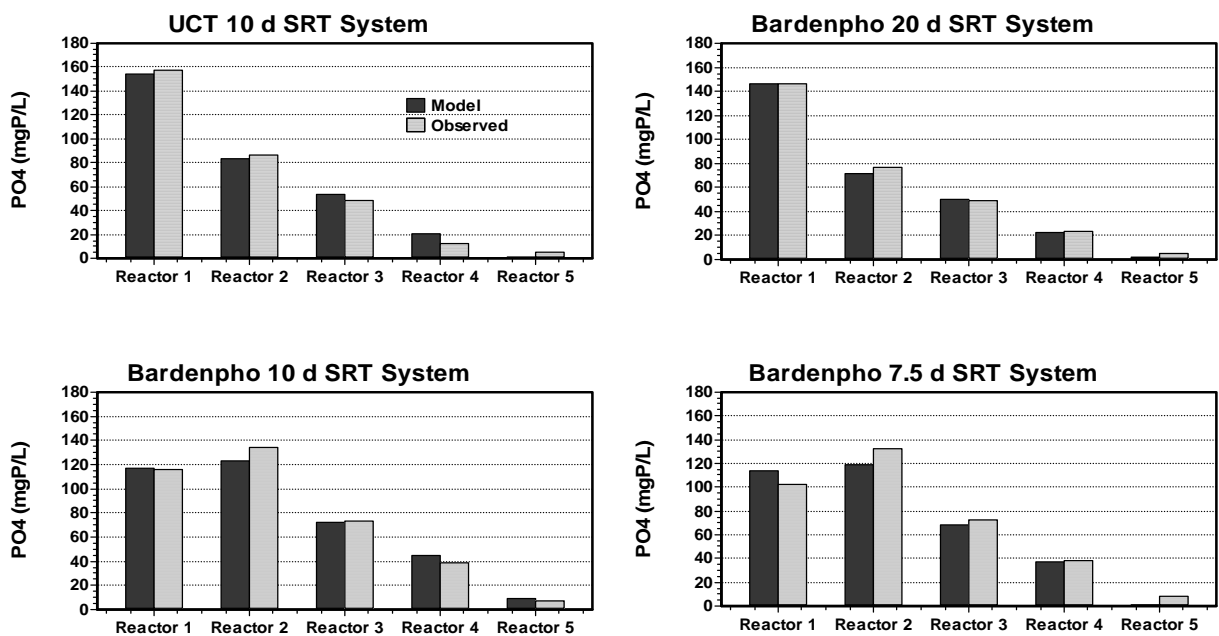
Figure 6.10. Orthophosphate profiles in bench scale BNR systems
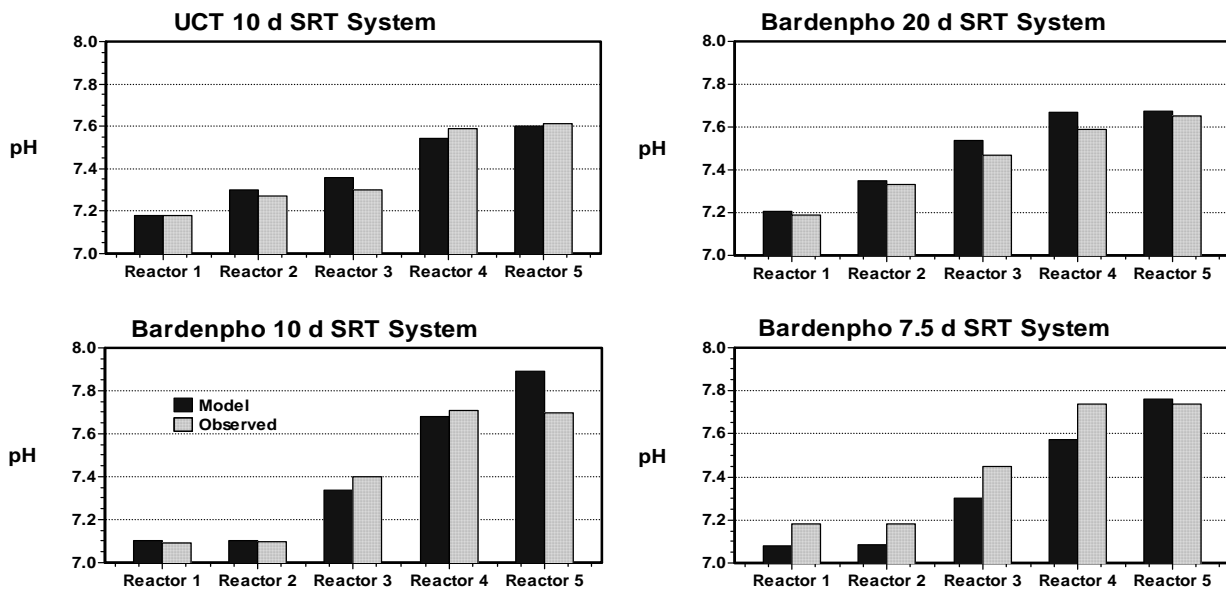
Figure 6.11. pH profiles in bench scale BNR systems

Figure 6.11 shows the simulated and measured pH profiles for the same experiments as shown in Figure 6.10. The equilibrium part of the pH model does not have parameters to calibrate, as ionization constants are known from literature. An estimation of the CO_2 mass transfer coefficient is required, using the same area for transfer as in the existing oxygen transfer model. The mass transfer coefficient used for all four systems was 10.0 m/d.

In addition to nitrification/denitrification and CO_2 transfer, pH in a BNR system is affected by the dynamic uptake and release of phosphorus and cations, such as calcium, magnesium and potassium. If these phenomena are not considered, it is not possible to model the pH accurately. This section focussed on the equilibrium chemistry element of the pH model, but the biokinetic model also requires additions and extensions to describe the processes that have an effect on ionic species.

6.5 Extension of the pH model for solutions with precipitate formation

6.5.1 General considerations

The water equilibrium system is significantly more complicated than the simplified model introduced so far suggests. There are potentially hundreds of soluble or solid species that exist even in the simplest solutions, and obtaining a numerical solution is very time consuming – i.e. not practical in conjunction with a dynamic activated sludge model that requires a new calculation of the whole system every few simulated seconds. Determining if precipitates form will further increase the complexity of the solution by orders of magnitude.

A general iterative method exists called the Tableau method (Morel and Hering, 1993) that can be used in principle for solving equilibrium systems of unlimited complexity. A simple example is demonstrated in Appendix A. Water chemistry programs (MINEQL+ etc.) use this method for finding a numerical solution based on multivariate iterative optimization. The Tableau method is very flexible and generally implementable, but too slow for practical

88

application in conjunction with an ASM-type model. The computational load is orders of magnitude higher than solving an ODE. A practical alternative is outlined below:

1. Consider all components soluble.
2. Solve the system using the principle as described in Section 6.3 for all considered components.
3. Check the supersaturation index (SSI) for each potential precipitate. If the product of the activities of ions participating in a precipitate is larger than the solubility constant, the solution is supersaturated for the specific precipitate.
4. If there is no supersaturation, the solution is found. Otherwise, go to step 5)
5. If any solids is supersaturated (SSI>solubility product)
    a. Select solution containing precipitate with highest supersaturation index as a considered component.
    b. Repeat from 2.

This method in models with realistic complexity will result in multiple, large algebraic equation systems. If there is no precipitate, there is one (1) solution. With one (1) precipitate, two (2) solutions exist (with or without the precipitate). With two (2) precipitates, four (4) solutions exist (soluble only, one or the other precipitate forming, or both precipitate forming).

Table 6.2. Important solids precipitating in wastewater:

Aerobic environment	Anaerobic environment
Struvite (typically only in digester returns)	Struvite (if the pH increases)
Calcium phosphates (e.g. HDP)	Calcium phosphates (e.g., HDP, HAP)
Calcium carbonate	Calcium carbonate
Aluminium hydroxide (after chemical dosing)	Aluminium hydroxide (after chemical dosing)
Aluminium phosphate (only at low pH)	Ferrous hydroxide (after chemical dosing)
Ferric hydroxide (after chemical dosing)	Vivianite
Ferric phosphate (only at low pH)	

For "n" precipitates, 2^n solutions must be expressed, similar to Pascal's Triangle (Pascal, 1665). Pascal's Triangle is a geometric arrangement of the binomial coefficients in a triangle. In reality some of these solutions may not be physically feasible. From chemical equilibrium tables (NIST, 2001) about 30 potential precipitates can be identified. 2^{30} large equation systems are beyond the scope of this work (and practical applicability). The selection in Table 6.2 can be supported by typical plant operational sources and examination of the solubility of all precipitates. Many other precipitates will form only at extremely high pH values. However, the number of required algebraic solution sets can be reduced by solving selected potential precipitates with a fast kinetic rate. The fast rate will reduce the step-size and increase solution time, but the resulting simplification in the size of the Pascal Triangle (and code size) will outweigh the reduction of step size. In the following sections, a practical implementation is described that mixes the numerical handling of precipitates with equilibrium and kinetic approaches. Specifically, calcium and magnesium phosphates are

implemented using kinetic expressions, and iron or aluminium hydroxides and phosphates are implemented using equilibrium expressions.

6.5.2 Conversion between anaerobic and aerobic systems

Most ionic species occur both in aerobic and anaerobic environments (K^+, NH_4^+, etc) However, some are exclusive to one or the other (typically Fe^{3+} and SO_4^{2-} in aerobic environments, and Fe^{2+} and S^{2-} in anaerobic environments, etc.).

The conversion between the corresponding species is most often biologically mediated, a kinetic reaction. In some cases (oxidation of SO_3^{2-} to SO_4^{2-}) a kinetic chemical reaction occurs. These reactions have to be handled outside the equilibrium system, in a similar way (and in conjunction with) the biological reaction matrix.

6.5.3 Modelling magnesium precipitate formation

Reactions for spontaneous precipitation of calcium phosphates (hydroxy-dicalcium-phosphate, HDP: $Ca_2HPO_4(OH)_2$, and hydroxy-apatite, HAP: $Ca_5(PO_4)_2OH$) based on Maurer *et al.* (1999), as well as struvite (magnesium-ammonium phosphate) based on Musvoto *et al.* (2000) were incorporated in the general pH model. For practical reasons these reactions are implemented using fast kinetic rates.

The ASDM model implemented in BioWin (Barker and Dold, 1997; Dold *et al.*, 2007) is based on an integrated activated sludge – anaerobic digestion model that has been extended with water chemistry, simulation of pH, and various chemical reactions. Formation of struvite usually occurs in digesters or in output streams from digesters (particularly if there is an increase in pH). Necessary requirements for the formation of struvite are the presence of magnesium, ammonium and phosphate ions at a pH favouring precipitation. These conditions may be encountered in the digestion of waste sludge from a biological phosphorus removal system. There are several steps that are required in practice in order for struvite precipitation potential to exist in wastewater treatment plants:

1. **Magnesium, ammonia and phosphorus uptake in the bio-P process:** The model predicts phosphorus uptake and storage as polyphosphate (poly-P) and release in anaerobic, anoxic and aerobic activated sludge reactors. Along with the formation of poly-P, magnesium and other charge balancing cations are stored in the biomass according to an experimentally determined stoichiometric ratio. Assimilation of nitrogen is based primarily on the N content of biomass. The biomass containing stored phosphorus and cations (including magnesium), as well as nitrogen is removed from the activated sludge process through wasting and is directed to the anaerobic digester unit.

2. **Transport to the digester:** Waste sludge with its Mg, N, P content and other components is sent to the digester.

3. **Release of magnesium, ammonia and phosphorus in the digester:** Anaerobic degradation processes are included in the anaerobic digestion model. These result in the release of phosphate, cations associated with polyphosphate (including magnesium), and organic nitrogen which is converted to ammonia.

4. **Weak acid-base system in the digester:** The equilibrium based pH model accounts for the various species in the digester (phosphates, carbonates, ammonia, nitrate,

acetate, propionate, calcium, magnesium and other strong acids and bases), as well as gas transfer for CO_2 and ammonia. This results in pH and pH change calculations in the digester (and other parts of the plant).

5. **Struvite formation:** Struvite precipitation is described according to the solubility equation (implemented in a kinetic expression for numerical reasons), extended from Musvoto *et al.* (2000). This process is sensitive to pH because this impacts the ammonia and phosphate speciation. The reaction is expressed as:

$$NH_3 + H_3PO_4 + Mg(OH)_2 + 4\,H_2O \leftrightarrow MgNH_4PO_4 \cdot 6H_2O$$
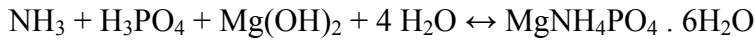
The equilibrium solubility equation is as follows:

$$[Mg^{2+}][NH_4^+][PO_4^{3-}] = Ksp_{Str}$$

where Ksp_{Str} is the struvite solubility constant

In kinetic expression:

$$r_{STR} = k_{STR}((f_2*[Mg^{2+}])^{1/3}*(f_1*[NH^{4+}])^{1/3}*(f_3*[PO_4^{-3}])^{1/3} - Ksp_{Str}^{1/3})^3$$

where k_{STR} is the rate of struvite precipitation/dissolution

Given sufficient residence time and fast enough rate (Musvoto *et al.*, 2000) the result of the equilibrium and kinetic methods will be identical.

6.5.4 Struvite formation potential

The formation of struvite precipitate depends on the available concentration of its constituents (magnesium ,ammonia, phosphate) and pH.

Struvite (mgTSS/L)
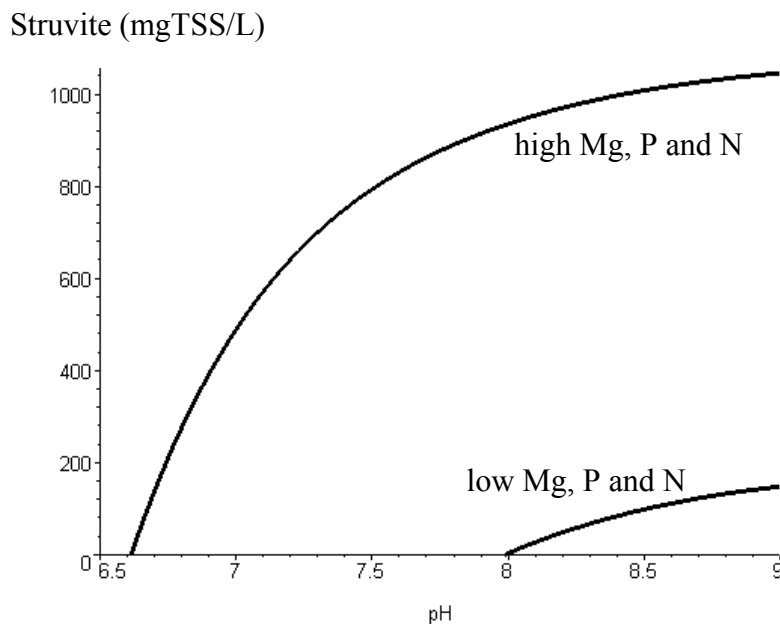
Figure 6.12. Struvite formation as a function of pH

91

If high ammonia, phosphate and magnesium concentrations are present, struvite can form even below pH 7. For example, one of the solutions shown in Figure 6.12 had 130 mg N/L ammonia, 140 mg P/L ortho-phosphate, and 110 mg/L magnesium. Under these conditions struvite starts to form at pH 6.6.

On the other hand, if one of the ions is present at low concentration, a substantially higher pH is required to induce precipitation of struvite. The other example shown in Figure 6.12 contains 30 mg N/L ammonia, 50 mg P/L ortho-phosphate, and 20 mg/L magnesium. Struvite only starts to form if the pH is raised above pH 8.0.

6.5.6. Simulation of swine wastewater aeration

The pH model was tested for a piggery wastewater by simulating a batch aeration test. Suzuki *et al.* (2002) investigated the precipitation of calcium, magnesium and phosphate in swine wastewater through aeration. A batch of 30L of screened piggery wastewater was continuously aerated for three hours. Measurements of the system pH, inorganic carbon concentration and the concentrations of soluble magnesium, calcium and PO_4-P were taken over the course of the experiment. The experiment was designed to determine whether significant precipitation could be achieved without the addition of chemicals to raise the pH.

Figure 6.13 shows the simulated and observed pH and inorganic carbon concentrations for the batch experiment. Inorganic carbon (IC) is defined as follows:

$$IC = \left[H_2CO_3^*\right] + \left[HCO_3^-\right] + \left[CO_3^{2-}\right]$$

The stripping of carbon dioxide and the effect of this on pH is accurately predicted by the combination of the gas transfer model and the pH model. The stripping of CO_2 will also be ineffective to raise the pH much above 9.0 as the carbonate equilibrium shifts almost completely towards the ionized forms (see Figure 6.13).
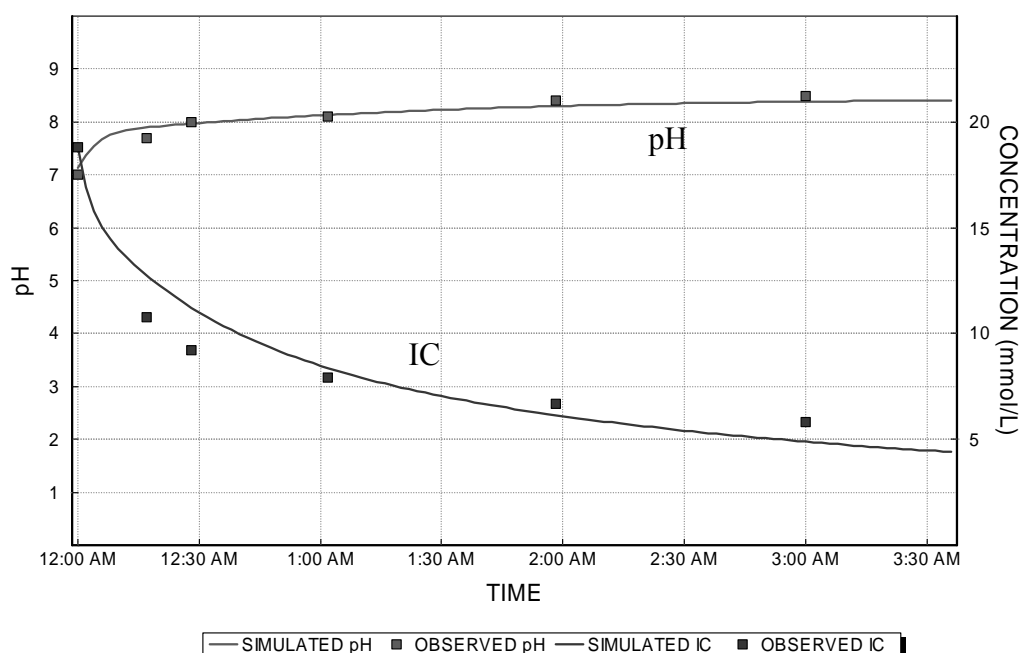
Figure 6.13. Response of inorganic carbon and pH during aeration of piggery waste.

Figure 6.14 shows the observed and simulated responses of the concentrations of soluble calcium, magnesium and PO₄-P during the aeration experiment. The simulated responses for magnesium and calcium accurately reflect the observed responses over the entire course of the experiment. The simulated response of calcium lags the observed response over the first hour and a half of the experiment, but provides reasonable estimates for the rest of the experiment. These results are presented to illustrate the importance of accurate determination of the pH and ionized species concentrations on simulation of precipitation behaviour.
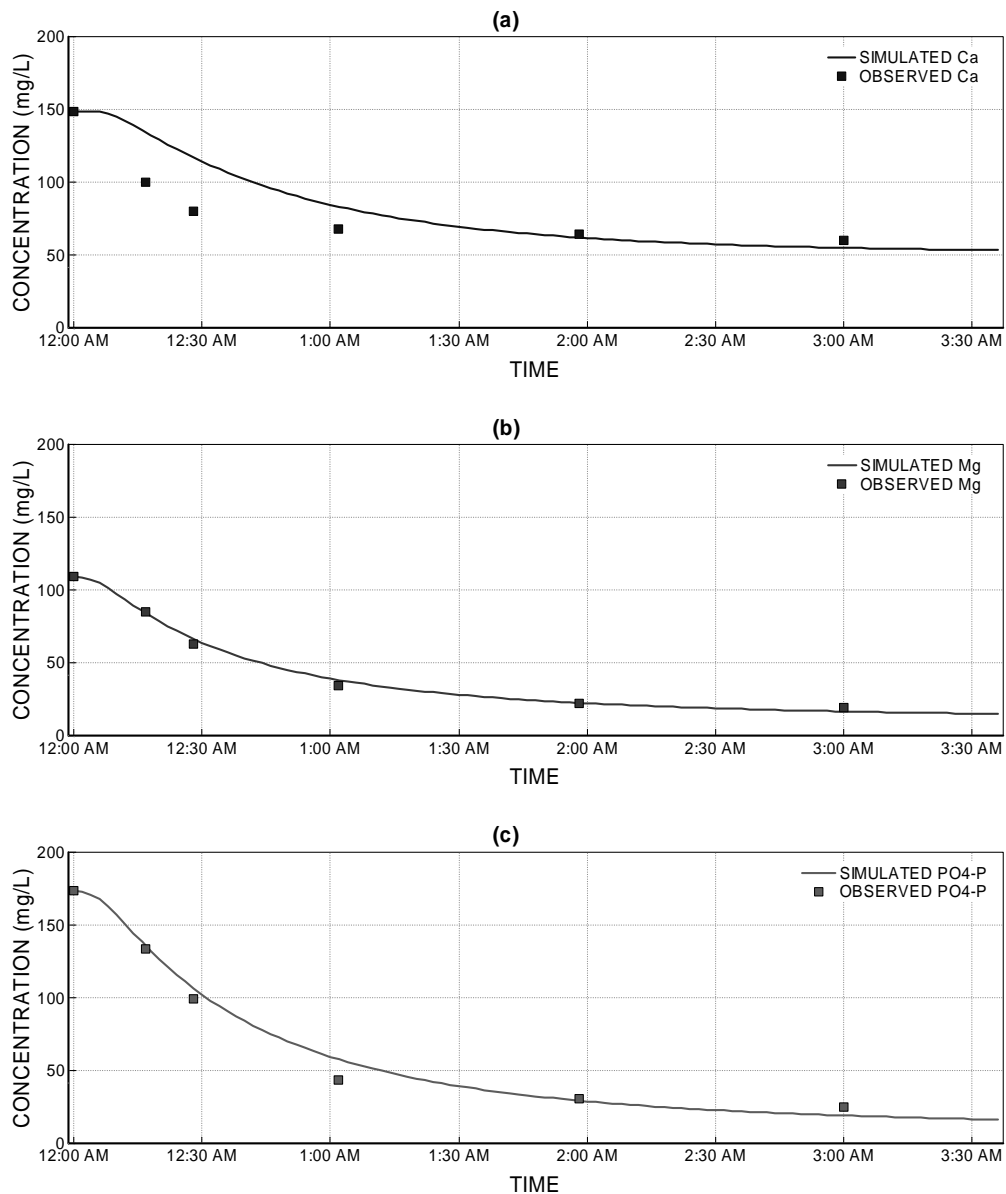
Figure 6.14. Observed and simulated soluble concentration responses during batch aeration of piggery waste for (a) calcium, (b) magnesium and (c) PO₄-P

6.6 Conclusions

A robust pH model is essential for reliable simulation of many important wastewater treatment operations. All the required information is available today to implement a general pH model that uses true chemical constants which do not require calibration at the plant.

Some developments made possible as a result of the ability to model pH are:

93

1. Gas phase modelling which is important for modelling anaerobic digestion and precipitation processes. Calculation of gas transfer rates requires knowledge of the ionization states of certain species (CO_2, NH_3) and consequently the pH of the system.
2. Inhibition of biological activity at low and high pH.
3. pH-dependent modelling of aluminium and ferric dosing for phosphorus precipitation, including hydroxide sludge formation, integrated into the biological model matrix.
4. pH-dependent modelling of the spontaneous precipitation of struvite and calcium phosphates, integrated into the biological model matrix. Accurate prediction of struvite precipitation also requires modelling of magnesium concentrations, both the soluble magnesium and that stored in organisms.

7 MODELLING IRON AND ALUMINIUM PRECIPITATION BASED ON EQUILIBRIUM CHEMISTRY[6]

7.1 Introduction

In many jurisdictions, especially in North America, total phosphorus limits in the effluent are extremely low – sometimes lower than our detection limit just a few years ago. To achieve phosphorus removal, particularly to very low levels, chemical, such as ferric (Fe^{3+}), ferrous (Fe^{2+}) or aluminium (Al^{3+}) salt dosing (and to a lesser extent, lime, i.e calcium, Ca^{2+}) is a widely used technology around the world. These cations readily form insoluble phosphate precipitates in a certain pH range. The technology is easy to control and can produce very low soluble phosphate residuals consistently. It can be used on its own, in side-stream treatment or to supplement biological phosphorus removal. In spite of the widespread use of chemical phosphorus removal, its mechanism is poorly understood. The mechanism in the complex organic environment of wastewater could be a combination of precipitation, co-precipitation, redissolution, adsorption and coagulation/flocculation processes. The required dose to achieve a certain residual concentration depends on many variables, such as phosphorus to be removed, type of metal salt, pH, alkalinity, mixing, dosage point, the presence or absence of colloidal materials, colloid stabilizing agents as well as many other factors. In this chapter a review, calibration and critique is provided for an equilibrium-based chemical phosphorus removal model, combined into the weak acid-base system of the wastewater as described in Chapter 6.

7.2 Extended chemical precipitation model

In engineering practice the required chemical dose at wastewater treatment plants is often calculated based on a simple flow proportional model. A chemical equilibrium based model (WEF, 1998; Jenkins and Hermanowicz, 1991) is available that introduces the amount of orthophosphate (OP) to be removed and pH sensitivity. The model is presented for both ferric and aluminium ions, but in this chapter only ferric will be considered. This model is able to predict the resulting OP residuals as a function of pH and dose. It includes the following chemical species:

1. ferric ion, in solution;
2. ferric phosphate – hydroxide complex as $Fe_{1.6}H_2PO_4(OH)_{3.8}$, a solid;
3. ferric hydroxide – $Fe(OH)_3$, a solid;
4. ferric phosphate complex, $FeH_2PO_4^{2+}$, a soluble component.

The ferric phosphate precipitate in this model has a fixed Fe/P molar ratio and was designed to force the experimentally observed Fe/P molar ratio (1.6 molFe/molP) at low iron doses. This precipitate will form under low dosing conditions (below 1.6 molFe/molP). At higher dosing conditions excess ferric is bound up in ferric hydroxide. The solubilities of these components are determined so as to match experimentally measured minimum OP concentrations. The model predicts a minimum of 35 µgP/L OP residual at the optimum pH 6.95. The reactions and parameter values of the WEF model are shown in Table 7.1.

The WEF chemical phosphorus removal model as described above (WEF, 1998) was combined with a general equilibrium based pH model to be able to determine the ionic composition of the solution. This allows the calculation of pH instead of using it as an input parameter, as well as determining the effect of chemical dosing on pH. The pH model includes weak acid/base dissociation reactions for water, phosphate, carbonate, ammonia and short chain fatty acids, as well as CO_2 gas transfer (Chapter 6). These species were selected since they are commonly found in wastewater and the rates at which they ionize are typically extremely rapid. The complete list of ionic species and dissociation constants is provided in Chapter 6. Temperature correction to the dissociation constants was also applied. Assuming that the strong acids and bases (and the calcium and magnesium not bound in precipitates) are fully dissociated and noting the electro-neutrality requirement, the set of equations describing the equilibrium state can be solved. This involves the simultaneous solution of the following equations:

1) The dissociation expressions (one equation for each ion species in each of the systems);
2) The solubility expressions (one equation for each solid present);
3) Material balances for each component (i.e. total species concentration is the sum of ionized and unionized species for one particular component);
4) The equation for ionic strength and the Davies equation (a simplification of the extended Debye-Hückel law) to provide an estimate of each of the activity coefficients. Activity coefficients are used to asses the impact of ionic strength on species dissociations (Loewenthal and Marais, 1976);
5) The charge balance equation (electro-neutrality requirement).

Table 7.1. Species and constants in the WEF chemical phosphorus precipitation model

Component	Reaction	Dissociation or solubility constant log(K)
Ferric phosphate	$\left(Fe^{3+}\right)^{1.6}\left(H_2PO_4^{2-}\right)\left(OH^-\right)^{3.8} = K_{sp,FeP}$	-67.1
Ferric hydroxide	$(Fe^{3+})(OH^-)^3 = K_{sp,FeOH3}$	-0.5
Soluble ferric phosphate complex	$\dfrac{\left(Fe^{3+}\right)\left(H_2PO_4^-\right)}{\left(FeH_2PO_4^{2+}\right)} = K_{iFeH2PO4}$	-21.3

The WEF model combined with pH calculations ("enhanced WEF model") was implemented with the General ASDM biokinetic model in BioWin (Barker and Dold, 1997; Dold *et al*, 2007) and used at a large treatment plant in Washington D.C.

7.3 Model calibration at the Blue Plains plant

The Blue Plains (District of Columbia Water And Sewer Authority, DCWASA) wastewater treatment plant in Washington, D.C. is the largest advanced treatment plant in the world. The plant treats an average daily influent flow of 1400 ML/d from the Washington area, and discharges through the Potomac river to the sensitive Chesapeake Bay. Yearly average effluent concentrations are 0.5 mgN/L ammonia, 4.5 mgN/L nitrate and 0.1 mgP/L (100 μgP/L) total phosphorus or lower. The plant employs a two-stage technology. A schematic plant configuration is shown in Figure 7.1.
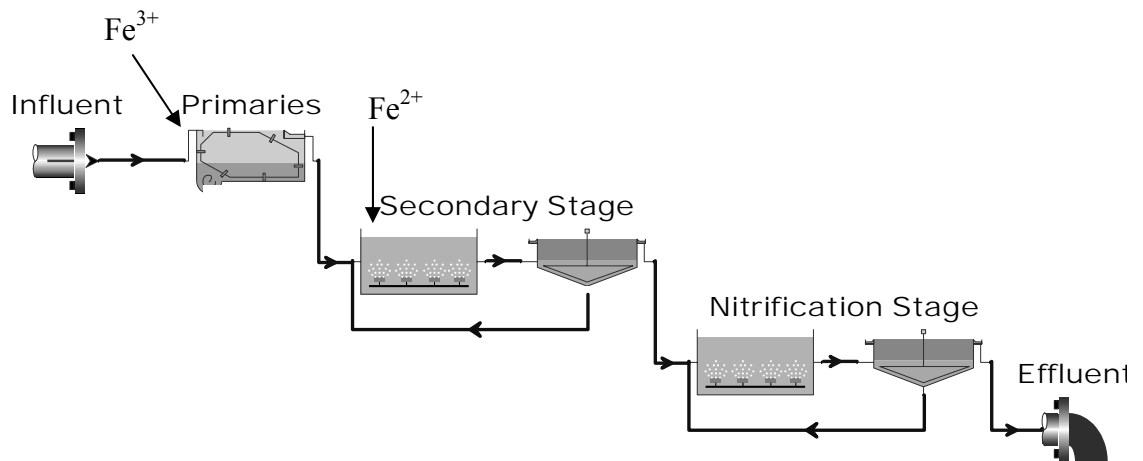
Figure 7.1. Schematic representation of the Blue Plains (Washington D.C.) plant

The first stage (called secondary stage, 2.5 days SRT) is for BOD removal. The second stage (15 days SRT) performs nitrification and denitrification using methanol. Chemical addition for phosphorus removal is at two points. Ferric is dosed to the primaries, and ferrous (pickle liquor) to the first stage. Ferrous ions are assumed to be oxidized to ferric in the aerated activated sludge environment. Typical pH values at the plant range from 6.6 to 6.9.
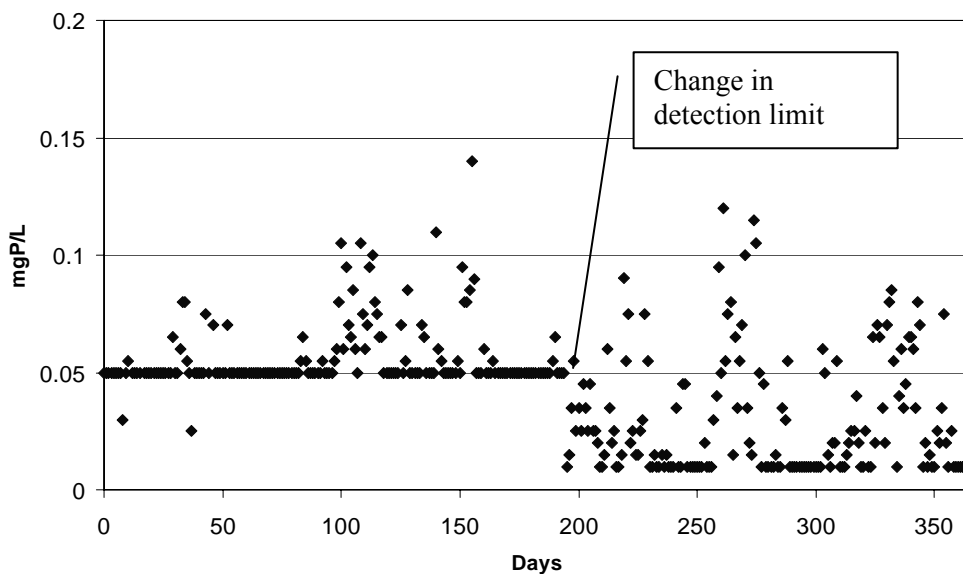
Figure 7.2. Soluble phosphorus measurements at the Blue Plains plant in 2002

Analysis of several years' worth of data from the Blue Plains plant showed that the plant can frequently achieve 10 µgP/L OP concentration (and possibly lower) over a wide pH range. OP (measured at the plant as total soluble phosphorus, TSP) detection limits at the plant were changed in mid 2002 from 50µgP/L to 10µgP/L. The effect of this change is shown in Figure 7.2. About one third of the measurements still fall below the new lower detection limit.

A similar data set was arranged and plotted as a function of pH (Figure 7.3). The lowest concentration in each pH category is shown by a larger symbol. The plant rarely encounters pH conditions lower than pH 6.0 or higher than pH 7.0. In this pH range OP concentrations can frequently reach the detection limit of 10 µgP/L, almost independently of pH. The enhanced WEF model was recalibrated to match these results (using an objective function of sum of squares). Only the ferric phosphate and ferric hydroxide solubility constants were changed. The residual OP concentrations using the original and new solubility constants are plotted against experimental data in Figure 7.4. The new model calibration provides less than 10 µgP/L OP concentration in the pH range of 6.2 to 7. The actual minimum OP concentration at pH 6.5 is 7 µgP/L.
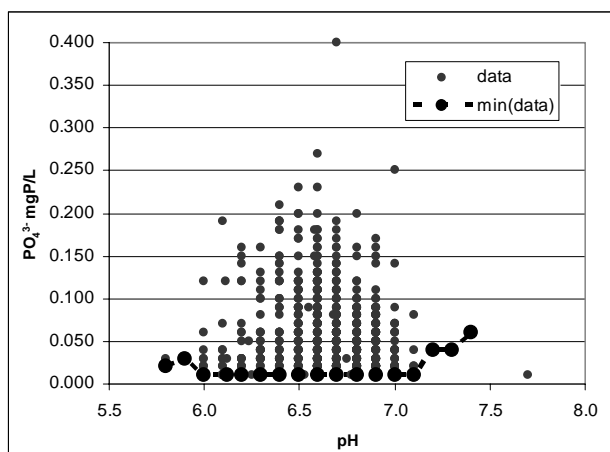
Fig. 7.3. OP concentrations, Blue Plains
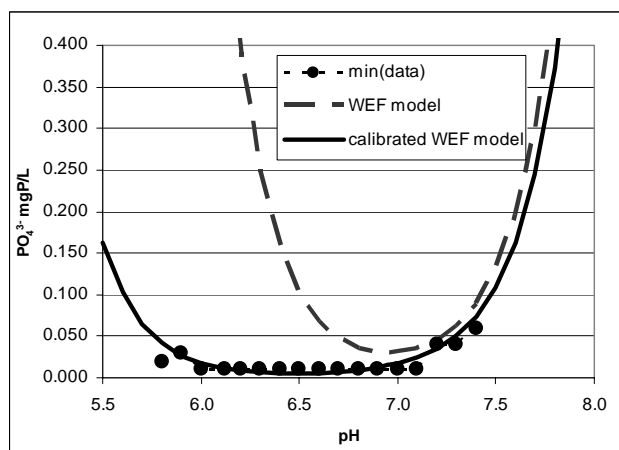
Fig. 7.4. OP concentrations in the model

The constants used in the model and important model results are summarized in Table 7.2.

Table 7.2. Summary of the constants and results from the enhanced WEF model

	WEF model defaults	Calibration
Model parameters		
log K_{sp} Fe$_{1.6}$H$_2$PO$_4$(OH)$_{3.8}$	-67.1	-70.9
log K_{sp} Fe(OH)$_3$	-0.5	-1.3
log K_i FeH$_2$PO$_4^{2+}$	-21.3	-21.3
Fe/P mole ratio	1.6	1.6
Model predictions		
Optimum pH range	6.8-7.1	6.0-7.2
Min. attainable OP [µgP/L]	**35**	**7**

The Fe/P molar ratio of 1.6 from the original WEF model was not changed for this calibration, since equilibrium concentrations apply as soon as an overdose of ferric is present.

Table 7.3 shows actual iron doses and phosphorus removed at various stages in the Blue Plains plant in 2002. The chemically removed P is estimated including the effect of particulate P hydrolysis and biological phosphorus uptake for synthesis. During model calibration to full scale data, the best "Fe added / P removed" molar ratio at the Blue Plains plant was 3.5 molFe/molP.

Table 7.3. Iron dose and phosphorus removed, Blue Plains, 2002.

Process	Fe dose	P removed	Molar ratio
	kg/d	kg/d	molFe/molP
Primaries	4190	572	4.1
Secondaries	4550	988.9	2.6

Significant variation in this molar ratio is expected from plant to plant. Since this molar ratio is incorporated into the composition of the ferric phosphate precipitate forming, upon its change it is necessary to provide a new solubility constant (Table 7.4). This ensures that the equilibrium OP concentrations are equivalent irrespective of the Fe/P molar ratio selected.

Table 7.4. Effect of Fe/P molar ratio on constants of the enhanced WEF model

	Calibration #1*	Calibration #2*
Model constants		
log K_{sp} $Fe_{1.6}H_2PO_4(OH)_{3.8}$	-70.9	**-154.8**
log K_{sp} $Fe(OH)_3$	-1.3	-1.3
log K_i $FeH_2PO_4^{2+}$	-21.3	-21.3
Fe/P mole ratio	**1.6**	**3.5**
Model predictions		
Optimum pH range	6.0-7.2	6.0-7.2
Min. attainable OP [μgP/L]	7	7

*There is no difference between the equilibrium concentrations provided by Calibration #1 and #2.

Full scale OP measurements for the year 2002 and model results using a complete plant model for Blue Plains are shown in Table 7.5. The model incorporates all unit processes on the plant including the activated sludge and sludge line, pH calculations and chemical precipitation. Automatic compensation of the ferric phosphate solubility constant for changes in Fe/P molar ratios is used to ensure that equilibrium OP concentrations are always at the determined values.

Table 7.5. Measured and simulated orthophosphate concentrations at Blue Plains.

Location	OP measured	OP simulated
	mgP/L	mgP/L
Influent	1.38	1.39
Primary Effluent	0.90	0.85
Secondary Effluent	0.04*	0.01
Nitrification Effluent	0.05**	0.01

* data measured partially with 0.05 and partially with 0.01 mgP/L as detection limit
**data measured with 0.05 mgP/L as detection limit

7.4 Towards a mechanistic chemical phosphorus removal model

The enhanced WEF model can predict residual OP concentration (depending on pH) and chemical sludge production in activated sludge systems, but it contains elements, such as the ferric hydroxo-phosphate complex and solubility and dissociation constants, that are empirically calibrated. Measured solubility and dissociation constants for the actual components existing in pure aqueous systems are available in the literature. The National Institute of Standards and Technology database (NIST, 2001) contains actual solubility constants for ferric phosphate ($FePO_4.2H_2O$) and ferric hydroxide, $Fe(OH)_3$, as well as the dissociation constant for the soluble $FeH_2PO_4^{2+}$ complex. However there are a number of other hydroxo and phosphate complexes with measured dissociation constants, such as $FeOOH$, $FeOH^{2+}$, $Fe(OH)_2^+$, $Fe(OH)_4^-$, $Fe_2(OH)_2$, $Fe_3(OH)_4$, $FeHPO_4^+$), that should be considered as well.

The solution of a model containing all these components showed a much wider optimal pH range for low OP concentrations (pH 3 to 7), and a minimum achievable OP concentration of 3.2 µgP/L (Table 7.6).

Table 7.6. Comparison of empirical and measured solubility/dissociation constants as well as model predictions.

	Calibrated WEF model	NIST database
Model constants		
log K_{sp} for ferric phosphate	-70.9	-26.4*
log K_{sp} Fe(OH)$_3$	-1.3	-38.6
log K_i FeH$_2$PO$_4^{2+}$	-21.3	3.47
Fe/P mole ratio	1.6	N/A**
Model predictions		
Optimum pH range	6.0-7.2	3-7
Min. attainable OP [µgP/L]	7	3.2

*for $FePO_4.2H_2O$
**ratio not available in NIST database

100

Additional naturally occurring cations (Mg^{2+} and Ca^{2+}) and organic acid complexes present in wastewater should also be considered in a more complete description of phosphorus precipitation reactions. In addition to these chemical precipitation reactions, adsorption of OP ions on ferric hydroxide and formation of hydroxo-phosphate complexes play a role in determining the equilibrium OP concentrations that can be achieved in plants depending on pH. Coagulation, a pH dependent process, and changes in particle size distribution of the precipitates and various complexes have an important impact on what is considered "soluble orthophosphate" in the laboratory measurements.

7.5 Conclusions and perspectives

An empirical chemical equilibrium-based model, the "enhanced WEF model" (based on WEF, 1998), was used successfully to simulate residual ortho-phosphate concentrations and required ferric doses at the Blue Plains plant in Washington D.C. The model predicts the pH change due to the chemical dose and the amount of chemical sludge generated in the system. Measurement of the ferric dose to phosphorus removed molar ratio (molFe/molP) is required in an experimental setup or based on available full-scale data for accurate use of the model.

Current chemical equilibrium-based models describe only partially the complex processes that occur during chemical phosphorus removal in wastewater. Using actual chemical species, and considering other kinetic processes in addition to precipitation, such as sorption and coagulation, is required for a more thorough understanding of the fundamental mechanisms of chemical phosphorus removal. A better understanding of the mechanisms will lead to more consistent effluent P levels at reduced dosage rates, reduced chemical sludge production and consequently substantial savings in chemical and sludge treatment costs.

Chapter 8 describes the experimental program which was started to address the simplifications in the WEF model and the results obtained.

8 CHEMICAL PHOSPHORUS REMOVAL: PROCESSES, MODELLING AND DESIGN[7]

8.1 Introduction

Chemical phosphorus removal using metal salts is an important technology for achieving very low residual phosphorus concentrations in wastewater treatment plant effluents. In spite of its widespread use, the actual complex mechanism, likely consisting of iron and phosphate complexation through an oxygen atom, precipitation of hydroxides, co-precipitation of phosphate, chemisorption/adsorption, diffusion, coagulation and flocculation processes, has not been studied sufficiently. In practice this usually leads to high ("safe") doses and consequently unnecessarily high chemical costs and sludge production.

It is well known that, in chemical phosphorus removal, solids that contain variable ratios of metals and phosphate are formed (WEF, 1998). Measured residual phosphate concentrations both in plants (see Chapter 7) and in experiments shown in this chapter are highly variable. Therefore pure component, chemical equilibrium-based models which predict fixed equilibrium residual P concentration are not suitable to calculate chemical sludge formation and residual P concentration. Equilibrium models also assume ideal mixing and instant reactions. The effect of mixing on P removal was documented by Sagberg *et al.* (2006). In order to develop a comprehensive model that is able to describe these complex processes, an extensive measurement program was carried out as the first step.

The objective of the research project initiated by the Washington D.C. Water and Sewer Authority was to (1) determine the most important design and operating factors influencing P removal; (2) investigate the potential chemical, physico-chemical and physical mechanisms and their consequences on engineering design and operation of these systems.

A large number of laboratory batch and a series of continuous flow tests were used to establish the effect and role of initial and residual P, metal dose, pH, alkalinity, COD and solids concentration, kinetics, mixing, time, chemical solids formation, and the mechanism of chemical P removal. Experimental results and conclusions are presented in the first part of this chapter.

---

[7] Based on Szabó A, Takács, I., Murthy, S., Daigger, G., Licskó, I., Smith, S. (2008) The significance of design and operational variables in chemical phosphorus removal. Water Environment Research (accepted for publication) and Smith, S., Takács, I., Murthy, S., Daigger, G. and Szabó, A. (2008) Phosphate Complexation Model and its Implications for Chemical Phosphorus Removal. Water Environment Research (accepted for publication).

In the second part of the chapter, some of these variables (dose, pH and floc age) are investigated in more detail in order to develop a conceptual model for phosphate removal. The developed model is based on phosphate complexation: active oxygen sites bonding iron and phosphorus atoms according to chemical equilibrium principles. It was found that a phosphate complexation model predicts phosphate removal in the simple H^+-PO_4^{3-}-Fe^{3+} system. Conceptually, the model involves precipitation of hydrous ferric oxides (HFO), which can be simultaneous with complexation of phosphate species; this results in phosphate being occluded into the HFO floc. By varying the single model parameter proportional to reactive site density (referred to as the Active Site Factor (ASF)), the same chemical equilibrium framework can be used to describe phosphate removal by preformed HFO flocs. This highlights the importance of reactive site availability in predicting phosphate removal. Changes in particle characteristics with aging of HFO are demonstrated using electron microscopy and dye adsorption experiments, and implications of the proposed removal mechanism for wastewater treatment are highlighted.

8.2 Materials and methods

Environmental and operational conditions influencing P removal processes were investigated by using several different methodologies in laboratory experiments.

8.2.1 Jar tests

Coagulation-flocculation jar tests were carried out with model and real wastewater. More than 1500 model wastewater samples and 600 real wastewater samples were analyzed. Model wastewater contained a phosphate solution prepared from tap water and KH_2PO_4; raw wastewater was collected from municipal wastewater treatment plants in Hungary. All experiments were performed in 1-litre glass cylinders with a Kemira flocculator device (KEMIRA, 1990). In the first set of tests (examining the effects of dose, pH, initial P concentration, alkalinity, and organics), coagulant was added to a 1 L sample during intensive stirring (350 rpm, G = 425 1/s). The intensity of mixing is characterized in this work using the mean velocity gradient, "G" (Grady *et al.*, 2007). A calibrated relationship between the propeller speed and G provided by the manufacturer of the flocculator device was used to calculate the G values reported. After initial rapid mixing, the flocs were allowed to grow for at least 10 minutes while the sample was gently mixed (20 rpm; G = 6 1/s). In the case of raw wastewater, samples were settled for 20 minutes. pH was set before each experiment, but it was not readjusted during or after coagulation. Model systems (P solutions) were buffered by the natural alkalinity of tap water or by addition of $NaHCO_3$. Most of the wastewater experiments were carried out at original pH without pH control. Samples were taken at different times and were filtered immediately through a membrane filter with 0.45 μm nominal pore size. Phosphate was analyzed according to the ascorbic acid photometric method, with a detection limit of 10 μgP/L.

Coagulant types used in the experiments were: ferric-chloride, ferric-sulphate, aluminium-sulphate and pre-polymerized aluminium-chloride.

8.2.2 Investigating kinetics

Laboratory experiments to optimize chemical P removal from wastewaters are typically performed with fast mixing (G = 300 - 1000 1/s), providing optimal removal efficiency in short term experiments. In wastewater treatment plants, mixing at the dosage point is usually

poor (G = 20 - 100 1/s), and flocculation is hindered by insufficient flocculation time as well as several processes that disrupt floc formation, including pumping, aeration, phase separation etc. To gain a better understanding of P removal kinetics, the effect of mixing intensity (as measured by the mean velocity gradient, G) and floc aging in the process of chemical dosing were investigated in laboratory experiments.

In certain experiments the P removal capacity of ferric hydroxide flocs was investigated (similarly to earlier experiments, Licskó, 1976). Ferric hydroxide flocs were pre-formed in the absence of phosphate ions. This simulates the effect of dosage on plants with insufficient mixing, where these flocs are forming without coming into contact with the soluble P content of the wastewater. Subsequently, some of the pre-formed flocs were used immediately for phosphorus removal, while others were aged for various length of time and their soluble P removal (adsorption) capacity was tested in jar tests.

8.2.3 Continuous experiments: system setup

The objective of the continuous experiments was to compare P removal efficiency in systems with instantaneous reactions (very short SRT) and systems which operate in the normal SRT range. Biological components (activated sludge) were not included in the system, as the aim was to examine the chemical reactions independently.

The equipment consisted of two parallel systems including a coagulation tank (mixer), reactor (flocculator) and settling tank (Figure 8.1, Table 8.1).

Table 8.1 Operational parameters of the continuous experiments

Parameters		System "A"	System "B"
Q [L/h]		2.15	2.15
Raw water pH		7.5	7.5
Raw water PO_4-P [mg/L]		4.0	4.0
Fe_{dose}/P_{ini} [mol/mol]		1.4	1.4
HRT	mixer	2.5 min	2.5 min
	reactor	18 min	4.7 h
	settling tank	4.5 h	4.5 h
	total	4.8 h	9.3 h
V [L]	mixer	0.09	0.09
	reactor	0.64	10.16
	settling tank	9.68	9.68
	total	10.41	19.93
SRT		18 min	5.5 d

Raw water (P solution) prepared from tap water and KH_2PO_4 was supplied by a peristaltic pump at a rate of 2.15 L/h. Precipitant/coagulant (concentrated ferric-chloride solution) is introduced to the mixer unit (HRT = 2.5 min) where it is intensively mixed with raw water. A magnetic stirrer is used for mixing. Flocculation is carried out in a reactor which is slowly stirred by a magnetic stirrer. The produced ferric-hydroxide-phosphate flocs are allowed to settle in a settling tank with a hydraulic residence time of 4.5 h. An overwhelming part of the contact and dispersion effect for the proposed surface complexation mechanism is occurring in the reactors, before the flocs are separated in the clarifier. System "A" is a short SRT system, where the HRT of the reactor is 18 min, and no recycle is applied (SRT = HRT in this case, as there is no recycling). Chemical sludge (settled ferric hydroxide

flocs) is wasted intermittently from the settling tank. In System "B" all the settled sludge is recycled to the reactor (HRT = 4.7 h). Sludge is wasted from the reactor to sustain a SRT of 5.5 d.

System "A" represents typical conditions during primary precipitation (pre-precipitation), where the coagulant is well mixed and efficient flocculation is carried out before phase separation. However, in full scale treatment plants the settling time is about 1-3 hours, whereas the HRT of the laboratory sedimentation tank was 4.5 hours. The longer settling time provides better phase separation, and gives a higher possibility of surface reactions, which typically does not have a high significance in normal plant operations using primary precipitation.

System "B" simulates systems where contact time between the wastewater and the metal hydroxide flocs is longer, due to longer HRT and SRT. This occurs in simultaneous P removal systems where dosage of chemical is directly into the activated sludge reactor. The laboratory system is a representation of only one (rarely applied) configuration of such a system, where the coagulant is fed to a coagulator (mixer) unit prior to the reactor. Due to this setup, higher P removal rate is expected in the laboratory system with optimal mixing than would occur in a full scale plant configuration where the coagulant is introduced to the reactor under less favourable mixing conditions (low G values). A settling tank with a relatively large volume was chosen in order to ensure efficient phase separation in System "B" to promote recycling of all solids possible.
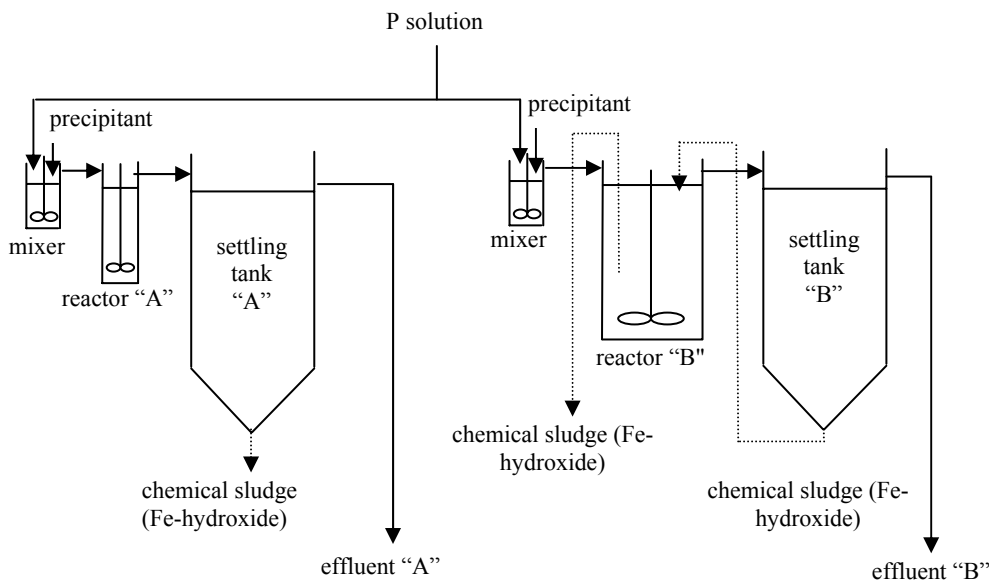
Figure 8.1. Flow scheme of continuous experiments

8.2.4 Phosphate sorption methodology

Batch sorption assays for chemically mediated phosphate removal were performed. All chemicals used were reagent grade or better. The general experimental protocol involved making a solution of 1 mgP/L from a stock tribasic sodium phosphate solution. Iron, as ferric chloride, is added to this solution to give the desired Fe/P ratio. While this initial solution is stirred, sodium hydroxide is added to adjust the pH to the desired value; initial pH is acidic because of ferric chloride. This sample is stored in a polyethylene bottle and shaken on a rotary shaker for 24 hours which is often taken as the operational definition of equilibrium for phosphate adsorption studies (Li and Stanforth, 2000). After 24 hours the samples are taken off the shaker and the pH is again tested. The samples are closed to the atmosphere so there is little drift in pH but the final pH value is taken as the "true" value. The solid

sample is filtered through a 0.45 μm filter and the filtrate is measured for soluble phosphate concentration using the method described below. The filter mass after filtration can be used to determine the mass of precipitate and, after digestion in nitric acid and flame atomic adsorption spectrophotometry (AAS), the iron concentration of the solid can be determined. The iron digestion and analysis was done according to EPA method No. 3050B using a Perkin Elmer model No. 3100 AAS.

8.2.5 Sensitive colorimetric determination of phosphate

Phosphate detection is based on the standard colorimetric technique (Riley and Murphy, 1962) and presented as the ascorbic acid technique in Standard Methods (1998). For samples above 0.01 mgP/L a Varian Cary 50 spectrometer was used with a 1 cm path length. For more dilute samples a one meter light path was used for a detection limit of approximately 0.0001 mgP/L. The 1 m light path consists of a hollow-fiber optic tube 1 m long from World Precision instruments (LWCC-2100), coupled to a Xenon lamp light source (Ocean Optics HPX-2000) and a QE5000 detector from Ocean Optics. The analytical methods were verified by spike recovery tests.

8.2.6 Dye adsorption experiments

Dye adsorption can be used to determine the surface area of particles suspended in solution. The advantage of dye adsorption techniques is that the sample is not dried, as it is in the BET technique (Brunauer *et al.*, 1938). By avoiding drying the sample, the surface area should be more representative of what solutes will actually "see" in solution. Dye adsorption using Methylene Blue is a common technique to determine surface area of clay minerals (Hang and Brindley, 1970). The method involved taking a suspension of HFO with a known particle density (mg/L) and adding increasing amounts of Methylene Blue in batches. The pH of these batches is fixed by addition of dilute sodium hydroxide and nitric acid as necessary. For the experiments reported here the pH was fixed at 4.0, even though this value is not representative of wastewaters, because that pH yielded the most reproducible results. It is suspected that samples closer to the zero point of charge of the solids had a greater degree of particle interactions and interfered with the dye adsorption technique. After 1 hour equilibration time these batches were filtered through 0.45 μm membrane filters and the concentration of dye in solution was determined using fluorescence spectroscopy at 600 nm excitation and 690 nm emission. Fluorescence was measured using a Varian Cary Eclipse spectrofluorometer. The difference between the total added dye and the measured solution dye concentration was used to determine the amount of dye bound to the surface of the HFO. In this way, a sorption isotherm for the dye molecule was generated and fitted to a Langmuir adsorption model using nonlinear regression analysis. Assuming monolayer coverage, the area of a single dye molecule can be used to determine the surface area of the particles in solution (Hang and Brindley, 1970).

8.2.7 Microscopy methods

Samples were prepared for microscopy by taking the original aqueous suspension and centrifuging it in order to collect the solid at the bottom of the centrifuge tube. The supernatant was decanted and replaced with pure water (MilliPore Synthesis A10 system with resistance > 18 MΩ/cm). The solid was distributed back into suspension and the process repeated three times. The final aqueous suspension was dispersed onto a thin slide for microscopic analysis. The water was evaporated and the solid was analyzed. This cleaning

procedure is necessary in order to remove salts from the aqueous solution. SEM measurements were performed on a Hitachi S-5200 SEM, using the accelerating voltages indicated in the figures without using conductive coating.

8.2.8 Acid-base titrations

Experimental and modelling methods for titration curves are detailed elsewhere (Smith and Ferris, 2001a) but in brief the method is based on measuring pH using a glass electrode during acid-base titration in a temperature controlled environment at a solution ionic strength adjusted to 0.02 M, close to typical wastewater. Each titration point was allowed to reach steady state before the next addition of titrant as determined by a maximum allowed drift rate in pH. The charge excess (*b*), calculated from the equation given below, is the amount of negative charge required for electroneutrality:

$$b = [Cations+] - [Anions-] + [H+] - [OH-] \tag{8.1}$$

Solutions of ferric chloride and sodium phosphate (80 mM) were titrated from pH 5 to 10. Titrations were performed using a Tanager 9501 automatic titrator and separate glass electrode and reference electrode half-cell electrodes. This method was used in determining dissociation and solubility constants in the pure orthophosphate and the Fe-P system.

8.3 Jar test results

8.3.1 Influence of metal to phosphorus molar ratio

The metal to phosphorus (Me/P) molar ratio is one of the main factors determining P removal efficiency. The Me/P molar ratio can be expressed in various forms. The three frequently used expressions are:

1. initial Me/P molar ratio (moles of metal dosed divided by moles of soluble P initially present, Me_{dose}/P_{ini});
2. Me/P molar ratio in the solid co-precipitate (Me_{prec}/P_{prec}); and
3. moles of metal dosed per moles of soluble P removed (Me_{dose}/P_{prec}). At typical pH values this latter is very similar to (Me_{prec}/P_{prec}) since most metal dosed will be incorporated in the co-precipitate.

Initial Me/P ratio For a given wastewater, applying higher coagulant doses (Me_{dose}/P_{ini} ratio) results in lower residual soluble P (PO_4-P) concentration. In the case of small coagulant doses (and relatively high residual P), the relationship between dose and the residual P is close to linear; however, specific P removal decreases with increasing coagulant dose (Figure 8.2). For the typical concentration ranges (initial soluble P concentration between 0.5-6.0 mg/L), to achieve 80-98% soluble P removal efficiency, doses above 1.5-2.0 Me_{dose}/P_{ini} are required even in "pure" P solutions and among the most favourable environmental circumstances (efficient mixing, optimal pH range, etc.). Reaching low (<0.1 mgP/L) residual PO_4-P concentration requires metal doses far in excess of the "stoichiometric" 1 molMe/molP ratio.
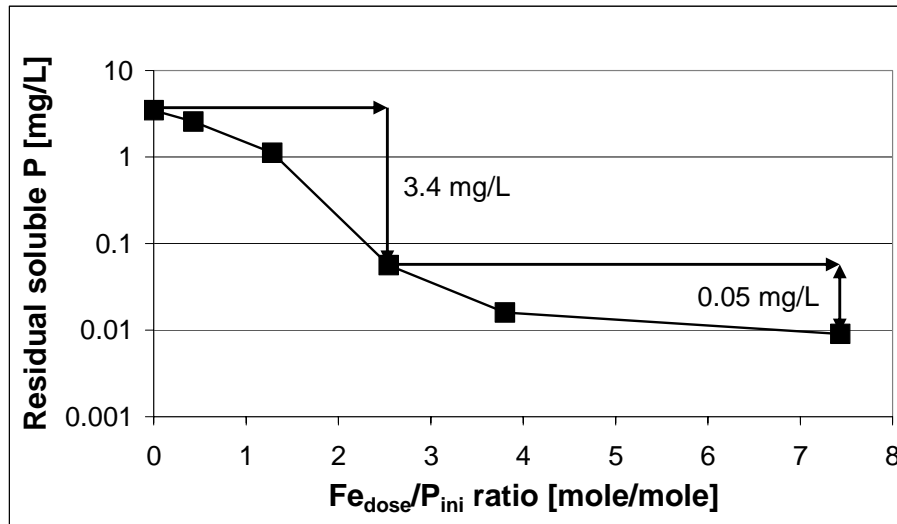
Figure 8.2. Residual soluble P in terms of initial Fe/P molar ratio (P solution; ferric-chloride; pH_{ini}= 6.5; P_{ini} = 3.5 mg/L; Alk_{ini}=125 mg $CaCO_3$/L)

Me/P ratio in the precipitate The amount of P incorporated into the precipitate (P_{prec}) can be calculated as the difference of initial (P_{ini}) and residual soluble P concentration (P_{res}) (i.e. P_{ini} - P_{res}). In the same way, the amount of metal in the solid precipitate is Me_{dose} - Me_{res}. According to lab experiments carried out by addition of ferric-chloride to P solution, above pH 5, the residual soluble iron (Fe_{res}) (measured by the standard phenanthroline method) is generally less than 0.1 mg/L and usually insignificant compared to the dose (Figure 8.3). At low pH, residual Fe is high because of the formation of soluble ferric complexes is dominant. In Figure 8.3, the lower Fe_{res} values that still occur at low pH may be attributed to $FePO_4$ (a solid) formation. $FePO_4$(s) is only expected to form at low pH (NIST, 2001).
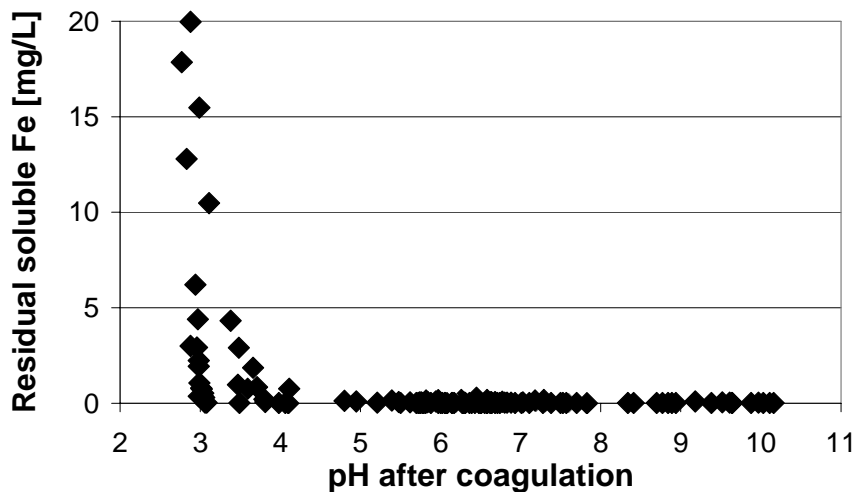
Figure 8.3. Residual soluble Fe concentration versus pH after the coagulation (P solution; ferric-chloride; P_{ini} = 0.5-12.5 mg/L; pH_{ini} = 3.0-10.2; Fe_{dose} = 0-50 mg/L; Alk_{ini} = 0-250 mg $CaCO_3$/L)

The amount of iron precipitated can be estimated by the amount added, as practically all the added iron precipitates in the usual operating pH range. Consequently, the Fe to P ratio in the co-precipitate depends on the initial Fe to P ratio. For Me_{dose}/P_{ini} > 1.0 mol/mol, the higher the initial molar ratio, the higher the Me_{prec}/P_{prec} will be in the co-precipitate (Figure 8.4).
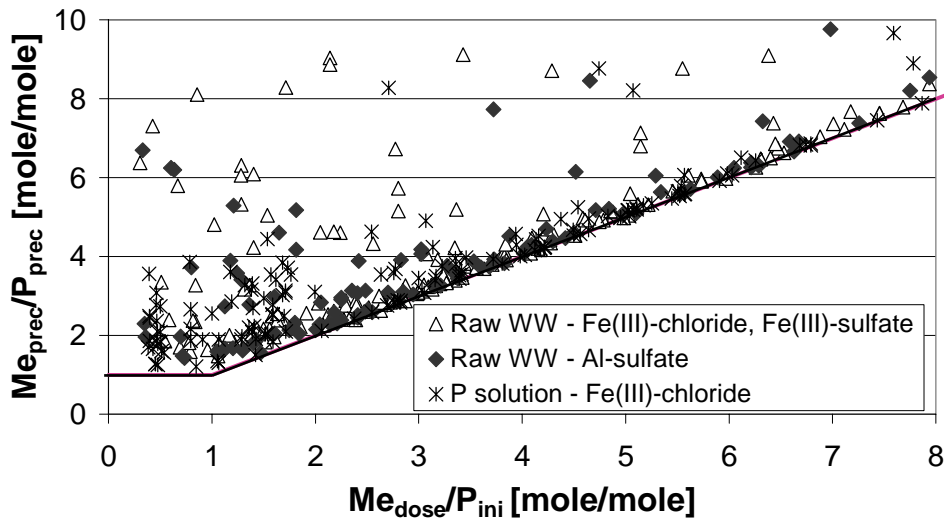
Figure 8.4. Me to P molar ratio in the precipitate in terms of initial Me/P ratio (P_{ini} = 0.5-12.5 mg/L; pH_{ini} = 3-10)

The slope on the bottom is the practical boundary and applies in those cases when almost no residual P is left behind (Me_{dose}/P_{ini} = Me_{prec}/P_{prec}). This is the optimal case. Points further from this boundary show data where environmental conditions were not optimal for P removal (such as higher pH levels and organic concentration, insufficient mixing, etc.).

8.3.2 Influence of coagulant type

Al^{3+} and Fe^{3+} containing coagulants show similar efficiencies (on a molar basis) for phosphate removal, both in model and real wastewaters. Figure 8.5 shows results of several experiments with raw wastewater treated by different coagulants.
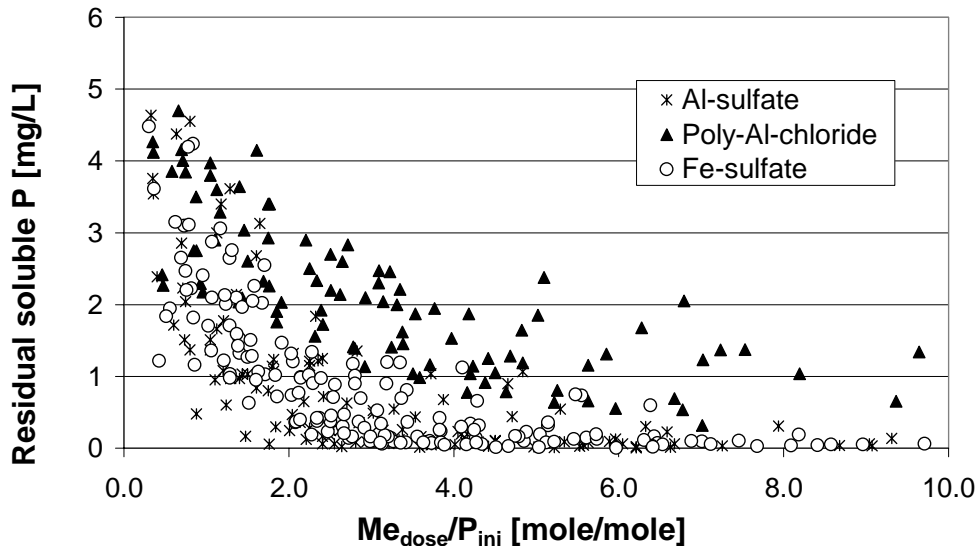
Figure 8.5. Residual soluble P applying different types of coagulants (different raw wastewater samples; pH_{ini} = 6.8-8.7; P_{ini} = 0.9-7.4 mg/L; TSS_{ini} = 50-2050 mg/L; COD_{ini} = 200-4000 mg/L; 500 samples)

The scatter in the data is due to the significantly different raw wastewater composition of many samples (initial PO_4-P, TSS, COD concentration, pH, etc.). Figure 8.6 shows results from a specific experiment using the same raw wastewater.
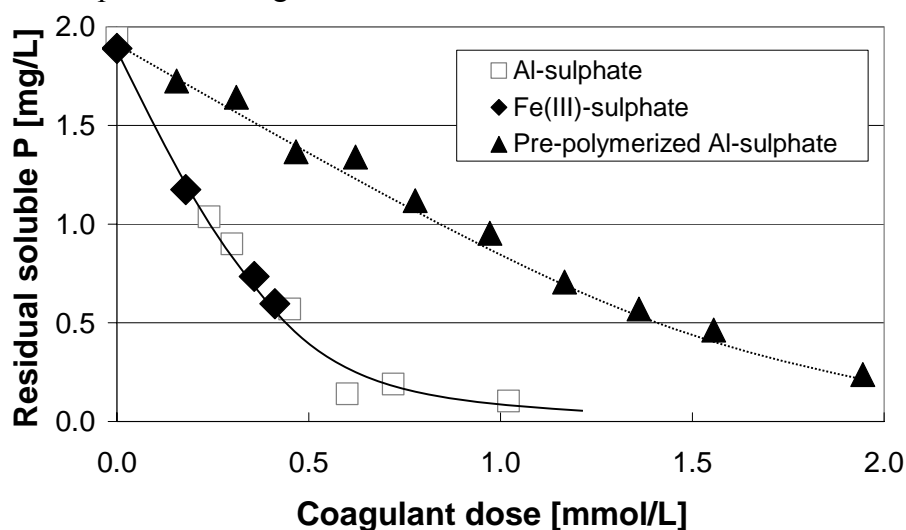
Figure 8.6. Residual soluble P in one raw wastewater sample, using different types of coagulants (P_{ini}=1.9 mg/L; pH_{ini} = 7.1)

Ferric and aluminium chemistry, the various ionic species formed and their ionization constants differ significantly for iron and aluminium ions. However, the most important reaction directly affecting phosphate removal is the formation of metal hydroxides (hydrous metal oxides, or specifically in the case of iron, hydrous ferric oxides, HFO), which is the dominant process in the case of both metals at typical plant pH values (NIST 2001). The phosphate complexation properties of these metal hydroxides were only investigated in detail for ferric ions in this work, but based on the results of these jar tests they are likely similar for aluminium.

Pre-polymerized salts are less efficient in removing PO_4-P as shown in Figures 8.5 and 8.6, in agreement with the works of Ratnaweera *et al.* (1992), Gillberg *et al.* (1996) and Fettig *et al.* (1990). Since precipitate formation decreases with increasing basicity (OH/Me ratio or degree of polymerization), the higher the basicity, the lower the phosphate removal efficiency will be (Ratnaweera *et al.*, 1992; Gillberg *et al.*, 1996).

8.3.3 Influence of pH

Full-scale and laboratory data show that, if conditions are favourable, very low soluble P residuals (P_{res}) can be achieved in the chemical P removal process in a wide pH range for both model water (P solution) and raw wastewater. Figure 8.7 contains full-scale plant data from the Noman Cole and Blue Plains wastewater treatment plants. The plants have been able to achieve very low (0.01-0.05 mgP/L) soluble P concentrations in the majority of effluent samples in a wide range of pH conditions (6.0-7.5).

111
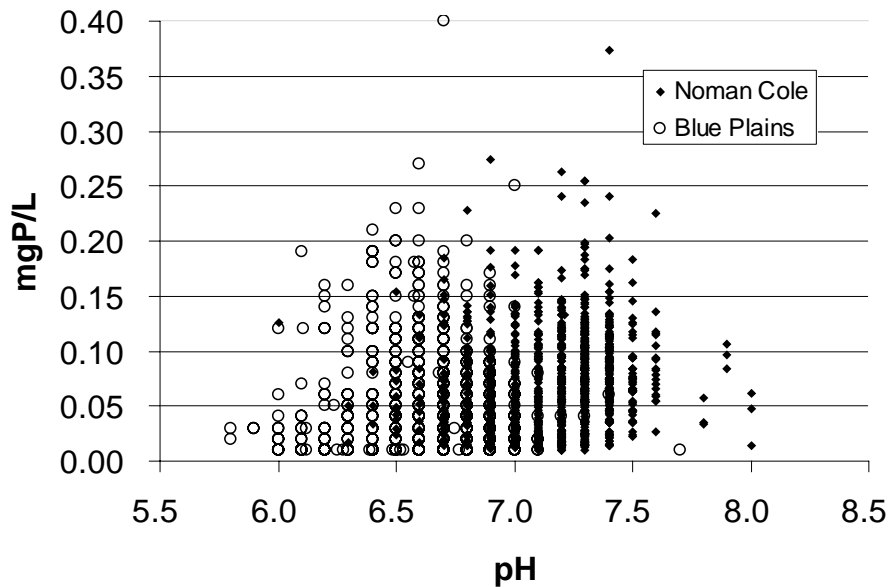
Figure 8.7. Residual soluble P in the effluent of two large plants

In lab experiments using tap water with initial soluble P concentrations (P_{ini}) of 0.5-12 mg/L, residual PO_4-P < 25 µg/L was achieved at pH 3.5-8.5 if other environmental conditions (e.g. mixing) were favourable and the coagulant dose was high enough (Figure 8.8). Similar residual PO_4-P concentrations could be reached in raw wastewater (COD_{ini} = 250-1000 mg/L, TSS_{ini} = 50-550 mg/L) between pH 5.0-7.0 without pH control. (The detection limit for the colorimetric phosphate method is 10 µg P/L. Some of the measured values were below the detection limit, these are shown to be 10 µg/L P). However, to achieve such low PO_4-P concentrations in the treated water, high metal doses were required even if other conditions were favourable. To assure P_{res} = 0.1 mg/L at least Me_{dose}/P_{ini} = 2.5 mol/mol was needed and Me_{dose}/P_{ini} = 5.0 mol/mol was necessary to get P_{res} = 0.01 mg/L in these experiments. In cases when environmental conditions were not optimal, the above residual P concentrations could not be reached. Figure 8.8 includes these cases, as well as the data without chemical dosage and using small coagulant doses. These laboratory results cannot be directly applied to predict full scale plant effluent P concentrations, as mixing and hydraulics will play a large role at these low concentrations (usually in the negative sense, increasing residuals).

In the WEF model (WEF, 1998, described in Chapter 7), the lowest soluble P concentration possible is 46 µg/L, and 0.1 mgP/L is achievable between pH values of 6.5 and 7.3 only. In some of our experiments, lower residual P concentrations were observed in a wider pH range than predicted by this chemical equilibrium model. This may be attributed to optimal experimental conditions which are not always achievable on full-scale plants, new, more sensitive analytical techniques and a more extensive dataset available.

At extremely low or high pH values, the minimum achievable P_{res}, and thus the efficiency of P removal depends on pH. At acidic pH the precipitation of metal-hydroxide is limited, and mostly soluble phosphate complexes form. Even the already precipitated phosphate will redissolve when decreasing the pH by adding more coagulant to the system (in spite of the higher coagulant dose).
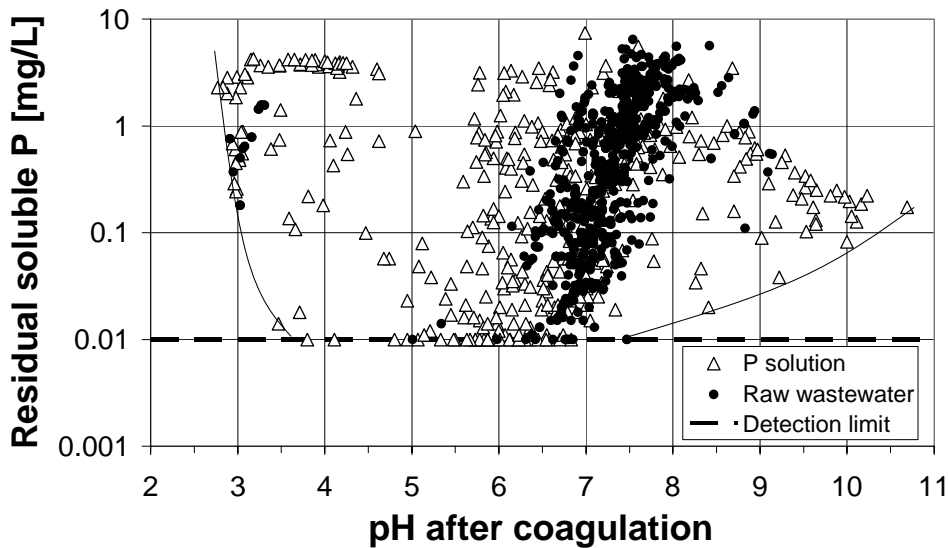
Figure 8.8. Residual soluble P concentration versus pH (model and real wastewater experiments; different types and doses of coagulants; P_{ini} = 0.5-12.5 mg/L)

At alkaline pH values (pH 7-10) the surface of the metal-hydroxides is more negatively charged, and soluble iron-hydroxide complexes (e.g. $Fe(OH)_4^-$) start to form (NIST, 2001). Thus the P removal efficiency decreases with increasing pH. At pH values larger than 10, the PO_4-P can form a precipitate with magnesium and calcium ions available in most wastewaters (Fettig *et al.*, 1990), and reduction of soluble P concentration can take place without iron or aluminium coagulant addition.

P removal at larger doses has the highest efficiency between pH 5.5 and 7.0. Within this pH range - which occurs most of the time in practice after metal salt addition - the effect of pH is not very important in co-precipitation and coagulation reactions. Neither the molar ratio in the precipitant nor the residual P concentration is significantly affected by pH within this interval (Figure 8.9).
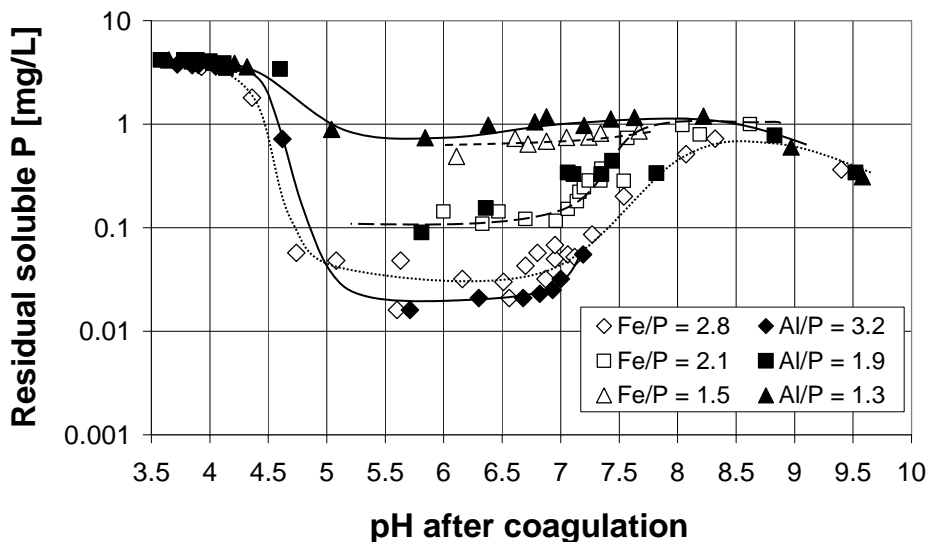
Figure 8.9. Residual soluble P concentration in terms of pH after coagulation (P solution; aluminium-sulphate; ferric-sulphate; P_{ini} = 3.6-4.0 mg/L)

113

These results are in contradiction to earlier studies (Lijklema, 1980; Fettig *et al.*, 1990; Jenkins *et al.*, 1971), where strong pH dependency was found between pH 5-8 with lower doses of Fe and Al coagulants. Further experiments are required to fully characterize the full dose - pH dependence – P residual relationship.

The results show that aluminium and ferric salts remove P with similar efficiency, and the pH dependency of residual P concentration is comparable (Figure 8.9). Therefore the choice between Fe and Al salts should depend on other factors, such as availability, price, sludge handling possibilities, etc. In this article, all of the other results and references relate to ferric salts, not alum.

8.3.4 Influence of alkalinity

Jar tests with model wastewater showed that phosphorus removal efficiency is influenced by the alkalinity of the raw wastewater. In the same pH range (though without pH control), higher alkalinity resulted in slightly higher residual soluble P concentrations (Figure 8.10).
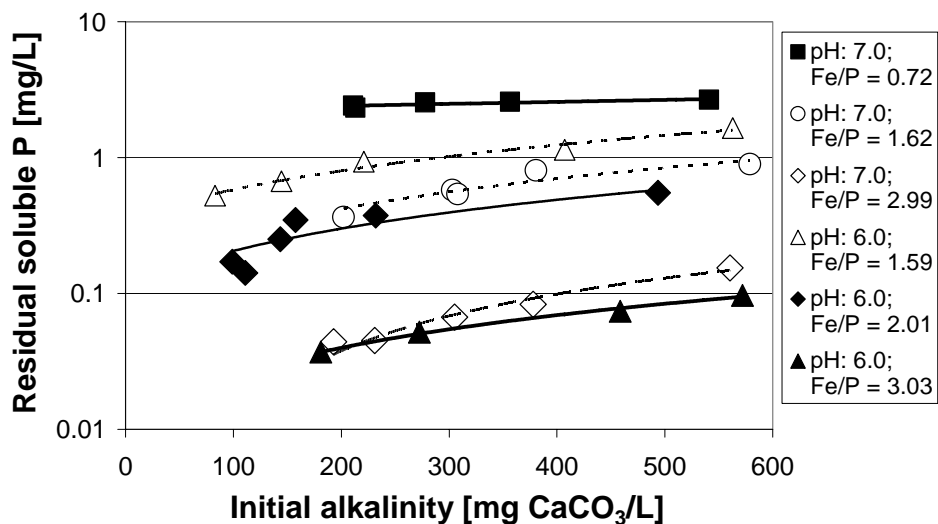
Figure 8.10. Residual soluble P concentration in terms of initial alkalinity (P solution, ferric-chloride; P_{ini} = 3.9-4.3 mg/L)

This phenomenon is currently not well understood. In waters with higher alkalinity the formation of metal hydroxides can be significantly faster, since the H^+ capturing capacity is higher. This creates a better chance (kinetic advantage) for fast precipitation of metal hydroxides and a lower probability for co-precipitation of phosphate and metal hydroxides. It is also possible that competition exists between the HCO_3^- ions and HPO_4^{2-} ions for the active sites. However, this phenomenon requires further investigation and confirmation.

8.3.5 Influence of initial PO$_4$-P concentration

P removal efficiency depends on the soluble P concentration of the raw wastewater. The higher the initial P concentration, the lower the Me_{prec}/P_{prec} ratio will be (Figure 8.11).
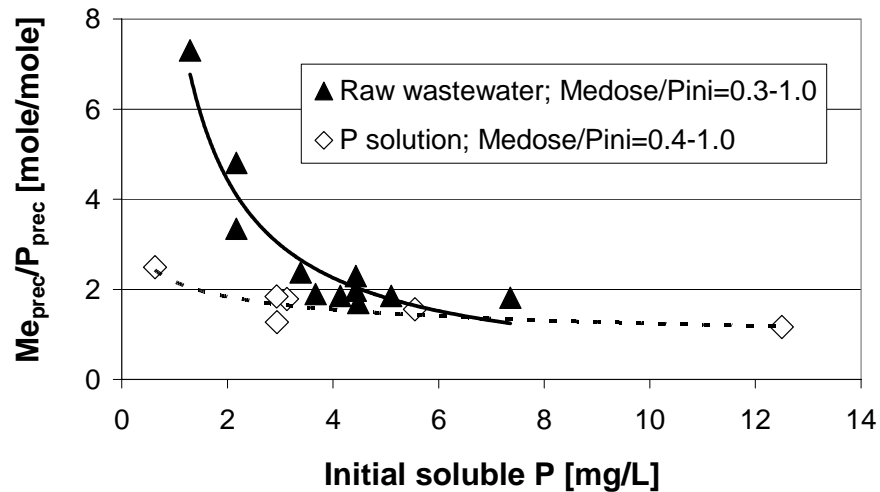
Figure 8.11. Me/P ratio in the precipitate in terms of initial soluble P concentration

This ratio can approach approximately one; though this is not necessarily an indication of the formation of a pure metal-phosphate precipitate. In P solution the ratio usually gets below 2.0 mol/mol at small relative doses ($Me_{dose}/P_{ini} < 2.0$ mol/mol) if the initial P concentration is higher than 2 mgP/L and pH is in the optimal range (5.5-7.0). A similar tendency was found in experiments done with raw wastewater; however, P removal efficiency was generally lower (and the Me_{prec}/P_{prec} ratio was higher) than in "pure" systems. The difference between the results gained in P solution and wastewater was more significant when the initial soluble P concentration was lower (<4 mgP/L).

Although the relative efficiency of P removal increases with increasing initial soluble P concentration (low Me_{prec}/P_{prec} ratios were observed when the initial P concentration was higher), to reach a certain residual P concentration, higher relative coagulant dose (Me_{dose}/P_{ini}) is needed when P_{ini} is higher (Figure 8.12).
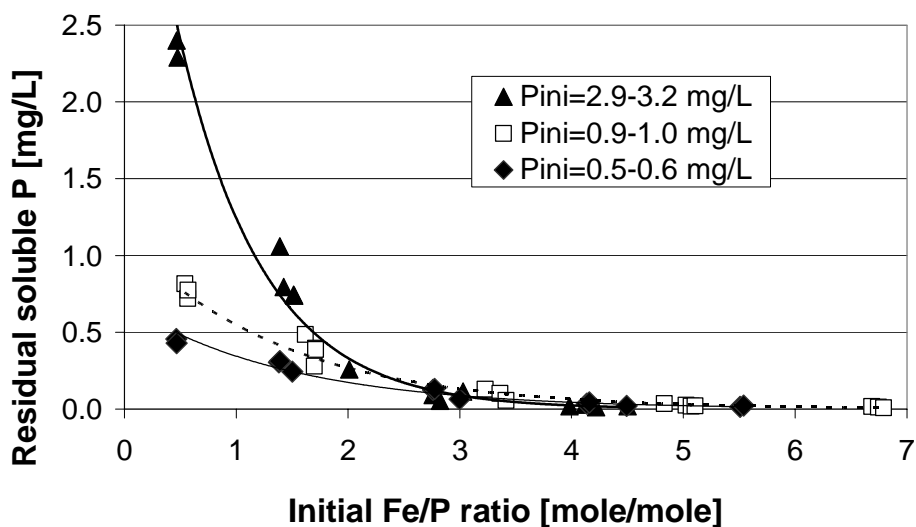
Figure 8.12. Residual soluble P concentration in terms of the initial Fe/P ratio (P solution in tap water; ferric-chloride)

115

8.3.6 Influence of raw wastewater COD concentration

Based on jar tests carried out with municipal wastewater, it is found that the amount of organic material present in raw wastewater significantly influences the P removal efficiency (Figure 8.13).
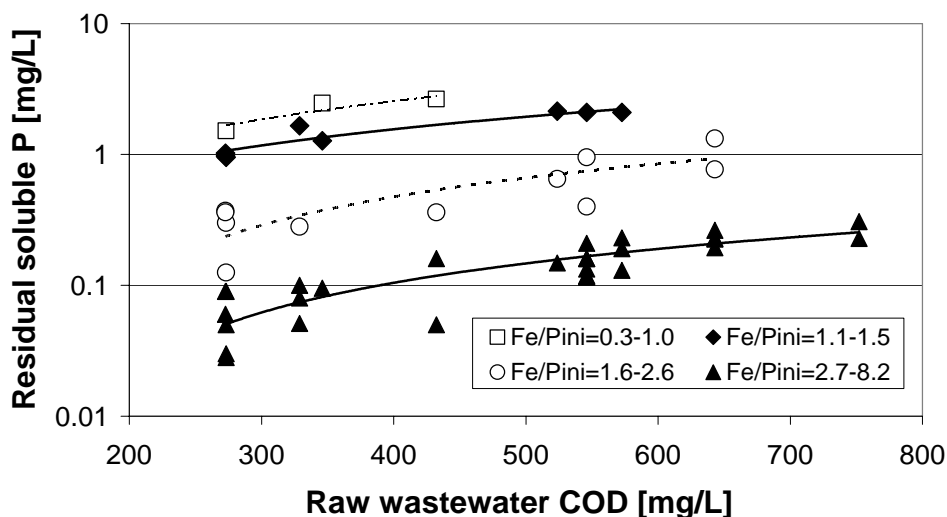
Figure 8.13. Residual soluble P concentration in terms of raw wastewater COD concentration (raw wastewater; $pH_{ini} = 7.5$-8.5; PO_4-$P_{ini} = 3.1$-5.2 mg/L; $TSS_{ini} = 80$-260 mg/L)

With increasing raw wastewater COD concentration chemical pre-treatment will result in higher residual soluble P concentration (applying the same dose). P removal efficiency can be negatively affected by both particulate and dissolved organic materials. In these experiments the two impacts could not be separated, as a higher dissolved COD concentration most often occurred together with a higher particulate organic matter concentration.

Parallel to higher initial COD concentration, the TSS concentration of the raw wastewater was also higher. At higher TSS concentrations, less efficient P removal was observed. Although the effects of COD and TSS cannot be separated, the observed tendency agrees with results found by other authors (Fettig *et al.*, 1990).

A phosphate complexation model (such as presented later in this chapter) is consistent with the observation that the presence of organic materials decreases removal efficiency. The mechanism could be that carboxylic and phenolic groups on the organic matter compete with phosphate for binding sites on the surface of the metal hydroxides.

8.4 Kinetics in phosphorus removal

8.4.1 Influence of time (kinetics) in P removal

Several parameters were investigated which have an effect on or relationship to kinetics or general, time-dependent reactions. The first one discussed below is the time dependent reaction rate itself. In the following two sections mixing (as measured in inverse time units, G 1/s) and age of preformed flocs are investigated more closely.

116

The reaction rate (kinetics) of phosphate removal was investigated in traditional jar tests, where the change in residual PO_4-P concentration was followed in time. Typical kinetics of P removal is shown in Figure 8.14. There is an initial fast removal of P occurring in less than 1 minute, or likely even in a much shorter timeframe (referred as "instantaneous P removal"). However, significant further removal can occur after a few hours or days (termed "slow P removal"). The following parameters were investigated concerning their effect on the rate of P removal: initial Me/P ratio, mixing conditions and the age of hydroxide flocs.
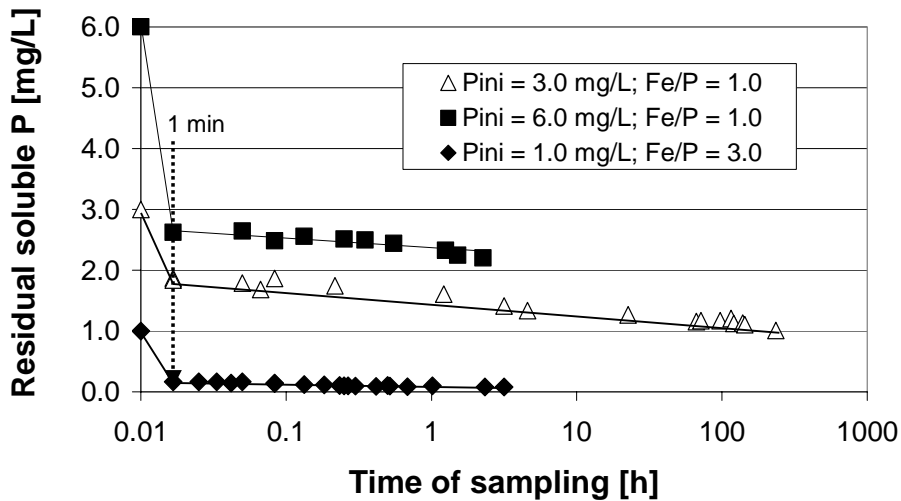
Figure 8.14. Kinetics of P removal (P solution; ferric-chloride; Me_{dose}/P_{ini} = 1.0-3.0 mol/mol; G = 425 1/s)
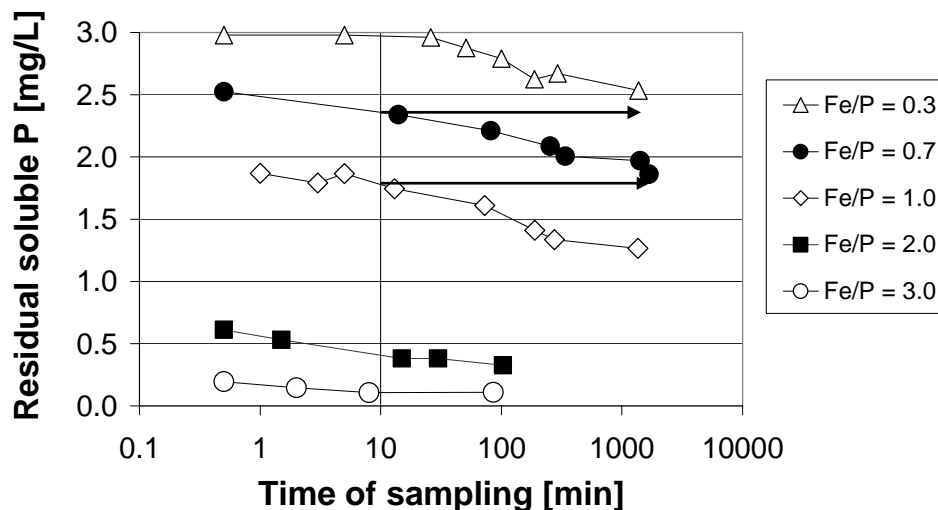
Figure 8.15. Kinetics of P removal (P solution; ferric-chloride; P_{ini} = 3.0 mg/L; Fe_{dose}/P_{ini} = 0.3-3.0 mol/mol; G = 425 1/s)

The importance of kinetic reactions resulting in slow P removal under typical plant conditions should be taken in context of Figure 8.2, where the removal of an additional 0.05 mg/L residual P required a significant increase in molar ratio (5.0 extra mole coagulant/mole P). Figure 8.15 shows the kinetics of P removal for different Fe/P ratios, starting at a similar initial P concentration (P_{ini} = 3.0 mg/L). As an example, 1.8 mg/L residual soluble P was reached by Me_{dose}/P_{ini} = 1.0 mol/mol dosage in 10 minutes. However, if the reactions are allowed to proceed for 30 hours, the same PO_4-P concentration can be reached by a dose of Me_{dose}/P_{ini} = 0.7 mol/mol only as indicated by the arrow on Figure 8.15. Although the

117

absolute P removal by the slow reaction is smaller when a higher dose is applied, achieving an additional small removal of residual P can be reached by allowing slow processes to occur, rather than by adding massive dosages of excess metal salts. Allowing for slow reactions can thus remove these small amounts of phosphates without a large dose requirement.

8.4.2 Influence of mixing intensity
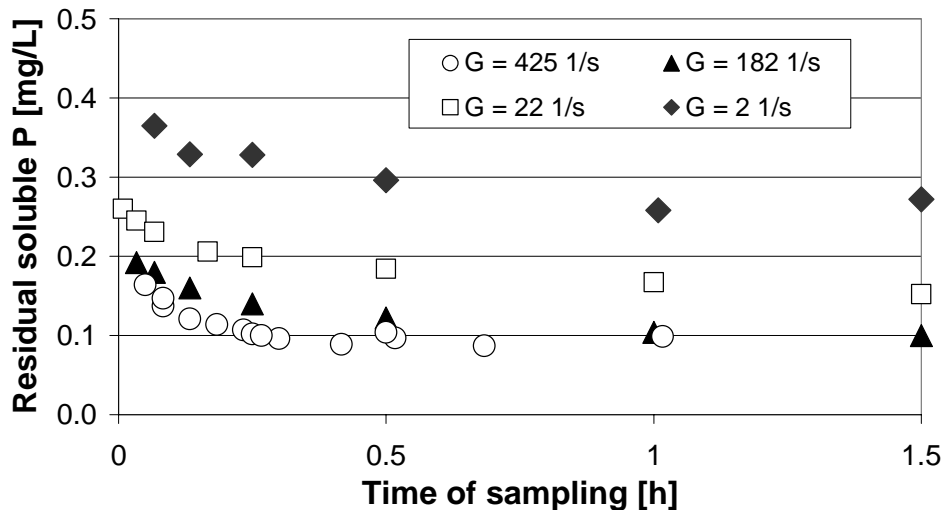
Figure 8.16. P removal kinetics at different G values (P solution; ferric-chloride; P_{ini} = 1.0 mg/L; Fe_{dose}/P_{ini} = 3.0 mol/mol)

There is a significant "instantaneous" reduction (very fast reduction, which is observed due to practical sampling limitations in a 0.5 to 1.0 minute timeframe) of P concentration under ideal mixing conditions (G = 425 1/s in this case). The majority of P removal (close to 90%) occurs within 10-20 minutes, and further removal occurs in the next few hours. When the intensity of initial mixing is low (G = 2-22 1/s) during coagulant addition, the "instantaneous" removal efficiency is impaired (residual P is 0.2-0.3 mg/L after 10-20 minutes). However, P removal continues even after several hours as a slow process (Figure 8.16). In both cases, the main P removal process is very fast, however, slow P removal provides a further decrease ("polishing") in soluble P concentration. The extent of the two different processes depends on mixing intensity. Ideally a very high mixing intensity should be achieved at the chemical dose point in full-scale plants – G-value higher than 200-300 1/s, similar to jar testing conditions.

Residual P concentration in a similar experimental series is shown in Figure 8.17 as a function of the G-value. Instantaneous phosphate removal is more efficient when metal hydroxides are being formed under high G conditions, which provides ample opportunity for contact between ferric and phosphate ions. This is the case when the metal salt is added to wastewater prior to the biological treatment step (pre-precipitation) or after biological treatment and phase separation (post-precipitation) under good mixing conditions. If pre-formed metal hydroxide flocs come in contact with phosphate ions (because of inefficient or incomplete mixing or because pre-polymerized metal salts are used), initial P removal (within the first few minutes) will be less effective. However this can be compensated to a degree by the long contact time in simultaneous precipitation, where coagulant is introduced to the activated sludge reactor and its residence time matches that of the biological solids.
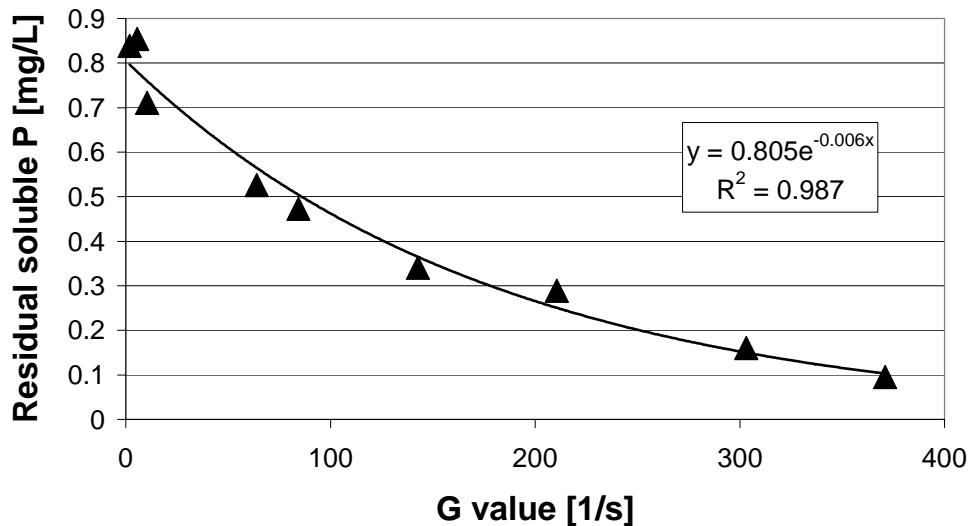
Figure 8.17. Effect of G-value on P removal (ferric-chloride; $P_{ini} = 4.1$ mg/L; $Fe_{dose}/P_{ini} = 1.8$ mol/mol; time of sampling: 11 min after coagulant addition)

In the case of pre- or post-precipitation (dosing the coagulant prior to the primary or after the secondary settling tank), where the contact time is short, it is very important to assure a high probability of phosphate ions getting in contact with ferric ions and freshly formed, positively charged ferric hydroxides. In typical wastewaters, the concentration of PO_4^{3-} is orders of magnitude lower than the concentration of HCO_3^- ions, which control $Fe(OH)_3$ precipitation. If the coagulant is intensively mixed at the dosage point, more efficient P removal will occur.

The extent of the slow adsorption (surface complexation) reaction also depends on the residual P after the fast reaction is completed. The residual P concentration after the first few minutes is mainly determined by mixing as described above, and the dosage, i.e. the Fe_{dose}/P_{ini} molar ratio. During the relatively short contact time due to phase separation in pre- or post-precipitation, P removal by the slow reaction is not significant.

8.4.3 Influence of the age of flocs

The age of hydroxide flocs has a significant influence on P removal efficiency. In a jar test, hydroxide flocs were separately formed and after a certain aging period (denoted as "Age of flocs" in Figure 8.18) they were added to the P solution. Samples were taken at different times after adding the flocs to the P solution ("Time of sampling" in Figure 8.18). According to the results, fresh ferric hydroxides (aged 1 minute) can achieve about 60% P removal in 20 minutes (Figure 8.18). For the same initial conditions ($P_{ini} = 1.0$ mg/L; $Fe_{dose}/P_{ini} = 3.0$ mol/mol), only 30-35% of the original PO_4-P is removed if the ferric hydroxide floc is aged 30 minutes before it comes in contact with orthophosphate. The result is in agreement with earlier observations (Lijklema, 1980) and with qualitative changes in iron hydroxide at different ages shown in electron microscope images later in this chapter. If preformed flocs (e.g. chemical sludge from drinking water plants) are used for P removal in a wastewater treatment plant, the fresher the sludge and the shorter the transportation and storage time, the better the efficiency that can be expected.

119
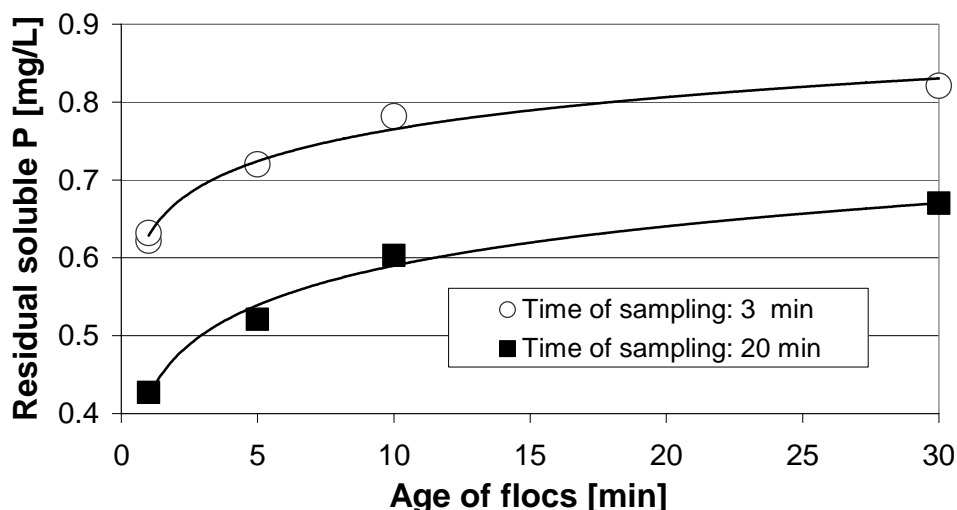
Figure 8.18. Effect of floc age on P removal (P solution; ferric-chloride; preformed ferric hydroxides; $P_{ini} = 1.0$ mg/L; $Fe_{dose}/P_{ini} = 3.0$ mol/mol)

8.5 Continuous laboratory experiments

Two continuous flow systems as described in Section 8.2.3 were operated for several weeks. Due to recycling of the chemical sludge, the concentration of suspended solids in steady state was 24 times higher in System "B" than in System "A". The HRT of Reactor "B" itself was 15 times longer than the HRT of Reactor "A"; however, the total system HRT (including HRT of the coagulation tank, the reactor and the settling tank) was only 2 times longer in System "B". Based on our previous batch tests (see Figure 8.14 and 8.15), the long contact time provides opportunity for sorption reactions, causing additional P removal if the contact of ferric hydroxides and PO_4 ions is ensured. This phenomenon was verified in the continuous system where the average soluble effluent P concentration was 15% lower in System "B" (with recycle). 0.47-0.81 mg/L residual soluble P was achieved without recycling (System "A"); while only 0.40-0.58 mg/L PO_4-P remained in the effluent of the long SRT system with recycle. The effluent P concentration varied less in System "B", where the standard deviation was about 10%. System "A" showed more instability, as the standard deviation of the residual PO_4-P was almost 15% (Figure 8.19).

Based on the results of the batch tests, there are two important factors that should be considered during evaluation of the above data. First, the unusually long settling time might provide a possibility for removal of soluble P through surface reactions in the settling tank of System "A". However, the difference in PO_4-P concentration in the reactor and in the effluent was not significant (see Table 8.2), proving that phosphorus removal almost exclusively occurred in the mixing tank and the reactor (flocculator). The pH of the two systems was different due to the longer HRT in System "B" resulting in a more efficient gas exchange with the atmosphere (an artefact of laboratory testing) (Figure 8.20). Without pH control, the pH of the tap water solution increases with time due to CO_2 loss. This was experienced in long term batch tests as well. This artificially reduced the measured benefit of solids recirculation and retention because increased pH results in reduced phosphorus removal efficiency (Figures 8.8, 8.9, and 8.21).
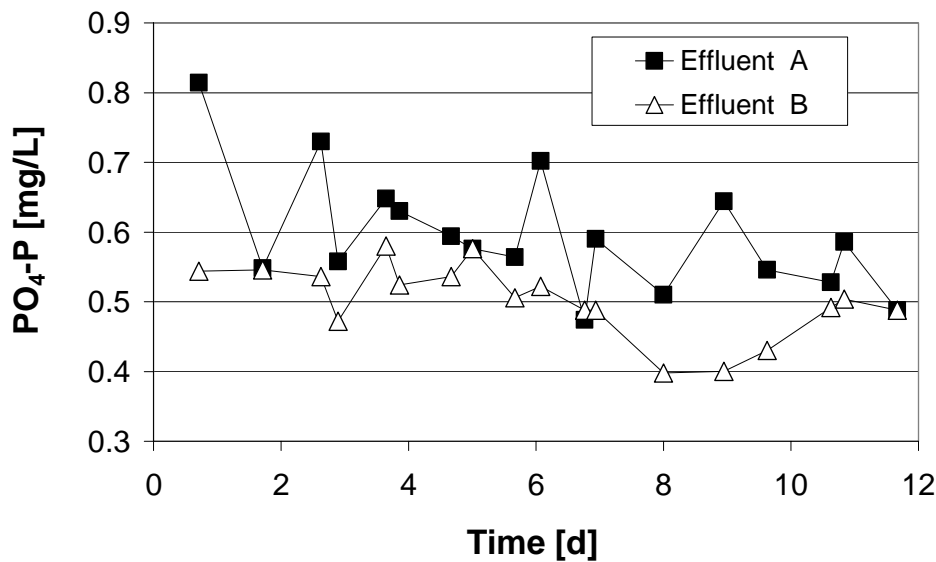
Figure 8.19. Effluent PO$_4$-P concentrations in continuous experiments

Another question of importance to practitioners is whether the jar test results could be used to estimate continuous flow systems in practice. The average residual P in System "A" was 0.60 mg/L (0.47-0.81 mg/L) for Fe$_{dose}$/P$_{ini}$ = 1.4 mol/mol and pH of 6.8. The residual P in batch jar tests for similar Fedose/Pini and the same final pH was 0.6. This residual P is the same in the continuous and the batch systems under similar conditions, indicating that batch jar tests could probably represent low SRT continuous flow systems. This, however has to be confirmed with more detailed experiments.

Table 8.2. Water quality parameters in the continuous experiments

Parameters	System "A"	System "B"
TSS [mg/L]	25 (17-30)	610 (565-665)
Effluent pH	6.8 (6.60-7.00)	7.2 (6.85-7.27)
Effluent PO$_4$-P (P$_{res}$) [mg/L]	0.60 (0.47-0.81)	0.50 (0.40-0.58)
Effluent PO$_4$-P (P$_{res}$) standard deviation	14.6%	10.4%
Extra removal in System B ((P$_{resA}$-P$_{resB}$)/P$_{resA}$)		15% (0-38%)
P removal rate compared to raw PO$_4$-P	85% (79-88%)	88% (86-91%)
Reactor PO$_4$-P [mg/L]	0.62 (0.51-0.90)	
PO$_4$-P corrected for pH 7.2 [mg/L]*	0.90	0.50

*based on results of batch experiments (Figure 8.9 and 8.21), it is easier to remove P (residuals are lower) at pH 6.8 compared to pH 7.2. The estimated P residual would have been 0.90 mg/L instead of 0.62 had the pH been maintained at 7.2 (details in text).
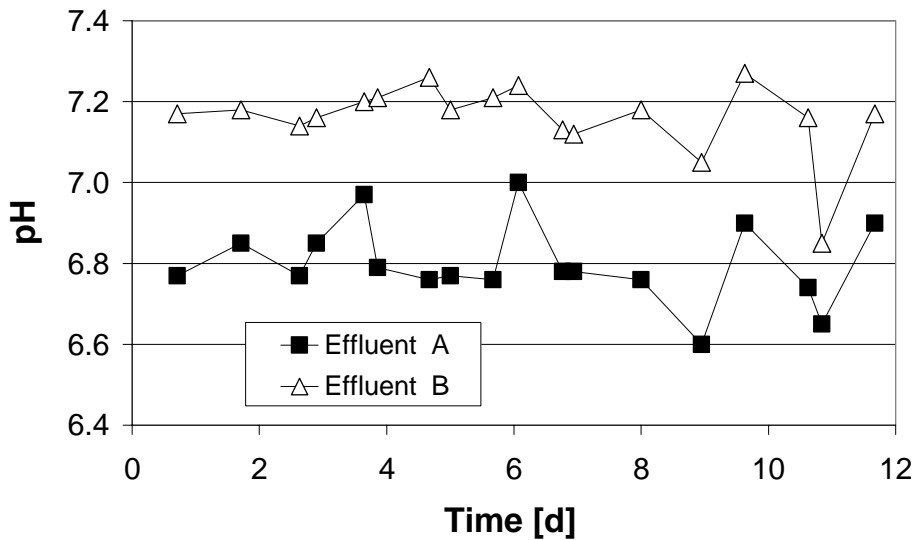
Figure 8.20. Effluent pH values in continuous experiment
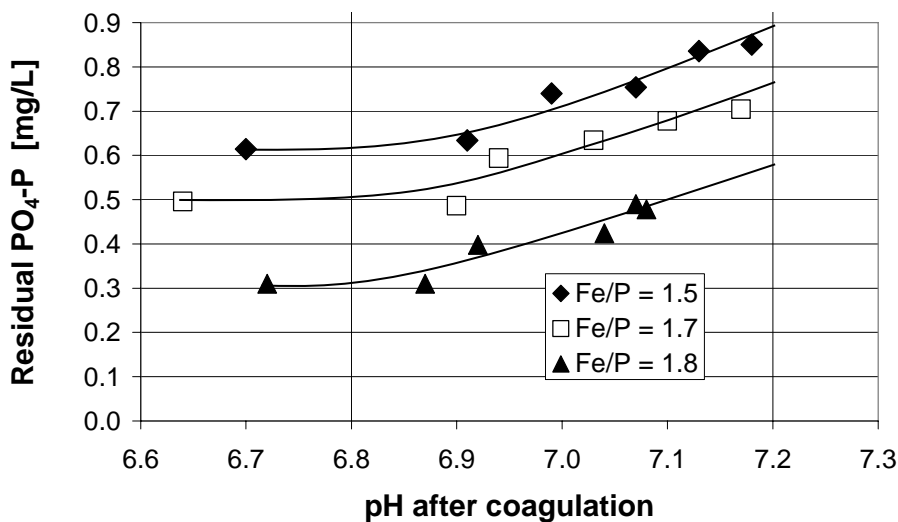
Figure 8.21. Effect of pH on the residual soluble P concentration (batch test; P solution; $P_{ini} = 4.0$ mg/L)

The efficiency of phosphate removal is influenced by the actual pH value in the pH range occurring in the continuous experiment. The average effluent pH in System "A" was 6.8, where the residual P concentration averaged 0.60 mg/L. At the same time, the average pH value of Effluent "B" was 7.2. According to batch test results with similar coagulant dose ($Fe_{dose}/P_{ini} = 1.5$), the residual PO_4-P concentration is about 0.3 mg/L higher at pH 7.2 than at pH 6.8 (Figure 8.21). Thus, if a correction to account for the pH difference is applied to Effluent "A" based on the results of batch tests shown in Figure 8.21, the average residual PO_4-P concentration would be about 0.9 mg/L in System "A".

The results of the continuous experiments show that a system with longer HRT and SRT can provide more efficient P removal than one with short HRT and SRT in the case of similar mixing conditions. This phenomenon is primarily due to the longer contact time between PO_4

122

ions and metal hydroxide particles, and it partially mitigates the effect of inefficient mixing in simultaneous P removal systems. It is important to realize that, in addition to this beneficial effect, many other aspects have to be considered when choosing between pre-, post-, or simultaneous dosing systems, such as availability of equipment, dosing configurations, sludge production, and the effect on the biological system.

8.6 Surface of Hydrous Ferric Oxides (HFO)

8.6.1 Aging of HFO: dye adsorption experiments

The batch phosphate removal tests demonstrate the importance of surface area in controlling phosphate removal via ferric chloride addition. There are several surface area determination techniques available. The most commonly used technique is BET analysis, which requires sample drying which will inevitably change the nature of the particles. To avoid this, solution speciation techniques are used, such as dye adsorption (Hang and Brindley, 1970). In the dye adsorption method, a known concentration of dye is added to the aqueous sample of particles, where it interacts with the surface and is removed from the solution. Thus, a measure of soluble dye can be used to determine how much dye is adsorbed to the surface by difference. The result is an adsorption isotherm for dye molecules onto the reactive surface. The isotherm can be mathematically fit to the Langmuir equation and the total sorptive capacity determined (Hang and Brindley, 1970). This total capacity can be converted to surface area if the size of the dye molecule is known and mono-layer coverage is assumed. Figure 8.22 shows data and corresponding best-fit isotherms for fresh and old HFO.
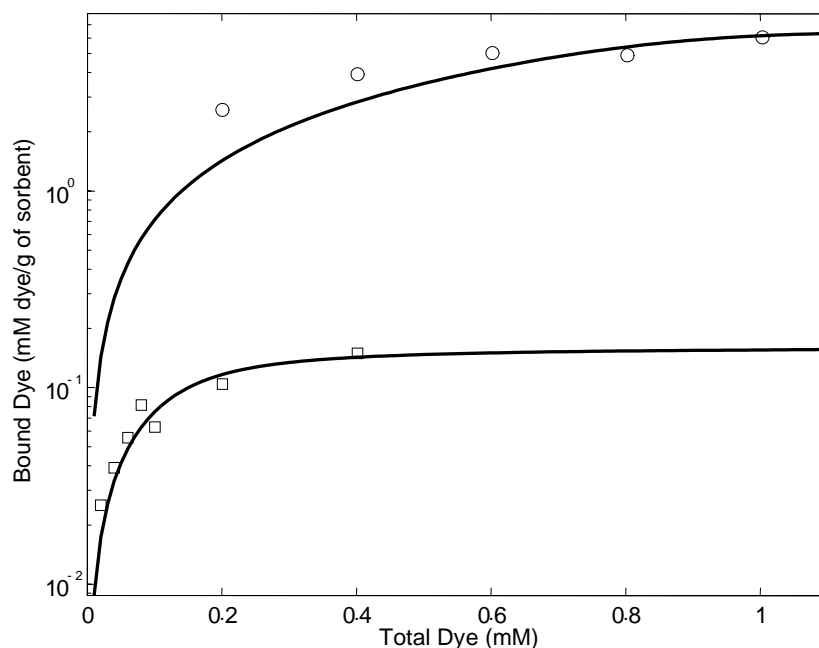
Figure 8.22. Dye sorption isotherms for fresh (circles) and old (squares) HFO. The solid lines correspond to Langmuir isotherm fits to the sorption data.

The fresh HFO was prepared according to the method in detailed in section 8.2.4 (i.e. neutralize a 10 mg Fe/L solution with base) and used immediately. The old HFO is material that was prepared in the same way but stored at 4 degrees Celsius for two years.

For fresh HFO the surface area was determined to be 5500 ± 170 m^2/g. The old HFO (2 years) was determined to have a surface area of 920 ± 170 m^2/g. For comparison the usual value for

consolidated HFO surface area based on BET analysis is taken as 600 m^2/g, with a reported range of 100 to 1200 m^2/g and 600 somewhat arbitrarily selected as a representative value (Dzombak and Morel, 1990). It is reasonable that the solution dye adsorption method should give higher surface areas than BET measurement, because the samples are not exposed to the compaction and reorganization associated with drying. The surface areas determined here show the expected qualitative trend; higher surface area for the fresh material. In terms of proportional decrease, the aged surface area has decreased to 17% of the fresh HFO value. For comparison, in the preformed floc experiments the ASF value decreases to 25% of the fresh value. The implication is that the ASF parameter can be related to available surface area and it might be possible to model phosphate interactions during aging of flocs by varying this single parameter.

Implications of aging for design and operations. As the HFO molecules age, they become denser (Dzombak and Morel, 1990) and should limit the ability of orthophosphate diffusion within the molecular structure (Makris *et al.*, 2004). In kinetic modelling of dynamic treatment processes the surface area changes of HFO must be taken into account. The age of flocs may be significant to practice. For example, whether to recycle iron or aluminium containing water treatment plant residuals for phosphorus removal may significantly depend on the floc age. Chapter 7 describes a plant that recirculates its relatively 'fresh' tertiary sludge to the primary process, resulting in substantial additional phosphorus removal in the primary process. Georgantas and Grigoropoulou (2005) present comparison data for phosphate removal using either fresh alum or spent alum sludge. It was found that the fresh material removed phosphate 5 times more efficiently, in terms of residual concentrations, than the old spent material.

8.6.2 Aging of HFO: microscopy

The batch sorption data (Figures 8.22) allows a model to be developed to quantitatively describe removal of phosphate. The important parameter in this model is the proportionality constant (ASF), to convert total iron into binding site density. An obvious question is how does binding site density change as the particles age? To address this issue SEM and TEM images were obtained for HFO particles of different ages. The freshest HFO that could be obtained was prepared in the lab from 10 mg Fe(III)/L and immediately "quenched" by rinsing with pure water. The image was obtained within 24 hours of particle formation. A TEM image of this sample is shown in Figure 8.23. TEM images can show size (about 50 nm short axis and 100 nm long axis) and density. The dark regions in the image are denser than the lighter regions of the image. This fresh HFO particle is much less dense, suggesting that significant potential exists for diffusion into the particle. The total particle size is consistent with the estimate of ASF of 1.18 for phosphate removal when HFO is formed *in situ*. For 50 nm particles the estimate of ASF is 1.3.
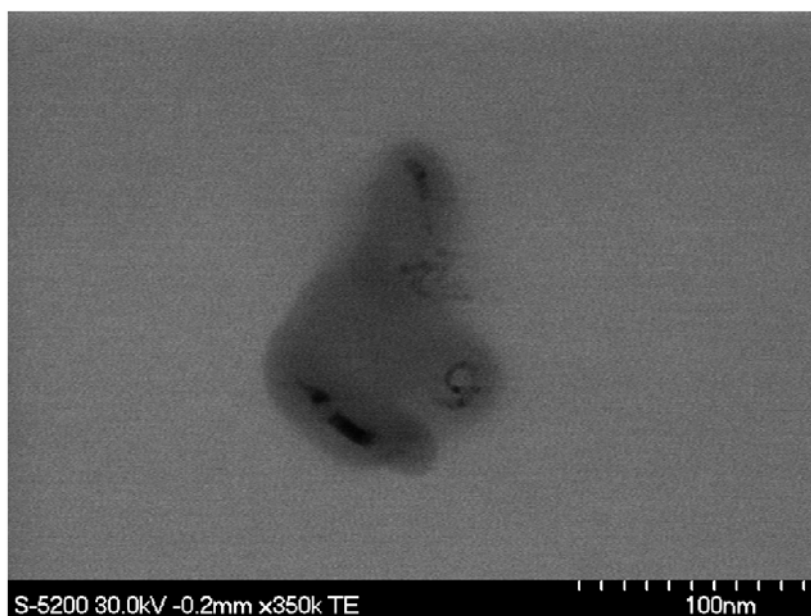
Figure 8.23. TEM image of fresh HFO

The sample shown in Figure 8.23 is a typical TEM image of HFO formed at circumneutral pH. Similar images are obtained when the HFO is formed in the presence of phosphate except at an acidic pH. At acidic pH $FePO_4$(s) was observed (see Figure 8.26).

A second TEM image is shown in Figure 8.24 for HFO that was prepared in the same way as the fresh HFO but allowed to age for 4 days before centrifugation and rinsing. The TEM image shows that the density has increase dramatically and the low density fresh HFO is now more like dense hard spheres. The total size of the particle has also increased, with a long axis greater than 200 nm and a short axis about 100 nm. An increase in particle size is consistent with decreases in surface area and a decrease in the ASF parameter. Smaller aggregates are apparent as constituents of this total particle though. Based on these images it seems likely that, as HFO particles age, the capacity for phosphate removal will decrease.
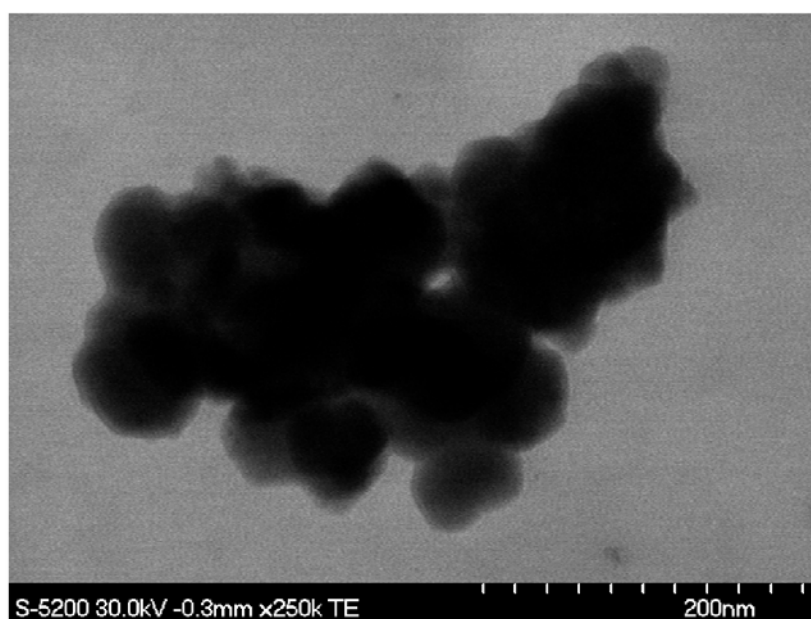
Figure 8.24. TEM image of young (4 day old) HFO

Further emphasis of the proposed decrease in removal capacity with age is provided by an image (Figure 8.25) of 2 year old HFO (actually crystallized goethite), which was prepared by rapid neutralization of ferric chloride and stored at 4 ^{o}C. This sample (Figure 8.25) shows very large particle size with a "mat" greater than 400 nm in size. In addition to the large particle size, there is evidence of crystallization. This demonstrates that not only does particle size change but the actual chemical structure of HFO evolves with time.
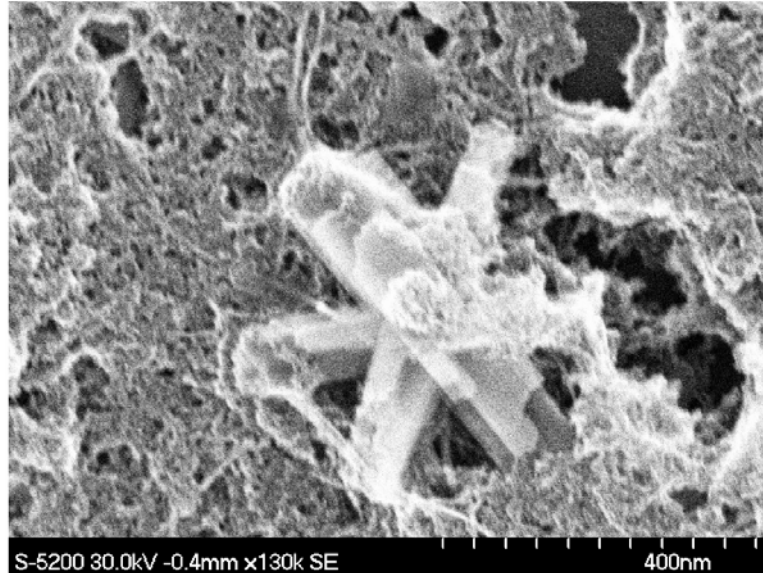
Figure 8.25. SEM image showing crystallization of HFO (likely to goethite) after 2 years

In freshly prepared solutions precipitating around circumneutral pH values, only amorphous HFOs are visible (Figure 8.23, 8.24). At lower pH values, a different type of well-defined crystal appears (Figure 8.26).
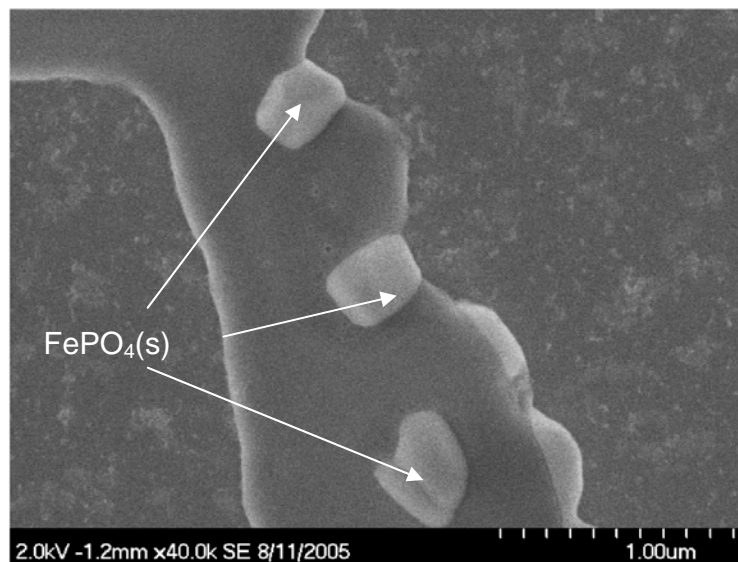
Figure 8.26. SEM image showing FePO$_4$ precipitated from a solution of 1 mg P/L as sodium phosphate and 10 mg Fe/L as ferric chloride and pH adjusted to 3.5 using sodium hydroxide)

Several samples were tested for these crystals at higher pH but no evidence indicating their presence was found at pH values above 5. This observation is consistent with the formation of $FePO_4(s)$ at lower pH and was further investigated in Section 8.7.1 in titrimetric studies.

8.7 Precipitates in the simple Fe-PO₄-OH system

8.7.1 Iron species formed in the presence of phosphate

Hydrous ferric oxide forms when acidic ferric chloride solutions are neutralized. The products of iron oxyhydroxide formation are variable depending on conditions. In particular, the rate of base addition and the aging of the sample are known to create products of variable structure (Schwertmann and Cornell, 2000). Since the conditions of HFO synthesis in this current work were variable in that different pHs were selected as the endpoint, it is necessary to determine whether the same HFO product was formed independent of the final pH. To accomplish this, the iron content of the HFO was determined by atomic absorption (AA) spectrophotometry. There were no trends versus pH in the %Fe by mass, although the value in the solid was quite variable (most of the values between 45% and 60%). The %Fe value for 6 observations on HFO formed between pH 7 and 10 was 52.7 ± 9.7 at 95% confidence level. These results suggest that the HFO prepared had a variable composition and that this variation was random and not dependent on the formation pH. For comparison the percent iron in $Fe(OH)_3$ without waters of hydration is 52 and for Geohite (FeOOH) it is 62.6. One proposed stoichiometry for HFO is $Fe_5(HO)_8 \cdot 4H_2O$ (Jambor and Dutrizac, 1998), which would have an iron composition of 57.9% by mass. The %Fe of $FePO_4(s)$ is 37.1%, so it is extremely unlikely that the precipitate has the stoichiometry of ferric phosphate.

From the literature (de Haas et al., 2000; WEF, 1998) and the data in this study it is clear that phosphate is removed from solution up to pH 8 and higher. It is proposed that co-precipitation and adsorption of phosphate ions on ferric hydroxide flocs is occurring around neutral pH values (Pierri et al., 2000). In this context, co-precipitation refers to phosphate removed during the precipitation of HFO. It is possible that the mechanism of removal is trapping of surface bound phosphate on tiny HFO flocs as the flocs accumulate and grow and does not involve pure ferric phosphate ($FePO_4$) formation.

8.7.2 Titrimetric investigation of the formation of solid FePO₄

To determine the relative significance of the precipitation and adsorption processes in P removal, titrations were performed on three systems:

1. Solution containing orthophosphate only (no ferric was added); for the calibration of the method.
2. Solution containing ferric only (no phosphate was added); in this case only $Fe(OH)_3$ solid forms.
3. Solution with ferric and orthophosphate; both $FePO_4$ and $Fe(OH)_3$ solids form.

The titration method is based on measuring pH using a glass electrode during acid-base titration in a temperature controlled environment. In all cases the ionic strength of the solution was adjusted to 0.02, close to typical wastewater. Each titration point was allowed to reach steady state before the next addition of titrant. The charge excess (b) is calculated from Eq. 8.1. This is the amount of negative charge required for electric neutrality.

The titration method was initially validated by detailed titrations of orthophosphate in the absence of iron. The method involved a fixed concentration of Na_3PO_4 (2 mM) at fixed ionic strength (0.02) and fixed temperature ($25^{o}C$). The pH of this phosphate solution was raised to 10 with sodium hydroxide and titrated to below pH 4 with standardized nitric acid. Phosphate in all dissociation states (H_3PO_4, $H_2PO_4^-$, HPO_4^{2-}, PO_4^{3-}) according to Loewenthal (1976) and NIST (2001) was considered in the model. Results are shown in Figure 8.27.
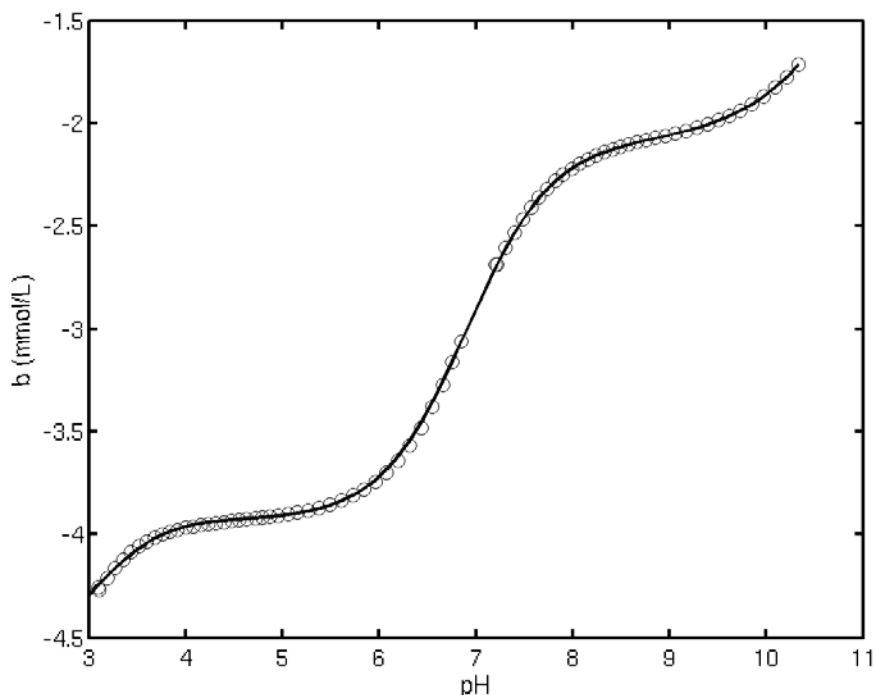
Figure 8.27. Charge excess titrating phosphate only

Subsequently, titrations were done with iron addition only, without phosphate. Ionic strength was 0.02 and total iron concentration was 1.8 mM. (Figure 8.28). Calculated charge excess is modelled with solubility constant (K_{sp}) for $Fe(OH)_3(s)$ as the only unknown. All other ionization constants for the soluble iron-hydroxide complexes $Fe(OH)^{2+}$, $Fe(OH)_2^+$ and $Fe(OH)_4^-$ are taken from NIST (2001) and corrected for ionic strength using the Davies equation. In addition, surface charging of the iron hydroxide solid is modelled using parameters from Smith and Ferris (2003).

Best-fit value of $\log K_{sp}$ for the $Fe(OH)_3(s)$ is -38.25. This compares well with the -38.6 value found in NIST (2001).

In the third set of experiments, ferric phosphate titrations were performed. Fixed ionic strength was 0.02 and total phosphate concentration was 80 mM. In Figure 8.29, three titrations are shown, with iron in varying molar ratios (0.5 to 2.0) relative to the phosphate concentration.
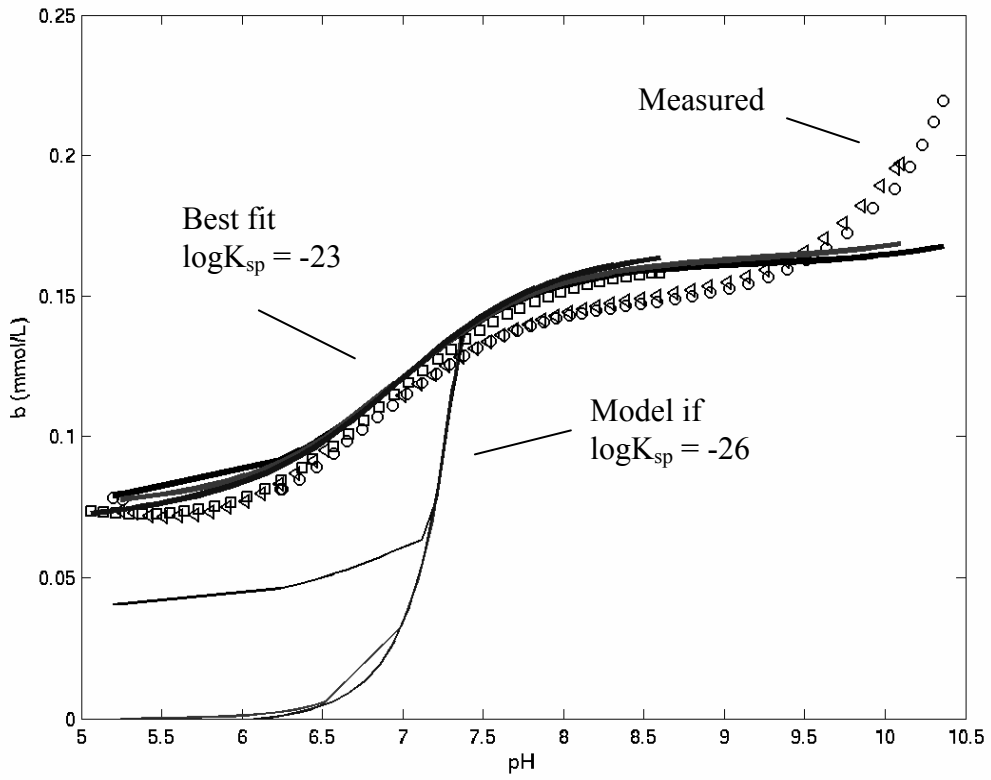
Figure 8.28. Charge excess versus pH in the ferric - phosphate system
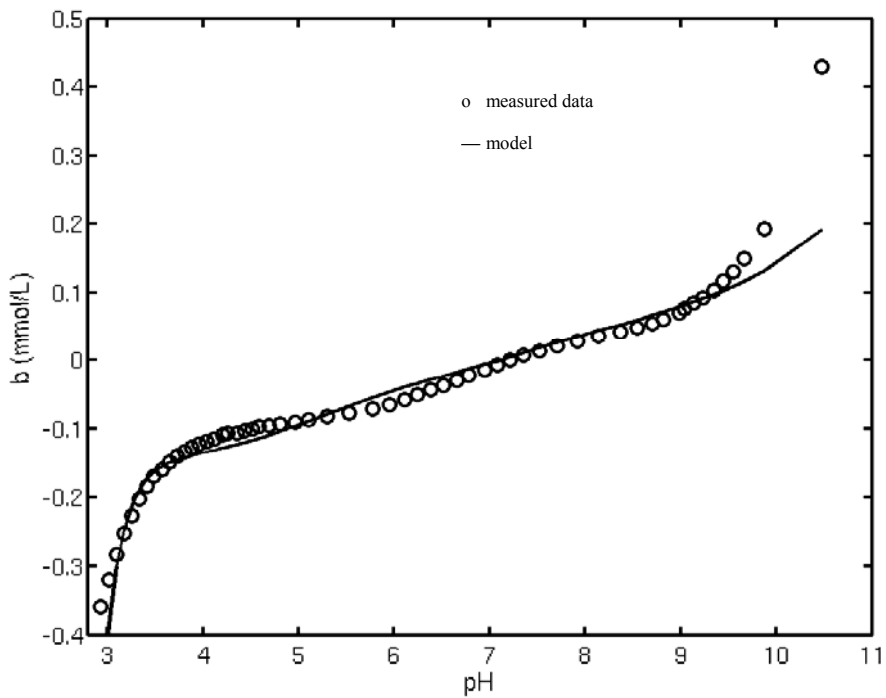
Figure 8.29. Charge excess titrating iron hydroxide

129

Calculated charge excess is modelled with K_{sp} for $FePO_4(s)$ as the only unknown. Parameters for soluble ferric-phosphate complexes $FeH_2PO_4^{2+}$ and $FeHPO_4^+$ are taken as NIST (2001) values and corrected for ionic strength using the Davies equation. $logK_{sp}$ for $Fe(OH)_3(s)$ is -38.25 from the previous experiment.

Based on these experiments, the best-fit value of $logK_{sp}(FePO_4(s))$ is lower than –23 (thick lines), meaning that no pure ferric phosphate precipitation occurs above pH 5. As an illustration, thin lines, using $logK_{sp}(FePO_4(s)) = -26$, show how charge excess would look if $FePO_4$ started to form around pH 7.2. NIST (2001) contains a range of $logK_{sp}$ values for $FePO_4(s)$, depending on particle size and form, between -21.8 (amorphous) and -26.8 (crystalline).

Based on these titrations, the following dissociation and solubility constants were obtained for the ferric-phosphate system (Table 8.3).

Using the -23 $logK_{sp}$ value for ferric-phosphate, the precipitated species are plotted in Figure 8.30 as a function of pH. Pure ferric phosphate precipitates below pH 3.5 only. A mixture of ferric phosphate and hydroxide with increasing molar ratios precipitates between pH 3.5 and 4.5. Pure ferric hydroxide precipitates above pH 4.5. From literature (de Haas *et al.*, 2000, WEF, 1998) and data in Fig. 8.1 it is clear that phosphate is removed from solution up to pH 8 and possibly higher. It is also known that co-precipitation and adsorption of phosphate ions on ferric hydroxide flocs is occurring around neutral pH values (Pierri *et al.*, 2000).

Table 8.3. Solubility and dissociation constants for the ferric-phosphate system

Component	log K (NIST)	log K (measured)
H_2O	-14.16	not measured
$H_2PO_4^-$	-2.13	not measured
HPO_4^{2-}	-7.21	-7.1
PO_4^{3-}	-12.02	not measured
$FePO_4$ (solid)	-21.8 to - 26.8	>-23
$Fe(OH)_3$ (solid)	-38.6	-38.25
$FeH_2PO_4^{2+}$	3.47	not measured
$FeHPO_4^+$	8.3	not measured
$Fe(OH)^-$	11.27	not measured
$Fe(OH)^{2-}$	21.8	not measured
$Fe(OH)^{4-}$	34.4	not measured

The model used to describe these experiments included adsorption of phosphate on ferric hydroxide (Geelhoed *et al.*, 1997). Parameters used were as in the experiment shown in Figure 8.30 (0.02 ionic strength, measured logK values where available from Table 8.3, other dissociation constants from NIST (2001), $logK_{sp}$ $FePO_4(s)$ -21.8, surface charging from Smith

and Ferris 2003). 0.08 mM orthophosphate (2.48 mg P/L) was used with Fe/P molar ratios of 2 and 4. These values are typical on the two plants investigated.
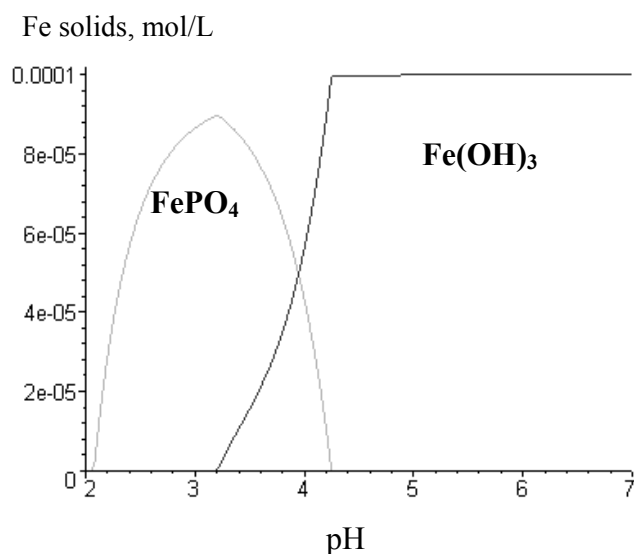
Figure 8.30. Two types of iron precipitates in
the ferric-phosphate system

8.8 Mechanism and surface complexation model

While the ferric iron solution added to the wastewater stream is acidic, sufficient alkalinity is generally present in the wastewater to neutralize it. The result is rapid precipitation of hydrous ferric oxides (HFO). These hydrous ferric oxides are probably most closely related to 2-line ferrihydrite and will occur alone or as coatings on particles (Small *et al*., 1999; Smith and Ferris, 2003). Simultaneously with the HFO precipitation, soluble phosphate is removed by either precipitation of iron phosphates, co-precipitation or adsorption of phosphate onto existing HFO particles. The removal of phosphorus can occur via many different pathways:

i.   adsorption of phosphate onto HFO;
ii. coprecipitation of phosphate into the HFO structure;
iii. precipitation of ferric phosphate;
iv. precipitation of mixed cation phosphates (*i.e.*, Ca, Mg, Fe, or Al phosphates, or hydroxyphosphates).

For consistent terminology the IUPAC definition of coprecipitation is adopted here. "The simultaneous precipitation of a normally soluble component with a macro-component from the same solution by the formation of mixed crystals, by adsorption, occlusion or mechanical entrapment." (McNaught and Wilkinson, 1997).

The work presented here focuses on the simple Fe, H, PO4 system as a starting point towards quantitative modelling of chemically mediated phosphorus removal. Most of the geochemical literature on iron and phosphate systems is devoted to item (i), the adsorption of phosphate onto preformed iron oxides (crystalline oxides or amorphous oxides, such as HFO). For example, Dzombak and Morel (1990) summarize cation and anion adsorption onto hydrous ferric oxides. This work, and extensions of it, have been included in various geochemical

131

modelling packages, such as MINEQL (Allison *et al.*, 1991). This type of modelling is a starting point since its use in wastewater treatment systems requires more mechanistic details to realistically predict chemical dose requirements and P residuals under engineering conditions. This starting point will be built upon in this model and will also incorporate pathway (ii).

Pathway (iii) was investigated and ferric phosphate precipitation in a simple Fe–PO4–H system was found to predominate only at acidic pH (5 or lower,) as described in Section 8.7.

The influence of more complicated water chemistry and the possibility of mixed precipitates (pathway iv) has received less quantitative attention but should be the emphasis of future work representing more realistic systems. Some work on item (iv) has shown that the presence of phosphate (and silicate) can dramatically affect HFO particle size (Magnuson *et al.*, 2001).

8.8.1 Complexation model for PO_4^{3-} removal

The model presented here for phosphate removal by ferric chloride addition is based on interactions between hydrous ferric oxide (HFO) and phosphate. The model is based on fundamental chemical binding principles and is designed to capture the effects of aging and mixing. The basis of the model is that iron and phosphorus share an oxygen atom. This can be represented by the following symbolic reaction (charges omitted) where the iron oxide surface is represented as FeOOH:

$$FeOOH + HOPO_3 \leftrightarrow FeOOPO_3 + H_2O \tag{8.2}$$

The exact reaction depends on the nature of the oxygen at the HFO surface, in particular the number of iron atoms sharing each oxygen. This aspect of the model is summarized by the MUSIC model applied to phosphate/goethite interactions by Geelhoed *et al.* (1997). Goethite is a crystalline iron oxide, but the mechanism of interactions is expected to be similar for amorphous iron oxide (HFO), as demonstrated by Smith and Ferris (2001a). These surface complexation reactions will also be pH dependent due to proton competition for surface oxygen and phosphate oxygen. The usual abbreviation for this type of modelling is surface complexation modelling (SCM). In the model developed here the SCM concept is generalized to include any set of molecules with similar short-range order similar to Goethite-like clusters.

The reactive oxygen atoms are termed "surface sites", the availability of which reflects mixing and aging conditions. Rapid mixing means that surface sites are readily available whereas with slower mixing much of the HFO would form in the absence of phosphate and make "internal" oxygen atoms unavailable for binding. Fresh HFO has a very open structure (see Figure 8.23) and surface sites are available. As the mineral ages though, the structure becomes more compact (Figures 8.24 and 8.25) and the surface oxygen atoms become less available for binding. Binding might still be possible but it will become diffusion limited (Makris *et al.*, 2004), which suggests that kinetics may be important. Longer term kinetic data presented in this chapter suggest that there is a two step process; a fast "equilibrium" step and a slower "kinetic" step. In this part of the work only the equilibrium process is considered. The majority of geochemical studies assume chemical equilibrium, but on timescales relevant to the wastewater treatment plant not all processes will reach equilibrium. There are competing sorption and aging limitations. The iron oxides change with time, and flocs can aggregate and change with age. This must be accounted for in a dynamic model.

8.8.2 Chemical equilibrium model

The chemical equilibrium model is divided into two parts for numerical reasons. The first part solves for the solid species present where $Fe(OH)_3(s)$ and $FePO_4(s)$ are allowed to precipitate, if thermodynamically favoured. Once the solid species are determined, a second chemical equilibrium modelling step is performed where phosphate is allowed to complex with active sites on the precipitated HFO. This second equilibration step is the phosphate complexation component of the overall model. Mechanistically, phosphate removal should be considered simultaneously with precipitation if phosphate is available. Thus, the SCM formalism is used to calculate removal during the coprecipitation step even though there are no defined surfaces present during the early stages of hydrolysis. The model describes this step through the use of the active site factor (ASF), which will be kinetically linked to initial mixing.

The first part of the chemical equilibrium modelling process is represented in Table 8.4 where the chemical reactions are represented in Tableau notation (Morel and Hering, 1993). The principle and nomenclature of the Tableau method is explained in detail in Appendix A. The reactants are given as the components across the top of the table, and the products are listed as the species in the last column. For example, the 9th row in Table 8.4 corresponds to the $FeH_2PO_4^{2+}$ formation reaction where it is necessary to combine 2 H^+, 1 Fe^{3+} and 1 PO_4^{3-} as reactants to yield the desired product. The log K value for this formation reaction is 22.11. The precipitation of potential solids is tested by comparing the reaction quotient (Q) to the solubility product Ksp. If Q is greater than Ksp, precipitation is allowed to occur. In the case of multiple precipitates the most insoluble (larger Q) is allowed to precipitate first, and iteration is subsequently performed to see if the second phase is still insoluble.

Table 8.4. Chemical equilibrium model expressed in tableau notation (Morel and Hering, 1993) for HFO and $FePO_4(s)$ precipitation.

H^+	PO_4^{3-}	Fe^{3+}	logK[1]	Species
-1	0	0	-14.04	OH^-
1	1	0	11.66	HPO_4^{2-}
2	1	0	18.64	$H_2PO_4^-$
3	1	0	20.65	$H3PO_4$
-1	0	1	-2.77	$FeOH^{2+}$
-2	0	1	-6.29	$Fe(OH)_2^+$
-4	0	1	-21.77	$Fe(OH)_4^-$
1	1	1	19.96	$FeHPO_4^+$
2	1	1	22.11	$FeH_2PO_4^{2+}$
Solids				
-3	0	1	-6.0	$Fe(OH)_3(s)$
0	1	1	21.9	$FePO_4(s)$

[1] The values for the parameters are determined from NIST (2001), and corrected for 0.02 M ionic strength using the extended DebyeHückel equation.

The numerical problem corresponding to solving for the equilibrium state of the system is to determine the value of **X** that minimizes the residuals in the mass balance. This calculation is performed as follows:

minimize R as a function of **X** where $\mathbf{R} = \mathbf{A'} \times (10^{\log C}) - \mathbf{T}$ (8.3)

and $\log\mathbf{C} = \mathbf{K} + \mathbf{A}\,\mathbf{X'}$

Minimization of the residual vector is performed using the Newton-Raphson method implemented in Matlab (The Mathworks, 2007) following the method of Smith and Ferris (2001b). In the absence of precipitate there are two elements in the **X** vector; the component concentrations, $[Fe^{3+}]$ and $[PO_4^{3-}]$. Here pH is fixed, so $[H^+]$ is known. The stoichiometry matrix **A** is 9×2 for 9 species and two components. The **T** and **K** vectors contain the total concentrations of iron and phosphate and the log K values respectively. Finally, **C** is a vector containing the concentration of each species. Concentrations in the **X** and **T** vectors are expressed as logarithms to the base 10 to ensure positive solution concentrations, and a well behaved numerical optimization.

When only one solid phase is present, either $[Fe^{3+}]$ or $[PO_4^{3-}]$ is fixed because one degree of freedom is lost and the optimization proceeds with one entry in **X**. When two solids precipitate there are no degrees of freedom and the concentrations of all species can be solved without iteration. If pH is unknown the same solution method can be used with a corresponding increase in the matrix dimensions as long as terms for the major cationic and anionic species are included so that the total hydrogen concentration can be estimated.

Once HFO is found to precipitate, a surface complexation model (SCM) calculation is run to determine how much phosphate is bound to the surface and other available oxygen binding sites as the precipitate is formed. The SCM model, shown in Table 8.5, still includes all aqueous reactions but the amount of precipitate is fixed. The stoichiometry of the surface reactions were determined based on Geelhoed *et al*. (1997). These possible surface reactions are based on spectroscopic studies as well as theoretical surface structural considerations (*i.e.*, the MUSIC model). These possible reactions on known Goethite are taken as reasonable reactions possible on the HFO surface. Even though the iron oxide formed here is amorphous and not crystalline it is reasonable that similar types of binding arrangements (Fe to O) will occur at their surface (Smith and Ferris, 2001a). These are the active phosphate binding sites. The values for the equilibrium constants in Table 8.5 were determined heuristically to describe the experimental data. The best description of the experimental data was taken as describing the lowest residual P concentrations. The idea is that these points are closest to equilibrium, which is expected to be the maximum removal of phosphate. While the exact values for log K's are different from the ones used in Geelhoed *et al*. (1997), the reaction stoichiometries are the same.

Soluble phosphorus is the sum of all phosphorus species not bound to the iron oxide surface or precipitated. In order to quantify a value for this it is necessary to determine how much phosphate capacity exists. In the tableau presented in Table 8.5 the total binding site capacity for Site 1 and 2 can be referred to as S1T and S2T. Using the same assumptions as Geelhoed *et al*. (1997), the concentration of these binding sites are taken to have the same value. These need to be related to the total iron concentration (FeT) in the precipitate, as follows:

S1T = S2T = ASF × (FeT in HFO) (8.4)

Table 8.5. Tableau notation for the SCM portion of the equilibrium model (charges omitted)

H	PO$_4$	S1[1]	S2[2]	Log K[3]	Log K[4]	Surface Species
2	1	2	0	27.65	30	S1H$_2$PO$_4$
3	1	2	0	33.8	35.5	S1H$_3$PO$_4$
1	1	0	1	15.5	20.5	S2HPO$_4$
1	0	1	0	9.2	9.2	S1H
1	0	0	1	9.2	9.2	S2H

[1] S1 is a singly coordinated surface oxygen, meaning that the surface oxygen is bound to only one iron (FeO).
[2] S2 is triply coordinated (Fe$_3$O) meaning that the surface oxygen is shared with three iron atoms.
[3] represent the log K values determined in the current work.
[4] are the log K values from Geelhoed et al. (1997) for comparison.

The crucial factor in modelling this system is the active site factor (ASF). This is related to available binding sites before, after and during precipitation and represents the fraction of reactive surface oxygen atoms per bulk Fe in the HFO. Best–fit values for ASF, given in the modelling results section, represent the only model parameter that needs to be varied to describe the data presented in Figures 8.31 and 8.32.
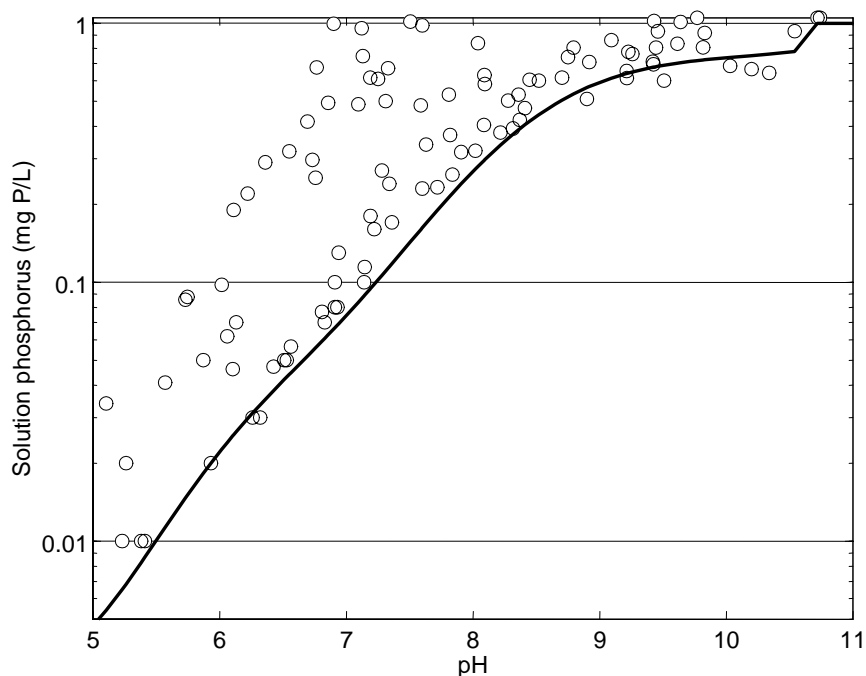
Figure 8.31. Residual P concentrations from original concentration of 1 mg P/L with 10 mg Fe/L. Iron was added from a stock solution of ferric chloride and was completely dissolved prior to pH adjustment. Data are represented as circles and the model calculation for ASF=1.18 is shown as a solid line
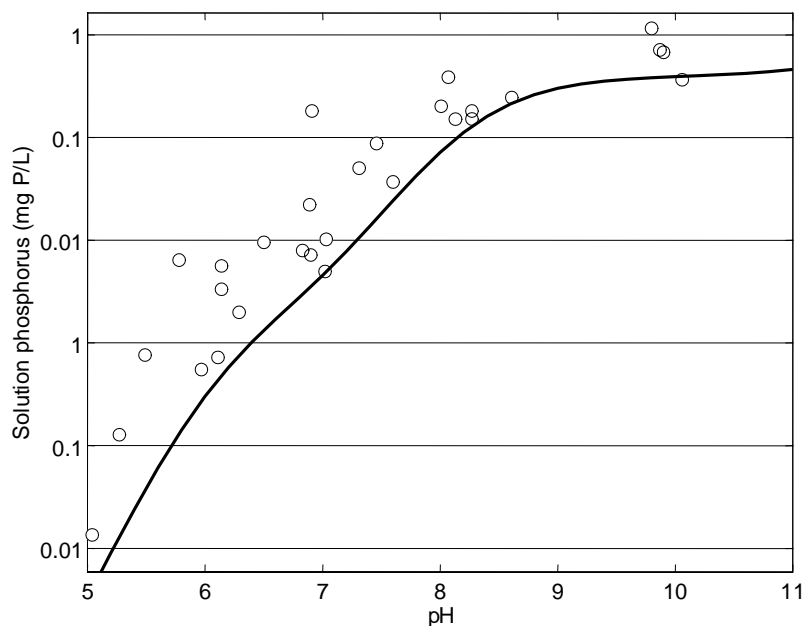
Figure 8.32. Residual P concentrations from original concentration of 1 mg P/L with 10 mg Fe/L as preformed HFO. Data are represented as circles and the model calculation for ASF=0.31 is shown as a solid line.

The value of the active site factor parameter is linked to the mixing conditions (G-value) and age of floc (SRT) through a kinetic function

$$ASF = f(G, SRT) \tag{8.5}$$

This function, together with expressions describing diffusion limitations within the floc, forms the kinetic part of the model. The exact form of the function and its parameters have not yet been determined and will be the subject of a future work.

8.8.3 Model description of the effect of pH and mixing

Figure 8.31 shows experimental data compared to the model calculation for more than 100 data points. Batch removal tests were performed with an initial concentration of 1 mg P /L dosed with 10 mg Fe /L, where a ferric chloride stock solution was the source of iron, followed by pH adjustment and 24 hour equilibration time. This corresponds to a 5.5 molar ratio of iron to phosphorus. The model qualitatively describes the data and captures the trend of greatest removal at low pH with gradual decrease in efficiency at more basic pH. Essentially no phosphate removal occurs at pH's above 9.5. With this high dose of iron it was possible to achieve residual phosphate concentrations of 10 μg/L for samples at pH values near 5.5. There is about half an order of magnitude scatter in the data, and 10 μg/L should be viewed as a best value. For pH values near neutrality the residual phosphate values were closer to 0.1 mg P/L.

Much experimental uncertainty exists in the data, likely reflecting the sensitivity of phosphate removal to the conditions of HFO formation. If the solution is well mixed then phosphate is removed as the HFO is formed; phosphate complexation occurs simultaneously with precipitation and can be termed co-precipitation. The experimental uncertainty is possibly a result of the difficulty in mixing reproducibly during base addition and HFO formation.

136

Fitting of the ASF parameter The chemical equilibrium parameters for the model plotted in Figure 8.31 are presented in Tables 8.4 and 8.5. The ASF value was the only parameter adjusted to allow the model to fit the data. The ASF value for HFO formed in the presence of phosphate was determined to be 1.18, which means that for every 100 iron atoms in the HFO there are 118 available oxygen sites for binding. Note, in surface complexation modelling these oxygen sites are just potentially available for binding but, as can be seen from the data, actual binding is pH dependent. The model takes this into account using protonation/deprotonation reactions for the reactive sites as well as the phosphate anion. To assess whether this model parameter (ASF) value is reasonable some simple scenarios are considered. For a hydrated iron atom ($Fe(H_2O)_6^{3+}$), in solution the ASF value would be 6. This is not a chemically realistic value; for energetic as well as steric reasons 6 phosphate ions would not bind to a single iron cation. But this theoretical value for a hexahydrated ferric cation does put an upper constraint on the value for ASF. For Bernalite, a mineral with stoichiometry $Fe(OH)_3(s)$ the unit cell is 0.7 nm × 0.7 nm × 0.7 nm. Using the crystal structure reported by Birch *et al*. (1993), and the visualization software Mercury (Cambridge Crystallographic Data Centre, Cambridge, UK), it is possible to estimate (count) reactive surface oxygen atoms per iron (total bulk iron). For a 1 nm cube there are 4.5 reactive oxygen atoms per iron, for a 2 nm × 2 nm × 2 nm cube this value decreases to 2.8 and the ratio is 1.3 for a 50 nm cube. Particles on the order of 50 nm in size are present in these samples (see Figure 8.23), so the maximum ASF value of 1.18 is reasonable.

This ASF value implies that 1.18 phosphate ions are bound per 1 iron atom. This ratio is very similar to the 1:1 stoichiometry for formation of the pure component $FePO_4$ which is potentially the source of the statements in applied wastewater treatment literature that $FePO_4$ is precipitating at pH range of 6-8. Indeed, $FePO_4$ is likely not precipitating as described in the previous subsection.

Figure 8.32 shows experimental data and model fit for preformed iron hydroxide flocs prepared by base addition prior to the addition of phosphate. These samples have the same total iron and total phosphate as for the data shown in Figure 8.31 but the reagents were added in a different order. The phosphate removed in this system has a minimum value of two orders of magnitude higher than in the system where HFO is generated in the presence of phosphate. This data directly shows the affect of order of addition of reagents, but also can be interpreted as demonstrating the importance of mixing in phosphate removal. Co-precipitation (the removal of phosphate via the SCM-like mechanism as HFO precipitates) is of less importance if the flocs are forming in the absence of solution phosphate, which is reflected in the ASF value of 0.31 used to describe the data in Figure 8.32. This is almost 25% of the value of the ASF value used in Figure 8.31 and results because the phosphate was not exposed to the particles as they were forming.

Implications of pH and mixing to design and operations. The data and modelling results in Figures 8.31 and 8.32 have implications for engineering design and practice. It can be inferred that mixing is important at the site of addition of acidic iron solution. Presence of dead zones (incomplete mixing) will result in a lower ASF value, thus impacting the efficiency of chemical dosage because a low sorptive capacity will result in low removal. As discussed earlier, in addition to complete mixing, the amount of mixing energy at the site of acidic iron addition is also important. Jar tests have also shown that pH has little effect between pH 5 and 7 if metal doses are large, resulting in very low residuals (less than 0.02 mgP/L). For solutions above pH 7 and for higher than 0.05 mgP/L residuals pH does effect removal as shown in Figure 8.31 and 8.32. Wastewater treatment plants typically operate in a

pH range of 6 to 8. Thus, mixing energy and pH in certain conditions are two factors that strongly influence removal efficiency, and it would be potentially beneficial to consider these factors in engineering practice.

8.8.4 Model description of iron dosing effects

A limited number of experiments were performed at higher and lower doses of iron with phosphate in the presence of HFO as it is forming. These experimental and model results are shown in Figure 8.33 using an ASF value of 1.18 for comparison purposes. High doses of iron do tend to remove more phosphate; based on model calculations levels as low as 0.1 μg/L are possible but in practice the lowest values measured were at the 5 μg/L level. It should be noted that the 0.1 μg/L value is a theoretical value calculated using the model presented in this chapter and was not measured. Also, to achieve such a low value an extreme iron dose of 55 times more iron than phosphorus would be necessary. As can be seen in Figure 8.34, obtaining reproducible data for such high iron doses is very difficult. Part of the reason for such scattered data is that the formation of HFO particles in the presence of high iron concentrations is likely different from the HFO formed in dilute solution. In practice, particles will associate with each other, and this association can be the predominant interaction in highly concentrated solutions (Anderson and Benjamin, 1990). The modelling presented in this chapter assumes no particle–particle interactions; the only surface reactions are between HFO and phosphate.
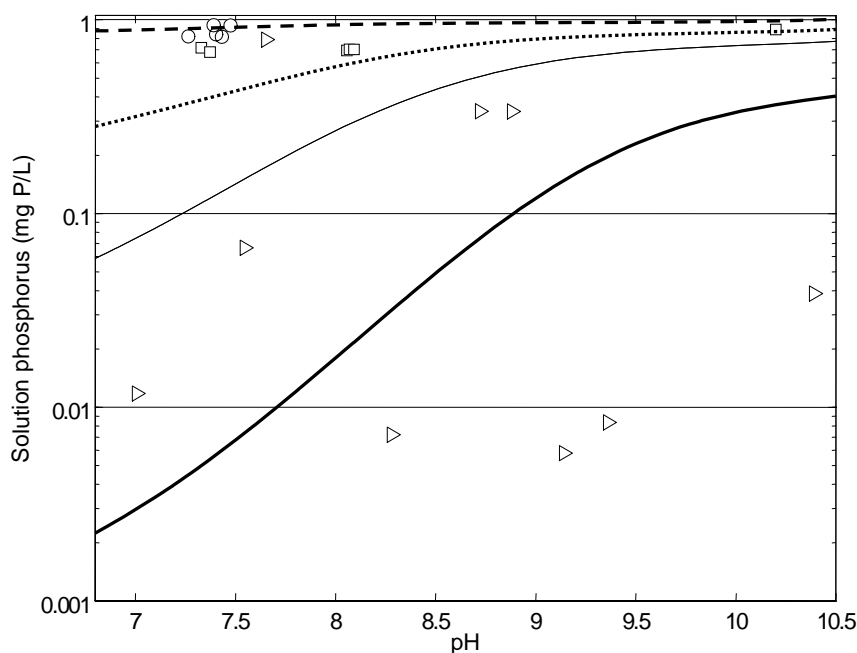
Figure 8.33. Residual orthophosphate from original concentration of 1 mg P/L with 1, 5 and 50 mg Fe/L dose from a FeCl$_3$ stock solution. Circles correspond to 1, squares to 5 and triangles to 50 mg Fe/L dose. The model calculation lines using an ASF value of 1.18 correspond to 50 (heavy), 10 (solid), 5 (dotted) and 1 (dashed) mg Fe/L.

Extreme Iron Doses To test for the particle–particle interactions mentioned above, iron overdose experiments were performed at fixed final pH of 7; HFO particles were formed by base addition in the presence of phosphate. The results of these experiments are shown in Figure 8.34. The right panel of Figure 8.34 shows that the residual phosphate decreases with

increasing molar iron dose of up to 100 moles Fe/mole P. At higher doses the removal efficiency starts to decrease, likely due to particle–particle interactions (Anderson and Benjamin, 1990). The solid line on the right side of Figure 8.34 is data interpolation (not a model calculation) to emphasize the trend. In the left panel of Figure 8.34 is a subset of the total data shown in the right panel, with model results. Phosphate removal at "lower" doses is more efficient in terms of concentration of phosphorus removed. The solid line in the right panel of Figure 8.34 represents an ASF value of 0.91, which reasonably represents the data at lower molar ratios. At higher molar ratios the 0.91 ASF value does not represent the data; a value of 0.2 is necessary to describe the higher dose data. The model calculations corresponding to an ASF value of 0.2 is shown as a dashed line in the left panel of Figure 8.34. The change in ASF can be interpreted as iron atoms predominantly being exposed to other iron atoms during the co-precipitation step and most of the HFO formation occurs in the absence of available phosphate. Thus, less reactive oxygen atoms are available for P sharing with Fe as HFO is formed.
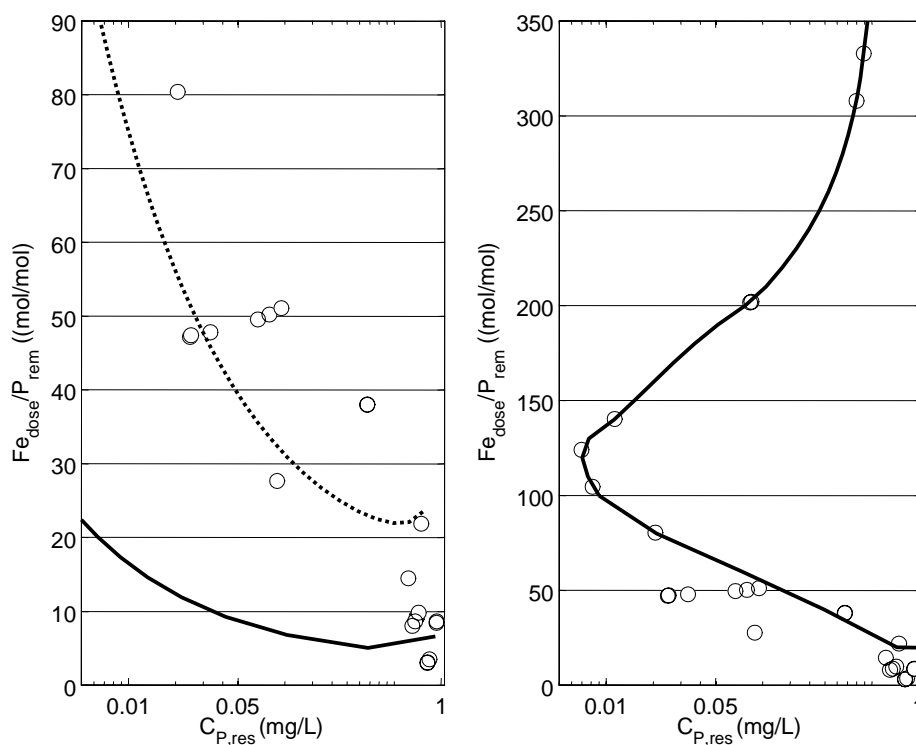
Figure 8.34. Ratio of Fe(III) dose to phosphorus removed as a function of residual soluble orthophosphate concentration. For all the batch tests the pH was fixed at 7.0 ± 0.1, and the equilibration time was set at 24 hours. In the left panel the dashed line corresponds to model calculations using ASF = 0.2 and the solid (lower) line corresponds to model calculations with ASF = 0.91. The line in the right panel is data interpolation. Symbols correspond to experimental data. Both panels represent the same data set on different scales

Implications of iron dosage to design and operations. If the mechanism proposed in this chapter is correct, then, as the molar ratio of iron to orthophosphate is increased based on random collisions, the iron particles are more likely to associate and interact with other iron particles rather than phosphate molecules, thus decreasing the efficiency of the process. At extreme Fe doses, the ASF factor is not only dependent on mixing and time, but it is also dependent on iron dose. It should be noted that the iron doses in Figure 8.34 are, for the most

part, well outside the range of engineering practice. These experiments were performed to investigate if there was a minimum measurable phosphate concentration. If phosphate is being removed by reaction with iron oxide surfaces, increasing the iron concentration should decrease the residual P. The question to address was: is there a lower limit on residual P via this removal mechanism? The minimum measured value was approximately 5 μg P/L (with large experimental uncertainty). Lower levels were not possible even with higher doses. In fact, higher doses lead to less efficient removal, which is likely due to particle-particle interactions, and these proposed particle-particle interactions limit the practical minimum residual P.

8.9 Discussion

A surface complexation model for chemical phosphorus removal using hydrous ferric oxide (HFO) was developed. Experimental results indicate that phosphorus removal occurs by two fundamental mechanisms: (i) adsorption of phosphate onto pre-formed HFO and (ii) co-precipitation of phosphate into the HFO structure. The direct precipitation of pure ferric phosphate does not appear to occur to any significant extent at pH values above 5. The second mechanism requires that phosphate be present when HFO is being formed, and it appears to occur very rapidly and is, therefore, significantly influenced by the specific mixing conditions occurring during the formation of HFO. Ortho-phosphate concentrations can be reduced to quite low values when this mechanism is functioning effectively. The first mechanism is significantly affected by the structure of the HFO, which changes with time as it "ages" and transitions from a more amorphous to a more crystalline structure. It should be noted that, on the timescale relevant to a wastewater treatment plant, the HFO should increase in density but is not likely to crystallize. The more open amorphous structure appears to allow more of the oxygen atoms in the HFO to be available for the diffusion of phosphate to active sites where oxygen atoms in the HFO and phosphate molecule can be shared via covalent bonds, thereby allowing phosphate to be removed from solution. As the HFO increases in density, diffusion is retarded which makes fewer active sites available for this reaction. The conceptual model presented here is supported qualitatively by the electron microscopic and dye adsorption experiments.

The HFO precipitation process progresses in the first few seconds and after this the oligomers accumulate and polymerize to form a network of solid HFO. If the system was well-mixed during polymerization, the HFO will contain associated phosphate occluded into the solid. In the case of typical, poorly mixed plant dosing conditions the HFO forms with much less phosphate occluded. Once this solid phase forms, the available sites for phosphate binding are drastically reduced on the surface. Deeper sites are expected to be kinetically limited through diffusion (Makris *et al.*, 2004).

The active site factor (ASF) refers to all the available sites as the HFO forms, not just terminal sites on the surface of the mineral at the end of precipitation. The ASF value of 1.18 found in the studied system corresponds to a phosphate capacity of essentially one mole of phosphate per mole of iron. Thus, the "co-precipitate" would have a stoichiometry similar to iron phosphate but a different chemical structure (*i.e.*, not a salt structure) as revealed by SEM images in this chapter.

The equilibrium part of the mathematical model does not differentiate between "soluble" and "solid" surface oxygen atoms and offers a unified description for the oxygen sharing mechanism itself. The initial fast removal in well-mixed systems and the slow removal

experienced later are described by varying ASF as a function of time and initial mixing. Further work is required to establish the form (empirical or more fundamentally based) and parameters of the function that can link initial mixing energy, the effect of time and floc aging, and diffusion to the ASF factor.

8.10 Conclusions

Batch and continuous flow laboratory experiments were conducted using synthetic and real wastewater to quantify the effect of numerous process variables on phosphorus removal efficiency using iron and aluminium salts. The following conclusions are based on the results of the experiments:

1. Residual soluble phosphate concentrations decrease as the molar dose of metal salt increases, although with diminishing returns.
2. For the practical range of pH values (above about 5), the metal content of the precipitate can be predicted based on the metal salt dose as essentially complete precipitation of the metal occurs.
3. Pre-polymerized metal salt is less efficient for phosphorus removal than freshly added and formed metal hydroxide.
4. Lowest values of soluble ortho-phosphate are obtained over the pH range of 5 to 7 for both aluminium and iron salts, with concentrations increasing for pH values outside of this range.
5. Phosphorus removal efficiency is adversely impacted by increased concentrations of alkalinity, soluble and total COD, and TSS.
6. Phosphorus removal is characterized by an initial fast removal upon the addition of metal salt, and a slower, long-term removal over time. Most of the removal occurs during the initial fast reaction, but the additional removal during the slower, long-term removal period can be significant relative to achieving low effluent soluble ortho-phosphorus concentrations.
7. Increased mixing intensity significantly improves the efficiency of the initial fast reaction.
8. Aging of flocs adversely impacts the long-term slow phosphorus removal reaction.
9. Continuous flow experiments verified the benefits of maintaining chemical flocs in contact with the process flow to achieve additional phosphorus removal.
10. An equilibrium based Surface Complexation Model (SCM) can describe the experimental results with fixed, mechanistically based chemical constants and one parameter, the Active Site Factor (ASF).
11. The ASF varies depending on mixing intensity and age of flocs and further work is required to develop a kinetic relationship that would be able to describe slow kinetic reactions in the iron-phosphate system.

PART THREE – BIOLOGICAL TREATMENT PROCESSES

9 MATHEMATICAL MODEL SUGGESTED FOR THE POWDERED ACTIVATED CARBON TREATMENT SYSTEM[8]

9.1 Objectives

The Powdered Activated Carbon Treatment (PACT) system uses a combination of activated sludge and powdered activated carbon to enhance the treatment performance in the case of high loading or difficult to degrade organics (such as in industrial plants). To be able to design a PACT system and for rigorous evaluation of experiments, a mathematical model was required that combines the biological and physico-chemical phenomena (bacterial growth, adaptation, adsorption and settling) occurring in the process. Model construction, as well as its lab-scale and full-scale calibration and verification is the subject of this Chapter.

9.2 Description of the base model

The dynamic model of Dold *et al*. (1980), a so-called bi-substrate death-regeneration model was the basis of this work. This structured model was chosen from the available set of models because it was easy to extend, flexible, yet simple enough to utilize for modelling the complex wastewater treatment technologies. In the following a short summary is given on those elements of the model, which were used in the extension. Only part of the model was used, describing the fate of organics. Nitrogen was not considered in this study.

A new concept in the above-mentioned model is the death-regeneration approach instead of the endogenous respiration theory, and the division of influent organics into four fractions. Regarding the biodegradable substances, the model takes into account the particulate matter, as a main form of influent organics. The model contains an initial adsorption step for the biodegradable suspended organics. The degradation of the stored and dissolved substrate is described by Monod-type equations. As experience shows, the utilization rate of particulate substrate is lower by about one order of magnitude than that of the soluble substrate. The rate-limiting step at the previous reaction is the extracellular enzymatic breakdown.

The structure of the Dold model is as follows:

---

[8] Based on Takács I. (1986) Application of a mathematical model for the activated sludge treatment. Water Science and Technology, Vol. 18. pp. 163-174. and Benedek P., Major V. and Takács I. (1985) Mathematical model suggested for carbon - activated sludge system. Water Research, Vol. 19, No. 4., pp. 407-413.

The raw wastewater with a COD concentration of S_0 contains four fractions of organics:

$S_{bs} = f_{bs} \cdot S_0$ soluble biodegradable fraction   (9.1)
$S_{bp} = f_{bp} \cdot S_0$ particulate biodegradable fraction   (9.2)
$S_{us} = f_{us} \cdot S_0$ soluble unbiodegradable fraction   (9.3)
$S_{up} = f_{up} \cdot S_0$ particulate unbiodegradable fraction   (9.4)

where
S_{bs} (gCOD/m^3)   biodegradable soluble substrate
S_{bp} (gCOD/m^3)   slowly biodegradable (particulate) substrate
S_{us} (gCOD/m^3)   unbiodegradable soluble organics
S_{up} (gCOD/m^3)   unbiodegradable particulate organics
S_0 (gCOD/m^3)   influent COD

with their relevant fractions (e.g. f_{bs} for S_{bs}), and the fractions necessarily add up to one:

$$f_{bs} + f_{bp} + f_{us} + f_{up} = 1 \qquad (9.5)$$

The relationship for the utilization of the soluble biodegradable substrate (S_{bs}) (degradation by Monod-kinetics):

$$\frac{dS_{bs}}{dt} = -\frac{K_{ms} \cdot S_{bs}}{K_{ss} + S_{bs}} \cdot X_a \qquad (9.6)$$

where
X_a (gVSS/m^3)   active fraction of the sludge
K_{ms} (gCOD/gVSS.d)   soluble substrate maximum utilization rate
K_{ss} (gCOD/m^3)   half-saturation coefficient for soluble substrate

The equation describing the change of the biodegradable fraction of the particulate matter S_{bp} (decreasing due to attachment to bacteria, increasing due to the organics coming from lysed cells):

$$\frac{dS_{bp}}{dt} = K_a \cdot S_{bp} \cdot X_a \left(f_{ma} - \frac{X_s}{X_a} \right) + P_a \left(1 - f_u \right) f_b \cdot X_a \qquad (9.7)$$

where
K_a (m^3/gVSS.d)   adsorption rate constant for particulate substrate
f_{ma} -   ratio of maximum substrate adsorbable on bacteria
P_a (gVOD/gVSS)   COD/VSS ratio
f_u -   unbiodegradable fraction of bacterial cell
f_b (1/d)   death rate of bacteria

The soluble, unbiodegradable organic matter passes through the system with no change.

The concentration of the particulate unbiodegradable organics (S_{up}) compared to the influent is increasing because of the organic material coming from the disintegrated cells:

$$\frac{d\,S_{up}}{dt} = f_u \cdot f_b \cdot X_a \tag{9.8}$$

The relationship for the substrate (X_s) stored on the bacteria (increasing due to adsorption and decreasing due to degradation):

$$\frac{d\,X_s}{dt} = K_a S_{bp} X_a \left(f_{ma} - \frac{X_s}{X_a} \right) \cdot \frac{1}{P_a} - \frac{K_{mp} \cdot X_s}{K_{sp} \cdot X_a \cdot X_s \cdot P_a} X_a \tag{9.9}$$

where

X_S	(gVSS/m^3)	stored substrate
K_{mp}	(gCOD/gVSS.d)	maximum utilization rate of particulate substrate
K_{sp}	(gCOD/m^3)	half-saturation coefficient for particulate substrate

The formulation for the change in the active fraction of the sludge (X_a) (increasing due to utilization of soluble and particulate substrate, decreasing because of organism death):

$$\frac{d\,X_a}{dt} = Y_h \left[\frac{K_{ms} \cdot S_{bs}}{K_{ss} + S_{bs}} + \frac{K_{mp} \cdot X_s \cdot P_a}{K_{sp} \cdot X_a + X_s \cdot P_a} \right] X_a - f_b \cdot X_a \tag{9.10}$$

where Y_h is organism yield coefficient in gVSS/gCOD

The equation for the oxygen requirement, OR (due to utilization of two types of substrate):

$$OR = \frac{dO_2}{dt} = (1 - P_a \cdot Y_h) \left[\frac{K_{ms} \cdot S_{bs}}{K_{ss} + S_{bs}} + \frac{K_{mp} \cdot X_s \cdot P_a}{K_{sp} \cdot X_a + X_s \cdot P_a} \right] X_a \tag{9.11}$$

The temperature-dependency of the substrate utilization constants:

$$K_{msT} = K_{ms,20} \cdot 1.2^{(T-20)} \tag{9.12}$$

$$K_{ssT} = K_{ss,20} \tag{9.13}$$

$$K_{mpT} = K_{mp,20} \cdot 1.029^{(T-20)} \tag{9.14}$$

$$K_{spT} = K_{sp,20} \cdot 1.1^{(T-20)} \tag{9.15}$$

where subscript T refers to parameter value at T is temperature (in ºC) and subscript 20 is parameter value at 20 ºC.

9.3 Extension of the model

As the model was intended for processing, analyzing and evaluating long-term operational results, first some simple changes were necessary. The model was implemented with variable

quantity and quality of raw wastewater simulating continuous operational conditions, (varying data series or approximate functions). The parameters involved are the organic content of the raw wastewater S_0 as well as the ratio of the different organic fractions (f_{bs}, f_{bp}, f_{us}, f_{up}) the temperature and flow rate of the sewage.

Substantial change was applied in the model by a different interpretation of the maximum substrate degradation rate constants (K_{ms}, K_{mp}). These coefficients are real constants only in the case of given environmental, operational conditions, influent sewage of certain composition and the characteristics of sludge adapted to it. When these conditions change, microbiological adaptation processes commence pushing the system toward a new equilibrium. The mathematical representation of the process consists of change of the K_{ms}, K_{ss} and K_{mp}, K_{sp} pair of constants corresponding to one state of equilibrium toward the new end conditions. The function in most cases is a simple linear function for the duration of the adaptation period:

$$K_{ms,t} = K_{ms,0} + K_{ad,m} \cdot t \qquad\qquad (9.16)$$

$$K_{ss,t} = K_{ss,0} + K_{ad,s} \cdot t \qquad\qquad (9.17)$$

where
t	(days)	time during adaptation period
$K_{ad,m}$ (gCOD/gVSS.d)		adaptation coefficient for soluble substrate (maximum utilization rate)
$K_{ad,s}$ (gCOD/m³.d)		adaptation coefficient for soluble substrate (half-saturation)

After adaptation, the value of the substrate degradation constants is kept at the final value achieved during adaptation.

The pair of constants for the degradation of the particulate substrate can be handled similarly, but for practical reasons discussed later these were left unchanged. The high value of $K_{ad,m}$ is characteristic for fast adaptation. In certain cases the function may differ from a linear equation, or even a lag-phase can be observed sometimes.

The most characteristic example for the application of the formulae discussed above is the intensification of a wastewater treatment plant by activated carbon powder (PAC) addition. This technology influences the environment of the bacteria in the activated sludge by providing support media and by means of sorption processes. As a result, the value of the K_{ms}, K_{ss} constants changes significantly.

Introducing an adsorption equation, the model was able to simulate the PAC-adding technology. Benedek *et al*. (1985) described the applied changes and assumptions, which can be summarized as follows:

In the suggested model, the PAC-addition affects the activated sludge treatment by three mechanisms:

1. The maximum specific substrate utilization rate constant "K_{ms}" for the soluble biodegradable substrate S_{bs} increases.

2. The unbiodegradable dissolved fraction of the organics present in the wastewater (S_{us}) is decreased by the activated carbon by adsorption. This phenomenon was modelled by the Langmuir-isotherm. Since this process is considerably faster compared to the biological degradation, it can be assumed as an instantaneous reaction. In the model it is taken into account by decreasing the influent S_{us} concentration with a ΔS_{us} value:

$$\Delta S_{us} = \frac{A_{m1} \cdot S_{us}}{B + S_{us}} \cdot c_c \tag{9.18}$$

where

A_{m1}	(gCOD/gPAC)	capacity of PAC for S_{us}
B	(gCOD/m^3)	half-saturation coefficient for adsorption
c_c	(g/m^3)	PAC-addition per unit influent volume

A simplifying assumption is that no adsorption of suspended solids occurs, and the effect of the PAC for the dissolved substrate is already taken into account by increasing the K_{ms} value. So adsorption is generally considered only in connection with the dissolved, unbiodegradable organic matter. This statement can be supported by two considerations:

- unbiodegradable molecules are adsorbed easier – due to their structure – on the active surface of the carbon particles,
- in the case of a biological system at steady state the ratio of biodegradable/unbiodegradable molecules is low.

Of course, under extreme conditions, e.g. at the step-like, large PAC-dosing at the start of a batch experiment, the adsorption of dissolved biodegradable molecules is also involved by an equation similar to eq. (9.18), but instead of S_{us} and A_{m1}, S_{bs} and A_{m2} (capacity of PAC for S_{bs}), respectively, are applied.

3. The settleability of the activated sludge flocs is usually enhanced, therefore the suspended solids content of the effluent decreases. This effect is modelled by decreasing the Pflanz-constant (k_{pf}, Equation 9.19).

A further modification is implemented when - for the purposes of continuous operation - the Pflanz equation (Pflanz, 1969), was introduced to the model for the description of effluent suspended solids:

$$X_E = k_{pf} \cdot v_F \left(1 + R\right) \cdot X_1 \tag{9.19}$$

where

X_E	(gVSS/m^3)	volatile suspended solids content of the effluent
k_{pf}	(h/m)	Pflanz constant for final settling
v_F	(m/h)	hydraulic surface load of settling tank
R	-	recirculation ratio
X_1	(gVSS/m^3)	activated sludge concentration

the mixed liquor total suspended solids (X_1) in the aeration basin contain four fractions:

$$X_1 = X_a + X_s + X_i + X_c \tag{9.20}$$

where

X_i	(g/m^3)	inert material (residue after volatilization)
X_c	(g/m^3)	concentration of PAC in the sludge

The model code includes a conditional statement for instantaneous withdrawal of excess sludge, by which the value of X_1 can be set to a predetermined level.

The extended model written in FORTRAN language was run first on a medium category mainframe computer (R-10, Hungarian product). The differential equations were solved using the fourth-order one step Runge-Kutta method. For practical reasons the program was afterwards rewritten in BASIC, and run on the Hewlett-Packard 85 personal computer of the Institute (RAM: 16 Kbyte). This way the model became more easily alterable and applicable in the case of in-situ experiments. Due to the limited memory capacity, two different models (though utilizing the same fundamental equations) were written for batch and continuous operation.

Under batch conditions the model describes the processes in a mixed and aerated tank filled with wastewater of known organic content after the addition of a given amount of activated sludge.

The input parameters are: S_0, T, $X_{a(t=0)}$, $X_{c(t=0)}$, and the constants shown in Table 9.1 and Table 9.2.

The model calculates the time variation of the following parameters: S_{bs}, S_{bp}, S_{us}, S_{up}, X_s, X_a and OR, as well as in the treated water:

$$COD_{filtered(t)} = S_{bs(t)} + S_{us(t)} \tag{9.21}$$

For continuous operation the model is capable of simulating a conventional or a PAC-fed activated sludge treatment plant with wastewater load of fluctuating quantity and quality. The model describes the processes taking place in the aeration basin and final clarifier under particular conditions of recirculation and withdrawal of sludge.

Input functions and parameters for the continuous model are:

Influent COD ($S_{o(t)}$), influent flow ($Q_{(t)}$), MLSS ($X_{1(t)}$), initial active biomass concentration ($X_{a(t=o)}$), PAC dose (c_c), initial activated carbon content $X_{c(t=o)}$, F_u, V_L, the frequency of excess sludge withdrawal and the parameters shown in Table 9.1 and Table 9.2. The time-based variation of the following parameters is computed: S_{bs}, S_{bp}, S_{us}, S_{up}, X_s, X_a, X_c, and in the effluent: $COD_{unfiltered}$, $COD_{filtered}$, and X_E. In addition to these the hydraulic residence time, sludge age and extracted sludge mass are determined, too.

9.4 Calibration of the model

9.4.1. Calibration in a batch system

The model was first calibrated based on batch experimental results from the literature.

Experiments of Lee and Johnson (1979) carried out in two 3 1iter vessels, fitted with a magnetic stirrer, were chosen for this purpose. The vessels were kept at 20°C, and both were filled with 300 mg/L powdered skimmed milk and 2g/L activated sludge. One of the vessels was fed with 3g/L powdered activated carbon. The mixed liquor was aerated and the samples, taken at certain predetermined intervals, were filtered for TOC determination.

Since the model requires chemical oxygen demand (COD) data representing the organic content of the water, the TOC values published (Lee and Johnson, 1979) were transformed to COD by a correlation equation. It should be mentioned, however, that the model is capable of determining the concentration of organics also in TOC if the constants are defined in appropriate units.

The substrate utilization rate parameters for the experiment with and without PAC-addition were determined from the data plotted in Figure 9.1 using a graphical method. The determined values are shown in Table 9.5. With those constants filtered COD vs. time was computed for both systems and good agreement was found between measured and computed data. The initial values of the variables are in the caption of Figure 9.1
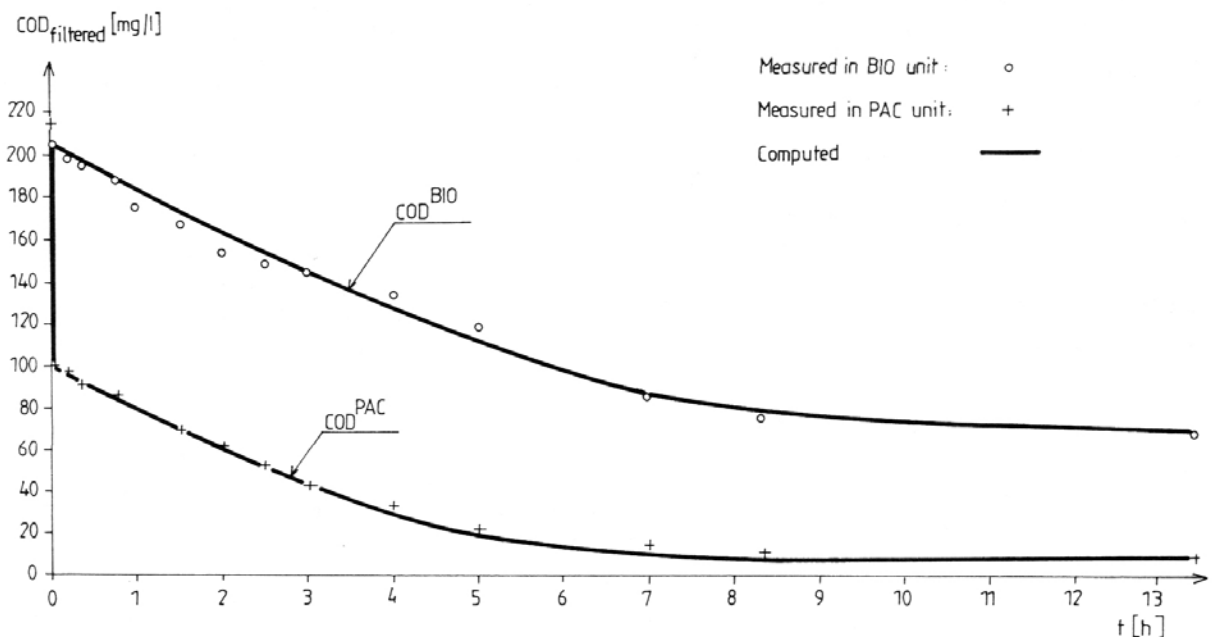
Figure 9.1. Verification of the model in batch operation. Notes: temperature 20˚C, substrate (powdered milk) 300 mg/L, substrate COD 206 mg/L, PAC 3000 mg/L, activated sludge 2000 mg/L.

Table 9.1 contains the model parameters, taken from Dold *et al*. (1980) and left unchanged in the new model.

Table 9.1. Parameters from literature

Symbol	Unit	Value
K_{mp}	gCOD/gVSS/d	3.00
K_{sp}	gCOD/m^3	0.04
F_{ma}	-	1.00
F_u	-	0.08
F_b	1/d	0.62
K_a	m^3/gVSS/d	0.25
P_a	gCOD/gVSS	1.48
Y_h	gVSS/gCOD	0.45
R*	-	1.00
* Not included in the original model		

The effect of the activated carbon powder is indicated by:

- the decrease of the soluble unbiodegradable fraction (S_{us}) from 72 to 8.5 mg/L - experienced in a very short period;
- the decrease of the soluble biodegradable fraction (S_{bs}) from 132 to 90.5 mg/L already before the start of biological processes. The decrease of biodegradable substrate due to adsorption - which is neglected under continuous operation because of the insignificant effect - is caused by the addition of considerable amount of PAC at one time;
- the increase of maximum substrate utilization rate, K_{sm}, in the PAC-fed system (see Table 9.5).

9.4.2. Calibration in a continuous flow system

For the verification of the model in continuous operation, continuous flow bench-scale experiments and batch tests on the adapted sludge were carried out. First the continuous experiments have been completed in order to obtain adapted organisms. The wastewater chosen for the experiments carried out in Fleps-type respirometers (Fleps, 1974) was prepared daily by pouring 125 mL of skimmed milk to 50 L of water. The data of analysis for this synthetic wastewater is shown in Table 9.2.

The wastewater was fed to the two parallel apparatus by a peristaltic pump. The circumstances during the adapting period in the experimental instruments are shown in Table 9.3.

The adaptation period took about 3 weeks; reaching the steady state was indicated by the gradual improvement and stabilization of the effluent quality, and the white colour of the sludge. Parallel with the whitening of the sludge in the non-PAC unit the density of the flocs decreased sharply, causing a drop in the settleability due to the single component substrate. Therefore 100 mg fine quartz sand dose per day was added to unit "A" for the enhancement of settleability. This treatment was unnecessary in unit "B".

Table 9.2. Synthetic wastewater quality

Milk content	2.5 ml/L
Unfiltered COD	510 ± 15
Membrane-filtered COD	293 mg/L
Unfiltered BOD_7	360 mg/L
Membrane-filtered BOD_7	210 mg/L
Suspended solids	188 mg/L
Volatile fraction of SS	183 mg VSS/L
Total phosphorus	4.4 mg/L
NO_3 - N	4.2 mg/L

After 3 weeks the flow rate was decreased by 50% and the units were run for one more week with this load.

The results of this experiment are shown in Table 9.4. The statistical evaluation was performed using the Student's t-test at a 95% probability level.

Table 9.3. Parameters of continuous experiments

	Unit A (BIO)	Unit B (PAC)
Reactor volume (l)	1	1
Area of final settling tank (cm^2)	25	25
Flow rate (L/h)	0.33	0.33
Retention time (h)	3.0	3.0
Hydraulic load of settling tank (m/h)	0.13	0.13
Organic load (kgBOD/(kgMLSS·day))	0.98	1.03
Mixed liquor suspended solids (g/L)	2.9	4.0
PAC-addition (mg/L)	0	110
Ratio of PAC in sludge (%)	0	31
Frequency of sludge withdrawal (1/d)	1	1
Recirculation ratio (-)	1	1
Sludge age (d)	2.6	2.5

The simulations which were computed using the constants determined this way are shown in Figure 9.2. The fitting of curves to the measured data is satisfactory.

After the completion of the continuous experiments, batch tests were performed in 2 m high, 5 liter tubes aerated at the bottom. The activated sludge came from the continuous reactors, where previously it was concentrated to 5 and 6 g/L, respectively.

Table 9.4. Continuous experiment results

	Unit A (BIO)		Unit B (PAC)	
Analysed Parameter	Q=0.33 L/h	Q=0.15 L/h	Q=0.33 L/h	Q=0.15 L/h
Unfiltered COD (mg/L)	116 ± 16	100 ± 7	71 ± 9	59 ± 3
Membrane-filtered COD (mg/L)	60 ± 7	44 ± 3	33 ± 10	31 ± 2
Unfiltered BOD_7 (mg/L)	31 ± 11	20 ± 9	16 ± 5	14 ± 7
Membrane-filtered BOD_7 (mg/L)	18 ± 9	9 ± 2	9 ± 4	6 ± 5
Suspended solids (mg/L)	43 ± 6	39 ± 10	22 ± 8	18 ± 4

Before starting the experiment the sludge was washed and aerated with tap water for 24 h, to remove the stored substrate. Then the sludge was washed again and 15 ml of skimmed milk added, and, after an immediate sampling, PAC was added to the unit B to reach a PAC-concentration of 1.3 g/L. This unit was sampled again and the sampling continued for 7 h, with the last sample being taken the next day after 22 h. The samples were filtered and stored in a cold place. The analysed samples were membrane-filtered.
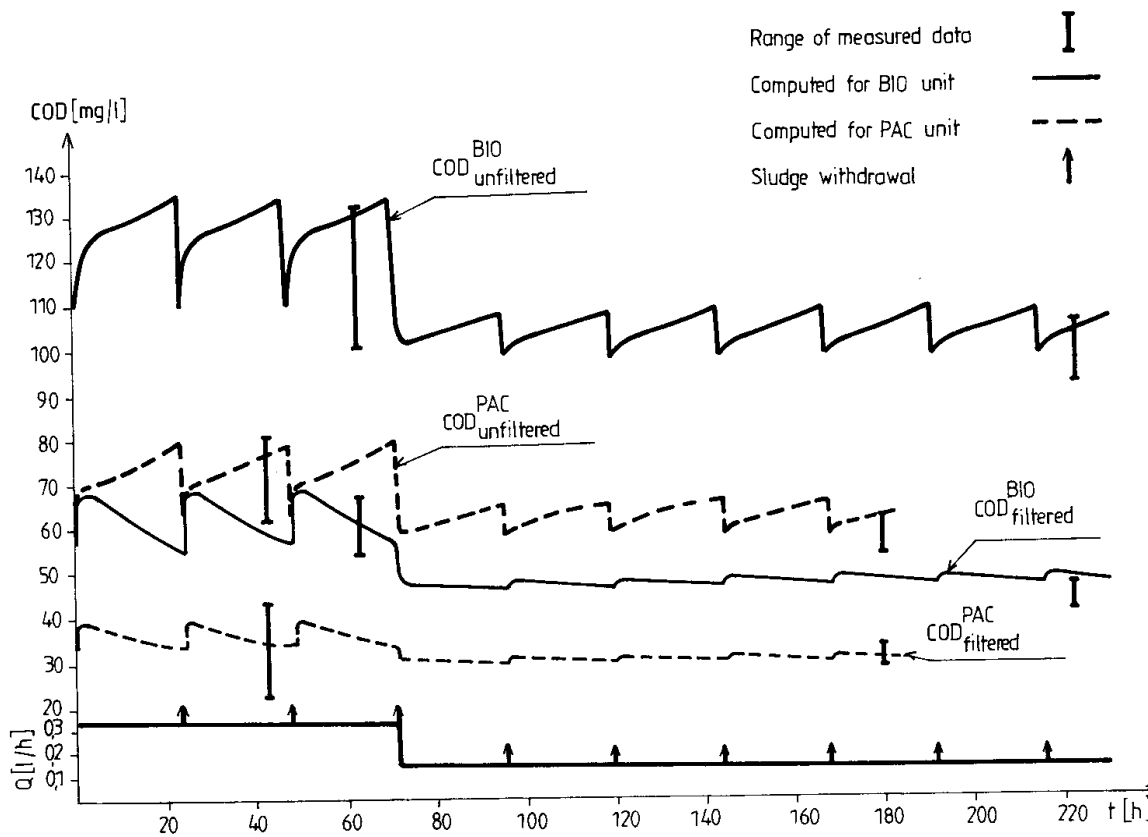
Figure 9.2. Simulation of the model in continuous operation. (The saw-like look of the simulated COD curves is due to intermittent sludge removal and the increase in sludge concentration (X_1) between two excess sludge removal events).

154
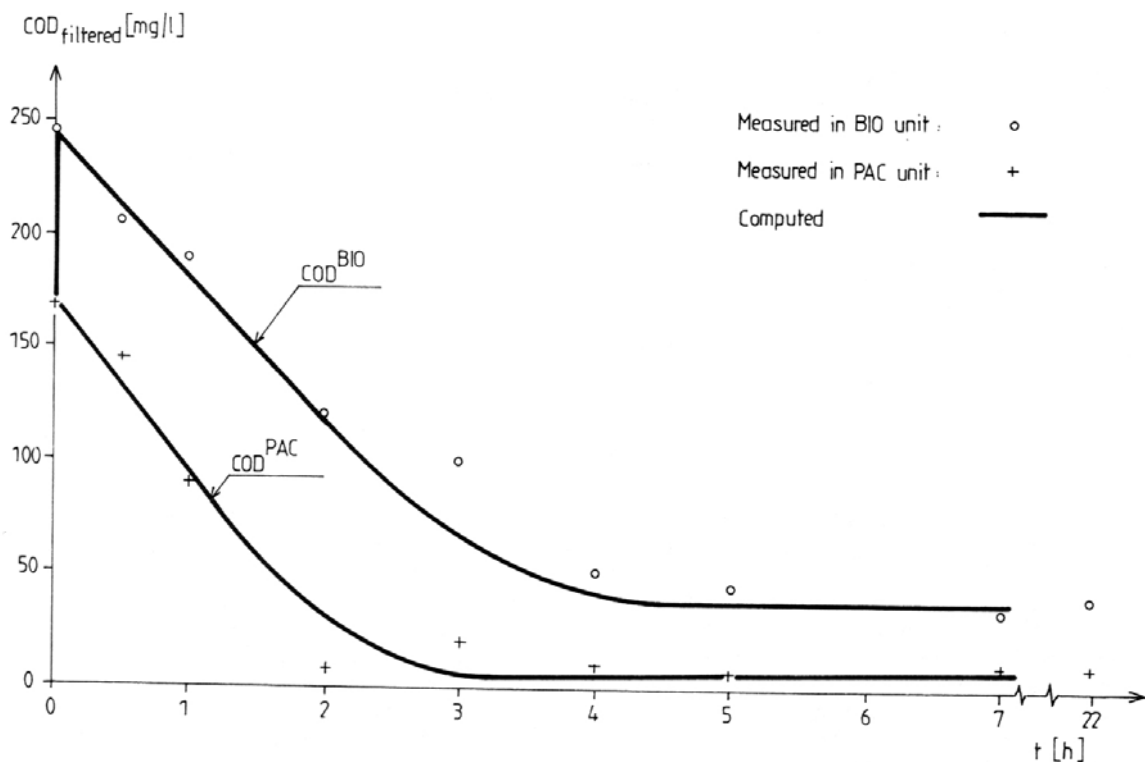
Figure 9.3. Verification of the model with batch experiments using the adapted sludge from the continuous tests.

The next step was the evaluation of these results. First the constants representing the organic fraction of the wastewater were determined on the basis of the data shown in Table 9.2 and of the equilibrium of the batch experiments. These constants can be found in Table 9.5 with the note "continuous model". The substrate utilization rate parameters were determined from the batch data shown in Figure 9.3 with the method described. The values of all the other constants were left unchanged as shown in Table 9.5

9.5 Application of the model in a chemical factory

In the fall of 1983 a full-scale experiment had been performed in Balatonfűzfő, at the wastewater treatment plant of the Nitrochemical Works (NIKE). The purpose of the experiment was to investigate the upgrading of the biological units, faced with overload and operational difficulties, by powdered activated carbon (PAC). The results of the experiment were published by Benedek *et al.* (1986). An evaluation of the results utilizing the mathematical model was performed, which is summarized below.

The wastewater to be treated on the biological treatment plant of the NIKE is a strong sewage typical to organic chemical industry. Prior to biological treatment it is submitted to neutralization, settling and equalization. There are two important properties of this wastewater. Firstly, its quality changes markedly in spite of the equalization and pretreatment due to start up and stopping of the different technological processes. Secondly, the organics present are mainly biologically degradable. Examining the composition of the sewage, this latter property is not evident as the main groups of the organic compounds contained in the wastewater are: substituted phenols, derivatives of benzene, nitrated aromatic substances, derivatives of aniline, chlorinated hydrocarbons, solvents, pesticides, etc. An unadapted activated sludge is not able to decompose these compounds; moreover it even loses a

155

significant part of its activity through contact with a greater concentration of them. However, the adapted sludge of the treatment plant consumes quickly and easily a large part of the above-mentioned organics.

During the three-month long experiment one of the biological units had been operated without PAC-addition, as a control unit, while the other had different doses of PAC. 19 parameters were tracked based on daily composite sampling. In addition, a gas chromatographic research started using a Perkin Elmer Sigma 3B GC for determining the change in the concentration of particular micropollutants.

The experimental results are plotted on Figure 9.4. The figure consists of three curves. The uppermost curve represents the direct chemical and total oxygen demand (COD and TOD) values (whichever was available) of the treated wastewater. In its original form this is hard to evaluate because of the large fluctuation of influent quality. Therefore, the relative performance is plotted below. Relative performance (RP) is defined by the following equation:

$$RP = 100 \left[\frac{1 - \eta_{PAC}}{1 - \eta_{BIO}} - 1 \right]$$

(9.22)

where η is treatment efficiency (-)
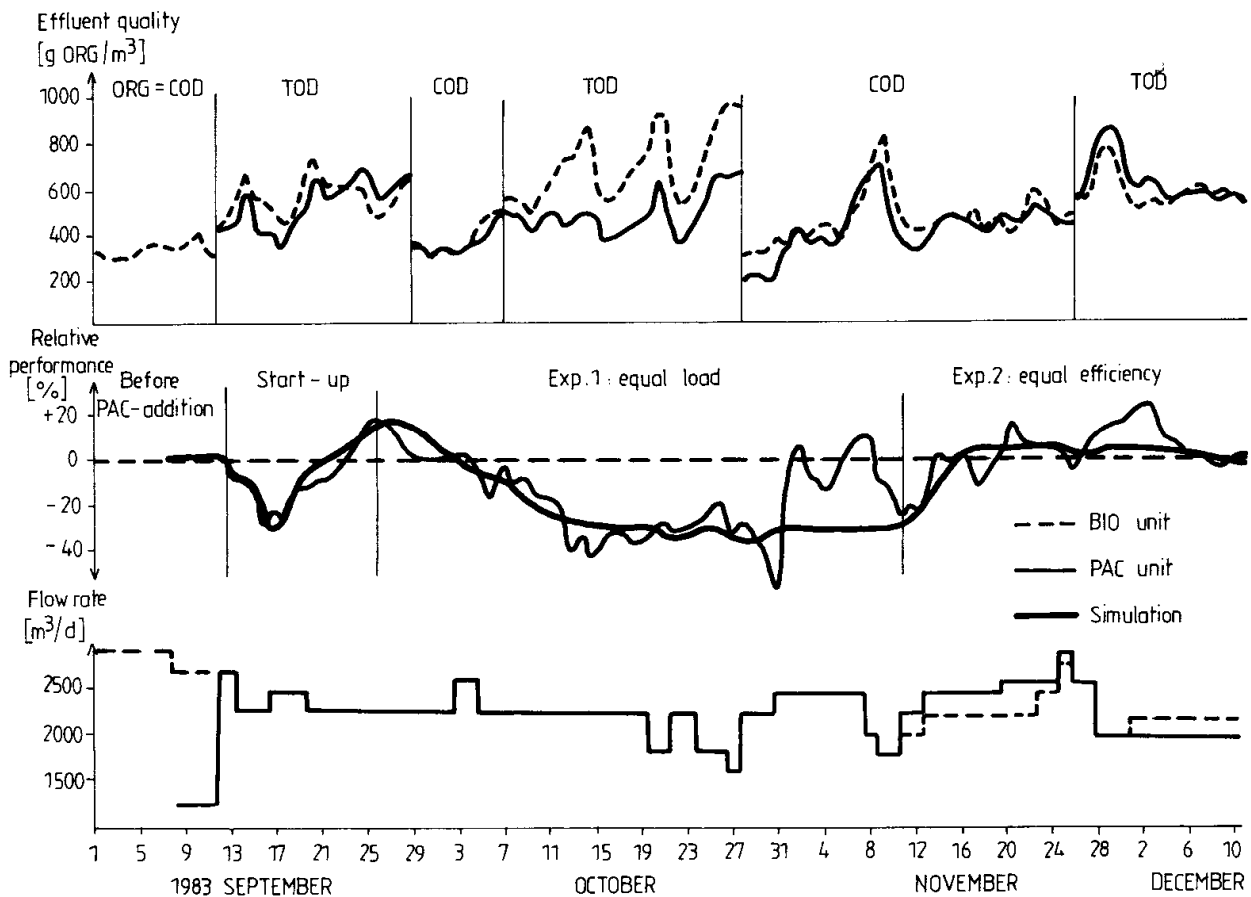
Figure.9.4. Experimental and simulation results for the Nitrochemical Works (dashed line - BIO unit; thin line – PAC unit; thick line: simulation)

156

On the lower part of the figure the flow rate is plotted. The experimental work can be divided into four well-defined periods, as indicated in the figure.

The experiment was started by adding an extra amount of PAC to the experimental unit on 15th and 16th of September 1983. The direct adsorption effect of the addition is easily observable in the sudden increase in the efficiency but then the PAC-unit became worse and only after a two weeks' adaptation period exceeded significantly the efficiency of the control unit. The organic content of the PAC-unit's effluent applying equal load and 70 g/m^3 PAC-dose in the first month was 30-40 % lower than that of the other unit, i.e. instead of an average 600 g/m^3 it decreased to 400 g/m^3. The treatment efficiency approached reliably the value of 85 %, while that of the control unit decreased below 80%, occasionally down to 67%.

After another two-week period a relative overload compared to the control unit was applied to the PAC-system in order to establish the potential increase in hydraulic capacity presuming equal effluent quality. The PAC-dose applied was 110 and 50 g/m^3, respectively, and 10 to 17 % increase in hydraulic load was achieved. It must be emphasized that this result was achieved in an under-aerated experimental system with DO limitation. Under proper operational conditions in the aeration basins 20-30 % capacity increase can easily be achieved based on sludge-activity determinations.

In the course of the experiment, batch degradation runs were performed with the sludge of both units. The K_{ms}, K_{ss} values indicated in Table 9.5 were obtained by evaluation of these results. As the values of these coefficients altered markedly during the experimental period, equations (9.16) and (9.17) were applied here with the determined $K_{ad,m}$ and $K_{ad,s}$ slopes (see Table 9.5). Also the various organic fractions were determined on the basis of daily COD and BOD tests. These values slightly varied, which was taken into account in the course of running of the program by data series. In addition, an approximate function was created for the temperature, which decreased continuously during the three months:

$$T_t = 5.7 \, e^{-0.03t} + 19.8 \qquad\qquad (9.23)$$

where t = 0 is the starting day of the experiment.

The value of the Pflanz-constant (K_{pf}) was determined by trial and error, fitting the simulation curve to the measured effluent suspended solids content. Four different values were determined for the four experimental periods.

Finally, only the adsorption constants represented in Equation 9.18 were unknown. Since these constants can be determined in separate wastewater - activated carbon system theoretically, a test was done and the values obtained this way. According to expectations the simulation curve differed from the experimental results in this case, as the activated carbon influences the treatment efficiency not only by simple adsorption, but by its continuously renewed active surface. This phenomenon of bioregeneration is well known in the literature. Its virtual effect is a large increase in the value of the A_{m1} constant. Accordingly it was increased until the best fit of the curves was reached.

At the start-up the added large amount of activated carbon certainly adsorbed also biodegradable organics, so in this period a value was assigned to the A_{m2} constant, too (see Table 9.5).

The program run utilizing the determined constants listed in Table 9.5 gave good match to the experimental results. The simulation curve is indicated in Figure 9.4. The fit is obvious, though evidently the model is unable to follow the stochastic fluctuation of the effluent quality, and the decrease in activity due probably to toxic substances encountered at the end of the third period. Due to the random character of toxic loads there is currently no way to include these in the simulation.

9.6 Discussion

On the basis of the experiences gained during the work and presented here the applicability of the model at operating industrial treatment plants is shown. Interesting conclusions can be drawn regarding the values of different parameters under varying conditions. The increase of the K_{ms} parameter in response to the PAC-addition indicates a direct relationship between the biological activity and the adsorbent present in the system. It is also worth noting that the value of this parameter is nearly as high in the case of chemical industrial wastewater as for the easily degradable synthetic solution containing milk (see Table 9.5).

Table 9.5. Values of parameters for different applications of the model

	Dold *et al.*	Lee and Johnson		Lab tests		Nitrochemical Works			
		BIO	PAC	BIO	PAC	Period 1	Startup	Exp. 2	Exp. 2
F_{bs}	0.24	0.22	0.22	0.40	0.40	0.42	0.41	0.42	0.39
F_{bp}	0.62	0.61	0.61	0.38	0.38	0.28	0.28	0.26	0.27
F_{us}	0.05	0.12	.012	0.07	0.07	0.21	0.22	0.24	0.25
F_{up}	0.09	0.05	0.05	0.15	0.15	0.09	0.09	0.08	0.09
K_{ms}	8.00	0.44	0.50	4.2	7.5	3.1	2.6	5.8	5.8
K_{ss}	20.00	37.1	37.7	34.0	27.0	28.0	33.0	26.0	26.0
$K_{ad,m}$	-	-	-	-	-	-	-0.04	0.15	-
$K_{ad,s}$	-	-	-	-	-	-	0.4	-0.33	-
K_{pf}	-	-	-	$2.2\ 10^{-3}$	$0.7\ 10^{-3}$	$3.3\ 10^{-3}$	$8.1\ 10^{-3}$	$5.2\ 10^{-3}$	$4.7\ 10^{-3}$
A_{m1}	-	-	0.03	-	0.14	-	0.40	2.8	2.8
A_{m2}	-	-	0.02	-	0.0	-	0.12	0.0	0.0
B	-	-	30.0	-	18.0	-	47.0	47.0	47.0
T	varies	20	20	18	18	Determined from Equation (9.23)			

There is a large difference between the value of the adsorption parameters determined for the two types of wastewater, probably due to the much greater portion of unbiodegradable molecules in the industrial sewage. The high value which is unrealistic in a non-biological system, is itself characteristic for the PAC-process. To make the applicability of the model as wide as possible the task will be to collect and compare these parameters (above all those

describing the substrate degradation and the adsorption processes) for different types of sewage and different operational conditions. After collecting suitable experience, reliable forecasts are expected by applying this model.

Nevertheless, the model still requires further improvement. For example, a fraction of the unbiodegradable organics can be considered as toxic, mostly in the case of industrial wastewater, like that of the Nitrochemical Works. A relationship is planned to be developed to describe the connection between this fraction and the biological toxicity tests, and the decrease of toxicity due to the treatment. Also the active microorganism content of the raw sewage is worth incorporating into the model, as in most cases it helps to restart a plant, the activated sludge of which has lost its activity due to some toxic effect. On the other hand, in the case of certain industrial wastes free of microbiological activity, this effect is not important, which makes them more vulnerable to toxic loads. The model seems to be suitable for this extension.

Some effort should be made to determine a better relationship between the hydraulic properties of the final settling tank, the settleability (Mohlmann index) and amount of active biomass and the effluent suspended solids with the aim of providing real forecasts for this important parameter. Also a method should be found for determining the parameters characteristic for the particulate substrate removal. In the course of the work, when such a parameter (without an accepted measurement method) was encountered, the value given by Dold *et al*. (1980) was accepted.

9.7 Conclusions

The mathematical model described in this chapter is an attempt to simulate an integrated wastewater treatment technology called the powdered activated carbon-fed activated sludge (PACT) system. Types of system equations describing biological (organics degradation and cell death), physico-chemical (adsorption and phase-separation) processes are included in the model. The main object of the study was to provide a useful model for engineering design. The model was calibrated for both batch and continuous operation on the basis of experiments carried out at VITUKI, in a full-scale industrial plant and from literature sources.

Using the model, more information can be obtained on the advantages and limits of the PAC-fed activated sludge system on the basis of simple bench-scale experiments in a relatively short period of time.

9.8 In context: the PACT model

From the late 60s and in the 70s of the last century several research groups, including the one at UCT, at that time with the direction of professor Marais, has been working on structured steady-state and later dynamic models for the activated sludge process. In spite of this, the standard in activated sludge modelling at the beginning of the professional career of the author was using traditional, unstructured models based on MLSS, BOD etc. and empirical relationships, such as observed yield. In these models, mass balance is not an important concept. The Dold model (Dold, 1980) was published (and became a precursor to all ASM models) as the first structured and rigorously mass (COD) balanced based approach. It speaks to the vision of Dr. Pál Benedek and his wide overview of the professional field, to have selected the Dold model as basis for the model development process that VITUKI was embarking on. Hungary had seen unprecedented growth in certain areas, specifically tourism

around Lake Balaton, and the local treatment plants were overwhelmed. Frequently, a community of 10000 people grew almost ten-fold during the summer months. Some plant operators were referring to their plants as "pumping stations"… and residence times of 20 minutes were known to have occurred. Powdered activated carbon dosing was a temporary help to alleviate the effects of organic and hydraulic overload for short periods of time. (It also provided entertainment to plant personnel when the Benedek team members, after manually dosing powdered carbon packaged in 30 kg bags with average particle size of 40 μm in the wind, resembled chimney-sweeps more than scientists). A model was required to be able to design these systems that utilized biological as well as physico-chemical (adsorption) processes within the activated sludge. Due to the limited computational capacity at hand in those days (before the superfast 1 MHz IBM XT was available), the model could only contain a few simple equations. It is worthwhile to remember that some of those equations that describe the biological activity in the Dold model, for example for sludge production and oxygen demand, still form the basis of the ASM series.

The PACT model has been cited several times in the literature (Specchia *et al.*, 1988; Márquez and Costa, 1996; Mesdaghinia *et al.*, 2001; Mazumder and Dikshit, 2004).

Much later the PACT model has been implemented in a commercial simulator and used in chemical treatment plants where powdered activated carbon added directly to the activated sludge was used primarily to improve the colour of the effluent and settling properties of the sludge (Takács *et al.*, 1998). Due to the workings of business environments both in wastewater modelling and in chemical industry, the author was unable to use the model or report on newly available data when assembling this thesis.

10 DIRECT PARAMETER EXTRACTION FROM RESPIROGRAMS FOR WASTEWATER AND BIOMASS CHARACTERIZATION[9]

10.1 Introduction

Respirometry is the measurement of the oxygen consumption rate of activated sludge under well defined experimental conditions. The measurement is often displayed by means of a respirogram, that is: a graphical representation of the respiration rate as a function of time. Respirometry is a well established method to deduce important kinetic information about the activated sludge (Spanjers and Vanrolleghem, 1995; Giroux et al., 1996; Vanrolleghem et al., 1999). Recently, methods have been developed to numerically fit model-generated and measured respirograms and thus optimise (identify) model parameters indirectly (Vanrolleghem et al., 1995). This Chapter proposes and describes the development of an alternative method to extract the information contained in a respirogram

The proposed method is novel in that it is "direct": it does not use a numerical optimisation routine, but through a series of numerical transformations the kinetic and stoichiometric parameters are directly calculated. The direct respirogram evaluation method described in this chapter tries to emulate the way an expert looks at a respirogram (but is not a knowledge based expert system). From the characteristic shape, the shoulders, tail end steepness, and areas associated with each component a scientist familiar with respirograms can estimate the number of identifiable wastewater components, and associated parameters. The proposed method, using the characteristics of first and second derivatives of the respiration rate, separates the respirogram into individual components, and calculates maximum respiration rate, saturation coefficient and oxygen to component conversion factor (or yield) for the components.

The method has advantages and limitations compared to parameter optimisation methods. A definite advantage is the simplicity of the straightforward evaluation method. There are no complications involving modelling, optimisation, and model identifiability. The parameter extraction calculation is model independent, even though the principle implies the Monod saturation term. The method can be used to evaluate numerous respirograms, generated by e.g. an automatic respirometer, and to help deciding about the proper model structure.

The most important limitation is that only certain types of respirograms can be identified. Individual components must be dominant (i.e. their rate of change must determine the shape of the respirogram) during a critical phase in the respirometric experiment, when the component concentration is nearing exhaustion. A properly performed respirometric

---

[9] Originally published as Spanjers H., Takács I. and Brouwer, H. (1999) Direct parameter extraction from respirograms for wastewater and biomass characterization. Water Science and Technology 39:4 pp. 137-145.

experiment, or series of experiments is necessary to generate respirograms with enough information content for the evaluation method.

This chapter describes in detail the direct respirogram evaluation method and the specific conditions that must be satisfied for correct evaluation. The method is tested on simulated respirograms and a number of real respirograms of various characteristics. The results from the direct respirogram evaluation method are compared to those from a parameter optimisation method.

10.2 Method

10.2.1 Characteristic features of a respirogram

The following features are identifiable in a properly developed respirogram (Fig. 10.1):

1. endogenous baseline before sample addition (first endogenous);
2. sudden increase in respiration rate due to sample addition;
3. peak respiration rate;
4. sustained respiration (very slow decline): one or several components close to saturation concentration;
5. shoulder (rapid drop): component is about to be oxidised;
6. baseline after complete substrate oxidation (second endogenous).
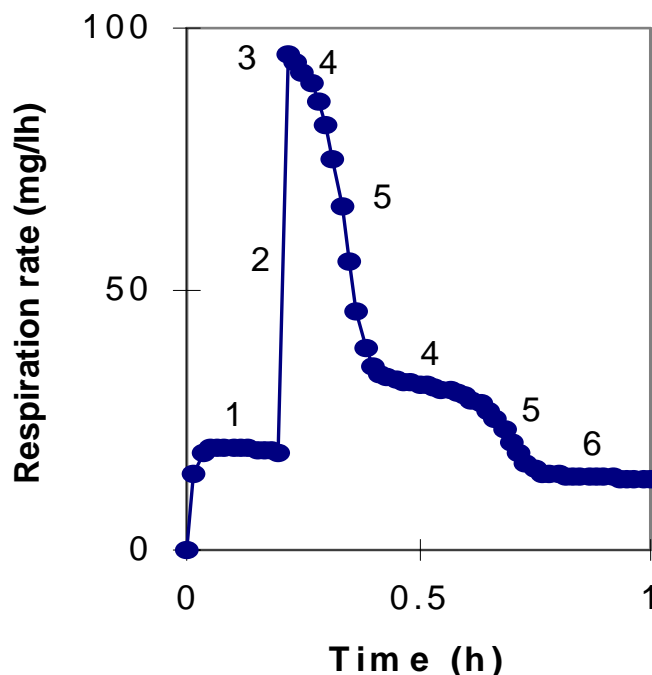
Figure 10.1. Characteristic features of a batch respirogram

There may be several repetitions of steps 4 and 5, according to the number of identifiable components. The example respirogram in Fig. 10.1 shows two components. Note the inflection points in the curve where the respiration rate drops rapidly. For Monod-type

162

kinetics this inflection point corresponds to a component concentration of half its saturation coefficient K.

The respiration rate associated with the oxidation of a component is given by:

$$r(t) = \frac{r_m S(t)}{K + S(t)} \tag{10.1}$$

where $r(t)$ is the measured (total) respiration rate $r_{tot}(t)$ minus the baseline respiration rate $r_b(t)$ for the particular component:

$$r(t) = r_{tot}(t) - r_b(t) \tag{10.2}$$

and the maximum respiration rate r_m is a parameter combination of yield Y, biomass concentration X_B and maximum specific growth rate μ_m of the biomass:

$$r_m = \frac{\gamma - Y}{Y} X_B \mu_m \tag{10.3}$$

where $\gamma = 1$ for carbon and 4.57 for ammonium. In the inflection point the second derivative of $r(t)$ equals zero. Solving $d^2 r(t)/dt^2 = 0$ yields:

$$\frac{d^2 r(t)}{dt^2} = 0 \quad \text{if} \quad S(t) = \tfrac{1}{2} K \tag{10.4}$$

The component concentration at any time is obtained by integrating $r(t)$ over the interval from t to the time instant t_e when the component is completely oxidised:

$$S(t) = \frac{1}{\gamma - Y} \int_t^{t_e} r(t) dt \tag{10.5}$$

Hence, by identifying the inflection points of a component in the respirogram we can obtain a numerical value of the component's saturation coefficient. Furthermore, it can be shown that the maximum respiration rate for a specific component can be obtained from the respiration rate at the inflection point:

$$r(t_{inflec}) = \tfrac{1}{3} r_m \tag{10.6}$$

10.2.3 Conditions required for respirogram evaluation

There are several analytical and environmental conditions which are required to produce a well-defined respirogram: the wastewater and sludge samples are representative for the treatment system under study; temperature and pH must be kept constant in the measuring system; the respirometer must be properly calibrated. These conditions belong to the actual measurement techniques and are not detailed here. We assume that the respiration rate values that are analysed are correct within a certain measurement error. The specific conditions that must be satisfied by the respirometric method are listed below.

163

Endogenous baseline — Correct results can only be obtained from full respirograms, where the measurement of respiration started before substrate addition, in an endogenous state, and was continued until all substrate added was oxidized and endogenous respiration was achieved again. Correct estimation of the endogenous respiration during the whole experiment is crucial. Endogenous respiration can change due to dilution (sample addition) and change in biomass activity. In an ideal case, the endogenous respiration is assessed both before and after sample addition (in Figure 10.1 stages 1 and 6, respectively). If endogenous values are only available from either the first part or the last part of a respirogram (stages 1 and 6, respectively), these values must be used to assess the endogenous rate during the course of the respirogram, taking into consideration the dilution. This method will reduce the accuracy of the respirogram evaluation.

Appropriate data frequency — To obtain a smooth respirogram it is necessary to gather data frequently enough - typically a minimum of 5 to 10 data points per identified component are desirable. This amounts to 30 to 50 data points in a typical respirogram, including the two endogenous stages. If less resolution is available, it is still possible to fit a smooth curve through fewer data points. The total biochemical oxygen demand may still be assessed with sufficient accuracy, but it is unlikely that the respirogram can be decomposed into individual components and their kinetics.

Components in substantial concentrations — Trace concentrations cannot be handled by the method described here. When the concentration of a component is less than its half *K*-value, the reaction rate becomes essentially first order, which cannot be identified by the second derivative technique applied.

10.2.4 Description of the evaluation method

In the following, a procedural description is given about the direct respirogram evaluation method.

1. Conversion of the measured data into the required format. This results in a database containing time marks, respiration rate values, accompanying analytical data, and possibly data concerning activated sludge and substrate used, all in the appropriate units.
2. Filtering of the measuring data. There are two reasons for this: (1) If data are not obtained with a constant measuring interval then a filter allows the extraction of equally timed data, which facilitates further evaluation. (2) Noise and outliers can be removed from the data without affecting the information content. In this research an Adaptive Data Filter (ADF) was used (Brannigan, 1990). This filter applies an optimised number of nodes to fit the least number of cubic splines to the data set, satisfying the Akaike Information Criterion. The entire evaluation, with the exception of the assessment of the endogenous respiration rate, is based on the filtered data.
3. Assessment of the endogenous respiration rate (r_b). This rate, which is generally low and does not change much during the time course of a respirogram, is derived from the respiration rate prior to the addition of substrate and the respiration rate after the substrate has been completely oxidised. A linear regression is performed on the actual data points starting with the last points and moving backward towards the active part of the respirogram. The slope of the linear regression is compared against a threshold value. The same procedure is repeated starting from the beginning of the respirogram. This step will attempt to identify the first endogenous level, and the time instant of the sample dosage. The latter is simply defined where the difference between two consecutive respiration

164

measurements exceeds a certain limit. r_b is subtracted from the total measured respiration rate (eq. 10.2). This yields the respiration rate associated with the oxidation of the components in the added wastewater only.

4. Assessment of the total biochemical oxygen demand of the added sample and the time necessary for complete oxidation. This is done by calculating the area under the respirogram between dosage and time instant of second endogenous respiration rate.

5. Decomposition of the respirogram into different components. This is done by identifying inflection points in the respirogram. A probability of components is calculated based on their relative areas on the first derivative. Components with a probability below a threshold value are rejected.

6. Calculation of model parameters. This involves maximum respiration rates r_m, saturation coefficients K_S and concentrations of the components in the added sample. As shown above, r_m and K_S can be obtained from the respirogram at the inflection points. As an alternative, parameters are also assessed from regression of the integrated respiration rate (Spanjers and Keesman, 1994).

7. Presentation of the results: reconstructed and decomposed respirogram, and result of calculations. In addition to the parameter values also the probability with which a component is identified (up to 100% for the principal component) and the accuracy of the values are reported. Conversion factors (component identity) are estimated from a knowledge base or are provided.

10.3 Examples

10.3.1 Simple model respirogram

To evaluate the numerical stability and accuracy of the evaluation method, simple model respirograms with a sampling interval of 60 seconds were generated and analysed. For this test the respirograms were generated and evaluated with the same Monod saturation term, so that a perfect evaluation would lead to exactly the same parameter values as were used in the simulation. Two substrates, comparable to ammonium and readily biodegradable carbon, were simulated separately and in combination. The initial substrate concentrations and parameters are as follows: substrate concentrations: 20-50 mg N/L and 20-80 mg COD/L; maximum specific growth rates: 0.4-1.3 mg N/L/h and 3-12 mg COD/L/h; saturation coefficients: 0.3-1.5 mg N/L and 5-20 mg COD/L were varied. The following model, with substrate consumption as the only process, was used to generate the respirograms:

$$\frac{dS}{dt} = -\frac{\mu_m S X_B}{Y(K+S)}$$

(10.7)

$$r = \frac{(\gamma - Y)\mu_m S X_B}{Y(K+S)}$$

(10.8)

Because growth, decay and hydrolysis are not modelled there is no endogenous respiration and r_b=0 (or can be set to any other positive value). Furthermore there is no dilution effect because the initial substrate concentration is brought about with no volume change.

The evaluation results show that in many cases the original values of parameters and concentrations are returned with a reasonable small error (10-20%). However, the following observations indicate that errors may become unacceptable. First, low initial concentrations

lead to large errors in estimated μ_m and K. The initial concentration must be at least twice the substrate's K-value in order to obtain a reliable estimate of these parameters. Secondly, larger μ_m's tend to be underestimated. Thirdly, at the applied sampling interval (60 s) low K-values cannot be assessed reliably. Finally, certain combinations of sample dosages cannot be identified (shoulders masking each other).

10.3.2. ASM No. 1 respirogram

To evaluate further the direct respirogram evaluation (DRE) method it was applied to respirometric data generated with an interval of 60 s from the Activated Sludge Model No. 1 (ASM1). In this model, respiration is the result of the degradation of several components. The death regeneration concept used in the model implies an endogenous respiration associated with the oxidation of substrate released from decay and subsequent hydrolysis. Assuming that ASM1 represents the state of the art of our knowledge of activated sludge processes, and including the dilution effect upon sample addition, we can simulate respirograms with maximum reality. Table 10.1 summarises the values of the components and parameters used in the ASM1 simulation and Figure 10.2 shows the resulting respirogram.

Table 10.1. Components and parameters used in the ASM1 simulation. Other parameters: Henze *et al*. (1987)

Components			Parameters	
	Activated sludge	Wastewater	K_S (mg COD/L)	20
S_I	0	0	K_{NH} (mg N/L)	1.0
S_S	1.4	200	r_{mH} ($=\mu_{mH} X_{BH} (1-Y_H)/Y_H$) (mg O$_2$/L/h)	125
X_I	1000	0	r_{mA} ($=\mu_{mA} X_{BA} (4.57-Y_A)/Y_A$) (mgO$_2$/L/h)	56
X_S	3.8	100	Y_H	0.67
X_{BH}	1000	0	Y_A	0.24
X_{BA}	100	0		
X_P	100	0		
S_O	8.3	0		
S_{NO}	20.0	0		
S_{NH}	0.1	55		
S_{ND}, X_{ND}	1.0	0		
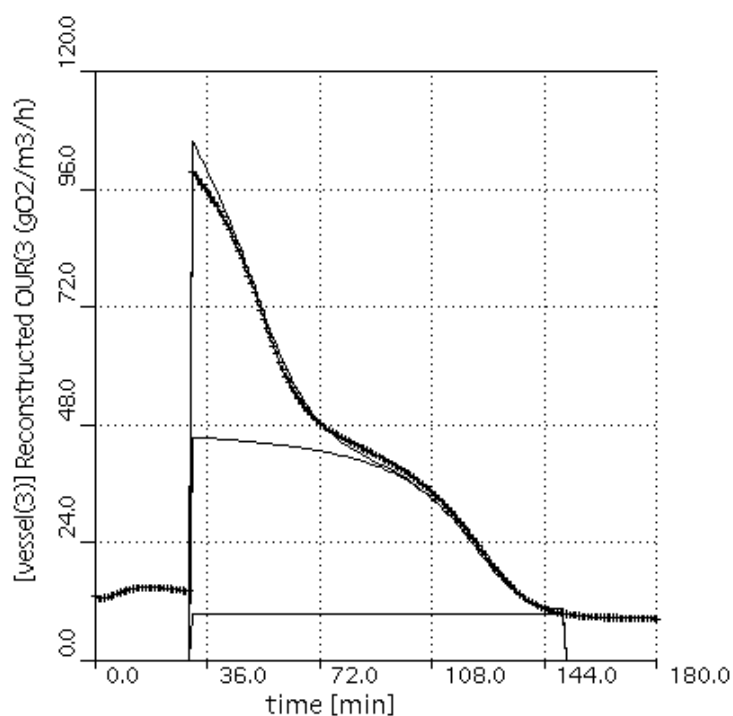
Figure 10.2. ASM1 Respirogram showing DRE results.

The respirogram shows the different levels of endogenous respiration due to dilution, and two distinct stages corresponding to different degradation processes. The DRE method is applied to these data, resulting in a smoothed respirogram from the data filter and a decomposition into two components. The numerical values of the analysis are summarised in Table 10.2.

Table 10.2. Results of direct respirogram evaluation (DRE) applied to ASM1 respirogram.

Parameter	DRE	ASM1
Goodness of ADF-fit (r^2)	1.000	—
Area under the respirogram (mg O_2/L)	70.3	—
Short-term BOD wastewater (mg O_2/L)	246	—
First component (assumed COD)		
Concentration in wastewater [a] (mg COD/L)	241	200 (S_s) + 100 (X_s)
r_m (mg O_2/L/h)	138	125
K (mg COD/L)	37	20
Second component (assumed N)		
Concentration in wastewater [b] (mg N/L)	40	55
r_m (mg O_2/L/h)	56	56
K (mg N/L)	1.3	1.0

[a] Assuming 0.33 mg O_2 per mg component; [b] Assuming 4.26 mg O_2 per mg component

167

The goodness of fit indicates a good agreement between the smoothed respirogram and the individual data. The calculations are done on the smoothed respirogram. The area under the respirogram represents the short-term BOD of the wastewater sample. Each of the two components is separately subjected to a parameter extraction to obtain their concentration in the sample as well as their characteristic values of r_m and K. To convert units from oxygen concentration to component concentration, the type of component and associated conversion factor have to be assumed. The estimated concentration of degradable material is larger than the ASM1 S_S but smaller than the sum of S_S and X_S. The reason is that the DRE value consists of S_S originally present plus partially hydrolysed X_S; a phenomenon that also exists in the evaluation of real respirograms. The DRE method overestimates both r_m and K, probably because the initial concentration is rather low (a bit more than twice the K-value). The estimation of the parameters of the second component is better. The concentration is underestimated, which can be explained from nitrogen uptake for heterotrophic growth: 7% of the COD consumed, that is 14 mg N/L, is not oxidised but used as nutrient.

10.3.3 Real respirogram

A number of real respirograms were analysed. The respirograms were obtained from an automatic respirometer operated at a full-scale activated sludge plant. An example of an analysed respirogram is depicted in Fig. 3.
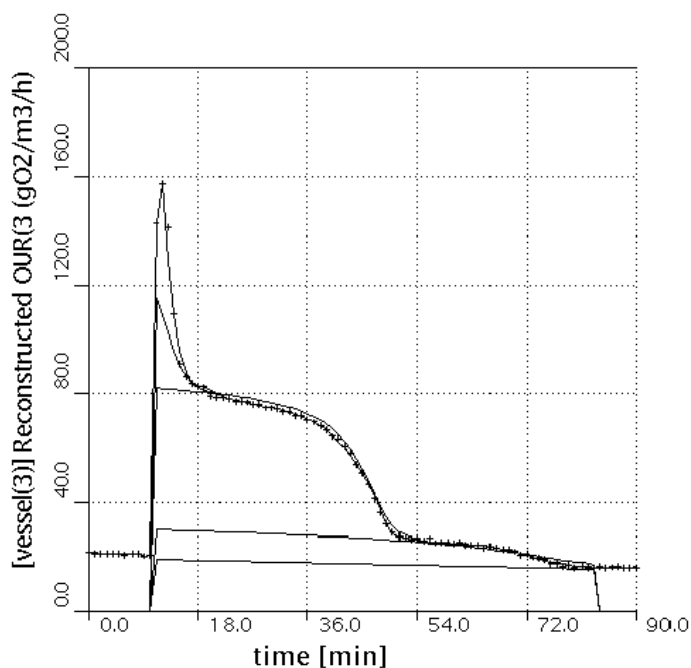
Figure 10.3. Respirogram from a nitrifying full-scale plant.

The respirogram was obtained by adding 0.600 litre of pre-settled wastewater (COD: 333 mg/L, BOD$_5$: 195 mg/L) to 2.3 litres of nitrifying activated sludge (MLSS: 2.09 g/L). The results of the DRE are summarised in Table 10.3. The goodness of fit indicates a good agreement between the smoothed respirogram and the data-points. Notice that the short-term BOD of the wastewater is in the same order of magnitude as its BOD$_5$. Four components are found, but the second one (just after the initial peak (Fig. 3) is rejected because of low probability. The other components are identified based on knowledge of experimental conditions and typical rates, and the associated conversion factors are assigned.

168

In addition to the results in Table 10.3, a number of other properties of the respirogram are assessed and reported in the software implementation of the DRE method (coded in GPS-X), such as endogenous respiration rate, time instants of the different stages in the respirogram, number of components detected and components rejected due to low probability.

Table 10.3. Results of direct respirogram evaluation applied to the respirogram in Figure 10.3.

	Full respirogram		
Goodness of ADF-fit (R^2)		0.998	
Area under the respirogram (mg O_2/L)		43.3	
Short-term BOD wastewater (mg O_2/L)		209	
	Decomposed respirogram		
	Component 1	Component 2	Component 3
Component assumed	Carbon	Ammonium	Nitrite
Concentration in wastewater (mg COD/L, mg N/L)	19.3	45.9	—
Conversion used (mg O_2/mg component)	0.40	3.20	1.10
r_m (mg O_2/L/h)	73.5	55.7	14.0
K (mg COD/L, mg N/L)	8.9	0.2	1.4

To judge the overall performance of the DRE method five different respirograms from a full scale plant (18.08 l wastewater plus 22.74 l activated sludge) were evaluated and the DRE results were compared with those from a parameter optimisation method (Brouwer *et al*., 1998). Parameter optimisation methods use a more or less simplified model that is fitted to the measured data. Numerical techniques are used to find parameter values that lead to the smallest deviation between model predicted and measured respiration rates. Here, the following modifications were made: two-step nitrification, first order hydrolysis, no ammonification and constant endogenous respiration. The two-step nitrification parameters were assessed from separate experiments with nitrite and ammonium additions. The concentration of slowly degradable matter and the hydrolysis coefficient are not reported here because these are not assessed in the DRE method. The two methods show no agreement with respect to carbon. In all respirograms the fraction of this component to the total oxygen consumption was not enough for a reliable assessment for both methods. The results for the nitrogen components are summarised in Table 10.4.

The third respirogram was obtained on a rainy day and showed only one component: ammonium. The optimisation method failed to estimate the parameters reliably, whereas the DRE method yields a very high r_m. This can partly be explained with the observation that there is almost no nitrite oxidation shoulder in the respirogram, so that the method is not able to subtract nitrite oxidation from total oxidation.

For ammonium and nitrite the two methods show reasonable agreement. The DRE method yields a somewhat higher value for the ammonium concentration than the optimisation method. A possible explanation is that the latter attributes part of the measured oxygen consumption to slowly biodegradable matter. In addition, the DRE method produces consistently lower values for the maximum ammonium oxidation rate and higher values for

the maximum nitrite oxidation rate. Because the DRE method does not comprise stoichiometry it assumes instantaneous high nitrite oxidation rate from the beginning of the respirogram. However, in the first part of the oxidation process nitrite is increasing from zero and its oxidation rate is sub-maximum. Hence, the DRE method underestimates the maximum ammonium oxidation rate. Apparently the two methods credit different portions of the measured rate to the two processes.

Table 10.4. Comparison of the direct respirogram evaluation (DRE) method and the model optimisation method.

Units are: concentration (S^{ww}) in mgN/L, r_m in mgO$_2$/L/h, K in mgN/L.

Res. No.	Comp. No.	Parameter	DRE	Optimisation
1	Ammonium	S^{ww}	50	45
		r_m	55	65
		K	0.4	0.3
	Nitrite	r_m	24	18
		K	1.2	0.2
2	Ammonium	S^{ww}	50	49
		r_m	48	65
		K	0.2	0.3
	Nitrite	r_m	20	18
		K	0.6	0.2
3	Ammonium	S^{ww}	14	13
		r_m	122	137
		K	0.1	0.5
4	Ammonium	S^{ww}	54	45
		r_m	53	55
		K	0.3	0.2
	Nitrite	r_m	22	16
		K	1.8	0.15
5	Ammonium	S^{ww}	39	35
		r_m	68	62
		K	0.2	0.2
	Nitrite	r_m	27	18
		K	0.2	0.2

10.4 Discussion

The DRE method is simple and straightforward because there are no complications involving modelling, optimisation and identifiability. It decomposes the respirogram into components and applies a simple technique based on the identification of inflection points to assess Monod parameters and component concentrations (eqs. 10.3 and 10.5). As an alternative, non-linear regression of the Monod functions around the inflection points should also be investigated.

In many cases a tailing can be observed after the initial peak, indicating hydrolysis of slowly degradable matter (more pronounced than in Fig. 10.3). This process, typically described with a first order model, cannot be identified using inflection points. A method should be developed that allows handling of this type of model. The main limitation of the DRE method is that individual components must be dominant during a sufficiently long time of the oxidation. This condition can only be satisfied through good experimental design in which respirograms with enough information content are generated.

The adaptive data filter is useful to obtain equally timed data and to handle noisy respirograms. However, in many cases human intervention is required to adjust the position of nodes for the cubic splines. This operation should be further automated to allow fully automatic analysis of respirograms.

The DRE method is intended to replicate how an expert looks at a respirogram by using a natural approach mainly based on identifying inflection points. The method should be improved by adding more intelligence, for example a knowledge base for component identification, so that large numbers of varying respirograms can be analysed. However, for reliable estimation of model parameters from individual respirograms a model optimisation technique can yield more accurate results. The DRE method may, however, be used as a first step to help deciding model structures. Likewise, the DRE method can provide initial values for a subsequent optimisation. This should allow for automatic handling of large numbers of respirograms, because the optimisation will converge faster when started from better initial conditions.

10.5 Conclusions

The direct respirogram evaluation method (DRE) makes use of the characteristic shape of respirograms. Parameters are directly identified without a model based on inflection points that can be visually observed and extracted using a second derivative identification method. The DRE is able to evaluate respirograms provided that these are obtained from properly designed and recorded experiments. However, the two methods, DRE and parameter optimisation, are not always in agreement, especially when a component is present in low concentration. The method fails to evaluate inferior respirograms without intervention of a specialist. Further development of the method is needed in particular with respect to:

- handling first order reactions or low concentrations;
- repeated inflection point detection on separated components;
- the detection of components;
- incorporation of a knowledge base for component identification.

11 SENSITIVITY ANALYSIS IN PRACTICE[10]

11.1 Background

Sensitivity analysis can be used by the modelling practitioner to identify those model parameters that have the largest effect on the model variables. The objective of this chapter is not to discuss the theory behind sensitivity analysis. This is done in a detailed way in many publications, for example in Dochain and Vanrolleghem (2001) and others. The objective is to provide practical guidance and practical engineering conclusions for a typical (although simplified) case study. The term "parameter" is used in a general sense, referring to all parameters that are inputs to the model (e.g. not only model kinetics, but also influent characteristics and operational variables). Likewise, "model variables" are state variables in the model along with all other calculated outputs. The three main practical uses of sensitivity analysis are:

1. Help in the selection of model parameters that can be estimated with the most accuracy, given a set of available measurements;
2. Help in developing a sampling program to gather additional data for the particular process objective so as to target the most sensitive elements of the model;
3. Identify those parameters that have negligible effect on model variables – or conversely, identify those variables that are not sensitive to any model parameters. These parameters usually can be left at default values and the variables do not warrant inclusion in a detailed sampling program.

Sensitivity analysis can be classified into non-linear and linear methods. Since biological and settling models applied in wastewater treatment modelling usually are fairly non-linear, non-linear analysis should provide a more information-rich snapshot of the model variable responses to changes in parameters. Non-linear sensitivity analysis is based on the calculation of the probability distribution of model variables from the probability distributions of the parameters. In theory, the derivation could be performed analytically, but this is impractical due to the large number of varying sets of equations that are employed by the typical models to describe different wastewater treatment plant configurations. Monte Carlo analysis will approximate the non-linear sensitivity functions numerically, and is used sometimes in model development exercises, but it is still impractical in typical engineering work due to the large computational effort required. Consequently, non-linear sensitivity analysis will not be discussed any further in the context of this chapter.

---

[10] Based on Melcer, H., Dold, P.L., Jones, R.M., Bye, C.M., Takács, I., Stensel, D.H., Wilson, A.W., Sun, P., Bury, S. (2002) Methods for Wastewater Characterization in Activated Sludge Modeling. Water Environment Research Foundation, Alexandria, Virginia, USA.

Linear sensitivity analysis consists of developing (generally numerically approximating) sensitivity functions around a certain operating point (typical state of the model). There are different ways to express the results. In this study, the relative change in state y_j for a 100% change in parameter θ_i is used, i.e.:

$$\delta_{i,j} = \frac{\theta_i}{y_j} \frac{\partial y_j}{\partial \theta_i} \tag{11.1}$$

where $i=1\ldots n$ (n number of parameters), and $j=1\ldots m$ (m number of states).

The advantage of this expression over other forms (containing absolute values) is that different parameters become easily comparable. Parameters for which $\delta_{i,j} > 100$ percent are generally considered very sensitive; though for a complete evaluation relative sensitivities between the parameters should be taken into account. An illustrative example is provided later in this chapter.

The analysis is performed by perturbing each individual parameter one at a time by an appropriately selected perturbation value $\Delta\theta$, i.e., approximate Eq. 10.1 by:

$$\delta_{i,j} = \frac{\theta_i}{y_j(\theta_i)} \frac{y_j(\theta_i) - y_j(\theta_i + \Delta\theta_i)}{\Delta\theta_i} \tag{11.2}$$

The simplest practical approach is to develop the sensitivity functions in steady state, around a certain operating point. Since the wastewater treatment plant is governed by non-linear processes, and the models are expected to reflect this reality, the sensitivity functions will largely depend not only on the model structure, but on the operating point itself. A sensitivity function, developed around a low SRT, non-nitrifying process, will not be representative for the same plant when it does nitrify.

The result of a steady-state sensitivity analysis is a two-dimensional matrix, one dimension containing the parameters, and the other the model states (n x m). Processing of such a matrix can provide valuable insight into the model structure and importance of parameters.

It is often important to observe the sensitivity functions under dynamic conditions. There are processes that are never in steady state, such as SBRs. For these, a simple steady-state analysis is not possible although it is still possible to generate an averaged sensitivity table. Also, the sensitivity functions will be quite sensitive themselves, not only to the long-term average operating point, but also to short-term system disturbances, diurnal variation, storms and upsets. Dynamic sensitivity analysis will provide more detailed information. For example, a parameter would affect a variable differently before, during and after a high load event.

The reasoning in the previous paragraphs can be rigorously extended by incorporating one more dimension (t, time) into the sensitivity matrix. Then the same methodology is used to perform n dynamic simulations. The computational effort increases, however (unless the software used does not have a steady-state solver to start with, in which case steady-state analysis already takes a significant time). Also, multi-dimensional matrices rapidly lose their illustrative value. The proposed approach from the practical standpoint is to select the

important parameters based on the steady-state sensitivity functions and develop dynamic sensitivity functions for this subset only.

Proper consideration must be given to the selection of the dynamic event, more precisely the forcing functions (influent and dynamically varying operational settings). Depending on the calibration task and data available, representative dynamic datasets should be chosen for the analysis. For example, if the task is to establish the effect of normal diurnal variation, then a typical diurnal flow and concentration profile, along with usual daily operational changes, such as periodic wastage, is required for a meaningful analysis.

11.2 Parameters and states in sensitivity analysis

11.2.1 Model parameters

Model parameters, in a general sense, are those constants and variables that are inputs into the calculations and have an effect on the calculated results of the model. Table 11.1 lists all types of parameters for a typical activated sludge plant model, whether they are normally included or not in sensitivity analyses.

Two parameter categories are typically excluded *ab ovo* from the analysis. One set are those that are supposed to be known to a high degree of accuracy, for example physical parameters. One notable exception is the number of tanks in series in the representation of a plug-flow tank. Initial conditions is a special category that is typically not considered in a sensitivity analysis either. Steady-state initialization will remove the effect of these variables from a typical activated sludge plant model. In special cases (e.g., simulation of a batch test or respirogram), the initial conditions are meaningful, and can be included in the analysis. Even in this case though, they need to be properly developed and cannot be randomly selected.

The two most important parameter categories that are usually included in sensitivity analysis are the actual mathematical model parameters (stoichiometric and kinetic parameters), and influent composition (wastewater fractions). The actual parameters are model dependent. For example, ASM1 has 19 model parameters that can be incorporated in the analysis (Henze *et al*., 1987). Sensitivity analysis (or *a priori* knowledge of the model) can be used to select the most sensitive subset for more detailed analysis, as shown in the example in this chapter.

11.2.2 Calculated variables

There are several categories of calculated variables in any model that are useful to include in the sensitivity analysis. The main categories and examples are:

- Model states in reactors (concentration of dissolved oxygen and heterotrophs…).
- Combined variables in reactors (VSS, MLSS…).
- Combined variables in settlers (effluent solids, RAS, sludge blanket…).
- Rates, saturation and inhibition functions, other internal model expressions (OUR, NUR…).

Table 11.1. Parameter categories in sensitivity analysis

Parameter category	Parameter sets	Examples	Used in sensitivity analysis	Note
Physical	Reactor configuration, environmental, physical constants	Volume, surface area, temperature, Henry constant…	No	Exception: number of CSTRs in series sometimes
Driving functions	Influent flow and concentrations	Influent COD, TKN, TP…	Sometimes	
	Influent composition/fractions	Biodegradable fraction, soluble inert organic fraction…	Yes	
	Operational variables	Recycle and wastage flows, airflow, chemical dosage, time schedules…	Sometimes	
Model	Stoichiometric	N, P content, yields…	Yes	
	Kinetic	Max. spec growth rates, half-saturation constants…	Yes	
	Settling	Vesilind and double-exponential constants…	Yes	
	Initial conditions	Initial concentrations of heterotrophs, autotrophs…	No	In special circumstances (e.g. simulation of short-term batch tests)

Inclusion or omission of any of these will not affect the results of the analysis. Consequently, the ones that will be displayed are selected based on the importance they play for a particular application. An important set is the model state variables. Most of the other categories can be calculated based on this set.

11.3 Sensitivity analysis example

11.3.1 The wastewater treatment plant

To illustrate the practical application of sensitivity analysis, a simple nitrifying activated sludge plant is used, consisting of one process train, as summarized in Table 11.2.

This plant was modelled (in BioWin) as a single CSTR bioreactor, using the ASM1 model, and a simple settler model with 99.8 percent solids capture in the effluent and mass balance based RAS calculation. Wastage was withdrawn from the aeration tank to allow hydraulic

SRT control. The plant was run to steady-state under two different operating conditions: 3.3 d SRT, partially nitrifying, and 15 d SRT, complete nitrification. After the steady-state analysis results, a selected dynamic example is discussed.

Table 11.2. Activated sludge plant specifications

	Item	Value	Units
Reactor	# of reactors	1	-
	Reactor volume	20,000	m^3
	HRT	6	hr
	DO setpoint	2.0	gO_2/m^3
	Wastage (3.3 d SRT)	6,000	m^3/d
	Wastage (15 d SRT)	1,333	m^3/d
Influent	Flow (DWF)	80,000	m^3/d
	COD	500.0	$gCOD/m^3$
	TKN	40.0	gN/m^3
	Alkalinity	6.0	mmol/L
Settler	Surface area	2,500	m^2
	Recycle flow	40,000	m^3/d

11.3.2 Selected parameters

The analysis was performed by providing a 1 percent positive perturbation. The perturbation has to be small enough such that the change in model response can be considered linear, but large enough that numerical accuracy issues do not arise. Three different sets of parameters were perturbed in the model.

Stoichiometric and kinetic parameters. The 19 stoichiometric and kinetic parameters in the ASM1 biokinetic model were analyzed. Default values were used in the base case as shown in Table 11.3. In an actual analysis, the default values might provide an initial starting point – then based on the results and the calibration values obtained, the sensitivity analysis can be repeated for the final calibrated model and parameter values.

Influent (driving function) parameters. The effect of influent flow rate, organic and nitrogen loading as measured by total COD and TKN concentration, readily biodegradable fraction ($S_S/(S_S+X_S)$) and soluble inert fraction ($S_I/(S_I+X_I)$), was analyzed in this example. Table 11.4 provides default values. Perturbation was +1 percent.

Table 11.3. ASM1 default parameters used in the sensitivity example

Parameters	Default value	Units
Stoichiometric		
N content of active biomass (i_{XB})	0.086	gN/gCOD
N content of endogenous/inert mass (i_{XE})	0.06	gN/gCOD
Fraction of biomass leading to particulate products (f_P)	0.08	gCOD/gCOD
Heterotrophic yield (Y_H)	0.666	gCOD/gCOD
Autotrophic yield (Y_A)	0.24	gCOD/gN
Kinetic		
Heterotrophic maximum specific growth rate (μ_H)	6.0	1/d
Readily biodegradable substrate half-saturation coefficient (K_S)	20	gCOD/m^3
Oxygen half-saturation coefficient ($K_{O,H}$)	0.2	gO$_2$/m^3
Nitrate half-saturation coefficient (K_{NO})	0.5	gN/m^3
Anoxic growth factor (η_g)	0.8	-
Heterotrophic decay rate (b_H)	0.62	1/d
Autotrophic maximum specific growth rate (μ_A)	0.8	1/d
Ammonia half-saturation coefficient for autotrophs growth (K_{NH})	1.0	gN/m^3
Autotrophic decay rate (b_A)	0.04	1/d
Oxygen half-saturation coefficient for autotrophic growth ($K_{O,A}$)	0.4	gO$_2$/m^3
Maximum specific hydrolysis rate (K_h)	3.0	1/d
Hydrolysis half-saturation (K_X)	0.03	gCOD/gCOD
Anoxic hydrolysis factor (η_h)	0.4	-
Ammonification rate (k_a)	0.08	m^3/gCOD/d

Table 11.4 Default influent (driving function) values

Parameters	Default value	Units
Influent flow rate, Q_{inf}	80000	m^3/d
Influent COD, COD_{inf}	500	$gCOD/m^3$
Influent TKN, TKN_{inf}	40	gN/m^3
Readily degradable fraction, $S_S/(S_S+X_S)$	24.4	%
Soluble inert fraction, $S_I/(S_I+X_I)$	27.8	%
Ammonia fraction of TKN	75	%
Soluble TKN fraction $S_{ND}/(S_{ND}+X_{ND})$	50	%

Operational parameters. DO concentration setpoint and waste flow rate (defining the operational SRT) were selected as the two most important operational parameters on this simple plant. Perturbation was +1 percent.

Table 11.5. Operational parameters analyzed

Parameters	Default value	Units
DO setpoint	2.0	gO_2/m^3
Wastage flow (3.3 d SRT)	6000	m^3/d
Wastage flow (15 d SRT)	1333	m^3/d

11.4 Sensitivity analysis - the procedure

The plant as specified above was implemented in BioWin (based on the ASM1 model equations) and run to steady state with the default set of parameters using an absolute error criteria of maximum 0.01 $g/m^3/d$ residual derivative of the state variable with the largest derivative. Results for state variables and a few other selected operational variables are listed in Table 11.6. Values are recorded to 4 decimal digits even though there is no process meaning attached to this accuracy. For an accurate determination of the sensitivity functions in a non-linear system a small perturbation must be chosen, thus necessitating the use of this high numerical accuracy.

The following steps were performed for the preparation of the steady-state sensitivity tables (Tables 11.7-11.10, presented at the end of the chapter) around the two operating points:

- Steady state was established (one for each base case and one for each perturbed parameter). The results of the runs were saved into a spreadsheet (two sheets – one for each operating point). Steady state can be achieved using an iterative method if

available in the software, or with a long dynamic run using constant influent and operational settings. Attention has to be paid to numerical accuracy.

- The sensitivity functions according to Eq. 11.2 were calculated in a matrix, one for each operating point, expressed as percent change in calculated variables for 100 percent change in parameters. Since the models are non-linear, and both parameters and calculated variables have physical bounds, generally it would be meaningless to change parameters by 100 percent. Expressing the results of a 1 percent perturbation scaled up to 100 percent change is solely for the purpose of presentation and must be taken as the approximation of the derivative at the parameter default value.

Table 11.6. Results of the Two Base Cases

	Value		Units
Operational variables			
SRT	3.3333	15.0000	days
VSS[1]	2196.3930	6315.0828	$gVSS/m^3$
State variables			
Readily biodegradable substrate (S_S)	3.5166	2.4647	$gCOD/m^3$
Slowly biodegradable substrate (X_S)	40.1013	47.7716	$gCOD/m^3$
Soluble inert organics (S_I)	25.0000	25.0000	$gCOD/m^3$
Inert particulate organics (X_I)	834.9390	3,310.6961	$gCOD/m^3$
Heterotrophs ($X_{B,H}$)	2,030.9831	3,666.4450	$gCOD/m^3$
Autotrophs ($X_{B,A}$)	50.0365	207.8064	$gCOD/m^3$
Endogenous decay products (X_P)	294.6018	2,113.6034	$gCOD/m^3$
DO (S_O)	2.0000	2.0000	gO_2/m^3
NH3-N (S_{NH})	1.1238	0.2174	gN/m^3
NO3-N (S_{NO})	12.7435	18.1798	gN/m^3
Particulate biodegradable organic N (X_{ND})	1.8672	2.7823	gN/m^3
Soluble biodegradable organic N (S_{ND})	0.6899	0.6410	gN/m^3
Alkalinity (S_{ALK})	3.0272	2.5741	mol/m^3

[1]VSS is calculated from particulate COD using a 1.48 mgCOD/mgVSS conversion factor

The matrix at this point contains all the information, but is not easily readable. The (arbitrarily chosen) sum of absolute values of sensitivities for each row and column were calculated as an

additional row and column for the matrices. The absolute value of the calculated variables was also added as this contains important information in addition to the relative sensitivities.

The matrices were sorted by the sum of absolute values, both for parameters and calculated variables. Sorting left to right and top to bottom in descending order results in the most sensitive cells being moved to the top left corner. The order of parameters and variables, their rank, becomes an important aid for the analysis. To further enhance readability of the sensitivity tables, low sensitivity values ($\delta_{i,j} < 10$ %) were discarded, and the highest sensitivity fields appear in bold font ($\delta_{i,j} > 150$ %).

11.4.1 Steady-state sensitivity analysis - results

The sensitivity tables for both the 3.3 d SRT and the 15 d SRT operating points were divided into two tables for convenience. One type of table (Tables 11.7 and 11.9) contains the results of the analysis performed on model parameters, and the other (Tables 11.8 and 11.10) for influent and operational parameters.

As an example, the number -208 in the ammonia (S_{NH}) column and maximum specific autotrophic growth rate (μ_A) row in Table 11.7 represents a strong sensitivity of ammonium to the growth rate in a negative direction. For 1 percent increase in the growth rate, the ammonium variable will drop 2.08 percent. (-208 percent sensitivity for 100 percent change).

The conclusions that can be drawn for each table and for the whole of the example analysis are listed below.

11.4.2 Sensitivity to model parameters at 3.3 d SRT

Variables at the right side of Table 11.7 (X_I, S_I, S_O, SRT, ranked 12-15) are not sensitive at all to model parameters and cannot be modified by changes to the model parameter set. There are various reasons for this. Inert organics (X_I, S_I) are not undergoing any transformations in the model and their concentration will only depend on mass balance. DO and SRT, on the other hand, are controlled variables in the system.

Variables with high ranks (X_{ND}, S_{NO}, $X_{B,A}$, S_{NH}, X_S) can be readily affected by varying the model parameters. Some (ammonia, S_{NH}), are strongly dependent on one or two parameters (in this case μ_A and K_{NH}) only, while others are influenced by a whole range of parameters (e.g., X_{ND})

The model parameters themselves are ranked – parameters on the top, for example heterotrophic yield (Y_H), tend to have a larger effect on several variables, as opposed to the parameters ranked towards the bottom rows of the table. The parameters on the top are obviously the more important ones for the model calibration exercise, while the less important ones can be left at their default values.

The absolute values of the variables (listed under the "variables" row) provide an additional guideline when evaluating the impact of sensitivity. For a 1 percent increase in heterotrophic yield (Y_H) about the same relative change (1.5 percent) will occur to the endogenous products (X_P) and the heterotrophs ($X_{B,H}$), but for X_P this means about 4 mg COD/L increase, while for $X_{B,H}$, around 30 mg COD/L.

A few other practical points that can be obtained from Table 11.7 are listed below. It must be kept in mind that these are specific to the system and the operating point it is in (one mixed tank, fully aerobic, 3.3 d SRT,…).

Nitrate concentration is strongly dependent on heterotrophic yield – through N assimilation (since only the residual ammonia can be nitrified).

If the predicted alkalinity is higher than the measured, there are three parameters available to reduce the predicted value in the model (Y_H, i_{XB} and μ_A). μ_A achieves this through more nitrification (strong effect on ammonia). If effluent ammonia was predicted correctly though, this points to a measurement error on influent or effluent ammonia or alkalinity.

VSS (MLVSS) is mostly dependent on Y_H as expected. Based on practical experience VSS is even more strongly affected by influent loading and composition, as well as wastage. This will be discussed in association with Table 11.8.

For the calibration of effluent nitrate and ammonia, the most important parameters are the μ_A, governing nitrification, and Y_H, i_{XB} which have a large effect on assimilation.

11.4.3 Sensitivity to influent and operational parameters at 3.3 d SRT

These parameters are presented in a separate table as "sensitivity" has a different meaning in relationship to influent and operational parameters. The model cannot be "calibrated" by changing influent COD, for example. Some general pointers to evaluate the information content in Table 11.8 are provided below.

In general, these parameters affect a large number of variables in the model. 41 percent of the fields have an entry, as compared to 14 percent in Table 11.7.

Ranking of the variables is different from Table 11.7, but can be used the same way to establish important and not as important parameters and variables.

Influent COD has the largest effect, even on nitrogen variables (except ammonia). The link between COD and N is through the assimilation process.

Ammonium is very sensitive (+182 percent) to wastage flow. This is an indication of the sensitivity of the nitrification process around the 3.3 d SRT operating point.

Wastewater soluble versus particulate fractions have a relatively small effect on the process.

11.4.4 Sensitivity to model parameters at 15 d SRT

Several key conclusions can be drawn when comparing the results in Table 11.9 generated at 15 d SRT, with a system that is under higher loaded conditions (3.3 d SRT):

The list of insensitive (inert and controlled) variables did not change, and hence does not depend on the operating point.

There are changes in the rank of the parameters compared to the 3.3 d SRT operating point, but the general ranks did not change much: high-ranked, important parameters and less important ones are still in their respective positions.

Hydrolysis and decay parameters (K_h, K_X, f_P) gained a few positions in the ranking system for long SRT conditions, while the growth parameters (μ_A) decreased in importance.

When considering variables, the nitrification process is a lot less sensitive at 15 d SRT, based on the lower ranks of both ammonia and autotrophs.

11.4.5 Sensitivity to influent and operational parameters at 15 d SRT

The analyzed parameters (Table 11.9) generally retained their order of importance between the 3.3 d and 15 d SRT system.

The most important change in the rank of the variables concerns the two primary substrates, S_S and S_{NH}. Both become very insensitive at this high SRT.

11.5 Dynamic sensitivity analysis

Sensitivity functions in a dynamic model are sensitive not only to the general operating point the system is in, but to the effect of time-varying forcing functions. A steady-state value of ammonia (1.1 mg N/L at 3.3 d SRT) can vary as much as 1-5 mg N/L under normal diurnal loading conditions. It is expected that the sensitivity of this variable will be different during the morning peak and the late night low loaded situation.
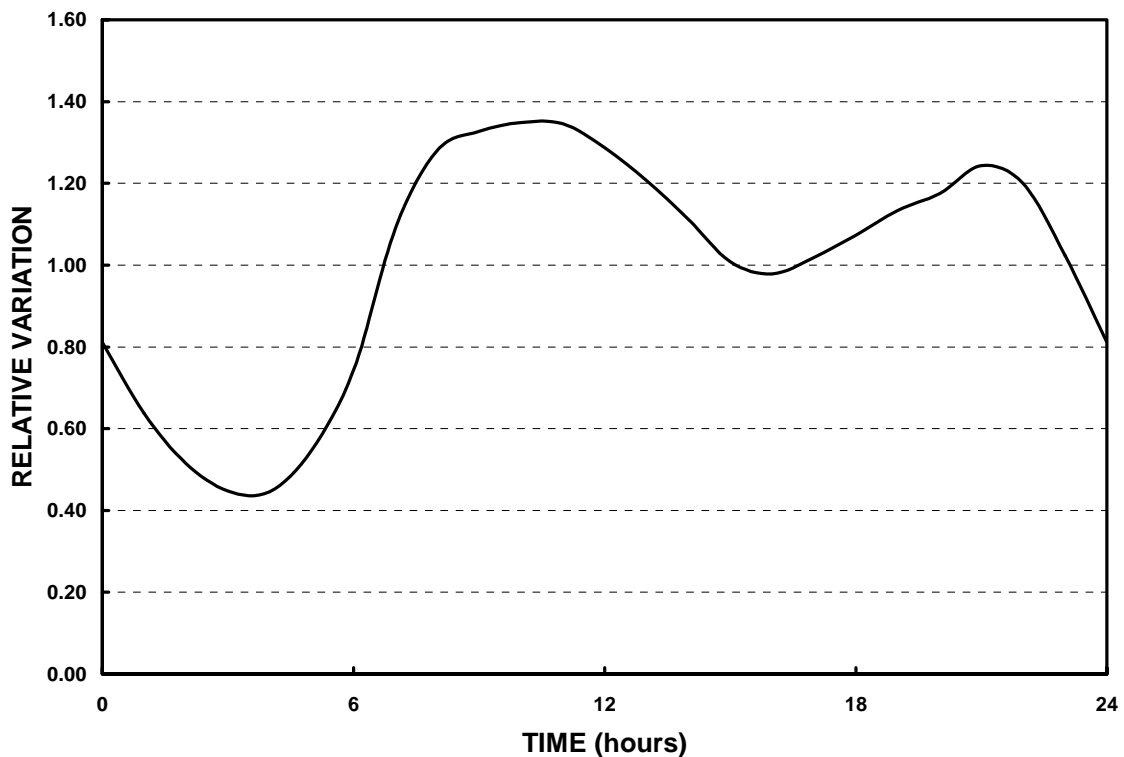
Figure 11.1. Normalized Diurnal Pattern Used for Dynamic Analysis

183

The steady-state sensitivity analysis performed above does not provide information on model sensitivity with respect to the effect of time-varying load. To illustrate a dynamic sensitivity analysis, the two most sensitive parameters, μ_A and K_{NH} as well as ammonia as output variable were selected. The steady-state average value of the influent was maintained, but diurnalized using the function in Figure 11.1. This diurnal profile was applied to influent flow rate, COD and TKN. 10 days of diurnal runs were performed with the same diurnal pattern, starting from the steady-state condition in Table 11.7 (3.3 d SRT), and ammonia was recorded in the aeration tank during the last day. Following the base case (μ_A = 0.8 1/d and K_{NH} = 1.0 g N/m^3), two more runs were performed applying +1 percent perturbation to each parameter, individually. The resulting diurnal ammonia concentration, along with the perturbation cases, is plotted in Figure 11.2.
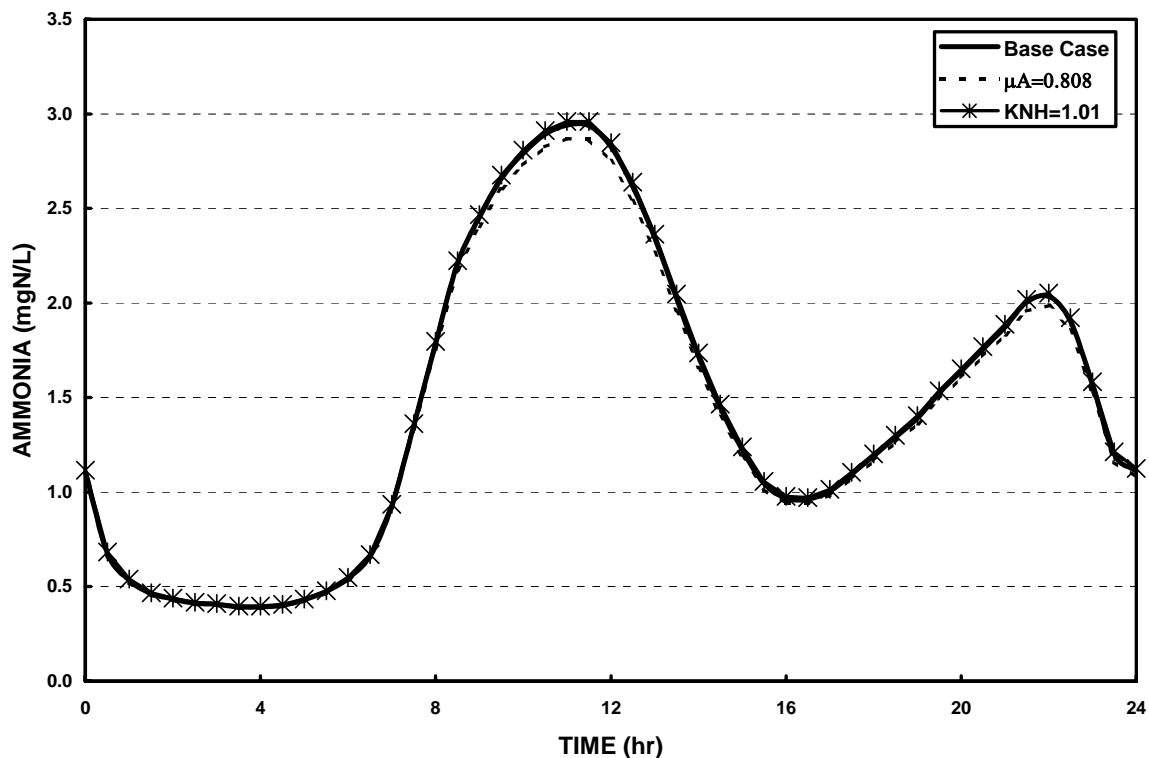
Figure 11.2. Diurnal Ammonia Profile

The sensitivity functions now can be approximated using Eq. 11.2 for these parameters. This is plotted in Figure 11.3.

The following conclusions can be drawn from Figure 11.3.

The average of the dynamic parameter sensitivity does not correspond exactly to the steady-state value (-222 percent instead of -208 percent and 96 percent instead of 100 percent for μ_A and K_{NH}, respectively), though there is a strong correlation. This is a well-known phenomenon in dynamic simulation of diurnal versus steady-state systems – steady state does not equal the average of a diurnal time series.

The variation in the sensitivity of μ_A is much larger than that of K_{NH}. If K_{NH} is increased in the model, it will result in an almost uniform increase of effluent ammonia concentration throughout the day. If μ_A is increased, it will result in a slight decrease during low loaded

periods (when most of the ammonia is oxidized) and a larger decrease and faster recovery of concentration peaks.

Ammonia is least sensitive to growth rate (consider the negative scale) during low loaded periods, more sensitive during high loaded periods, and reaches the highest sensitivity during recovery from a high loaded situation, when the rate of change of the concentration is the greatest in the negative direction.
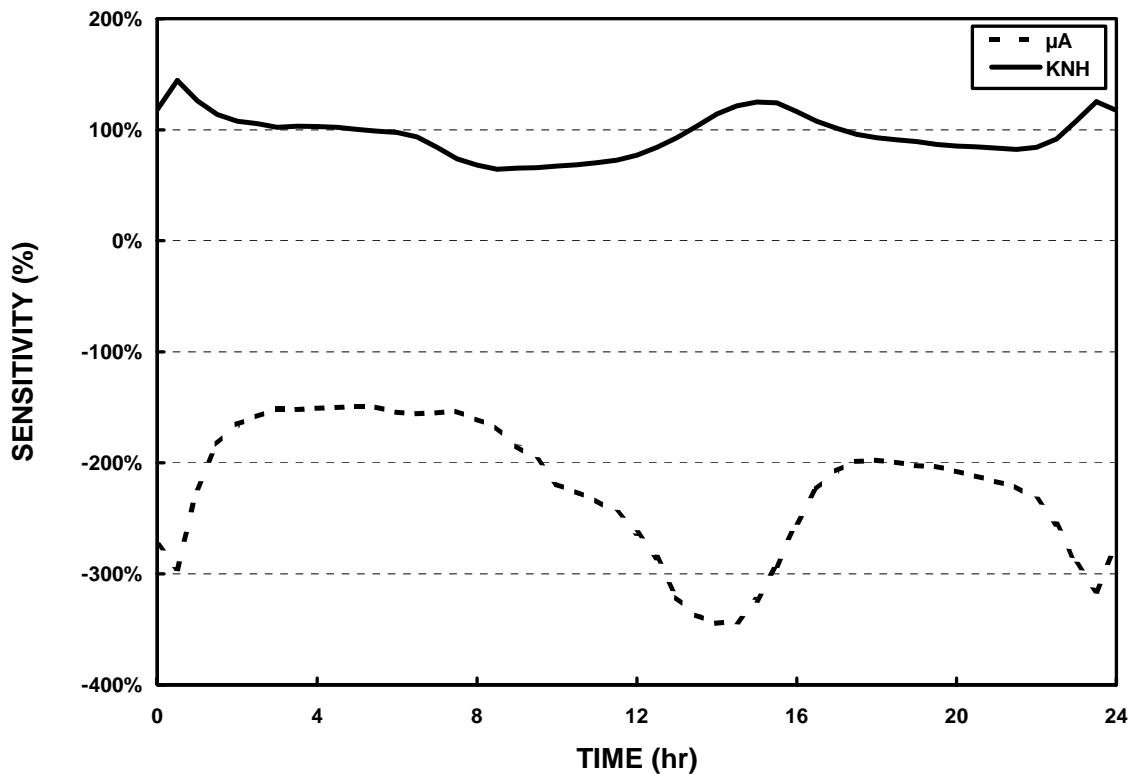
Figure 11.1. Diurnal Sensitivity Functions

11.6 Conclusions

This chapter describes the methodology of sensitivity analysis in modelling with a practical perspective, and provides examples for a simple aerobic system as simulated by the ASM1 model. Guidance is given on various forms of sensitivity analysis and how to deduce useful model and calibration information from the results of the analysis. The results as presented here are provided as examples to illustrate the methodology only – it is likely that parameter ranking and sensitivity would be significantly different for more complex systems describing nitrification, denitrification and excess phosphorus removal. In those cases (and even for simple aerobic systems under different loading conditions or simulated using other models than in the example in this chapter), the sensitivity analyses have to be performed with the actual model setup to generate valid sensitivity functions.

Table 11.7. Model parameter sensitivity table (3.3 d SRT)

% Sensitivity Rank	Rank	1	2	3	4	5	6	7	8	9	10	11	12	13	14	15
	Variables	$X_{N,D}$	$S_{N,O}$	$X_{B,A}$	S_{NH}	X_S	X_P	S_{ND}	S_S	X_{BH}	S_{ALK}	VSS	X_I	S_I	S_O	SRT
Rank	Value	1.9	12.7	50.0	1.1	40.1	294.6	0.7	3.5	2031.0	3.0	2196	834.9	25	2	3.3
1	Y_H	83	**-241**	-123		17	**153**	-26		**154**	72	108				
2	b_H	95	23	23		72	57	87	76	-42		-20				
3	i_{XB}	95	-111	-78				86			33					
4	K_h	**-157**				**-162**										
5	μ_A		18	13	**-208**						-11					
6	K_X	96				99										
7	f_P	-11					94									
8	μ_H								-116							
9	K_{NH}				100											
10	k_a							-97								
11	K_S								100							
12	Y_A			98												
13	η_g		-40													
14	$K_{O,A}$				36											
15	b_A			-13	24											
16	$K_{O,H}$															
17	i_{Xun}		-10													
18	η_h															
19	K_{NO}															

Table 11.8. Analysis of influent and operational parameters (3.3 d SRT)

% Sensitivity	Rank	1	2	3	4	5	6	7	8	9	10	11	12	13	14	15
	Variables	S_{NO}	X_{BA}	X_P	X_I	VSS	$X_{B,H}$	S_{ALK}	$X_{N,D}$	X_S	$S_{N,H}$	S_I	S_O	SRT	$S_{N,D}$	S_S
Rank	Value	12.7	50.0	294.6	834.9	2196	2031.0	3.0	1.9	40.1	1.1	25	2	3.3	0.7	3.5
1	COD_{inf}	**-190**	-104	100	100	97	101	57	79	100		100			-32	
2	Q_{was}	-40	-120	**-152**	-95	-76	-57	17	-32		**182**			-99		40
3	Q_{inf}		97	96	97	98	98		97	100						
4	TKN_{inf}	301	213					**-162**	19						35	
5	DO setp	45						-15			-35		100			
6	$S_I/(S_I+X_I)$	13			-38							100				
7	$S_S/(S_S+X_S)$								-11	-29						

Table 11.9 Model parameter sensitivity table (15 d SRT)

% Sensitivity	Rank	1	2	3	4	5	6	7	8	9	10	11	12	13	14	15
	Variables	X_{ND}	X_S	S_{ND}	X_P	S_S	S_{NO}	X_{BH}	S_{NH}	X_{BA}	VSS	S_{ALK}	X_I	S_I	S_O	SRT
Rank	Value	2.8	47.8	0.6	2113.6	2.5	18.2	3666.4	0.2	207.8	6315	2.6	3310.7	25	2.0	15
1	Y_H	**152**	88	-22	**201**		**-176**	**202**		-67	124	89				
2	b_H	62	55	95	26	99	12	-74		13	-23					
3	K_h	-138	-141													
4	i_{XB}	99		94			-39			-28		19				
5	K_X	97	100													
6	f_u	-15	-12		90			-10				16				
7	μ_A									-120						
8	μ_H					-111										
9	Y_A										98					
10	k_a			-98												
11	K_{NH}									101						
12	K_S					100										
13	b_A									41	-34					
14	η_g						-38					19				
15	i_{XE}						-13									
16	$K_{O,H}$															
17	$K_{O,A}$									23						
18	η_h															
19	K_{NO}															

Table 11.10. Analysis of influent and operational parameters (15 d SRT)

% Sensitivity / Rank	Rank → Variables → Value	1 S_{NO} 18.2	2 X_{BA} 207.8	3 X_I 3310.7	4 X_P 2113.6	5 S_{ALK} 2.6	6 VSS 6315	7 X_S 47.8	8 X_{BH} 3666.4	9 X_{ND} 2.8	10 S_I 25	11 S_O 2.0	12 SRT 15	13 S_{NH} 0.2	14 S_{ND} 0.6	15 S_S 2.5
1	COD_{inf}	-110	-50	100	99	56	96	100	100	86	100				-20	
2	Q_{inf}		92	90	87		92	99	97	96						
3	Q_{was}	-14	-69	-84	-107		-65	-10	-23	-18			-99	69		12
4	TKN_{inf}	**213**	**153**			**-191**					12				22	
5	DO setp	39				-19						100		-18		
6	$S_I/(S_I+X_I)$			-38			-13				100					
7	$S_S/(S_S+X_S)$							-18								

PART FOUR – THEORETICAL ASPECTS OF MODELLING

12 THE DYNAMIC SOLIDS RESIDENCE TIME[11]

12.1 Introduction

The Solids Residence Time (SRT) has long been recognized as one of the key process parameters of the activated sludge process. The SRT is routinely used for design and operation of wastewater treatment plants. Its popularity stems from two facts: ease of understanding and its large effect on the process.

By definition, the SRT is calculated as the mass of solids in the system divided by the mass flow of solids produced in a day under steady-state conditions. Variations of the SRT exist depending on the way the mass of solids is calculated. For example, in calculating the *aerobic SRT* only the solids in the aeration tank are taken into account, while the *complete SRT* takes into account the total mass of solids including those in the settler. Another refinement takes into consideration the solids lost in the effluent. It should be noted that all these definitions of solids residence time are based on steady-state conditions. As a result, the calculation of the SRT based on daily records can lead to large and unexpected variations. Vaccari *et al*. (1985, 1988) provide an excellent summary and analysis of the problems related to the steady-state sludge age. The authors suggest the use of a Dynamic Sludge Age (DSA) variable, similar in many ways to the proposed Dynamic Solids Residence Time (DSRT). However, the DSRT differs from the DSA in the way it is calculated. Vaccari *et al*. (1985) derive a general analytical solution and specific equations to be used under different conditions, "cases", to calculate DSA at time "*t*" if initial age, sludge mass in the system and solids production are known.

A more generic approach would be to define the rate of change in the age of the solids, then integrate it with a numerical integration method from a known initial condition to arrive at the appropriate sludge age. This method is generally well suited when dealing with systems described by a large number of coupled differential equations, such as the biokinetic processes in the activated sludge system. This approach has many advantages over a closed-form analytical solution. These will be addressed along with the mathematical development necessary for the justification of the method of calculation.

Intuitively, it can easily be said that sludge production, due to influent loading, has a more direct effect on the age of the solids in the system than wastage. This is contrary to what the steady-state SRT calculation, based on sludge wastage, seems to suggest. If a sludge mass in

---

[11] Based on Takács I, Patry, G: (2002) The Dynamic Solids Residence Time. Proceedings of IWA 2002, Melbourne, Australia, and as yet unpublished work with Anne-Emmanuelle Stricker

an activated sludge system does not have any influent loading (being off-line for maintenance, for example), consequently no new growth and no sludge production occur for one day, then, at the end of the day, irrespective of the amount of solids wasted from the system, the remaining solids will be exactly one day older. At the other extreme, if the new solids production in a day, due to a very high load, matches the amount of solids that were retained in the system at the beginning of the day, then the biomass, on average, will become "substantially" younger, even if no sludge is wasted during the day. Under these conditions, the traditional SRT calculation method, based on steady-state conditions, fails to reflect the true age of the solids. The development of a simple, intuitive, and generic method to calculate the DSRT is presented.

12.2 The Dynamic Solids Residence Time equation

The change in the average age of the solids in an activated sludge system is due to aging of the existing solids plus the effect of new (young) solids arriving and generated in the process.

The basis of the mathematical development is the mass weighted age balance, written for a finite time Δt as follows:

(Age x mass) of solids = (age x mass) of old solids remaining + (age x mass) of new solids

$$A_t M_t = (A_0 + \Delta t)(M_0 - M_L) + \Delta t M_P \tag{12.1}$$

where

Δt Time interval [d]

A_0 Age (Solids Residence Time) of solids at the beginning of Δt [d]

A_t Age (Solids Residence Time) of solids at the end of Δt [d]

M_0 Mass of solids at the beginning of Δt [kg]

M_t Mass of solids at the end of Δt [kg]

M_L Mass of solids lost during Δt [kg]

M_P Mass of solids produced during Δt [kg]

The mass balance for Δt is:

$$M_t = M_0 - M_L + M_P \tag{12.2}$$

$M_0 - M_L$ can be expressed from Equation 12.2 and substituted into 12.1 to reduce the number of variables:

$$A_t M_t = (A_0 + \Delta t)(M_t - M_P) + \Delta t M_P \tag{12.3}$$

expanding Equation 12.3 allows the cancellation of the $\Delta t M_P$ term

$$A_t M_t = A_0 M_t - A_0 M_P + \Delta t M_t - \cancel{\Delta t M_P} + \cancel{\Delta t M_P} \tag{12.4}$$

194

Rearranging 12.4:

$$A_t M_t - A_0 M_t = \Delta t M_t - A_0 M_P \tag{12.5}$$

Expressing the age change from 12.5, dividing by $\Delta t M_t$

$$\frac{A_t - A_0}{\Delta t} = 1 - \frac{A_0 M_P}{M_t \Delta t} \tag{12.6}$$

taking the differential form of 12.6 and recognizing that the true sludge production (F_P, in kg/d) is the mass produced over Δt :

$$\frac{dA}{dt} = 1 - \frac{A F_P}{M} \tag{12.7}$$

Using SRT instead of A, the ordinary differential equation (ODE) describing the age change in activated sludge systems can be expressed in the following form:

$$\frac{dSRT}{dt} = 1 - \frac{SRT \cdot F_p}{M} \tag{12.8}$$

where:

$\dfrac{dSRT}{dt}$ Age change [d/d; age of solids in days per days of real time]

M Mass of solids in the system [kgTSS]

F_p Mass flow of solids (true solids production) produced in the system [kgTSS/d]

Equation 12.8 expresses that the age change in a day is maximum one day, or (usually) less, and can even be negative (the sludge getting younger) depending on the relative amount of fresh sludge produced.

In a dynamic modelling environment, the ODE presented in (12.8) can be integrated from an instantaneous or steady-state initial condition using a suitable numerical solver. Under real plant conditions, only composite samples are typically available. Assuming that daily composite samples are available, the sludge production must be estimated daily. Using the true sludge production and MLSS mass values, the derivative (i.e., age change) can be calculated and added to the previous day's SRT to arrive at the actual SRT value.

$$SRT_{today} = SRT_{yesterday} + 1 - \frac{SRT_{yesterday} \cdot F_p}{M_{today}} \tag{12.9}$$

This simple algorithm (i.e., Euler integration with a fixed one-day step size) provides a close estimate of the actual dynamic SRT. This is illustrated in Figure 12.1 for a selected dynamic period of the experiment described in Section 12.4.
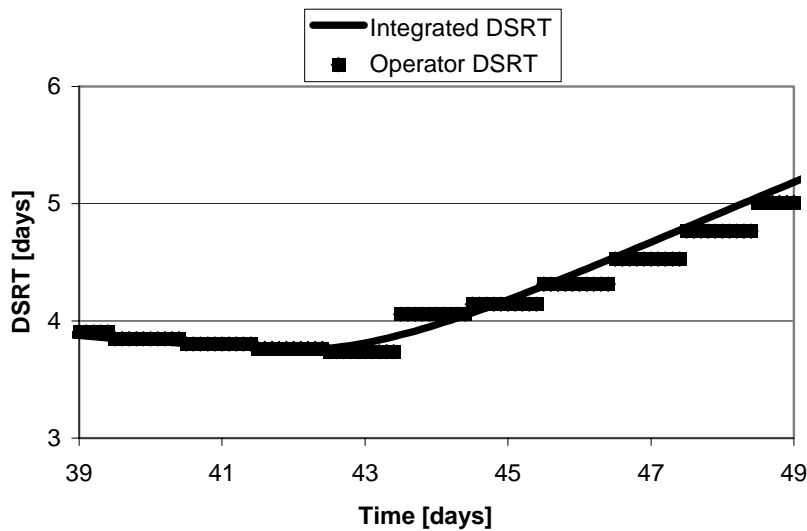
Figure 12.1. Operator calculation of the DSRT

The key parameter is estimating the correct amount of sludge produced (F_P) in the activated sludge system.

12.3 Estimating sludge production for the dynamic SRT equation

Plants lose solids mass in three different ways., with wastage, effluent and through endogenous respiration.

At most plants only wastage is considered, and is taken to approximate true sludge production. The strong practical justification for this is that the solids line will have to process only the wasted solids. The planet, however, sees the full effect of effluent solids discharged into the receiving water body, as well as mass lost through endogenous respiration in the form of CO_2 in the atmosphere. The actual residence time of the mixed liquor also depends on all three terms.

Two different methods to estimate the true sludge production are outlined in the following sections, depending on whether detailed influent fractionation is available or not. It must be emphasized that the dynamic SRT requires a dynamic (time dependent) approach, and that F_P is the instantaneous rate or (in lack of on-line data) the previous day's production. Consequently sludge production and decay formulae obtained from a steady-state approach cannot be used here.

12.3.1 Empirical method without influent fractionation

If only one or a few general measurements (BOD, COD, TSS, VSS or similar) are available for the influent at the plant, true solids production can be estimated as the sum of observed sludge production plus mass which is not observed since it is lost due to endogenous decay.

$$F_P = F_{P,obs} + F_d \qquad (12.10)$$

where

F_P True sludge production (kg/d)

$F_{P,obs}$ Observed (net) sludge production (kg/d)

F_d Mass lost by endogenous decay (kg/d)

For $F_{P,obs}$, a linear relationship can be established using recent historical data between daily sludge production and one or several of the above variables, using the concept of yield (Y).

$$F_P = Y_Q.Q_{\text{inf}} \qquad\qquad (12.11)$$

or $F_P = Y_{COD}.F_{COD}$ (12.12)

or $F_P = Y_{BOD}.F_{BOD}$ (12.13)

or $F_P = Y_{BOD}.F_{BOD} + Y_{TSS}.F_{TSS}$ (12.14)

Relationships using BOD_5 (12.13 or 12.14) usually give the best (most linear) prediction. The units of the yield and influent concentration must be selected such that they result in kg TSS produced (e.g. kgTSS/kgBOD if influent BOD loading is known).

F_d can be estimated using the mass of MLVSS (M_{VSS}) and a decay coefficient (b_{VSS}):

$$F_d = b_{VSS}M_{VSS} \qquad\qquad (12.15)$$

The default decay coefficient is 0.05 to 0.06 1/d (Eckenfelder and Weston, 1956; Eckenfelder and O'Connor, 1961). However the value of this parameter has been widely discussed, and updates suggest that it depends on influent composition, temperature and loading rate.

12.3.2 Estimation of true sludge production with influent fractionation

Total sludge produced is the sum of several distinct fractions:

$$F_p = F_B + F_E + F_I + F_{II} + F_{prec} \qquad\qquad (12.16)$$

where

F_B Mass of new biomass grown during Δt [kgTSS/d]

F_E Mass of inert endogenous products produced by the decay of the pre-existing biomass during Δt [kgTSS/d]

F_I Mass of organic inert suspended solids accumulated from the influent during Δt [kgTSS/d]

F_{II} Mass of inorganic inert suspended solids accumulated from the influent during Δt [kgTSS/d]

F_{prec} Mass of inorganic solids generated from internal processes such as chemical precipitation during Δt [kgTSS/d]

Based on sludge production equations (Dold, 2007)

$$F_B = Y_H F_{bCOD} \qquad\qquad (12.17)$$

$$F_E = f' b'_H M_H \tag{12.18}$$

$$F_I = \frac{F_{X_I}}{f_{CV,\text{inf}}} \tag{12.19}$$

where

Y_H Cellular yield of heterotrophs [kgTSS/kgCOD]
F_{bCOD} Influent mass flow of biodegradable COD [kgCOD/d]
f' Fraction of endogenous decay products in the endogenous model approach [-]
b'_H Decay coefficient of heterotrophs in the endogenous model approach [1/d]
M_H Mass of heterotrophic biomass present in the plant [kgCOD]
F_{XI} Influent mass flow of inert particulate COD [kgCOD/d]
$f_{CV,\text{inf}}$ COD:VSS ratio of influent particulate [gCOD/gVSS]

The mass of heterotrophs can be determined by adding the freshly grown biomass and subtracting the decayed biomass from the previous day's estimate. To initialize the calculation, a steady-state estimate from the steady-state model (Dold, 2007) or a dynamic estimate from a dynamic model can be used, similar to initializing the SRT itself. Over several days, the calculation will converge towards the best estimates, depending on data availability.

The use of this formula requires the prior determination of the COD fractions of the influent (Melcer *et al.*, 2002). For the endogenous parameters, the following default values can be used as guidelines (Dold, 2007):

f' = 0.2 [-]

$$b'_H = 0.24 \cdot 1.029^{T-20} \; [1/d] \tag{12.20}$$

where T is the temperature of the activated sludge [^{o}C].

12.4 Application examples

Equation (12.8) can be examined under different conditions.

At *Steady-State*, i.e. when the SRT does not change with time, ($\frac{dSRT}{dt} = 0$), and the net solids production can be approximated by the wastage, ($F_p = F_w$), the equation reduces, as expected, to the traditional steady-state SRT calculation:

$$\frac{M}{F_w} = SRT \tag{12.21}$$

The value of the derivative ($\frac{dSRT}{dt}$) in (12.8) is *never larger* than one, since there are only positive variables on the right-hand side of the equation, after the minus sign. This is equivalent to stating that the solids in any system can never age faster than real time, i.e. one day a day.

If for some period of time there is *no loading* and consequently no sludge production in the system, the age of the sludge will increase by one day a day (the maximum possible rate). The sludge wastage rate has no effect on this in agreement with the intuitive description in the introduction.

If there is an *influent load* and if sludge is being produced in the system (as most of the time in real activated sludge plants), the effect will depend on the proportion of new solids generated compared to the mass of old sludge.

In a highly loaded system the changes are fast. If the system is producing half the amount of solids present every day, the SRT at steady-state is 2 days. If, however, the initial condition is a 10-day SRT before the high load condition, the derivative will be -4 day/day and after the first day the DSRT will change to 6 days (i.e., a -40% change).

In a low loaded system, more time is necessary to attain the new equilibrium. As an example, in a 10 day SRT plant one-tenth of the existing mass of solids is generated every day. (At steady-state one-tenth of the solids must be wasted - hence the 10 day SRT). If the system was at steady-state, Equation (12.8) yields a value of zero for the derivative, confirming the stabilized state of the system. If, however, the system was operating at a 5-day SRT, the first day the sludge will age by 0.5 day (i.e., +10%) and the DSRT will be 5.5 days.

In practice, the transition from a 5-day to a 10-day SRT takes several weeks. This is much more indicative of the true performance of the activated sludge, as demonstrated in the following example.

The instantaneous and dynamic SRT calculations were implemented in the IWA Denitrifying Benchmark Plant (Copp *et al.*, 2002) in GPS-X™. In the first run, no dynamic data file was used (i.e., no change in influent flow rate or concentrations). The plant was simulated for 12 weeks starting from the dry weather steady-state condition with wastage changing according to the schedule shown in Table 12.1.

Table 12.1 Wastage schedule

Time	Wastage
[week]	[m3/d]
0	385
1	770
4	1055
6	385

The resulting traditional SRT calculation, a 7-day moving average applied to this value, and the Dynamic SRT are shown in Figure 12.2.
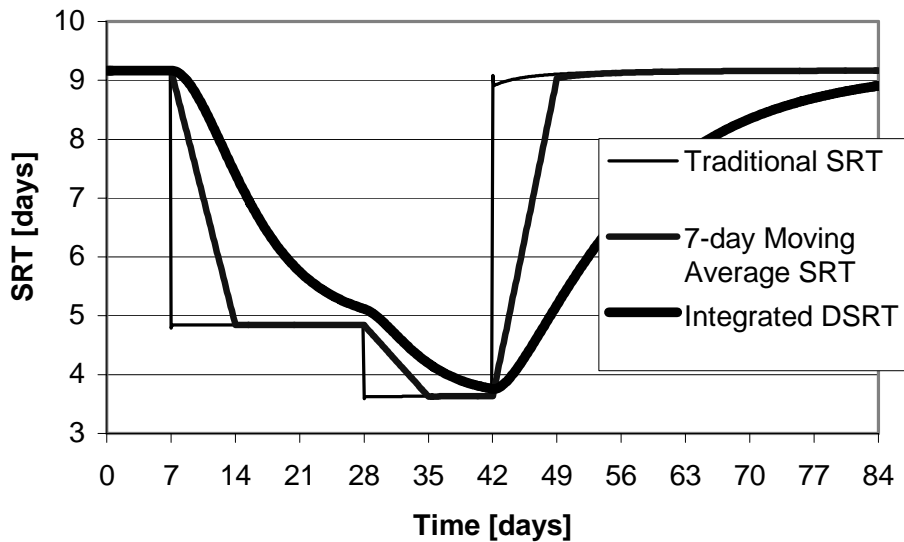
Figure 12.2. Comparison of SRT calculation methods

It can be concluded that in extreme cases the traditional SRT calculation is misleading and may lead to inappropriate control actions on part of the plant operators.

A smoothing method like applying a moving average can give similar results to the dynamic SRT in a certain SRT range, but the time window will need to be dynamically varied depending on the SRT in the system. I.e. longer SRT systems need a longer moving average window. The window essentially is the time constant of the system.

In contrast, the DSRT does not have these drawbacks and is representative of the true age of the biological solids. To demonstrate this, another simulation was performed with the same benchmark layout. In this case, the dry weather data file in Copp *et al.* (2002) (extended to 8 weeks) was used. To maintain a 5-day initial SRT on a steady-state basis, 744.5 m^3/d waste flow rate was necessary, while a 10-day SRT system required 367.5 m^3/d waste flow. The plant was converged to steady-state at 5 days SRT, then after one week dynamic run the waste flow rate was reduced and the plant was run for 7 more weeks. The two types of SRTs, along with the effluent ammonia (to indicate process performance), are plotted in Figure 12.3.
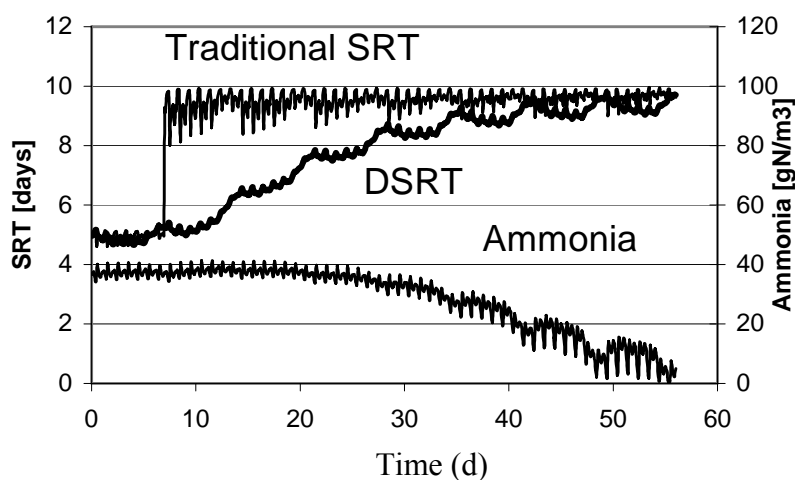
Figure 12.3. SRT, DSRT and process performance (effluent NH_3)

200

The dynamic SRT is inherently more stable and the real process performance (in this example start of nitrification) bears a closer relationship to the dynamic SRT than to the traditional, instantaneous SRT.

12.5 Plant example – SRT and nitrification at cold temperatures

The data from the operation of a wastewater treatment plant in Austria provides a case to illustrate the use of dynamic SRT in full-scale plants. The plant serves 14 mountain communities in the Alps drained with a combined sewer. The plant was designed for a Population Equivalent (PE) of 72000, and PE currently connected is 37000. The plant has the following main treatment steps and volumes:

Grit chamber 396 m^3
Primary clarifier 1200 m^3
Biological treatment $3 \times 1000 \text{ m}^3$ ($1/3^{rd}$ pre-anoxic)
Secondary clarifier $2 \times 2600 \text{ m}^3$

The maximum hydraulic loading is $28200 \text{ m}^3/\text{d}$ during dry weather and $52000 \text{ m}^3/\text{d}$ during rain weather. The process temperature varied between 4 and 15 ^{o}C in 2004. The plant is in a cold mountain climate, supplied by long sewers, as it is a centralized WWTP for a whole valley.

The pipes are embedded in cold ground, and cold groundwater. The pipes have large diameters so there may be heat loss to cold air. The plant operated at a total SRT of 6 to 8 days. Under these conditions, the process was only able to nitrify when temperature was above 10 ^{o}C, as shown in Figure 12.4.

The critical SRT for nitrifier washout was calculated according to Equation 12.22:

$$SRT_{crit} = \frac{1}{\mu_{A,T} * (1 - f_{ANOX}) - b_{A,T}} \qquad (12.22)$$

and

$$\mu_{A,T} = \mu_{A,20} \theta_\mu^{(T-20)} \qquad (12.23)$$

$$b_{A,T} = b_{A,20} \theta_b^{(T-20)} \qquad (12.24)$$

where

$\mu_{A,T}$ maximum specific nitrifier growth rate at actual temperature (T)
f_{ANOX} anoxic reactor volume fraction (33%)
$b_{A,T}$ nitrifier decay rate at actual temperature (T)
$\mu_{A,20}$ maximum specific nitrifier growth rate at 20 ^{o}C (0.9 1/d)
$b_{A,20}$ nitrifier decay rate at 20 ^{o}C (0.15 1/d)
θ_μ temperature sensitivity coefficient for μ_A (1.10)
θ_b temperature sensitivity coefficient for b_A (1.08)
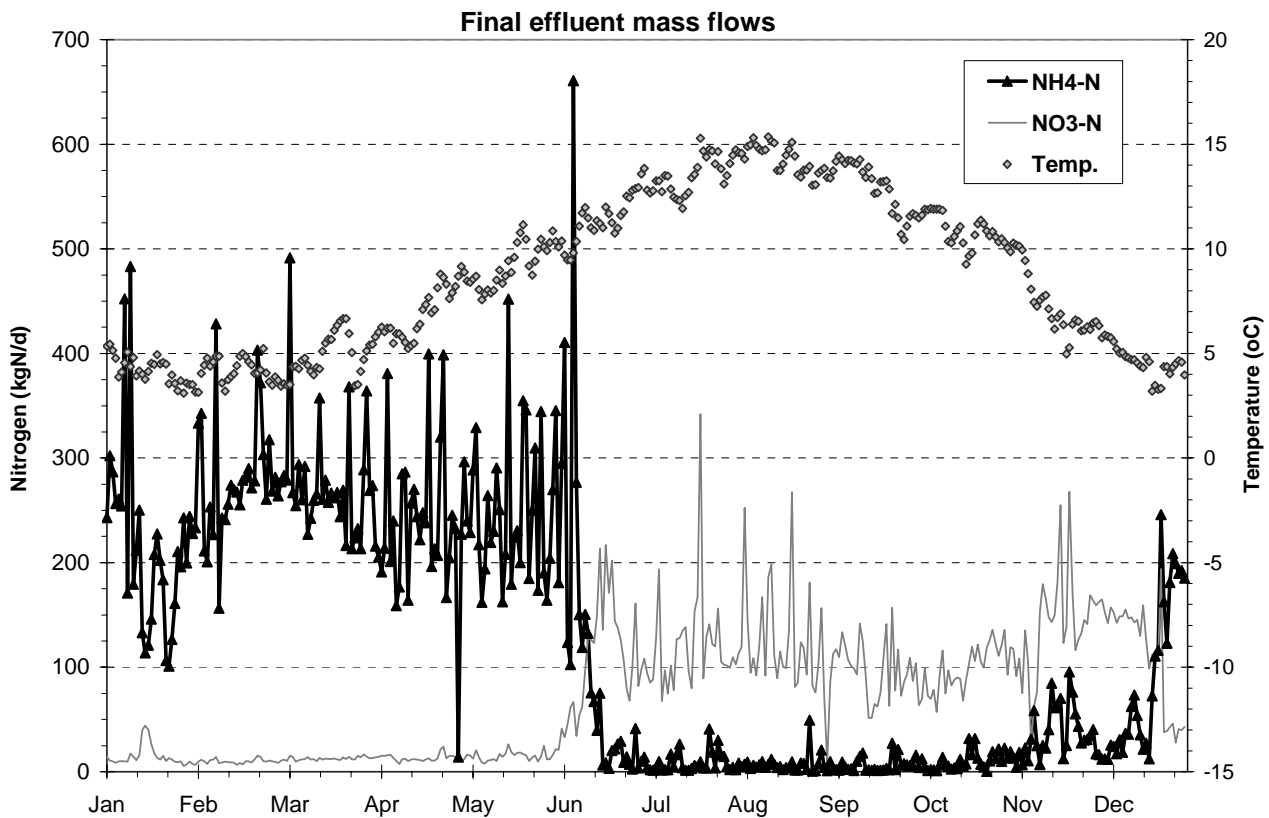
Figure 12.4. Stable nitrification above 10 ^{0}C at the example WWTP

The washout SRT, according to Equation 12.2, and the traditional SRT (smoothed by a 7-day moving average window) were calculated and plotted on Figure 12.5. It is clearly visible that during periods when the 7-day moving average SRT is below the washout SRT (grey areas until June and after early November), no nitrification occurs. The 7-day moving average SRT seems to be a good indicator of process performance, except between Christmas and New Year: on December 23rd, a loss of sludge mass occurred following emergency repair on one clarifier. The operators stopped wasting for the next 5 days, and the sludge concentration gradually recovered. The instantaneous SRT drops to 4 days on December 23rd as it takes into account the reduced sludge mass, then soars beyond 55 days for the following days as wastage is halted and effluent is the only solids output. The moving average smoothes out the one-day drop, and climbs from 8 to 45 days, while nitrification is lost.

On Figure 12.6 the dynamic SRT is plotted together with the washout SRT. The dynamic SRT agrees mostly with the 7-day moving average SRT except in two conditions. First, the dynamic SRT is able to explain why there was no nitrification during the Christmas season. The true age of the solids dropped instantaneously from 8.5 to 3 days due to the loss of older sludge mass on December 23rd. Even if there was no wastage for the following week, the fresh sludge produced daily limited the aging of solids to 0.4 day/day. The dynamic SRT remained below the critical washout SRT for the whole week, while the traditional SRT calculation failed due to the absence of wastage.

202
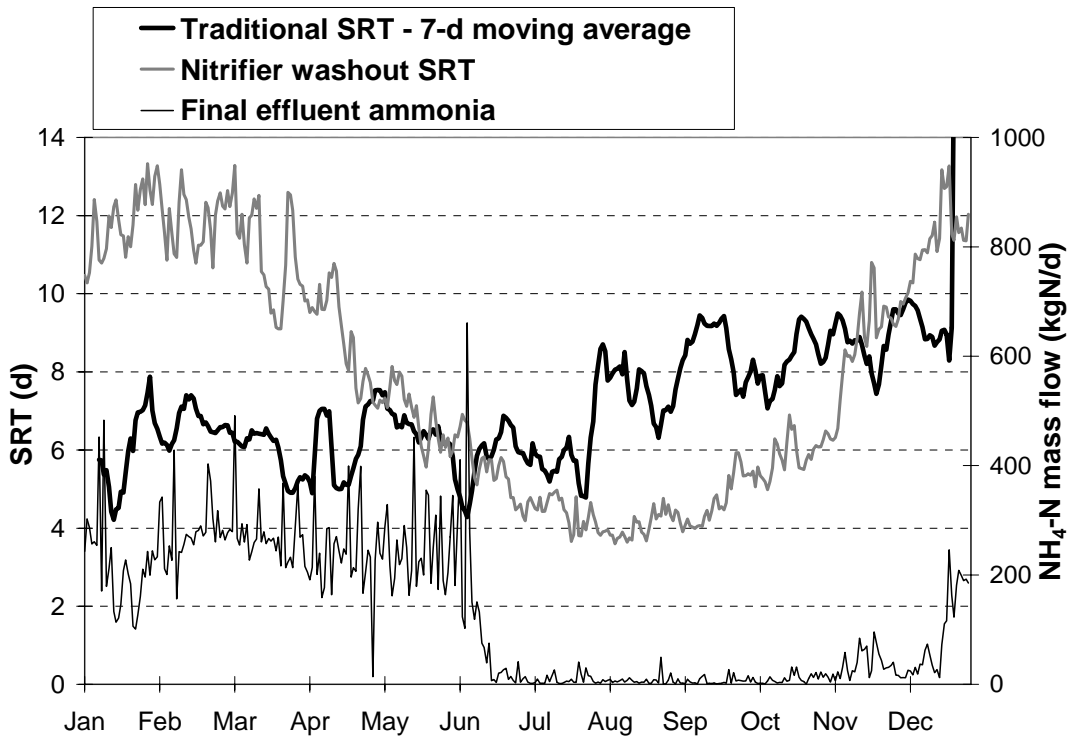
Figure 12.5. Traditional 7-day moving average SRT and nitrifier washout SRT. Grey periods: 7-day SRT is below the washout SRT, no nitrification is expected

The dynamic SRT may also be somewhat more accurate in indicating the marginal nitrifying conditions existing from June to mid July. There are several short periods when the actual dynamic SRT drops to the critical SRT, and there are corresponding small peaks in effluent ammonia.
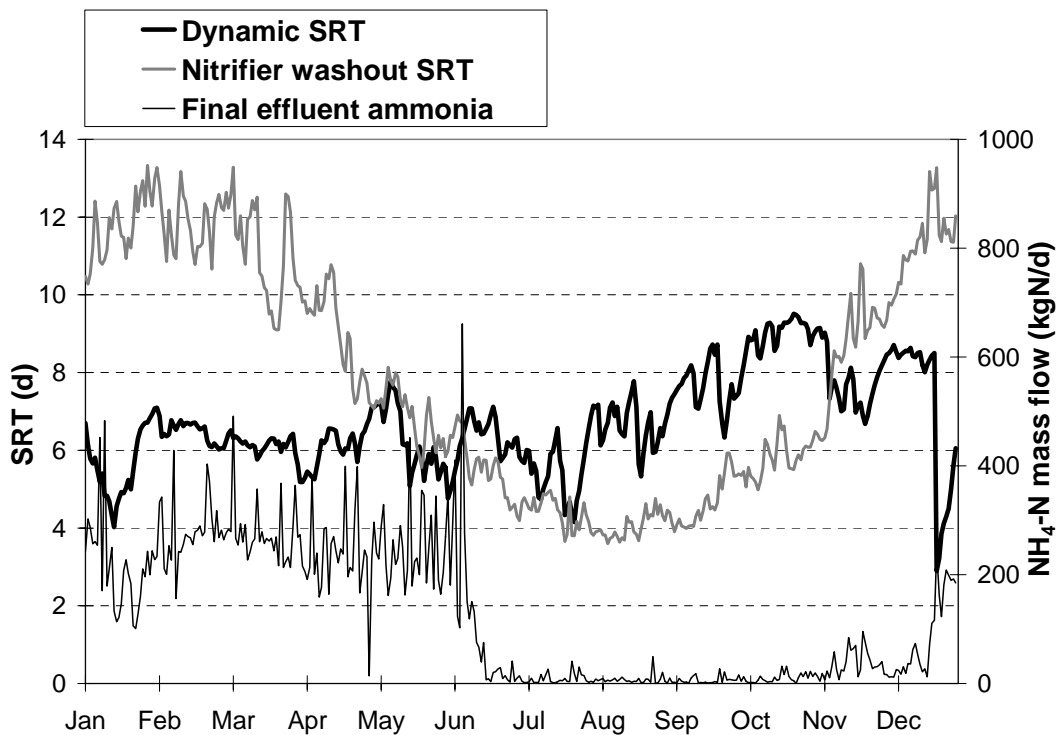
Figure 12.6. Daily dynamic SRT and nitrifier washout SRT. Grey periods: dynamic SRT is below the washout SRT, no nitrification is expected

The 7 day moving average SRT blurs these conditions due to the averaging period. In fact, the moving average method should consider the actual SRT as the length of the moving time window. While the results of such an advanced filtering method may be similar to the dynamic SRT, this may not be practical in a full-scale plant situation. For example, a 6.7 day moving average (and performing the moving average with a variable window) is difficult to do in an actual plant operating environment with only daily composite data available. The dynamic SRT, by its formulation, will take this effect into account.

12.6 Conclusions

Wastewater treatment plants rely on SRT as one of the most important process variables to maintain optimal operation. The widely used steady-state based calculation method fails to provide a useful estimate of the sludge age under dynamic conditions or requires more sophisticated filtering than a simple 7-day moving average, to reflect the true age of solids, and expected process performance.

The proposed Dynamic Solids Residence Time (DSRT) variable

- provides a representative estimate of the true age of the solids in an activated sludge system, even under extreme dynamic conditions (i.e. startup of nitrification);
- at steady-state is equivalent to the traditional, instantaneous SRT;
- is easy to calculate under real-world conditions or in a dynamic simulation.

Estimation of the true solids production at plants is the key for calculating both the steady-state and dynamic solids residence time.

13 ELEMENTAL BALANCES IN ACTIVATED SLUDGE MODELLING[12]

13.1 Introduction

Engineers and operators have to consider the whole treatment plant and the effect of individual processes, recycles on each other in their work. One of the approaches to full-plant modelling is to link existing process models (e.g. ASM1, ADM1 and others) through transformers to each other. The continuity-based interfacing method (CBIM, Vanrolleghem *et al.*, 2005) was recently proposed and applied to construct such interfaces. This systematic method of building model transformers is based on elemental composition (C, H, O, N, P, S content) of organic and inorganic matter in the models to be connected. The transformer must preserve mass balances (continuity) on all elements when mapping state variables between models. Thus, the CBIM requires information on the elemental composition of all state variables. The insight that specification of elemental composition is useful in modelling is not new; see for instance, see Hellinga *et al.* (1996), Henze *et al.* (2000) Reichert *et al.* (2001), Batstone *et al.* (2002).

The objective of this chapter is to investigate, using the example of ASM1, if existing models preserve elemental material balances, and to describe how to determine elemental composition of state variables. The Gujer (Petersen) matrix method is extended to ensure that these balances are preserved. Maple (Maplesoft, 2005) was used for most symbolic equation manipulations.

13.2 Do COD-based models preserve elemental balances?

The ASMx models were constructed using COD and N mass balances. The models in their current form do not close the balance on C, H, O and N. Consideration of dissolved nitrogen gas, CO_2 and water as reaction products is necessary to close elemental balances in these models. These state variables, particularly water, as a reaction product, do not need to be calculated (integrated) in the model but are necessary to write the complete reaction of the particular process (e.g. heterotrophic growth) according to accepted chemical reaction principles. Thus, the ASM1 model matrix, which is used here as the illustrative example since it considers only COD, N and charge balances, was extended with three new columns: dissolved N_2 gas (S_{N2} g N/m^3), total CO_2 (S_{CO2} mol/m^3), and water, (S_{H2O} mol/m^3).

Charge balance is maintained in ASM1 using alkalinity as a state variable and the effect of charged reactants on it (e.g. nitrification using NH_4^+ and producing NO_3^-). This aspect was not included in this chapter, since there is a contemporary and more accurate way of calculating

---

[12] Takács I. and Vanrolleghem P.A. (2006) Elemental balances in activated sludge modelling. In: Proceedings of the IWA World Water Congress, 10-14 September 2006, Beijing, China.

the pH effects of conversion processes, through an equilibrium pH-model outside the kinetic matrix. This was introduced in the River Water Quality Model No. 1 (Reichert *et al*., 2001), and then adopted in ADM1 (Batstone *et al*., 2002) and ASM models (Takács *et al*., 2004; Volcke *et al*., 2006), and is described in Chapter 6. The new method incorporates the effect of other processes (e.g. CO_2 gas transfer) on alkalinity, and does not depend on an approximate charge balance (e.g. the charge of total CO_2 is pH dependent, at pH=7 and typical wastewater ionic strength is 0.819). For these reasons charge balances will not be considered in this chapter focussing on elemental balances. Consequently, the alkalinity state variable was not included in this analysis and all state variables will be represented in their un-ionized form (e.g. NH_3 and HNO_3). These state variables represent the complete mass of the compound, e.g. the sum of ammonia (NH_3) and ammonium (NH_4^+).

13.3 Determination of elemental composition of state variables

In order to present an example of elemental balancing, the elemental composition of each state variable in the extended ASM1 matrix was determined. The N (and P and S) components in particulate organic matter can be directly measured by common analytical methods. Typical values in municipal wastewater are: N: 10-12% of VSS, P: 2-3% of VSS, S: 1% of VSS (Grady *et al*., 1999). To determine the C, O and H contents for one particular component, three independent measurements are required, e.g. COD, VSS, TOC. For each additional element (N, P, S) we need one more analytical measurement. In an example case we would have:

$$C_{\alpha,C}H_{\alpha,H}O_{\alpha,O}N + \gamma_{O2}O_2 \rightarrow \gamma_{CO2}CO_2 + \gamma_{H2O}H_2O + NH_3$$
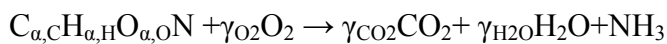
This equation has six unknowns. Carbon balance is trivial, and the rest can be found from the following balances:

COD/VSS ratio $\qquad iCOD = 2\gamma_{O2}O/(\alpha_{,C} C + \alpha_{,H} H + \alpha_{,O} O_{\alpha,O} + N)$

C/VSS ratio $\qquad iC = \alpha_{,C}C/(\alpha_{,C} C + \alpha_{,H} H + \alpha_{,O} O_{\alpha,O} + N)$

N/VSS ratio $\qquad iN = N/(\alpha_{,C} C + \alpha_{,H} H + \alpha_{,O} O_{\alpha,O} + N)$

Hydrogen balance $\qquad \alpha_{,H} = 2\gamma_{H2O} + 3$

Oxygen balance $\qquad \alpha_{,O} + 2\gamma_{O2} = 2 \alpha_{,C} + \gamma_{H2O}$

which lead, by using Maple (Maplesoft, 2005) symbolic manipulation software for ease of work, to the chemical composition deduced from simple measurements given in Table 13.1.

Table 13.1. Composition of organic matter obtained from simple analytical measurements and atomic weights.

Component considered $C_{\alpha,C}H_{\alpha,H}O_{\alpha,O}N$
$\alpha_C = iC \cdot N/(iN/C)$
$\alpha_H = (3 \cdot C \cdot iN \cdot O + 2 \cdot C \cdot iCOD \cdot N - 2 \cdot C \cdot iN \cdot N + 2 \cdot C \cdot N - 2 \cdot iC \cdot N \cdot C$ $- 4 \cdot iC \cdot N \cdot O)/iN/C/(2 \cdot H + O)$
$\alpha_O = - (2 \cdot C \cdot iCOD \cdot N \cdot H - 4 \cdot iC \cdot N \cdot O \cdot H + O \cdot C \cdot iN \cdot N + 3 \cdot O \cdot C \cdot iN \cdot H$ $- O \cdot C \cdot N + O \cdot iC \cdot N \cdot C) / iN/O/C/(2 \cdot H + O)$
$\alpha_N = 1$

13.3.1 Biomass composition

Bailey (1986) reports C and N contents for several microorganisms – the average is 49.9% C in VSS, and 13.3% N in VSS. Rittman (2000) presents data for COD/VSS ratios: 1.39 g COD/g VSS for pure and 1.33 g COD/g VSS for mixed cultures. ASM3 (Henze *et al.*, 2000) contains a COD/TOC ratio of 2.8. A typically used biomass composition is $C_5H_7O_2N$ after Hoover and Porges (1952), which was subsequently used by many schools (e.g. UCT) and incorporated into almost all modern modelling literature (Henze *et al.,* 1995; Henze *et al.*, 2000). This molecular formula, based on the reaction (assumed to occur during the COD test):

$$C_5H_7O_2N + 5 O_2 \rightarrow 5 CO_2 + 2 H_2O + NH_3$$
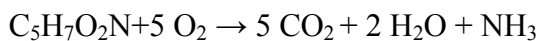
results in the following ratios: COD/VSS=1.42, N/VSS=0.124, C/VSS=0.53, and COD/TOC=2.7. Since these are close to typically measured ratios, the $C_5H_7O_2N$ formula is used in this chapter for both heterotrophs (X_H) and autotrophs (X_A), as well as their decay products (X_P). X_P is usually thought to contain less N than active biomass, but in lack of precise measurements of N, TOC and COD contents the same composition was accepted.

13.3.2 Substrate and inert composition

The elemental composition of biodegradable and inert organic state variables can be deduced using the following logic. COD/VSS ratios for X_S and X_I state variables can be calculated from COD/VSS ratios of influent wastewater and activated sludge mixed liquor, two typical mixtures with available measurements and known composition. Table 13.2 shows typical compositions of influent and MLSS, from simulations assuming 500 g COD/m^3 and 60% particulates in the influent at 8 d SRT.

Table 13.2. State variables in influent and MLSS

State	Unit	Influent	MLSS
$X_H + X_E$	gCOD/m^3	15	1722
X_I	gCOD/m^3	65	891
X_S	gCOD/m^3	220	88

Table 13.3. COD/VSS ratios for X_I and X_S

Measured		Assumed	Calculated	
Influent	MLSS	Biomass	Inert (X_I)	Substrate (X_S)
1.6	1.48	1.42	1.58	1.62
1.8	**1.48**	**1.42**	**1.55**	**1.90**
2.0	1.48	1.42	1.53	2.18
2.2	1.48	1.42	1.50	2.46

The calculation method is based on measured influent and MLSS COD/VSS ratios, assuming that they are a combination of the COD/VSS ratios of the three types of components present (two equations). The biomass and decay product COD/VSS ratios are assumed fixed at 1.42, and the two unknowns are the COD/VSS ratios for X_I and X_S. In Table 13.3, a series of COD/VSS ratios have been calculated for the two state variables, from increasing measured influent COD/VSS ratios.

From a practical modelling standpoint, this result seems to point to a) a relatively stable influent inert COD/VSS ratio, and b) a very sensitive COD/VSS ratio for substrates, depending likely on the composition of the sewage (protein/lipid/carbohydrate fractions) This may to a large extent explain the variability found in influent COD/VSS ratios, and points to the usefulness of a more fundamental modelling approach that includes several types of biodegradable organic material, similar to ADM1 (Batstone *et al.*, 2002). Table 13.4 contains composition data for several typical influent organic materials.

Table 13.4. Composition of typical influent organic substances

Component	Formula	Reaction	COD/VSS	C/VSS
Lipids/fatty acids (n~14)	CH_3- nCH_2 COOH	CH_3 nCH_2 COOH + (1.5n+2) O_2 = (n+2) CO_2 + (n+2) H_2O	2.87	0.87
Mixture of amino acids	Varies, average length is taken as 4 carbons	Varies	1.84	0.63
Biomass	$C_5H_7O_2N$	$C_5H_7O_2N + 5O_2 =$ $5CO_2 + 2H_2O + NH_3$	1.42	0.53
Proteins	$C_{3.5}H_{7.06}O_{1.75}N$	$C_{3.5}H_{7.06}O_{1.75}N + 3.64O_2 = 3.5CO_2 + 2.03H_2O + NH_3$	1.28	0.46
Carbohydrates	CH_2O	$CH_2O + O_2 = CO_2 + H_2O$	1.07	0.47

For the purpose of this chapter, for a "typical" influent with a COD/VSS ratio of 1.8, the following state variable COD/VSS ratios were selected: 1.55 for inert X_I and 1.9 for substrate X_S. Carbon contents were taken from Henze *et al.* (2000) as 2.8 COD/TOC ratio for X_I and 3.2 COD/TOC ratio for X_S. Based on the calculation of these combined COD/VSS and COD/TOC ratios from X_I and X_S elemental compositions, and the oxygen and hydrogen balance equations in the $C_{\alpha C}H_{\alpha H}O + \gamma_{O2}O_2 = \alpha_C CO_2 + \gamma_{H2O}H_2O$ reaction, four equations can be expressed for the four unknowns (α_C, α_H, γ_{O2}, γ_{H2O}), and thus the composition can be calculated. The resulting composition is shown in Table 13.5. In lack of filtered DOC/VS data, readily biodegradable substrate and soluble inert organics were assigned the same composition as their particulate counterparts. Organic nitrogen forms must be allocated the composition of NH3, since all associated carbon and COD is accounted for in the relevant organic state variables.

Table 13.5. Composition of state variables in ASM1 used in this study

State variable	Unit	Molar composition	Mass fraction of elements
S_I	$gCOD/m^3$	$C_{1.90}H_{2.39}O$	C=0.553; H=0.058; O=0.388;
S_S	$gCOD/m^3$	$C_{2.43}H_{3.96}O$	C=0.594; H=0.081; O=0.325;
X_I	$gCOD/m^3$	$C_{1.90}H_{2.39}O$	C=0.553; H=0.058; O=0.388;
X_S	$gCOD/m^3$	$C_{2.43}H_{3.96}O$	C=0.594; H=0.081; O=0.325;
X_H	$gCOD/m^3$	$C_5H_7O_2N$	C=0.531; H=0.062; O=0.283; N=0.124;
X_A	$gCOD/m^3$	$C_5H_7O_2N$	C=0.531; H=0.062; O=0.283; N=0.124;
X_E	$gCOD/m^3$	$C_5H_7O_2N$	C=0.531; H=0.062; O=0.283; N=0.124;
S_O	$gO2/m^3$	O_2	O=1.00;
S_{NO}	gN/m^3	HNO_3	H=0.016; N=0.222; O=0.762;
S_{NH}	gN/m^3	NH_3	H=0.176; N=0.824;
S_{ND}	gN/m^3	NH_3	H=0.176; N=0.824
X_{ND}	gN/m^3	NH_3	H=0.176; N=0.824

Note: Atomic weights used are: C = 12.011g/mol, H = 1.0079g/mol, O = 15.9994g/mol and N = 14.007g/mol

13.4 Extended Gujer matrix

It is proposed that the Gujer (Petersen) matrix be extended with the necessary state variables (N_2, CO_2, H_2O and others for more detailed models) to allow the continuity check on conservation of elements. Table 13.6 contains the extended ASM1 stoichiometry matrix. Stoichiometric parameters and their values are listed in Table 13.7.

Table 13.6. Extended ASM1 stoichiometry matrix

Process	S_I	S_S	X_I	X_S	X_H	X_A	X_P	S_O	S_{NO}	S_{NH}	S_{ND}	X_{ND}	S_{N2}	S_{CO2}	S_{H2O}
	g COD/m³							g O₂/m³	g N/m³					mol/m³	
1		$-\frac{1}{Y_H}$			1			$-\frac{1-Y_H}{Y_H}$		$-i_{XB}$				$\frac{\gamma_{CO_2,1}}{160}$	$\frac{\gamma_{H_2O,1}}{160}$
2		$-\frac{1}{Y_H}$			1				$-\frac{1-Y_H}{2.86Y_H}$	$-i_{XB}$		$\frac{1-Y_H}{2.86Y_H}$		$\frac{\gamma_{CO_2,2}}{160}$	$\frac{\gamma_{H_2O,2}}{160}$
3						1		$-\frac{4.57-Y_A}{Y_A}$	$\frac{1}{Y_A}$	$-\frac{1}{Y_A}-i_{XB}$				$-\frac{\gamma_{CO_2,3}}{160}$	$\frac{\gamma_{H_2O,3}}{160}$
4				$1-f_P$	-1		f_P					$i_{XB}-f_P*i_{XP}$		$\frac{\gamma_{CO_2,4}}{160}$	$-\frac{\gamma_{H_2O,4}}{160}$
5				$1-f_P$		-1	f_P					$i_{XB}-f_P*i_{XP}$		$\frac{\gamma_{CO_2,5}}{160}$	$-\frac{\gamma_{H_2O,5}}{160}$
6										1	-1				
7		1		-1											
8											1	-1			

Note: 160 g COD/m³ is the COD of one mole of biomass. Processes: 1. Aerobic growth of heterotrophs 2. Anoxic growth of heterotrophs 3. Aerobic growth of autotrophs 4. 'Decay' of

heterotrophs 5. 'Decay' of autotrophs 6. Ammonification 7. Hydrolysis of slowly biodegradable substrate 8. Hydrolysis of particulate biodegradable organic nitrogen

Table 13.7 Extended ASM1 stoichiometric parameters

Stoichiometric parameter	Unit	Value
Y_H	gCOD/gCOD	0.667
Y_A	gCOD/gN	0.24
f_P	gCOD/gCOD	0.08
i_{XB}	gN/gCOD	0.088
i_{XP}	gN/gCOD	0.088
$\gamma_{CO2,i}$ and $\gamma_{H2O,i}$	Mole	From the relevant process in Table 13.9

For clarity, a column with the chemical reactions should be added after the process rates to describe the specific process as a reaction, according to accepted chemical principles. This information can be expressed in three different ways:

1. Generally (for any composition of state variables and any value of stoichiometric constants);
2. For a chosen fixed composition of state variables and any value of stoichiometric constants;
3. For fixed composition of state variables and selected stoichiometric constants.

Table 13.8. Different ways of expressing process rates (example: aerobic heterotrophic growth)

For variable Y_H and any component composition

$$\frac{A}{Y_H B}C_{\alpha_{C,S}}H_{\alpha_{H,S}}O + \frac{A(Y_H - \alpha_{C,S})}{4Y_H}O_2 + NH_3 \rightarrow C_{\alpha_{C,B}}H_{\alpha_{H,B}}O_{\alpha_{O,B}}N + \frac{Y_H\alpha_{C,B}B - \alpha_{C,S}A}{Y_H B}CO_2$$

$$+ \frac{\alpha_{H,S}(4\alpha_{C,S} - 2\alpha_{O,B} - Y_H\alpha_{H,B}) - Y_H\alpha_{H,B}B + 3Y_H B}{2Y_H B}H_2O$$

where

$A = 4\alpha_{C,B} + \alpha_{H,B} - 2\alpha_{O,B}$

$B = 4\alpha_{C,S} + \alpha_{H,S} - 2$

Notation for number of atoms in formula (α) = $\alpha_{element,state}$ element is C, H or O, state is Biomass or Substrate

For variable Y_H and component composition listed in Table 5:

$$\frac{1.71}{Y_H}C_{2.43}H_{3.96}O + 5\frac{1-Y_H}{Y_H}O_2 + NH_3 \rightarrow C_5H_7O_2N + \frac{4.16-5Y_H}{Y_H}CO_2 + \frac{3.39-2Y_H}{Y_H}H_2O$$

For Y_H=0.667 and component composition listed in Table 5:

$2.57\ C_{2.43}H_{3.96}O + 2.50\ O_2 + NH_3 \rightarrow C_5H_7O_2N + 1.24\ CO_2 + 3.09\ H_2O$

Table 13.8 shows the three ways of expressing the reactions (example for the aerobic growth process in ASM1). In order to present a complete example of the simplest presentation mode of ASM1 reactions, with fixed constants, Table 13.9 is given. Since reactions are expressed for one mole of biomass, and the stoichiometry matrix (Table 13.6) is expressed in g COD/m^3 units, it is necessary to convert reaction coefficients using the COD content of one mole of biomass (e.g. 160 g COD/m^3).

Table 13.9. ASM1 reaction column

Process	Reaction
Aerobic growth of heterotrophs	$2.57\ C_{2.43}H_{3.96}O + 2.50\ O_2 + NH3 \rightarrow$ $C_5H_7O_2N + 1.24\ CO_2 + 3.09\ H_2O$
Anoxic growth of heterotrophs	$2.57\ C_{2.43}H_{3.96}O + 2.0\ HNO_3 + NH_3 \rightarrow$ $1.24\ CO_2 + C_5H_7O_2N + N_2 + 4.09\ H_2O$
Growth of autotrophs	$48.59\ NH_3 + 5\ CO_2 + 90.19\ O_2 \rightarrow$ $C_5H_7O_2N + 47.59\ HNO_3 + 45.59\ H_2O$
Decay of heterotrophs	$C_5H_7O_2N + 1.28\ H_2O \rightarrow$ $1.58\ C_{2.43}H_{3.96}O + 0.08\ C_5H_7O_2N + 0.92\ NH_3 + 0.77\ CO_2$
Decay of autotrophs	$C_5H_7O_2N + 1.28\ H_2O \rightarrow$ $1.58\ C_{2.43}H_{3.96}O + 0.08\ C_5H_7O_2N + 0.92\ NH_3 + 0.77\ CO_2$
Hydrolysis of particulate substrate	$C_{2.43}H_{3.96}O \rightarrow C_{2.43}H_{3.96}O$
Hydrolysis of particulate nitrogen	$NH_3 \rightarrow NH_3$
Ammonification	$NH_3 \rightarrow NH_3$

13.5 Concluding remarks

The proposed methods will increase the information contained in wastewater process models used today, enable modellers to construct models that preserve elements, will make reading of the models more informative, and will make constructing CBIM-based transformers between submodels more rigorous, by significantly reducing the number of degrees of freedom from estimating state variable elemental compositions.

It was found that not all data are readily available for elemental balancing of municipal wastewater components. TOCs, as well as DOC and VS measurements on filtrates would help to establish typical state variable compositions. Direct chemical component measurement (e.g. protein extraction, ether extractable lipids) would be useful as well.

The composition of certain state variables (e.g. biomass, inerts) seems to be stable. Others (influent substrate) vary significantly. Proper handling of this may lead to models based on

more fundamental components like proteins, lipids and carbohydrates (similar to ADM1, Batstone *et al.*, 2002). This should lead to more stable stoichiometric parameters and more predictive power for the models.

There is evidence (e.g. Pramanik and Keasling, 1997) that elemental composition changes even for variables that are considered stable. For example, biomass can have different N content in high-loaded, low-loaded or nutrient-limited conditions. Current modelling methodology does not deal with this in an elegant way and is in need of more research and development. Hence, in today's models, composition parameters have to be considered for calibration as well.

Elemental balancing increases the complexity and data requirements of models, while at the same time increasing the amount of information contained in models. On a process model basis, this is not always required. For example, O_2 uptake and sludge production predictions do not change in the proposed extended ASM1 matrix. However, elemental balancing provides a rigorous integrity check for models, leads to new insights into the behaviour of wastewater treatment systems, and facilitates the use of the continuity-based interfacing method to link different models.

14 ELEMENTAL BALANCE-BASED METHODOLOGY TO ESTABLISH REACTION STOICHIOMETRY IN ENVIRONMENTAL MODELLING[13]

14.1 Introduction

Strous *et al.* (1998, 1999) described a newly discovered lithotroph, anaerobically converting ammonia and nitrite to nitrogen gas according to the following stoichiometry:

$$NH_4^+ + 1.32\ NO_2^- + 0.066\ HCO_3^- + 0.13\ H^+ \rightarrow$$

$$0.26\ NO_3^- + 1.02\ N_2 + 0.066\ CH_2O_{0.5}N_{0.15} + 2.03\ H_2O$$
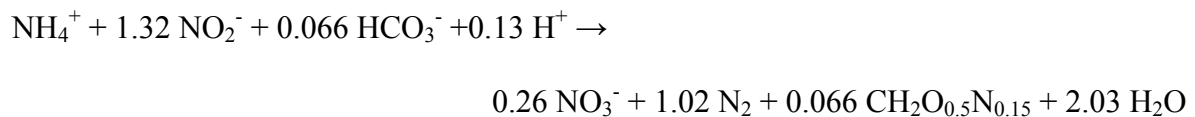
This new microorganism, a planctomycete, is an anaerobic ammonia oxidizer and was named Anammox.

A kinetic model for the growth of the Anammox biomass was proposed by Koch *et al.* (2002). Only the stoichiometry is investigated here. The basis of the growth reaction is 1 g Anammox biomass COD. The stoichiometric coefficients in the Koch model are shown in row 1 of Table 14.1.

Table 14.1. Proposed stoichiometric coefficients for the Anammox growth reaction

Components →	Ammonia S_{NH}	Nitrite S_{NO2}	Nitrate S_{NO3}	Nitrogen gas S_{N2}
Koch *et al.* (2002)	$-1/Y_{NH3}$	$-1/Y_{NH3} - 1/1.14$	$1/1.14$	$2/Y_{NH3}$
Hao *et al.* (2002)	$-1/Y_{NH3}$ $-i_{NBN}$	$-1/Y_{NH3} - 1/1.14$	$1/1.14$	$2/Y_{NH3}$
Dapena-Mora *et al.* (2004)	$-1/Y_{NH3}$ $-i_{NBN}$	$-1/Y_{NH3} - 1.52$	1.52	$2/Y_{NH3}$

$Y_{NH3} = 0.114$ g COD / g N, $i_{NBN} = 0.087$ g N / g COD

A full elemental balance cannot be established for this model since carbon (bicarbonate) is not included. Also, N for synthesis is not included. The authors recognize this but claim that this causes only a small error due to low biomass production. The remaining N balance is trivial and agrees only approximately with Strous *et al.* (1999). Concerning N_2 production, half of

---

[13] Originally published as Takács, I., Vanrolleghem, P.A., Wett, B., Murthy, S. (2007) Elemental balance based methodology to establish reaction stoichiometry in environmental modelling. Water Science & Technology 56. 9. p37-41.

the N comes from NH_3 and half from NO_2^-. The nitrate production stoichiometry is significantly different from Strous *et al.* (1999): 0.88 g NO_3-N is produced per g biomass COD instead of 1.52 g NO_3-N. Since one mole of this biomass representation contains 36.4 g COD, 0.26 mole of nitrate production per 0.066 mole of biomass converts to 1.52 g NO_3-N produced per g biomass COD (0.26 x 14.0 / (0.066 x 36.4)) according to Strous *et al.* (1999).

Hao *et al.* (2002) included N for synthesis (adding a $-i_{NBN}$ term to the S_{NH} column) and kept the same stoichiometry (Table 14.1).

Dapena-Mora *et al.* (2004) retained the same ammonia and nitrite stoichiometry (but introduced a typo missing the stoichiometric coefficient in the Anammox state variable column). The authors, based on the original Strous *et al.* (1998) publication, revised the 1/1.14 nitrate production stoichiometry to the correct 1.52 (Table 14.1).

An assumption in these modelling approaches is that half the nitrogen in the nitrogen gas produced is originating from ammonia, and the other half from nitrate. Elemental balancing can provide further insight into this assumption and help identify the proper stoichiometric coefficients.

14.2 Method description (example: ASM1 aerobic heterotrophic growth)

The well-known heterotrophic growth reaction under aerobic conditions in ASM1 (Henze *et al.*, 2000) is used to demonstrate the principle of the proposed elemental balancing method.

The proposed methodology relies on the following steps:

1) Establish the elemental composition of each state variable. In this section, the composition as developed in Chapter 13 for the extended ASM1 is used. Biomass composition is $C_5H_7O_2N$ and substrate composition is $C_{2.43}H_{3.96}O$.
2) Establish the COD content of the state variables (using the chemical reaction for complete oxidation). In this case, 1 mole of biomass is equivalent to 5 moles of O_2, and 1 mole of substrate is 2.92 moles of O_2.

   $C_5H_7O_2N + 5O_2 \rightarrow 5CO_2 + NH_3 + 2H_2O$

   $C_{2.43}H_{3.96}O + 2.92O_2 \rightarrow 2.43CO_2 + 1.98H_2O$
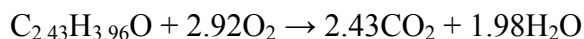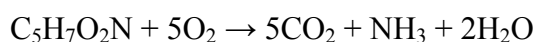
3) Set up an elementally balanced reaction with unknown stoichiometry to generate (an arbitrarily selected) 1 mole of biomass. This example is for aerobic heterotrophic growth, in the neutral form as described in Chapter 13, specifically for elemental balancing:

   $\gamma_{Ss}C_{2.43}H_{3.96}O + \gamma_{O2}O_2 + NH_3 \rightarrow \gamma_{CO2}CO_2 + C_5H_7O_2N + \gamma_{H2O}H_2O$
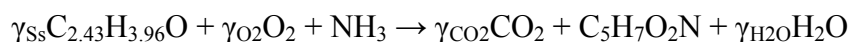
   Note that synthesis ammonia is explicitly identified, resulting in a trivial N balance. The reaction can be expressed in the usual charged form or using uncharged species. The uncharged form yields simpler symbolic manipulation and the resulting stoichiometric coefficients will be the same. Charge balance is maintained by using exclusively neutral, undissociated or unionized components.

4) There are four unknowns (γ_{Ss}, γ_{O2}, γ_{CO2}, γ_{H2O}) in the equation and three elemental balances can be set up. The degree of freedom is one – the measured yield. Set up three elemental balances and the expression for yield.
   - Carbon balance: $\gamma_{Ss} \cdot 2.43 = \gamma_{CO2}+5$;
   - Oxygen balance $\gamma_{Ss} + \gamma_{O2} \cdot 2 = \gamma_{CO2} \cdot 2+2+ \gamma_{H2O}$;
   - Hydrogen balance $\gamma_{Ss} \cdot 3.96+3 = 7+ \gamma_{H2O} \cdot 2$;
   - Yield expression $Y = (5 \cdot O_2)/(\gamma_{Ss} \cdot 2.92 \cdot O_2)$; (necessarily incorporating biomass and substrate COD equivalents, $O_2=32$g/mole).

5) Solve the linear equation system (manually or preferably using a symbolic solver, e.g. Maple (Maplesoft, 2005)). In ASM1 we are only interested in substrate, oxygen and biomass coefficients (though the method provides coefficients for CO_2 and H_2O as well), thus:

   For substrate, $\gamma_{Ss} = 1.712328767/Y_H$, for oxygen, $\gamma_{O2} = 5(1-Y_H)/Y_H$, for biomass, the coefficient is 1.

6) Do a mass balance check on the reaction to verify results.
7) The coefficients in 5) are per mole of biomass. A conversion to grams of biomass COD (which is the basis of the ASM1 process rate) is necessary, using values from 2). This results in:
   - Substrate coefficient: $1/Y_H$
   - O_2 coefficient: $(1-Y_H)/Y_H$
   - Biomass coefficient: 1
   - Synthesis N coefficient: $1 \cdot N/(5 \cdot O_2) = 0.087$ (N=14g/mole, $O_2=32$g/mole)

14.3 Method application (example: Anammox)

The elemental balance methodology described in the first section was applied to the Anammox growth reaction (Wett *et al.*, 2007).

1. The biomass composition was selected as: $C_{41.3}H_{64.6}O_{18.8}N_{7.04}P$. This elemental composition includes P and results in the following, widely accepted stoichiometric values for biomass: VSS/COD=1.42, N/COD=0.07, P/COD=0.022, C/VSS=0.50 (Van Denmark and Batzing, 1987).

   The biomass used in Koch (2002) had a different composition, $CH_2O_{0.5}N_{0.15}$. This biomass results in the following, slightly different ratios: VSS/COD=1.51, N/COD=0.09, C/VSS=0.50, and does not contain phosphorus.

2. 1 mole of biomass is equivalent to 44.02 moles of COD, and 1 mole of substrate is 2.92 moles of COD.

   $$C_{41.3}H_{64.6}O_{18.8}N_{7.04}P + 44.02O_2 \rightarrow 41.3CO_2+18.98H_2O + 7.04NH_3 + H_3PO_4$$

   $$C_{2.43}H_{3.96}O + 2.92O_2 \rightarrow 2.43CO_2 + 1.98H_2O$$
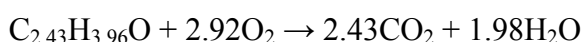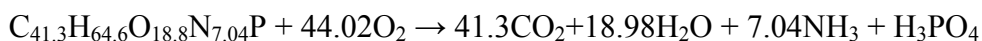
3. The Anammox reaction is set up as:

$$\gamma_{NH3}NH_3 + 7.04NH_3 + \gamma_{HNO2}HNO_2 + 41.3CO_2 + H_3PO_4 \rightarrow$$

$$C_{41.3}H_{64.6}O_{18.8}N_{7.04}P + \gamma_{N2}N_2 + \gamma_{HNO3}HNO_3 + \gamma_{H2O}H_2O$$
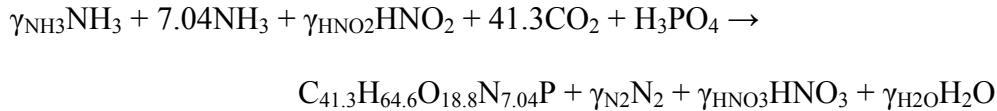
4. There are five unknowns (since C and P balances are trivial) and three elemental balances for H, O and N. The number of degrees of freedom is 2, selected as:

   - the amount of biomass COD grown on one mg electron-donor ammonia N (Y_{NH3}), according to Koch (2002), and
   - the amount of nitrate N produced on one mg electron-donor ammonia N used for growth (Y_{NO3}), which describes the 1/1.14 or 1.52 constants in previous works.

5. The resulting molar coefficients ($44.02O_2$ is the COD of one mole of biomass) are:

γ_{NH3} = $(44.02O_2)/(Y_{NH3}N)$

γ_{HNO2} = $(44.02O_2)/(Y_{NH3}N) + (73.367Y_{NO3}O_2)/(Y_{NH3}N)$ - 58.693

γ_{N2} = $(44.02O_2)/(Y_{NH3}N) + (14.673Y_{NO3}O_2)/(Y_{NH3}N)$ - 29.3467

γ_{HNO3} = $Y_{NO3}(44.02O_2)/(Y_{NH3}N)$

γ_{H2O} = $2(44.02*O_2)/(Y_{NH3}N) + (14.673Y_{NO3}O_2)/(Y_{NH3}N)$ - 49.5867

Considering N = 14.0067 g/mol and O_2 = 35.9988 g/mol, the reaction becomes:

$$889.2NH_3 + 1205.7HNO_2 + 41.3CO_2 + H_3PO_4 \rightarrow$$

$$C_{41.3}H_{64.6}O_{18.8}N_{7.04}P + 929.3N_2 + 229.4HNO_3 + 1791.2H_2O$$
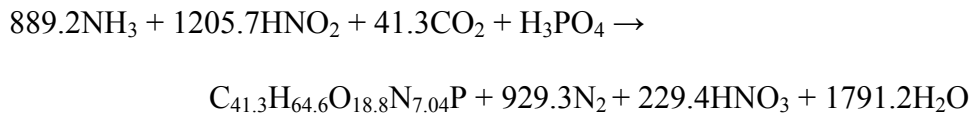
Converting this back to one mole of ammonia used yields:

$$NH_3 + 1.37HNO_2 + 0.047CO_2 + 0.0011\ H_3PO_4 \rightarrow$$

$$0.0011\ C_{41.3}H_{64.6}O_{18.8}N_{7.04}P + 1.05N_2 + 0.26HNO_3 + 2.03H_2O$$
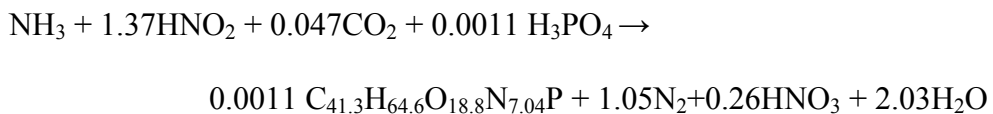
This reaction is rather similar to the original Strous equation. The main differences are due to the "higher molecular weight" of the biomass and the inclusion of P (as well as the slightly different elemental composition of the biomass).

6. These coefficients must be expressed for 1 g COD biomass to be included in the Anammox growth reaction. The resulting row in the Gujer matrix is presented in Table 14.2.

Table 14.2. Proposed stoichiometric coefficients for the Anammox growth reaction

	S_{NH}	S_{NO2}	S_{NO3}	S_{N2}
Anammox growth	$-1/Y_{NH3}$ $-i_{NBN}$	$-1/Y_{NH3} - 5/3Y_{NO3}$ $+ 4/3*N/O_2$	Y_{NO3}	$2/Y_{NH3}+2/3 \cdot Y_{NO3}$ $-4/3 \cdot N/O_2$

Some of the stoichiometric coefficients are different from the literature:

S_{NH}:   same as in Hao *et al*. (2002);
S_{NO2}:   new expression (the value of the $4/3 \cdot N/O2$ term is 0.584);
S_{NO3}:   same as Dapena-Mora *et al*. (2004) if $Y_{NO3} = 1.52$;
S_{N2}:   new expression.

These stoichiometric coefficients can be developed, using the same methodology, for a biomass of arbitrary composition, i.e. $C_{\alpha,C}H_{\alpha,H}O_{\alpha,O}N_{\alpha,N}P$. (Using elemental balancing, the COD of one mole of this biomass is $\alpha,C +1/4 \cdot \alpha,H -1/2 \cdot \alpha,O -3/4 \cdot \alpha,N + 5/4$ moles of O_2). All elemental molar fractions (α,C, etc.) cancel out during the development, resulting in the same formulation as in Table 14.2, proving that all of these stoichiometric coefficients are independent of biomass composition.

Based on calculations using this stoichiometry and $Y_{NH3}=0.114$ and $Y_{NO3}=1.52$, 47.5% of the nitrogen in the N_2 gas originates from ammonia, the rest from nitrite.

14.4 Conclusions

A method based on elemental balances simplifies deriving stoichiometric coefficients and serves as a rigorous check on reaction continuity. The method's steps are easy to follow, and the result it produces is demonstrated to agree with stoichiometry of well-known reactions, such as the aerobic heterotrophic growth on readily degradable substrate. The method is applied to develop stoichiometric coefficients for the Anammox growth reaction. It is shown that the currently published models use simplifying assumptions for these stoichiometric coefficients.

GENERAL CONCLUSIONS

Wastewater treatment plant modelling, with its roots in research, has found its place in the past two decades as a useful engineering tool in plant-wide process design, operation, training and control. Four different areas in plant-wide wastewater treatment plant modelling are investigated in the four parts of this work:

1. Phase separation, with special attention to one-dimensional modelling of final clarifiers.
2. Chemical processes, including pH calculation in wastewater and chemical phosphorus removal.
3. Biological processes, specifically additions and evaluation methods that extend the well-established principles of biological process models.
4. Theoretical aspects of modelling wastewater treatment plants.

The **final clarifier** is an important process unit in most treatment plants providing clarified effluent, thickened return solids and temporary storage of solids during high flow periods in the sludge blanket. A model that can approximate these functionalities is crucial from the perspective of predicting the performance of the whole plant. The Vesilind settling velocity function forms the basis of flux theory used in one-dimensional dynamic models. The Vesilind settling velocity function, however does not account for discrete settling occurring in the clarified water column of the settler, nor for compression in the sludge blanket. In *Chapter 1,* a model based on the solids flux concept and on a mass balance around each layer of a one-dimensional settler is presented. This model can simulate the solids profile throughout the clarifier, including the underflow and effluent suspended solids concentrations under steady-state and dynamic conditions. Examples based on full-scale and pilot-scale experimental data taken from the literature illustrate the application of the model to secondary settlers. Results of the analysis confirm that the model can predict the effluent and underflow suspended solids concentrations under a variety of conditions. The model is based on a modification of the Vesilind settling function. The new function is a double-exponential settling formula designed to simulate the settling velocity of dilute and more concentrated suspensions. Compression effects are approximated through the use of a low number of layers (8-15) and the minimum of fluxes in neighbouring layers.

Chapter 2 shows the rationale behind the modified Vesilind function: a relationship exists between the average settling velocity of floc particles in the upper layers of a secondary clarifier and the concentration of suspended solids within that layer. While it can be theoretically argued that the average settling velocity of particles in the flocculent settling zone is independent of concentration, the practical and operational constraints of secondary clarifiers lead to the conclusion that the average settling velocity of flocculent suspensions is correlated to the suspended solids concentration. Analytical expressions describing the

219

concentration and average settling velocity of a suspension as a function of particle size distribution are presented. Finally, the relationship between particle size distribution and overflow rate is addressed.

In *Chapter 3* this knowledge is used to directly link compression to the double-exponential settling function, resulting in a model containing four exponential terms that account for discrete, zone and compression settling. This model formulation allows a model structure that is independent of the number of layers. To enhance the use of the model in practice, an extensive set of batch settling tests were conducted at different scales, from a 1 liter cylinder to a large pilot-scale reactor. The experimental method to determine the Vesilind parameters from series of bench-scale zone-settling velocity tests is reviewed. It is confirmed that slow stirring of settling cylinders and not their volume is important in order to represent settling performance of full-scale plants for the whole range of solids concentrations. Based on these experiments, two new methods are proposed to extract the Vesilind parameters from zone-settling velocity test series. The methods can be automated and perform similarly as the traditional manual method, that requires human expert evaluation. The same tests are used through model calibration (simulating the zone-settling velocity tests) to extract parameters that are characteristic for the compression phase.

The model, through proper selection of parameters, can describe the adverse process effects caused by bulking sludge, but it is not able to predict when such conditions will occur. Two common causes of filamentous bulking of activated sludge are low DO and low F/M conditions in the activated sludge system. In *Chapter 4,* a dynamic mathematical model is presented that simulates the population dynamics of two groups of bacteria, floc-formers and filaments within the microenvironment of the activated sludge floc. An arbitrary grid of 50 by 50 elements was applied to a hypothetical floc of maximum 100 μm in diameter. The concentration of DO and soluble substrate was calculated inside the floc core under different bulk concentration conditions in order to simulate the effect of heterogeneous, gradient-governed micro-environments on dual species composition. Dynamic simulation runs were performed to calculate the growth of the two morphological types of microorganisms inside the floc under diffusion governed conditions. The results indicate that the method can predict the onset of the excessive filamentous growth (directly linked to bulking) even when traditional models neglecting diffusion limitation fail to do so. The positive feedback effect of the non-random (unidirectional) growth on the selective enrichment of filamentous organisms under electron acceptor (DO) or soluble substrate (F/M) limited conditions is demonstrated.

Several results in the preceding chapters were developed and published in the early years of wastewater modelling. *Chapter 5* provides a brief retrospective (not designed to be an exhaustive literature review) on a few key areas of development that occurred since.

Equilibrium chemistry and pH play a fundamental role in all biological processes, including the activated sludge and anaerobic digestion process. Due to the complexity of calculating pH in wastewater, IWA ASM type models use alkalinity as an indicator for pH instability. If alkalinity is low, there is a potential for rapid pH changes. However, this is represents a weak correlation and does not allow modelling of high pH inhibition or gas transfer. In *Chapter 6,* a general pH model is described that includes all of the major acid-base systems and strong ions typically found in municipal wastewaters. The objective of the model is to provide a method to calculate the pH throughout the activated sludge plant, including the liquid and solids lines. This is necessary to support accurate modelling of biological and physico-chemical processes,

such as nitrification, CO_2 gas transfer, struvite and calcium phosphate formation in digesters, and simultaneous chemical precipitation for phosphorus removal.

Metal (iron and aluminium) salts are frequently used to control effluent soluble phosphorus levels in wastewater treatment plants. Full-scale data from two plants in the Washington D.C. area were analysed in **Chapter 7** to establish phosphate behaviour in the presence of iron. A chemical equilibrium-based phosphorus precipitation model was used to evaluate the results. The model, after recalibration, can describe the low residual phosphate concentrations measured in practice and the relative insensitivity of the residual phosphate concentration to pH. In this work, however it was realized that many iron-phosphate complexes occurring in solution have to be taken into account and that phosphate chemistry cannot be comprehensively described with equilibrium equations alone.

An experimental program to investigate the effect of all significant factors on chemical phosphorus removal was initiated as described in **Chapter 8.** Batch and continuous experiments using model and real wastewaters were conducted to investigate the effect of metal salt (ferric and aluminium) addition in wastewater treatment and the corresponding phosphate removal from a design and operational perspective. Key factors expected to influence the phosphorus removal efficiency, such as pH, alkalinity, metal dose, metal type, initial and residual phosphate concentration, mixing, reaction time, age of flocs, and organic content of wastewater, were investigated. The lowest achievable concentration of orthophosphate under optimal conditions (0.01 – 0.05 mg/L) was similar for both aluminium and iron salts with a broad optimum pH range of 5.0 to 7.0. Thus, in the typical operating range of wastewater treatment plants pH is not a sensitive indicator of phosphorus removal efficiency. The most significant effect for engineering practice apart from the metal dose is that of mixing intensity and slow kinetic P removal of phosphorus in contact with the chemical sludge formed. Experiments show that significant savings in chemical cost could be achieved by vigorously mixing the added chemical at the point of dosage, and if conditions allow, providing a longer contact time between the metal hydroxide flocs and the phosphate content of the wastewater. These conditions promoted the achievement of less than 0.1 mg/L residual orthophosphate content even at lower metal to phosphorus molar ratios. A phosphate complexation model was developed in an attempt to understand the mechanistic basis of chemically mediated phosphate removal. The model presented is based on geochemical reaction modelling techniques and utilizes known surface reactions possible on hydrous ferric oxides (HFO). The types of surface reactions, their reaction stoichiometry and binding energies (logK values) are taken from the literature. The most important modelling parameter is the Active Site Factor converting moles of precipitated HFO to reactive site density. For well-mixed systems and phosphate exposed to ferric chloride during HFO precipitation there is a phosphate capacity of 1.18 phosphate ions per iron atom. In poorly mixed systems with phosphate exposed to iron after HFO formation the capacity decreased to 25% of the well-mixed value. The same surface complexation model can describe multiple data sets by varying the single ASF parameter in proportion to the availability of reactive oxygen functional groups. Electron microscope images and dye adsorption experiments demonstrate changes in reactive surface area with aging of HFO particles. Further work is required to establish the dependence of the ASF parameter on initial mixing, kinetics and age of flocs.

Several different subjects were investigated related to the core technology used in **biological wastewater treatment plants**: the activated sludge process itself. The development and application of a structured dynamic mathematical model for the powdered activated carbon treatment (PACT) system is discussed in **Chapter 9**. Part of the "Dold model" (Dold, 1980),

221

before the era of the ASM approach, was used as the basis in model development. The base model consists of six differential and a few algebraic equations, and describes the fundamental biological processes, e.g. the biodegradation of carbonaceous material, growth of microorganisms and their oxygen requirement. These principles still form the basis of activated sludge modelling today. In the additional development the model was extended by the Langmuir isotherm for simulation of the adsorption effect of powdered activated carbon addition to the process. Adaptation that occurs in the PACT systems is described by changing the maximum substrate degradation rate parameters according to a simple linear function when the system is moving towards a new equilibrium under new operational conditions (e.g. at the start of dosing activated carbon to a plant). A full plant model was constructed including mass-balance based settler modelling, extended by the Pflanz-equation for description of effluent solids. The extended model, coded and run on an HP85 using 16Kb of RAM, was calibrated to a set of batch and continuous experiments. The first industrial application of the model was carried out at the Nitrochemical Works in Balatonfűzfő, based on a 3-month full-scale experiment. Today, larger computer capacity and more accurate measurement principles, such as respirometry allow deeper insight into the processes occurring at wastewater treatment plants.

In *Chapter 10,* a method is proposed that directly calculates activated sludge model parameters and components through a series of numerical transformations on respirometric data. The method is "direct" because it does not use a model optimization technique. This direct respirogram evaluation (DRE) method separates the respirogram into individual components, and calculates maximum respiration rate, saturation coefficient and yield factor for the components. An advantage of the DRE method is its simplicity; there are no complications involving modelling, optimisation, and model identifiability. The calculations are model independent, even though the principle implies the Monod saturation term. The most important limitation is that only certain types of respirograms can be identified, that is: individual components must be dominant at a critical stage of their oxidation. The DRE method was tested on simulated respirograms and a number of real respirograms of various characteristics, and the results from the latter were compared to those from a parameter optimisation method. It is concluded that the two methods are not always in agreement, especially when a component is present in a minor fraction.

Sensitivity analysis can help determine whether these parameters are of prime interest in the specific model calibration study. The theory and practice of sensitivity analysis has been extensively described and used in the literature. In *Chapter 11,* a simple, practical example is developed, based on the ASM1 model and its parameters. It is shown how practical conclusions can be drawn from sensitivity analysis using simple tools. The primary objective of this example is to demonstrate to practitioners, who may not have the background or time to investigate the theory and methods in details, the benefits of sensitivity analysis. As an example, sensitivity analysis highlights how a parameter that seems to be unrelated to nitrification (the nitrogen content of heterotrophic biomass) has almost the same effect on nitrification performance as the maximum specific nitrifier growth rate parameter itself (through removing synthesis nitrogen that does not need to be nitrified).

The last part of the thesis considers various subjects in **theoretical modelling** of the wastewater treatment plant. A method to calculate the true age of solids (the Dynamic Solids Residence Time, DSRT) in the activated sludge system is proposed in *Chapter 12*. The DSRT extends the definition and use of the traditional steady-state Solids Residence Time (SRT). The new method is based on an age balance performed on the activated sludge in a manner

similar to that of a typical mass balance. At steady state the DSRT is equivalent to the SRT. Under dynamic conditions, the DSRT gives a better approximation of the true age of the solids in the system, and can replace empirical smoothing methods (e.g., seven-day moving average, etc.) routinely used to filter the sudden fluctuations in the instantaneous SRT calculation. The new process variable is useful for plant operators, engineers and modellers who are interested in the dynamic performance of the activated sludge process.

In *Chapter 13*, activated sludge models, based on COD and N balances, presented using the Gujer (Petersen) matrix description are investigated from the standpoint of maintaining elemental (C, O, H, N) balances. ASM1 is used as an example. The ASM1 Gujer matrix is extended with N_2, CO_2 and H_2O state variables to close elemental balances. The typical composition of state variables is determined using standard COD, TOC, VSS and TKN measurements. Chemical reactions are derived for each process in the ASM1 model for general composition and stoichiometric parameters, as well as for the most likely composition of state variables and best estimates for stoichiometric parameters (yield, endogenous fraction, etc.). For more accurate evaluations, data that are not always collected are needed on total and filtered influents, mixed liquor and effluents (VSS or VS, COD, TOC or DOC, N, and P with and without filtration). The availability of such data at plants would also provide the possibility for a data quality check. The elementally balanced model matrix can be used to verify model integrity and is necessary in linking different models using the CBIM transformer method, in view of plant-wide modelling and simulation.

At the same time, elemental balancing provides a simple and rigorous way to establish the stoichiometric coefficients of reactions represented in the Gujer matrix. Kinetic models in activated sludge, anaerobic digestion and other environmental modelling fields rely on the proper formulation of stoichiometric coefficients. The deduction of these coefficients is frequently trivial, from basic mass-balancing considerations. In more complex cases, such as the Anammox growth reaction, rigorous elemental balancing is required to establish the proper formulation. *Chapter 14* demonstrates the methodology based on a simple aerobic heterotrophic growth reaction where stoichiometry coefficients (such as the $-(1-Y_H)/Y_H$ term for oxygen) are well known. In the second step, the methodology is applied to the Anammox growth reaction. The fraction of N_2 gas in current models originates from the NH_4^+ and the NO_2^- electron donor/acceptor pair in equal proportion. This chapter demonstrates that this stoichiometry is a simplification leading to elemental balance errors. The proper stoichiometric coefficients are derived.

Wastewater treatment plants use many different physical, chemical and biological principles and their practical engineering implementation to produce treated effluent. The experimentation based on observation of these principles and mathematics as described in this dissertation is a path of discovery. Its objective is twofold: to improve our understanding of how the whole plant and its functional elements work together, and based on this knowledge, extend the toolkit engineers and operators use in their daily work to improve our environment.

In my work in the past 28 years I have been involved in research in a wide variety of topics: intensification of overloaded treatment plants; treatment of industrial wastewater; modelling of phase separation; modelling of various biofilm systems; nutrient removal including nitrogen and phosphorus removal to very low levels; external carbon addition; chemical equilibrium models for calculation of pH and precipitate formation in wastewater, including phosphorus removal; side stream treatment including advanced technologies using the ammonia to nitrite to nitrogen gas direct pathway and Anammox biomass; as well as whole plant modelling. Only a fraction of these are discussed in detail in this thesis.

The wonderful thing in research is that it leads to unexpected discoveries. Since wastewater treatment research is an applied engineering field, we have to be careful about keeping the focus, that we answer the actual problem that initiated the research. But it is equally important to notice those little gems on the roadside – some of them may turn into important new directions in the future.

I noticed what looked like such gems in a distance during my work on this PhD, and due to my limitations or just constraints on time, I was unable to collect them.

Dealing with so many different subjects, I struggled with the formal language, the symbolism of describing topics that belong to different principles. Biology and chemistry, settling, activated sludge and chemical phosphorus removal... Notation and methods to describe complex systems within the fence of the treatment plant should mature. Colloids are soluble if you measure them by filtration, slowly degradable, if you measure them by their degradation kinetics. In activated sludge modelling the Gujer matrix has had a huge positive effect, putting complex equation systems into an easy to understand framework. Our subject now is the whole plant. We must develop a common system of notation that can be used across all processes we have to deal with during whole plant modelling. We must develop the Super-Gujer matrix equivalent, or a matrix of matrices (see CBIM) for describing whole plant models, including their biokinetic, equilibrium chemistry, gas transfer and phase separation elements.

In Chapter 5, I attempted to clarify (for myself at least), the place of 1-D and CFD modelling in process predictions and detailed design. When I look at the astonishing simplicity of a 1-D model, there is an obvious question: how can such a simple model be so successful, so accurate in its predictions for process modelling? A CFD model contains detailed knowledge of tank geometry, flow patterns, temperature, liquid densities, etc. Without any of this, a 1-D model will provide a darn good overall prediction of effluent and return solids, sludge blanket and mass variations. This must mean that the vertical flow and settling component (the only thing the 1-D model has an understanding of) is an overwhelming part of the processes in the

clarifier. Even though the liquid has to move 30 or even 50 meters from the inlet of the clarifier to the effluent weirs, the more important component is the mere 3-4 meters that the sludge has to cover during settling in the vertical dimension.

In Chapter 12, I raised the question – we are losing solids three different ways from an activated sludge plant (effluent solids, wastage and endogenous decay). How come we don't take all three of those into consideration when calculating the real age (Solids Residence Time) of the biomass?

In Part 2, Chemical processes, one of my objectives at the start of the PhD was to come up with a comprehensive plant-wide chemical phosphorus removal model, including oxidizing and reducing environments, full equilibrium chemistry and kinetics as well as flocculation. These are the main mechanisms involved in the fate of phosphorus as it cycles through the various streams and process units in the plant. Now I better recognize the size of this challenge, and it is enormous. I believe that many more PhDs will be required to cover the most important processes that various forms of phosphorus take part in at the plant.

At this point we have to consider how do we analyze and model a complex system. To be able to approach a complicated system, we have to break it down into simpler elements. Consider the chemical and biological reactions concerning phosphorus. We try to isolate the main reactions without the interference of others. Experiments are performed when there is no biomass in the system, not even phosphate. What happens to iron in solution? Now what if phosphorus is in the system? And magnesium or calcium? And biological activity? And will the results obtained in a simplified system still be representative of the whole system?

A simple example (the simplest I can think of) will serve to highlight some of the challenges. To determine aerobic degradation rates of readily and slowly biodegradable substrate, a targeted respirometric experiment can be performed. There is enough oxygen, nitrogen, phosphorus, cations, anions, micronutrients, mixing, CO_2, and pH is at the optimum. The model that is fitted to determine kinetic parameters can be as simple as a first order rate with respect to biomass concentration, extended with a Monod term for substrate. The maximum specific growth rate is easily determined.

We take this value and use it in a complex model environment where a series of other Monod or similar switches are used necessarily. Even when there is no real limitation of any of the environmental conditions listed above, the individual Monod terms will not be exactly one. At 2 mg/L O_2 concentration, depending on the half-saturation concentration determined, the Monod function value will be at 90 to 97%. If we multiply six of these terms together, the result is in the range of 56 to 86 %. That is, our model in which we do not intend to simulate any environmental limitation will still use a slower (much slower) rate than what we measured in the experiment.

When reconstituting complex models based on simple elements, investigating the practical application of Liebig's Law (Principle of the Minimum) may prove crucial.

The challenge for the research community is not in isolating the simple subsystem. There are lots of studies looking at one specific process in P removal, or a specific unit process in the plant for that matter. However the useful lifetime of a PhD student is fairly limited. One that works on biological P removal will not be able to afford to look at chemical P processes. At the end, who will put all the pieces together?

A whole plant model that can be used in practice by the engineering community necessarily has to contain many different processes and mechanisms. Activated sludge, fixed film, anaerobic digestion, side stream treatment, chemical treatment, at least three-four different phase separation (various settling and filtration) processes, polishing, disinfection all act together.

It is our challenge as a profession to integrate processes found in these isolated experimental subsystems, reconcile them with data from the full-scale, complex plant and provide a good model that can be reliably used by practitioners.

Chemical plants that manufacture a product all look after their raw material and the chemicals, as well as the energy they use very carefully or they lose money and go out of business. As it has been proven at several plants, wastewater can be a valuable raw material, from which expensive products (N, P, energy) can be derived. Over time we will change our approach trying to get rid of wastewater and will build plants that process it into those valuable components it contains. The models we build today play a small but important role to get to this (however distant) objective with less hiccups along the road.

REFERENCES

Aiba S. and Nagatani M. (1971) Separation of Cells from Culture Media. In: Advances in Biochemical Engineering (Edited by Ghose T. and Fiechter A.), Vol. 1, pp. 31-54. Springer-Verlag, Berlin.

Aiba S., Humphrey A.E. and Millis N.F. (1965) Biochemical Engineering. University of Tokyo Press, Tokyo, Japan.

Allison, J.; Brown, D.S.; Novo-Gradac, K. (1991) MINTEQA2/PROEFA2. A geochemical assessment model for environmental systems. U.S. Environmental Protection Agency, Athens, Georgia:Environmental Research Laboratory.

Anderson P.R. and Benjamin, M.M. (1990) Modelling adsorption in aluminum-iron binary oxide suspensions. Environ. Sci. Technol. 24, 1586-1592.

Atkinson B. and Daoud I.S. (1976) Microbial Flocs and Flocculation in Fermentation Process Engineering. In: Advances in Biochemical Engineering (Edited by Ghose T., Fiechter A. and Blakebrough N.), Vol. 4, pp. 41-124. Springer-Verlag, Berlin.

Bailey J.E (1986) Biochemical Engineering Fundamentals. McGraw Hill, New York.

Barker, P.S. and P. L. Dold (1997) General model for biological nutrient removal activated sludge systems: model presentation. Wat. Env. Res., 69(5):969-984.

Batstone D.J., Keller J., Angelidaki I., Kalyuzhnyi S.V., Pavlostathis S.G., Rozzi A., Sanders W.T.M., Siegrist H. and Vavilin, V.A. (2002) Anaerobic Digestion Model No.1. IWA Scientific and Technical Report No.13, IWA Publishing, London, UK.

Benedek, P., Major, V. and Takács, I. (1985) Mathematical model suggested for carbon - activated sludge system. Water Research, Vol. 19, No.4, pp.407-413.

Benedek, P., Takács I. and Vallai I. (1986) Upgrading of a wastewater treatment plant in a chemical factory. Wat. Sci. and Tech., 18 (1), 75-82.

Birch, W.D., Pring, A., Reller A., Schmalle, W.H. (1993) Bernalite, Fe(OH)3, a new mineral from Broken Hill, New South Wales : description and structure. American Mineralogist, 78, 827-834.

Blackbeard, J.R., Ekama, G.A., Marais, G.v.R. (1986) A Survey of Filamentous Bulking and Foaming in Activated Sludge Plants in South Africa. Water Poll. Control. 85, 95-100.

Blackbeard, J.R., Gabb, D.M.D., Ekama, G.A., Marais, G.v.R. (1988). Identification of Filamentous Organisms in Nutrient Removal Activated Sludge Plants in South Africa. Water SA, 14, 29-33.

Brannigan, M. (1990) An adaptive data analyser. The C Users Journal, May 1990, 113-118.

Brouwer, H., Klapwijk, A., Keesman, K.J. (1998) Identification of activated sludge and wastewater characteristics using respirometric batch-experiments. Wat. Res., 32, 1240-1254.

Brunauer, S., Emmett, P.H. and Teller, E. (1938) Adsorption of gas in multimolecular layers. J. Am. Chem. Soc., 60, 309-319.

Bryant, J. 0. (1972) Continuous time simulation of the conventional activated sludge wastewater renovation system. Ph.D. dissertation, Clemson University, Clemson, S.C.

Busby, J. B. (1973) Dynamic modeling and control strategies for the activated sludge process. Ph.D. dissertation, Clemson University, Clemson, S.C.

Camp, T. R. (1945) Sedimentation and the design of settling tanks. Trans. Am. Soc. Civ. Engrs 94, 895-958.

Chambers, B. (1982) Effect of Longitudinal Mixing and Anoxic Zones on the Settleability of Activated Sludge. In: Bulking of Activated Sludge: Preventative and Remedial Methods, Eds: Chambers, B. and Tomlison, E. 166-186. Ellis Horwood Ltd, England.

Chapman, D. T. (1984) The influence of dynamic loads and process variables on the removal of suspended solids from an activated sludge plant. Ph.D. dissertation, University of Alberta, Edmonton, Alberta.

Charaklis, W.G. and Marshall, K.C. (1990) Biofilms. Wiley Intersci. Publ.

Chudoba, J. (1985) Control of Activated Sludge Filamentous Bulking. VI: Formulation of Basic Principles. Wat. Res. 19, 1017-1022.

Copp, J.B., Spanjers, H., Vanrolleghem, P.A. (2002) Respirometry in Control of the Activated Sludge Process: Benchmarking Control Strategies. IWA Scientific and Technical Report, IWA Publishing, London, United Kingdom.

Dapena-Mora, A., Van Hulle, S.W.H., Campos, J.L., Méndez, R., Vanrolleghem, P.A. and Jetten, M. (2004) Enrichment of Anammox biomass from municipal activated sludge: experimental and modelling results. J. Chem. Technol. Biotechnol., 79, 1421-1428.

De Clercq, B. (2003) Computational Fluid Dynamics of Settling Tanks: Development of Experiments and Rheological, Settling and Scraper Sub Models", PhD Thesis, Ghent University, Belgium

De Clercq, J. (2006) Batch and continuous settling of activated sludge: in-depth monitoring and 1D compression modelling. PhD Thesis, Ghent University, Belgium.

De Clercq, J., Nopens, I., Defrancq, J., Vanrolleghem, P.A. (2008) Extending and calibrating a mechanistic hindered and compression settling model for activated sludge using in-depth batch experiments. Water Research , 42, 781-791.

de Haas, D.W., Wentzel, M.C., Ekama, G.A. (2000) The use of simultaneous chemical precipitation in modified activated sludge systems exhibiting biological excess phosphate removal Part I: Literature review. Water SA, 26, 439-452.

Dick, R. I. and Ewing, B. B. (1967) Evaluation of the activated sludge thickening theories. J. Sanit. Engng Div., Am. Soc. Civ. Engrs 93, 9-29.

Dochain, D. and P.A. Vanrolleghem (2001) Dynamical Modelling and Estimation in Wastewater Treatment Processes. London UK: International Water Association

Dold, P.L. (1990) Incorporation of Biological Excess Phosphorus Removal in a General Activated Sludge Model, Proc. 13th Int. Symposium on Wastewater Treatment, Montreal, Canada, 83-113.

Dold, P.L., Ekama, G.A. and Marais, G.v.R. (1980). A general model for the activated sludge process. Progress in Water Technology, Vol.12, No 6.pp.47-77.

Dold, P.L. (2007) Quantifying Sludge Production in Municipal Treatment Plants. Proceedings of the Water Environment Federation 80th Annual Technical Exhibition & Conference, San Diego, California, USA, October 13 - 17, 2007.

Dold, P.L., Fairlamb, P.M., Jones, R., Takács, I. and Murthy, S. (2007) Sidestream Modelling Incorporated Into Whole Plant Simulation. Clonic Workshop, Barcelona, Spain

Dreier, D.E. (1945) Summary of the Experience In Mechanical Activated Sludge Operation. Sewage Works Journal, 17, 101-126.

Dzombak D.A., Morel, F.M.M.M. (1990) Surface complexation modeling, hydrous ferric oxide. Wiley-Interscience, New York.

Eckenfelder, W.W. and Weston, R.F. (1956) Kinetics of biological oxidation. Pp. 18-34 in B.J. McCabe and W.W. Eckenfelder, eds. Biological treatment of sewage and industrial wastes. Vol. 1. Rheinhold Publishing Company, New York.

Eckenfelder, W.W. and O'Connor, D. J. (1961) Biological Waste Treatment. Pergamon Press, New York, USA, 289 pp

Eikelboom, D.H. (1977) Identification of Filamentous Organisms In Bulking Activated Sludge. Progr. Wat. Techn., 8, 153-161.

Eikelboom, D.H. and van Buijsen, H.J.J. (1981) Microscopic Sludge Investigation Manual. TNO Research Inst. for Environ. Hygiene. The Netherlands.

Ekama, G.A., Barnard, J.L., Gunthert, F.W., Krebs, P., McCorquodale, J.A., Parker, D.S. and Wahlberg, E.J. (1997) Secondary Settling Tanks. Theory, Modelling, Design and Operation. Scientific and Technical Report No.6., IWA publishing, London, UK.

Fettig, J., Ratnaweera, C., Ødegaard, H. (1990) Simultaneous Phosphate Precipitation and Particle Destabilization Using Aluminium Coagulants of Different Basicity. In Chemical Water and Wastewater Treatment, Proceedings of the 4th Gothenburg Symposium 1990. H. H. Hahn and R. Klute (eds.), Springer-Verlag Berlin Heidelberg New York, 221.

Fick, A (1855) Poggendorff's Annel. Physik. 94, 59.

Fleps, W. (1974) Új laboratóriumi szennyvízvizsgáló készülék (respirométer). A készülék ismertetése [New laboratory instrument for examining wastewater (respirometer).Overview of the instrument]. Hidrológiai Közlöny.

Geelhoed, J.S., Hiemstra, T., Van Riemsdijk, W.H. (1997) Phosphate and sulphate adsorption on geohite: single anion and competitive adsorption. Geochim. Cosmochim. Acta, 61, 2389-2396.

Georgantas, D.A., Grigoropoulou, H.P. (2005) Phosphorus removal from synthetic and municipal wastewater using spent alum sludge. Water Science and Technology, 52, 525-532.

Gillberg, L., Nilsson., D., Åkesson, M. (1996) The Influence of pH when Precipitating Orthophosphate with Aluminum and Iron Salts, In: Chemical Water and Wastewater Treatment IV. - Proceedings of the 7th

Gothenburg Symposium Edinburgh 1996. H. H. Hahn, E. Hoffmann and H. Ødegaard (Eds.), Springer-Verlag Berlin Heidelberg New York, 95.

Giroux, É.Y., Spanjers, H., Patry, G.G. and Takács I. (1996) Dynamic modeling for operational design of a respirometer. Wat. Sci. Tech., 33(1), 297-309.

Gernaey, K., Vanrolleghem, P.A., and Lessard, P. (2001) Modelling of a reactive primary clarifier. Water Science and Technology Vol 43 No 7 pp 73–81.

Grady, C.P.L.Jr., Daigger, G.T. and Lim, H.C. (1999) Biological Wastewater Treatment. 2nd Edition Martin Dekker Publishing, New York.

Grady, C.P.L., Daigger, G.T., Love, N.G. (2007) Biological Wastewater Treatment, Third Edition. Taylor&Francis, London, UK, 1096.

Gujer, W. (2002) Microscopic versus macroscopic biomass models in activated sludge systems. Water Science and Technology Vol 45 No 6 pp 1–11

Hamilton, J., Jain, R., Antoniou, P., Svoronos, S.A., Koopman, B. and Lyberatos, G. (1992) Modeling and pilot-scale experimental verification for predenitrification process. J Environ Eng, 118:38–55.

Hang, P.T., Brindley, G.W. (1970) Methylene Blue Adsorption by Clay Minerals: Determination of Surface Areas and Cation Exchange Capacities. Clays and Clay Minerals, 18, 203-212.

Hao, X, Heijen, J.J., van Loosdrecht, M.C.M. (2002) Sensitivity analysis of a biofilm model describing a one-stage completely autotrophic nitrogen removal (CANON) process. Biotechnol. Bioeng., 77(3), 266-277.

Hao, O.J., Richard, M.G., Jenkins, D. (1983) The Half-Saturation Coefficient for Dissolved Oxygen: A Dynamic Method for Its Determination and its Effect on Dual Species Composition. Biotech. & Bioengin. 25, 403-416.

Hellinga, C., Vanrolleghem, P.A., van Loosdrecht, M.C.M. and Heijnen, J.J. (1996) The potentials of off-gas analysis for monitoring and control of waste water treatment plants. Wat. Sci. Tech., 33(1), 13-23.

Hellinga, C., v Loosdrecht, M. M. and Heijnen, J.J. (1999) Model based design of a novel process for nitrogen removal from concentrated flows. Mathematical and Computer Modelling of Dynamical Systems, 5 (4):351-371.

Hellweger, F.L. (2007) Accounting for intrapopulation variability in biogeochemical models using agent-based methods.Environ Sci Technol. 41 (8):2855-60

Henze, M., Grady, C. P. L. Jr, Gujer, W., Marais, G. v. R and Matsuo, T. (1987) Activated Sludge Model No. 1. IAWPRC Scientific and Technical Reports No. 1. IAWPRC, London, England.

Henze, M., Gujer, W., Mino, T. and van Loosdrecht, M.C.M. (2000) Activated Sludge Models ASM1, ASM2, ASM2d and ASM3. IWA Scientific and Technical Report No.9, IWA Publishing, London, UK.

Henze, M., Harremoës, P., LaCour Jansen, J. and Arvin, E. (1995) Wastewater Treatment: Biological and Chemical Processes. Springer, Heidelberg.

Heukelekian, H. (1941) Mechanical Bioflocculation and Bioflocculation of Sewage. Sewage Works Journal, 13, 506- 522.

Hill, R. D. (1985) Dynamics and control of solids-liquid separation in the activated sludge process. Ph.D. dissertation, Rice University, Houston, Tex.

Hoover, S.R. and Porges, N. (1952) Assimilation of dairy wastes by activated sludge. II. The equations of synthesis and rate of oxygen utilization. Sew. Indus. Wastes J., 24, 306-312.

Jambor, J.L., Dutrizac, J.E. (1998) Occurrence and constitution of natural and synthetic ferrihydrite, a widespread iron oxyhydroxide. Chem. Rev. 98, 2549-2585.

Jenkins, D., Richard, M.G., Daigger, G.T. (1984) Manual on the Causes and Control of Activated Sludge Bulking and Foaming. Prepared for Wat. Res. Com. of Pretoria, SA

Jenkins, D., Hermanowicz, S.W. (1991) Principles of Chemical Phosphorus Removal. Sedlak, R.I. (Ed.). Phosphorus and Nitrogen Removal from Municipal Wastewater: Principles and Practice., 2nd ed., Lewis Publishers, Chelsea, MI.

Jeppsson, U. (1996) Modelling Aspects of Wastewater Treatment Processes. Lund, Sweden: Lund Institute of Technology. PhD Thesis

Jeppsson, U., Diehl, S. (1996) An evaluation of a dynamic model of the secondary clarifier. Wat. Sci. Tech., 34(5-6):19-26, 1996.

Jones, R. M., Bye, C. M., Dold, P. L. (2003) Nitrification Parameter Measurement for Plant Design: Experience with New Methods. Proceedings of the Water Environment Federation 76th Annual Technical Exhibition and Conference, Los Angeles, California, USA, October 11-15, 2003.

Keinath, T. M., Ryckman, M. D., Dana, C. H. and Hofer, D. A. (1977) Activated sludge unified system design and operation. J. Envir. Engng Div., Am. Soc. Civ. Engrs 103, 829-849.

KEMIRA KEMI AB Water Treatment, (1990) The Handbook on Water Treatment, KEMIRA KEMI, Helsingborg.

Kennedy, A. (1991) Modelling of clarifier dynamics under quiescent conditions. M.Eng. thesis, Department of Civil Engineering, McMaster University, Hamilton, Ontario

Koch, G., Egli, K, Van der Meer, J.R. and Siegrist, H. (2002) Mathematical modelling of autotrophic denitrification in a nitrifying biofilm of a rotating biological contactor. Wat. Sci. Tech., 41(4-5), 191-198.

Koch, L.A. (1990). Diffusion: The Crucial Process in Many Aspects of the Biology of Bacteria. Advances in Microbial Ecology, Plenum Press New York,& London, 37-70.

Kroiss, H. and Ruider, E. (1977) Comparison of Plug-Flow and Completely-Mixed Activated Sludge Processes. Progr. Wat. Techn. 8, 169-173.

Kynch, G. J. (1952) A theory of sedimentation. Trans. Faraday Society, Vol. 48: 166-176.

Lau, A.O., Strom, P.F., Jenkins, D. (1984a) Growth Kinetics of Sphaerotilus natans and a Floc Former in Pure and Dual Continuous Culture. Journal of Wat. Poll. Control Fed. 56, 41-51.

Lau, A.O., Strom, P.F., Jenkins, D. (1984b). The Competitive Growth of Floc-Forming and Filamentous Bacteria: A Model for Activated Sludge Bulking. Journal of Wat. Poll. Control Fed. 56, 52-61.

Lee, J. S. and Johnson, W. K. (1979) Carbon-slurry activated sludge for nitrification-denitrification, J. Wat. Pollut, Control Fed. 51. No 1. pp. 111-126.

Lee, S.A., Koopman, B., Bode, H., Jenkins, D. (1983) Evaluation of alternative Sludge Settling Indices. Water Research, 17, 1421-1426.

Li, S. and Stanforth, R. (2000) Distinguishing adsorption and surface precipitation on phosphate and goethite (α-FeOOH). J. Coll. Int. Sci., 230, 12-21.

Li, D. and Ganczarczyk, J.J. (1987) Stroboscopic determination of settling velocity, size and porosity of activated sludge flocs. Wat. Res. 21, 257-262.

Licskó, I. (1976) Micro processes in coagulation. Water Research, 10(2), 143-146.

Lijklema, L. (1980) Interaction of Orthophosphate with Iron(III) and Aluminum Hydroxides. Env. Sci. Techno., 14, 534-541.

Loewenthal, R.E., Marais, G.v.R. (1976) Carbonate Chemistry of Aquatic Systems: Theory and Application. Ann Arbor Science, Ann Arbor Michigan.

Magnuson, M.L., Lytle, D.A., Frietch, C.M., Kelty, C.A. (2001) Characterization of submicrometer aqueous Iron (III) colloids in the presence of phosphate by sedimentation field flow fractionation with multiangle laser light scattering detection. Anal. Chem. 73, 4815-4820.

Makris, K.C., El-Shall, H., Harris, W.G., O'Connor, G.A. and Obreza, T.A. (2004) Intraparticle P diffusion in a drinking water residual at room temperature. J. Colloid & Interf. Sci. 277 (2): 417-423.

Maplesoft (2005) Maple version 9.5 All purpose mathematics software tool. www.maplesoft.com.

Márquez, M. C. and Costa, C. (1996) Biomass concentration in PACT process. Water Research 30, 9, September 1996, Pp 2079-2085

Mazumder, D., Dikshit A.K. (2004) Hybrid reactor system for wastewater treatment – application and approach of modelling. International Journal of Environment and Pollution 2004 - Vol. 21, No.2 pp. 105 – 131

Matson, J.V., Charaklis, W.G. (1976) Diffusion into Microbial Aggregates. Water Research, 10, 877-885.

Maurer, M., Abramovich, D., Siegrist, H. and Gujer, W. (1999) Kinetics of biologically induced phosphorus precipitation in waste water treatment. Wat. Res. Vol.33, No.2, pp 484-493

McNaught A.D., Wilkinson, A. (1997) IUPAC Compendium of Chemical Technology, Blackwell Science.

Melcer, H., Dold, P.L., Jones, R.M., Bye, C.M., Takács, I., Stensel, D.H., Wilson, A.W., Sun, P., Bury, S. (2002) Methods for Wastewater Characterization in Activated Sludge Modeling. Water Environment Research Foundation, Alexandria, Virginia.

Mesdaghinia, A.R., Nouri, J., Naddafi, J. K., Rezaian, A.R. (2001) Investigation of Sahebgharanieh Wastewater Treatment Plan Operation in Tehran and Appropriate Methods for Its Upgrading. Iranian J. Publ. Health, Vol. 30, Nos. 1-2, PP. 9-14.

Mitchell and Gauthier Associates (1987) Advanced Continuous Simulation Language (ACSL). Reference Manual. Concord, Mass.

Morel, F. M. M., Hering, J.G. (1993) Principles and Applications of Aquatic Chemistry. New York: John Wiley and Sons.

Morgan, E.H. and Beck, A.J. (1928) Carbohydrate Wastes Stimulate Growth of Undesirable Filamentous Organisms in Activated Sludge. Sewage Works Journal, 1, 46-52.

Musvoto, E.V., Ekama, G.A., Wentzel, M.C., Loewenthal, R.E. (2000) Extension and application of the three-phase weak acid/base kinetic model to the aeration treatment of anaerobic digester liquors. Water SA, 26(4), pp. 417-438.

Musvoto, E.V., Wentzel, M.C., Loewenthal, R.E., Ekama, G.A. (1997) Kinetic-based model for mixed weak acid/base systems. Water SA, 23(4), pp. 311-322.

National Institute of Standards and Technology (2001) NIST Standard Reference Database 46, Gaithersburg, MD., U.S.A.

Nopens, I., Biggs, C.A., De Clercq, B., Govoreanu, R., Wilén, B.-M., Lant, P. and Vanrolleghem, P.A. (2001) Modelling the activated sludge flocculation process combining laser light diffraction particle sizing and population balance modelling (PBM) Water Science and Technology Vol 45 No 6 pp 41–49

Nopens, I., Nere, N., Vanrolleghem P.A., and Ramkrishna, D. (2007) Solving the inverse problem for aggregation in activated sludge flocculation using a population balance framework Water Science & Technology Vol 56 No 6 pp 95–103

Ossenbruggen, P.J. and McIntire, S. (1990) Using shock wave theory to predict secondary clarifier performance. In: Advances in Water Pollution Control (Edited by Briggs R.), pp. 479-486. Pergamon Press, London.

Palm, J.C., Jenkins, D., Kaufman, W.J. (1980) Relationship Between Organic Loading, Dissolved Oxygen Concentration and Sludge Settleability in the Completely Mixed Activated Sludge Process. Journal of Wat. Poll. Control Fed. 52, 2484-2493.

Parker, D.S., Kauman, W.J. and Jenkins, D. (1971) Physical conditioning of activated sludge floc. J. Wat. Pollut. Control Fed. 43, 1817-1833.

Parker, D.S., Kauman, W.J. and Jenkins, D. (1972) Floc breakup in turbulent flocculation processes. J. Sanit. Engng Div. Am. Soc. Civ. Engrs 98, 79-99.

Pascal, B. (1665) Traité sur la Triangle Arithmétique, Paris: Duprez 1665, translated as Treatise on the arithmetical triangle by R Scofield, pp. 447-473 of B Pascal, The Provincial Letters. Pensées. Scientific treatises. Vol. 33 of Great Books of the Western World, Chicago, IL: Encyclopaedia Britannica Inc. 1952 (MJ 75.5).

Patry, G. G. and Takács, I. (1990) Simulator-based modelling of wastewater treatment plants. In Proceedings Annual Conference and 1st Biennial Environmental Specialty Conference CSCE, Vol. I, pp. 491-505.

Patry, G.G., Takács, I. (1992) Settling of Flocculent Suspensions in Secondary Clarifiers. Water Research, 26, No 4., pp. 473-479.

Perry, R., Green, D. (1985) Perry's Chemical Engineer's Handbook, Sixth Edition. McGraw-Hill Inc.

Pflanz, P. (1969) Performance of (activated sludge) secondary sedimentation basins. In Advances in Water Pollution Research (Edited by Jenkins S. H.), pp. 569-58 1. Pergamon Press, London.

Picioreanu, C., Kreft, J., and van Loosdrecht, M.C.M (2004) Particle-Based Multidimensional Multispecies Biofilm Model. Applied and Environmental Microbiology, Vol. 70, No. 5 p. 3024-3040

Pierri, E., Tsamouras, D. and Dalas, E. (2000) Ferric phosphate precipitation in aqueous media. Journal of Crystal Growth, Vol. 213, Issues 1-2, pp 93-98.

Pramanik, J. and Keasling, J. (1997) Stoichiometric model of Escherichia coli metabolism: Incorporation of growth rate dependent biomass composition and mechanistic energy requirements. Biotech. Bioeng., 56, 398-421.

Ratnaweera, H., Fettig, J., Ødegaard, H. (1992) Particle and phosphate removal mechanisms with prepolymerized coagulants, In: Chemical Water and Wastewater Treatment II. - Proceedings of the 5th Gothenburg Symposium 1992, R. Klute and H. H. Hahn (Eds.), Springer-Verlag Berlin Heidelberg New York, 3.

Reichert, P., Borchardt, D., Henze, M., Rauch, W., Shanahan, P., Somlyódy, L. and Vanrolleghem P.A. (2001) River Water Quality Model No. 1. IWA Scientific and Technical Report No. 12. IWA Publishing, London, UK.

Riley J.P., Murphy, M.J. (1962) A modified single solution method for phosphate in natural waters, Anal. Chim. Acta, 12, 31-36.

Rittmann, B.E. and McCarty, P.L. (2000) Environmental Biotechnology: Principles and Applications. McGraw-Hill, New York.

Rombardo, F., Allen, A., Bashaw, W. and Shelhamer, M. (2005). Measuring activated sludge settling characteristics to optimize final clarifier design. Proceedings of the 78th Annual Technical Exhibition and Conference (WEFTEC.05), Washington, DC, USA, 29 October - 2 November 2005.

Roth, M. and Pinnow, P. (1981) Bestimmung der Grossenverteilung der suspendierten Stoffe in biologisch gereinigten Abwassern (Determination of the particle size distribution in secondary effluents). Vom Wass. 57, 309-327.

Sagberg, P., Ryrfors, P. and K.G. Berg (2006) 10 years of operation of an integrated nutrient removal treatment plant: ups and downs. Background and water treatment. Water Science & Technology Vol 53 No 12 pp 83–90

Schuler, A.J (2006) Distributed microbial state effects on competition in enhanced biological phosphorus removal systems. Water Science & Technology Vol 54 No 1 pp 199–207

Schwertmann, U., Cornell, R.M. (2000) Iron oxides in the laboratory: Preparation and characterization. Wiley, New York.

Sezgin, M., Jenkins, D., Parker, D.S. (1978) A Unified Theory of Filamentous Activated Sludge Bulking. Journal of Wat. Poll. Control Fed. 50, 362-368.

Small, T.D., Warren, L.A., Roden, E.E., Ferris F.G. (1999) Sorption of strontium on bacteria, Fe(III) oxide, and bacteria-Fe(III) oxide composites. Environ. Sci. Technol. 33, 4465-4470.

Smith, D.S., Ferris, F.G. (2001a) Proton binding by hydrous ferric oxide and aluminum oxide surfaces interpreted using fully optimized continuous pKa spectra. Environ. Sci. Technol. 35, 4637-4642.

Smith, D.S., Ferris, F.G. (2001b) Methods in Enzymology Volume 337: Microbial Growth in Biofilms part B Special Environments and Physiochemical Aspects, edited by R. Doyle (Academic Press, San Diego, 2001), pp. 225–242.

Smith, D.S., Ferris, F.G. (2003) Specific surface chemical interactions between hydrous ferric oxide and iron reducing bacteria determined using pKa spectra. J. Coll. Int. Sci. 266, 60-67.

Smith, P.G. and Coackley, P. (1984) Diffusivity, tortuosity, and pore structure of activated sludge. Wat. Res. 18, 117-122.

Smith, S., Takács, I., Murthy, S., Daigger, G. and Szabó, A. (2008) Phosphate Complexation Model and its Implications for Chemical Phosphorus Removal. Water Environment Research (accepted for publication).

Spanjers, H. and Takács I. (1998) Direct parameter extraction from respirograms for wastewater and biomass characterization. Water Science and Technology 39:4 pp. 137-145.

Spanjers, H. and Vanrolleghem, P.A. (1995) Respirometry as a tool for rapid characterization of wastewater and activated sludge. Wat. Sci. Tech., 31(2), 105-114.

Spanjers, H., Keesman, K. (1994) Identification of wastewater biodegradation kinetics. In: Proceedings 3rd IEEE Conference on Control Application. Glasgow, Scotland, August 24-26 1994. 1011-1016.

Specchia, V., Ruggeri, B., A. Gianetto, A. (1988) Mechanisms of Activated Carbon Bioremoval. Journal Chemical Engineering Communications, Volume 68, Issue 1 June 1988, pages 99 – 117.

Standard Methods (1998) Standard Methods for the Examination of Water and Waste Water, 20th ed., American Public Health Association, Washington DC.

Steiner, E. C., Blau, G. E. and Agin, G. L. (1987) Introductory Guide to SIMUSOLV. Dow Chemicals, Midland, Mich.

Stenstrom, M. K. (1976) A dynamic model and computer compatible control strategies for wastewater treatment plants. Ph.D. dissertation, Clemson University, Clemson, S.C.

Stolp, H. (1988) Microbial Ecology - Organisms, Habitats, Activities. Cambridge Univ. Press.

Stricker, A-E., Takács, I., Marquot, A. (2007) Hindered and Compression Settling: Parameter Measurement and Modelling. Proceedings of the IWA Particle Separation Conference, 2007, Toulouse

Strous, M., Fuerst, J.A., Kramer, E.H.M., Logermann, S, Muyzer, G., van de Pas-Schoonen, K.T., Webb, R., Kuenen, J.G. and Jetten, M.S.M. (1999) Missing litotroph identified as new planctomycete. Nature, 400, 446-449.

Strous, M., Heijnen, J.J., Kuenen, J.G. and Jetten, M.S.M. (1998) The sequencing batch reactor as a powerful tool for the study of slowly growing anaerobic ammonium-oxidizing microorganisms. Appl.Microbiol.Biotechnol., 50, 589-596.

Suzuki, K., Tanaka, Y. (2002) Removal of phosphate, magnesium and calcium from swine wastewater through crystallization enhanced by aeration. Water Research., 36, 2991-2998.

Szabó, A, Takács, S. Murthy, G. Daigger, I. Licskó, S. Smith (2008) The significance of design and operational variables in chemical phosphorus removal. Water Environment Research (accepted for publication).

Takács, I. (1986): Application of a mathematical model for the activated sludge treatment. Water Science and Technology, 18. pp. 163-174.

Takács, I. and Vanrolleghem, P.A. (2006) Elemental balances in activated sludge modelling. In: Proceedings of the IWA World Water Congress, 10-14 September 2006, Beijing, China.

Takács, I., Fairlamb, M., Dold, P.L., Bye, C., Jones, R. and Murthy, S. (2004) pH in wastewater treatment plant modelling. In: Proceedings 4th IWA World Water Conference. Marrakech, Morocco, September 19-24 2004.

Takács, I., Fleit, E. (1995) Modelling of the Micromorphology of the Activated Sludge Floc: Low DO, low F/M bulking. Water Science and Technology, 31, pp. 235-243.

Takács, I., Lockwood, S., Caplis, J.R. (1998) Simulation model helps manufacturing facility maintain regulatory compliance, optimize treatment processes, and train operators. Industrial Wastewater, May/June 1998 pp 44-46

Takács, I., Patry, G. (2002) The Dynamic Solids Residence Time. Proceedings of IWA 2002, Melbourne

Takács, I., Patry, G. and Nolasco, D. (1991) A Dynamic Model of the Clarification-Thickening Process. Water Research 25 (10), 1263-1271.

Takács, I., Murthy, S., Smith, S. and McGrath., M. (2006) Chemical phosphorus removal to extremely low levels: experience of two plants in the Washington, DC area. Water Science & Technology Vol 53 No 12 pp 21–28

Takács, I., Vanrolleghem, P.A., Wett, B., Murthy, S. (2007) Elemental balance based methodology to establish reaction stoichiometry in environmental modelling. Water Science & Technology 56. 9.

The MathWorks (2007) Matlab R2007b. High-level language for technical computing. www.mathworks.com.

Thompson, D. (1988) Activated sludge: step feed control to minimize solids loss during storm flow. M.Eng. thesis, McMaster University, Department of Chemical Engineering, Hamilton, Ontario, Canada.

Tomlison, E. (1982) The Emergence of the Bulking Problem and the Current Situation in the UK. In: Bulking of Acti-vated Sludge: Preventative and Remedial Methods, Eds: Chambers, B. and Tomlison, E. 17-28. Ellis Horwood Ltd, England.

Vaccari, D.A., Fagedes, T., Longtin, J. (1985) Calculation of Mean Cell Residence Time for Unsteady-State Activated Sludge Systems. Biotechnology and Bioengineering, Vol 27, pp. 695-703.

Vaccari, D.A., Cooper, A. and Christodoulatos, C. (1988) Feedback Control of Activated Sludge Waste Rate, JWPCF, v60, 1, p 1979-1985.

Van Denmark, P.J. and Batzing, B.L. (1987) The Microbes. The Benjamin/Cummings Publishing Company, Inc.

Vanderhasselt, A. and Vanrolleghem, P. A. (2000) Estimation of sludge sedimentation parameters from single batch settling curves. Water Research 34 (2), 395-406.

Vanrolleghem, P.A, van Daele, M. and Dochain, D. (1995) Practical identifiability of a biokinetic model of activated sludge respiration. Wat. Res. 29, 2561-2570.

Vanrolleghem, P.A., Rosen, C., Zaher, U., Copp, J., Benedetti, L., Ayesa, E. and Jeppsson, U. (2005) Continuity-based interfacing of models for wastewater systems described by Petersen matrices. Wat. Sci. Tech., 52(1-2), 493-500.

Vanrolleghem, P.A., Spanjers, H., Petersen, B., Ginestet, P. and Takács, I. (1999) Estimating (combinations of) Activated Sludge Model No. 1 parameters and components by respirometry. Water Science and Technology, Volume 39, Number 1, 1999, pp. 195-214

Vesilind, A. (1968) Design of prototype thickeners from batch settling tests. Water Sewage Works 115 (7), 302–307.

Vitasovic, Z. (1986) An integrated control strategy for the activated sludge process. Ph.D. dissertation, Rice University, Houston, Tex.

Vitasovic, Z. (1989) Continuous Settler Operation: A Dynamic Model. In : Dynamic Modeling and Expert Systems in Wastewater Engineering, Lewis Publishers, Inc., Chelsea Michigan, pp. 59-81.

Volcke, E.I.P., van Loosdrecht, M.C.M. and Vanrolleghem, P.A. (2006) Continuity-based model interfacing for plant-wide simulation: A general approach. Water Res, Vol. 40, No. 15. (August 2006), pp. 2817-2828.

Wagner, F. (1982) Study on the Causes and Prevention of Sludge Bulking in Germany. In: Bulking of Activated Sludge: Preventative and Remedial Methods, Eds: Chambers, B. and Tomlison, E. 29-40. Ellis Horwood Ltd, England.

Wanner, J. and Grau, P. (1989) Identification of Filamentous Organisms from Activated Sludge: A Compromise Between Wishes, Needs and Possibilities. Water Research, 23, 883-891.

Water Environment Federation (WEF), (1998) Biological and Chemical Systems for Nutrient Removal, Alexandria, Va. U.S.A. ISBN 1-57278-123-8.

Wentzel, M.C., Ekama, G.A., Loewenthal R.E., Dold, P.L., and Marais, GvR (1989) Enhanced polyphosphate organism cultures in activated sludge systems. Part II: Experimental behaviour. Water SA, 15(2), pp. 71-88.

Wentzel, M.C., Ekama, G.A., Marais, G.v.R. (1992) Processes and Modelling of Nitrification-Denitrification Biological Phosphorus Removal Systems - A Review. Wat. Sci. Tech. 25, No. 6, 59-82.

Wett, B., Murthy, S., Takács, I., Hell, M., Bowden, G., Deur, A., O'Shaughnessy, M. (2007) Key Parameters for Control of DEMON Deammonification Process. Water Practice, Volume 1, Number 5, November 2007, pp. 1-11(11) online at
http://www.ingentaconnect.com/content/wef/wp/2007/00000001/00000005/art00011

Zhang, D., Li, Z., Lu, P., Zhang, T. and Xu, D. (2006) A method for characterizing the complete settling process of activated sludge. Water Research 40 (14), 2637-2644.

The fundamentals of the activated sludge process are well understood and described in a series of mathematical models that predict oxygen demand, sludge production and many other process parameters. However, for the designer or operator, the whole wastewater treatment plant involves more than the activated sludge process itself. What part of the mixed liquor is in the settler at any given time? Effluent solid particles contribute significantly to effluent quality, why cannot their concentration be calculated from Stokes law? Under what conditions will sludge stored in the clarifier lead to gross clarifier failure? Activated sludge models necessarily treat bioreactors as "ideally" mixed – while, from the viewpoint of a microorganism inhabiting the center of an activated sludge floc, conditions may be quite different from those its neighbour at the surface of the floc experiences. Under what conditions do water chemistry and pH have an effect on biological and chemical processes and how to take that into account on a plant-wide basis? Iron or aluminium salt dosing does result in lowered effluent phosphate concentration – why is the residual concentration so variable and not depending directly on the dosage alone? How to size and operate an activated sludge system with powdered activated carbon dosage? How do adsorption and adaptation in this environment affect effluent quality? Respirograms contain important information about the component concentrations and degradation kinetics that is "obvious" to an expert from the shape of the respirogram– is there a way to evaluate those characteristic shapes and inflection points without detailed simulation and numerical optimization? Does sensitivity analysis give us practical information we would miss without it? What is the exact "age" (SRT) of the solids in the activated sludge reactor four days after the wastage has been stopped? (Cannot divide by zero for four days…). Influent COD/VSS ratios are highly variable – what is the composition of influent substrate in municipal wastewater, how does it relate to its lipid/carbohydrate/protein content? What does elemental balancing tell us about the stoichiometry of the Anammox growth reaction?

This dissertation is an attempt to answer these seemingly very diverse questions, in four main parts: physical, chemical and biological processes, as well as theoretical aspects of wastewater modelling.

In **Part One**, **Physical processes**, a dynamic model of the clarification-thickening process is presented. The model, the first of its kind, is able to describe the complete solids profile in a one-dimensional representation of the clarifier, including effluent solids, sludge blanket height and return solids concentration. It is shown that the average settling velocity of the discrete particles in the effluent can be related to their concentration. The modified (double-exponential) Vesilind settling function makes use of the relationship that exists between the concentration and the particle size distribution of effluent particles to predict effluent solids. A further extension of the Vesilind function with two logistic correction terms leads to a

generalized settling function that includes discrete, zone and compression settling. Such a general function can be implemented in a layered settler model independent of the number of layers. A low number of layers was traditionally used to mimic the effect of compression through numerical "blurring". The accuracy of the Vesilind settling function depends on proper evaluation of the interface vs. time slopes found from Zone Settling Velocity tests. A contribution is made in the form of an automatic method to extract the slopes after fitting an empirical function, alleviating the need to manually select the linear portion of the curve.

A major deficiency in activated sludge modelling is the inability of models to predict settling properties of the activated sludge. A floc model that describes substrate and DO gradients inside the microenvironment of activated sludge flocs, and incorporates non-random growth patterns of filamentous organisms is developed. The model can predict circumstances conducive to low DO and low F/M bulking depending on process conditions.

In **Part Two, Chemical processes**, a general pH model for municipal wastewater is developed. pH plays a fundamental role in biological and chemical reactions as well as in gas transfer, and its incorporation as the general underlying environment for activated sludge, digestion or sidestream models is a major step forward in reliable whole-plant modelling. Dissociation and solubility constants, as well as various numerical techniques for the solution of the complex algebraic equations are well-known in the literature. The contribution consists of selecting the required chemical species and most important precipitates occurring in municipal wastewater, verifying selected dissociation and solubility constants, and developing a practical method that uses influent pH and alkalinity, as well as a mixture of equilibrium and kinetic expressions and the Supersaturation Index, to bring the computational effort for pH calculation to a practical level.

In an investigation of an empirical, equilibrium based chemical phosphorus removal model, important kinetic effects are found affecting phosphorus residuals that cannot be described using pure equilibrium chemistry principles. An extensive set of experiments is used to support a new surface complexation model, with a new key parameter (Active Site Factor). Variation of the Active Site Factor, essentially the number of reactive oxygen atoms per iron atom, enables the model to describe the effect of mixing at dosage point, and that of floc structure and age, on residual phosphorus concentration. The equilibrium constants of the new model are not empirically fitted, but are based on literature values that are widely accepted and validated.

In **Part Three, Biological processes**, an extension of an early ASM model with adsorption and microbial adaptation is described. These processes play a key role in the Powdered Activated Carbon Treatment (PACT) system, particularly when applied to industrial wastewaters. The model has been calibrated to a series of batch, bench- and full-scale experiments.

Estimation of model parameters using a respirogram is an accepted method to determine influent state variable concentrations, kinetic and stoichiometric parameter values. An alternative, Direct Respirogram Evaluation (DRE) method is described that relies on the characteristic shape (as determined by first and second derivatives found in multi-component respirograms) and does not depend on numerical optimization techniques. Understanding the effect of all model parameters is sometimes difficult due to the interlinked nature of the ASM structure. A step-by-step procedure of a sensitivity analysis serves as a guideline for practitioners, highlighting key relationships in the model structure.

In **Part Four, Theoretical aspects,** an ordinary differential equation (ODE) is developed that can be numerically integrated to provide the true age of solids in the reactor. This equation based on an age balance forms the theoretical background to the SRT calculation in steady-state, but is also applicable in dynamically changing conditions or when there is no wastage at all. It is shown that instead of wastage, the true age of the biomass depends more on how much fresh solids form daily.

In other theoretical aspects of modelling, it is shown how elemental balancing can be used to extract new information about the composition of influent state variables, based on standard COD and VSS measurements available. It is shown that influent inerts (X_I) likely have lower and less varying COD/VSS ratios than substrate (X_S). An elementally balanced version of ASM1 (including N_2, CO_2 and H_2O state variables) is presented, with the proposition to include elemental balancing in biokinetic modelling. Elemental balancing is used to investigate the Anammox growth reaction and correct a stoichiometric coefficient in the literature. A simple, generalized method is presented that can be used to develop stoichiometric coefficients of biokinetic models.

These results, although seemingly scattered in very different areas of wastewater plant modelling, all improve our understanding of how the whole plant works, and extend the toolkit that is available for the design engineer or operator to get the most out of his installation.

De grondbeginselen van het actiefslibproces worden goed begrepen en in een reeks van wiskundige modellen beschreven die de zuurstofvraag, slibproductie en veel andere procesparameters voorspellen. Nochtans, voor de ontwerper of de exploitant, impliceert de gehele afvalwaterzuiveringsinstallatie meer dan het actiefslibproces alleen. Welk deel van het slib bevindt zich op een gegeven moment in de nabezinktank? Zwevende stoffen in het effluent dragen beduidend bij tot de effluentkwaliteit bijdragen, waarom kan hun concentratie niet worden berekend met de wet van Stokes? In welke omstandigheden zal het slib opgeslagen in de nabezinker leiden tot een volledige faling van de nabezinker? Actiefslibmodellen beschouwen bioreactoren noodzakelijkerwijs als "ideaal gemengd" - terwijl, vanuit het gezichtspunt van een micro-organisme dat zich in het centrum van een actiefslibvlok bevindt, de voorwaarden vrij verschillend kunnen zijn van die van zijn buur aan het oppervlak van de actiefslibvlok. Onder welke omstandigheden hebben waterchemie en pH een effect op biologische en chemische processen en hoe moeten deze aspecten in overweging genomen worden in een model van een volledige installatie? Dosering van ijzer of aluminiumzouten resulteert in verminderde concentraties van fosfaat in het effluent - waarom is de residuele fosfaatconcentratie zo veranderlijk en niet direct afhankelijk van die dosering? Hoe moet een waterzuiveringsinstallatie met actiefkooldosering ontworpen worden en bedreven worden? Hoe beïnvloeden de adsorptie en aanpassing van het actiefslib in dit milieu de effluentkwaliteit? Respirogrammen bevatten belangrijke informatie over de concentraties aan afvalwatercomponenten en de degradatiekinetiek die door een expert uit de vorm van een respirogram kan afgeleid worden - is er een manier om die kenmerkende vormen en buigpunten zonder gedetailleerde simulatie en numerieke optimalisatie te bekomen? Geeft de gevoeligheidsanalyse ons praktische informatie die wij zonder de analyse zouden missen? Wat is de juiste "leeftijd" (SRT) van het slib in een actiefslibreactor vier dagen nadat de slibspui is onderbroken? (Er kan niet door nul gedeeld worden gedurende vier dagen...). De influent CZV/VZS verhoudingen zijn hoogst veranderlijk - wat is de samenstelling van influent substraat in huishoudelijk afvalwater en hoe verhoudt het zich met de vet/koolhydraat/eiwit-samenstelling? Wat vertellen elementaire balansen ons over de stoechiometrie van de Anammox-groeireactie?

Dit doctoraal proefschrift is een poging om deze schijnbaar zeer diverse vragen, in vier delen te beantwoorden: fysische, chemische en biologische processen, naast theoretische aspecten van de modellering van afvalwaterzuiveringsinstallaties.

In **Deel Een, Fysische processen**, wordt een dynamisch model van het klarings/indikkingsproces voorgesteld. Het model, eerste van zijn soort, kan het volledige slibconcentratieprofiel in een ééndimensionale beschrijving van de nabezinker berekenen, met inbegrip van de effluent zwevende stoffen, de slibdekenhoogte en de concentratie van de zwevende stoffen in de terugvoer. Er is aangetoond dat de gemiddelde bezinkingssnelheid van

de individuele partikels in het effluent afhankelijk is van hun concentratie. De gewijzigde (dubbel-exponentiële) bezinkingsfunctie van Vesilind maakt gebruik van het verband dat tussen de concentratie en de grootteverdeling van de effluentpartikels bestaat om de effluent zwevende stoffen te voorspellen. Een verdere uitbreiding van de Vesilind-functie met twee logistische correctietermen leidt tot een algemene bezinkingsfunctie die de discrete, de zone- en de compressie-bezinking omvat. Een dergelijke algemene functie kan in een gelaagd bezinkermodel onafhankelijk van het aantal lagen geïmplementeerd worden. Een laag aantal lagen werd traditioneel gebruikt om het effect van compressie door numerieke "dispersie" na te bootsen. De nauwkeurigheid van de Vesilind bezinkingsfunctie hangt echter af van een juiste evaluatie van de bezinkingscurven die resulteren uit batch bezinkingsexperimenten. Een bijdrage wordt geleverd in de vorm van een automatische methode om de hellingen af te leiden door het aanpassen van een empirische functie, waardoor de behoefte wegvalt om het lineaire gedeelte van de bezinkingscurve manueel te selecteren.

Een belangrijke beperking in actiefslibmodellering is het onvermogen van modellen om bezinkingseigenschappen van het actiefslib te voorspellen. Een vlokmodel werd ontwikkeld dat substraat- en zuurstofgradiënten binnen het micromilieu van actiefslibvlokken beschrijft, naast niet-willekeurige groeipatronen van filamenteuze organismen. Het model kan de omstandigheden voorspellen die bevorderlijk zijn voor lage zuurstof en lage F/M "bulking", afhankelijk van de procesvoorwaarden.

In **Deel Twee, Chemische processen**, wordt een algemeen pH-model voor huishoudelijk afvalwater ontwikkeld. pH speelt een fundamentele rol in biologische en chemische reacties evenals in gasoverdracht, en zijn integratie als algemeen onderliggende conditie voor actiefslib-, vergistings- of zijstroombehandelingsmodellen is een belangrijke stap voorwaarts in betrouwbare modellering van volledige zuiveringsinstallaties. De dissociatie- en oplosbaarheidsconstanten , evenals diverse numerieke technieken voor de oplossing van de complexe algebraïsche vergelijkingen zijn reeds goed beschreven in de literatuur. De bijdrage bestaat uit het selecteren van de vereiste chemische species en de belangrijkste neerslagen die in huishoudelijk afvalwater voorkomen, de verificatie van de geselecteerde dissociatie- en oplosbaarheidsconstanten, en het ontwikkelen van een praktische methode die gebruik maakt van de influent-pH en -alkaliniteit, evenals een set van evenwicht- en kinetische uitdrukkingen en de Oververzadigingsindex, om de rekentijden nodig voor pH berekening op een praktisch niveau te brengen.

In een studie van een empirisch, op evenwichten gebaseerd model van de chemische fosforverwijdering, worden belangrijke kinetische effecten vastgesteld die de residuele fosforconcentratie beïnvloeden en die niet kunnen worden beschreven op basis van de principes van de evenwichtschemie alleen. Een uitgebreide reeks experimenten werd gebruikt om een nieuw oppervlakte-complexvormingsmodel op te stellen, met een nieuwe zeer belangrijke parameter (de Actieveplaatsfactor). De variatie van de Actieveplaatsfactor, in essentie het aantal reactieve zuurstofatomen per ijzeratoom, laat het model toe om het effect van de menging op het doseringspunt, en de vlokstructuur en -leeftijd, op de residuele fosforconcentratie te beschrijven. De evenwichtsconstanten van het nieuwe model worden niet empirisch gefit, maar zijn gebaseerd op literatuurwaarden die algemeen worden aanvaard en gevalideerd.

In **Deel Drie, Biologische processen**, wordt een uitbreiding van een vroeg actiefslibmodel (ASM) met adsorptie en microbiële aanpassing beschreven. Deze processen spelen een belangrijke rol in poeder actiefkool waterbehandelingssystemen (PACT), in het bijzonder

wanneer toegepast op industriële afvalwaters. Het model is gekalibreerd aan een reeks van batch, lab- en volschalige experimenten. De schatting van modelparameters uit een respirogram is een aanvaarde techniek om de influentconcentraties van de toestandsvariabelen, de kinetische en de stoechiometrische parameterwaarden te bepalen. In dit werk wordt een alternatieve, Directe Respirogram Evaluatiemethode (DRE) beschreven die zich op de kenmerkende vorm baseert (zoals bepaald door de eerste en tweede afgeleiden te nemen van respirogrammen met meerdere componenten) en niet van numerieke optimaliseringstechnieken afhangt. Inzicht in de effecten van alle modelparameters is soms moeilijke te bekomen door de onderlinge afhankelijkheden in de ASM structuur. Een stap-voor-stap procedure voor gevoeligheidsanalyse, die de zeer belangrijke verbanden in de modelstructuur benadrukt, werd opgesteld als richtlijn voor de mensen in de praktijk.

In **Deel Vier, Theoretische aspecten**, wordt een gewone differentiaalvergelijking ontwikkeld die numeriek kan worden geïntegreerd om de echte slibleeftijd van de zwevende stoffen in de reactor te berekenen. Deze vergelijking die op een leeftijdsbalans wordt gebaseerd, vormt ook de theoretische achtergrond voor de berekening van de slibleeftijd in evenwichtstoestand, maar is nu ook toepasselijk onder dynamisch veranderende voorwaarden of wanneer er bijvoorbeeld geen enkele slibspui is. Er is aangetoond dat de echte leeftijd van de biomassa niet zozeer afhangt van de slibspui maar wel van de hoeveelheid nieuwe zwevende stoffen die zich dagelijks vormen. In andere theoretische aspecten van modellering, wordt bewezen hoe elementenbalansen kunnen worden gebruikt om nieuwe informatie over de samenstelling van de influent toestandsvariabelen te halen gebaseerd op standaard beschikbaar CZV- en VZS-metingen. Ook wordt aangetoond hoe inerte stoffen in het influent (X_I) waarschijnlijk lagere en minder variabele CZV/VZS-verhoudingen vertonen dan particulair substraat (X_S). Een elementengebalanceerde versie van ASM1 (met inbegrip van N_2, CO_2 en H_2O toestandsvariabelen) wordt voorgesteld, met de suggestie om in de toekomst elementenbalansen standaard in te bouwen in toekomstige biokinetische modellen. Element-balancering werd gebruikt om de Anammox groeireactie te onderzoeken en een in de literatuur gerapporteerde stoichiometrisch coëfficiënt te corrigeren. Een eenvoudige, veralgemeende methode werd voorgesteld die kan gebruikt worden voor het berekenen van stoichiometrische coëfficiënten van biokinetische modellen.

Deze resultaten, hoewel schijnbaar sterk verspreid over zeer verschillend gebieden van de modellering van afvalwaterzuiveringsinstallaties, laten ons echter wel toe ons inzicht in de werking van gehele installaties te verhogen, en de toolkit die beschikbaar is voor de procesingenieur of de operator te verbeteren zodat deze het meest uit een installatie kunnen halen.

Les principes fondamentaux des procédés à boues activées sont bien compris et décrits dans une suite de modèles mathématiques capables de prédire la demande en oxygène, la production de boues et bien d'autres paramètres du procédé. Cependant, pour l'ingénieur concepteur ou l'exploitant, la station de traitement des eaux usées ne se réduit pas au seul procédé à boues activées. Quelle fraction de la liqueur mixte se trouve dans le clarificateur à un instant donné ? Les matières en suspension ont un impact significatif sur la qualité de l'eau traitée; pourquoi ne peut-on pas prédire leur concentration avec la loi de Stokes ? Dans quelles conditions les boues stockées dans le clarificateur vont-elles provoquer son débordement et des pertes de boues ? Les modèles de boues activées considèrent que les bioréacteurs sont parfaitement mélangés, alors que du point de vue d'un microorganisme, les conditions régnant au centre d'un floc peuvent être très différentes de celles à la surface du floc. Dans quelles conditions la chimie de l'eau et le pH ont-ils un effet sur les processus biologiques et chimiques, et comment représenter ceci au niveau de la station entière ? Les sels de fer ou d'aluminium réduisent la concentration de phosphates dans l'eau traitée, mais pourquoi la concentration résiduelle de phosphates est-elle si variable et pas directement fonction du seul dosage ? Comment dimensionner et exploiter un procédé à boues activées avec addition de charbon actif en poudre ? Comment les phénomènes d'adsorption et d'adaptation affectent-ils la qualité de l'eau traitée ? Les respirogrammes contiennent de l'information importante sur la composition des eaux usées et les cinétiques de dégradation qu'un expert peut extraire de la forme de la courbe, mais y a-t-il moyen d'interpréter les formes caractéristiques et les points d'inflexion sans le recours de simulations approfondies et de l'optimisation mathématique ? Les analyses de sensibilité nous donnent-elles des informations pratiques qu'on ne pourrait obtenir autrement ? Quel est l'âge exact des particules dans un réacteur à boues activées après quatre jours sans extraction (puisqu'on ne peut pas diviser par zéro) ? Les ratios DCO/MVS des eaux usées sont très variables : quelle est la composition des substrats des effluents urbains, et quelle est sa relation avec les teneurs en lipides/glucides/protéines ? Que nous apprennent les bilans de masse par élément chimique à propos de la stœchiométrie des réactions de croissance dans le procédé Anammox ?

Ce mémoire tente d'apporter des réponses à ces questions très diverses en apparence, avec quatre parties principales: processus physiques, chimiques, et biologiques, et enfin aspects théoriques de la modélisation du traitement des eaux usées.

Dans la **partie I, Processus physiques,** un modèle dynamique des processus de clarification/épaississement est présenté. Ce modèle, premier en son genre, est capable de décrire le profil complet de concentrations en matières en suspension (MES) dans une représentation unidimensionnelle du clarificateur, y compris la concentration en MES de l'eau traitée, la hauteur du voile de boue, et la concentration de la boue recirculée. Il est démontré que la vitesse moyenne de décantation des particules individuelles de l'eau traitée peut être

exprimée en fonction de leur concentration. Cette relation, qui sous-entend l'existence d'une relation entre la concentration et la granulométrie des particules, est incorporée dans l'équation de Vesilind modifiée (double exponentielle), afin de pouvoir prédire la concentration en MES de l'eau traitée. Une seconde extension de la fonction de Vesilind avec deux termes de correction logistiques mène à une fonction de décantation généralisée qui inclut les phénomènes de décantation discrète, de décantation freinée, et de compression. Une telle fonction peut être utilisée dans un modèle de clarificateur en couches indépendamment du nombre de couches. Traditionnellement, un faible nombre de couches était défini pour pouvoir représenter les effets de la compression par un effet de "flou numérique". La précision de la fonction de Vesilind dépend de la détermination correcte des pentes de la hauteur de l'interface de la boue en fonction du temps mesurée au cours des tests de décantation freinée. Une méthode automatisée est proposée pour extraire les pentes en ajustant une fonction empirique sur les données, évitant ainsi de devoir sélectionner manuellement la portion linéaire des courbes de décantation.

Une limitation importante de la modélisation des boues activées est l'incapacité des modèles à prédire les propriétés de décantation de la boue. Un modèle décrivant les gradients de substrats et d'oxygène à l'intérieur de l'environnement microscopique des flocs des boues activées, et incluant des motifs de croissance non-aléatoires d'organismes filamenteux, est développé. Le modèle est capable de prédire les circonstances qui conduisent au foisonnement dû à des carences en oxygène et à des faibles charges massiques.

Dans la **partie II, Processus chimiques,** un modèle général de pH est développé pour les eaux usées urbaines. Le pH joue un rôle fondamental dans les réactions biologiques et chimiques, ainsi que dans le transfert des gaz. Son incorporation pour définir les conditions chimiques du milieu aqueux dans les modèles de boues activées, de digestion et de traitement des retours concentrés en tête représente un pas majeur vers la modélisation fiable des stations de traitement au complet. Les constantes de dissociation et de solubilité sont bien établies dans la littérature, de même que diverses techniques numériques pour résoudre les équations algébriques complexes. La contribution apportée consiste à sélectionner les espèces chimiques requises et les principaux précipités pertinents pour les eaux usées urbaines, à vérifier les constantes de dissociation et de solubilité retenues, et à développer une méthode pratique utilisant les mesures de pH et d'alcalinité des eaux usées, une combinaison d'expressions d'équilibres chimiques et de cinétiques de réactions, et l'index de sursaturation, afin de ramener les demandes de calcul pour la détermination du pH à des niveaux acceptables en pratique.

Lors de l'étude d'un modèle empirique de déphosphatation chimique fondé sur des équilibres, des effets cinétiques importants sont identifiés qui affectent les concentrations résiduelles de phosphore et ne peuvent pas être décrits en utilisant uniquement des principes de chimie des équilibres. Un large ensemble d'expérimentations est utilisé pour développer un nouveau modèle de complexation de surface, avec un nouveau paramètre clé (Facteur de Sites Actifs). Les variations de ce facteur, qui représente essentiellement le nombre d'atomes d'oxygène réactifs par atome de fer, permettent au modèle de décrire l'effet du mélange au point d'injection, et celui de l'âge et de la structure des flocs sur la concentration résiduelle de phosphore. Les constantes d'équilibre de ce nouveau modèle ne sont pas ajustées de manière empirique, mais correspondent aux valeurs de la littérature qui sont largement acceptées et validées.

Dans la **partie III, Processus biologiques,** une extension développée afin d'ajouter les processus d'adsorption et d'adaptation microbienne dans un des premiers modèles de boues activées est décrite. Ces processus jouent un rôle clé dans les systèmes à boues activées avec addition de charbon actif en poudre, particulièrement pour les eaux usées industrielles. Le modèle a été calé avec une séries d'expériences en réacteur batch, pilote et sur site réel.

L'utilisation de la respirométrie est une méthode reconnue pour déterminer les concentrations des variables d'état de l'eau usée, et des paramètres cinétiques et stœchiométriques des modèles. Une méthode alternative d'évaluation directe d'un respirogramme est proposée, qui est fondée sur la forme caractéristique de la courbe (déterminée par les dérivées premières et secondes trouvées dans les respirogrammes à plusieurs composants) et ne dépend pas des techniques d'optimisation mathématique.

Comprendre les effets de tous les paramètres d'un modèle est parfois difficile à cause de la structure complexe des modèles de boues activées. Une procédure pas-à-pas pour conduire une analyse de sensibilité est décrite, qui peut servir de référence pour les applications pratiques en mettant en évidence les relations clés dans la structure du modèle.

Dans la **partie IV, Aspects théoriques,** une équation différentielle ordinaire pouvant être intégrée numériquement pour déterminer l'âge réel de la boue dans le réacteur est développée. Cette équation, issue d'un bilan pondéré de l'âge des particules, forme la base théorique pour le calcul de l'âge de boue en régime permanent, mais elle s'applique aussi dans des conditions dynamiques et même en l'absence d'extraction de boues. Il est démontré que l'âge réel de la biomasse dépend plus de la quantité de boue fraîche produite chaque jour que de la quantité extraite.

Concernant d'autres aspects théoriques de la modélisation, il est montré comment les bilans de masse par élément chimique (bilans élémentaires) peuvent être appliqués pour extraire de l'information nouvelle sur la composition des variables d'état des eaux usées en utilisant les concentrations disponibles en DCO et MVS. Il est démontré que la matière particulaire inerte des eaux usées (X_I) a probablement un ratio DCO/MVS plus faible et moins variable que le substrat particulaire (X_s). Une version modifiée de l'ASM1 est présentée, dans laquelle les bilans élémentaires sont fermés (en incluant les variables d'état N_2, CO_2 et H_2O), et il est proposé d'inclure les bilans élémentaires dans la modélisation biocinétique en général. La méthode des bilans élémentaires est utilisée pour étudier la réaction de croissance de la biomasse du procédé Anammox et corriger un coefficient stœchiométrique de la littérature. Une méthode simple et généralisée est présentée pour calculer les coefficients stœchiométriques des modèles biocinétiques.

Tous ces résultats, bien qu'ils apparaissent disséminés dans des domaines très différents de la modélisation du traitement des eaux usées, contribuent à l'amélioration de notre compréhension du fonctionnement global des stations, et s'ajoutent aux outils disponibles pour l'ingénieur et l'exploitant pour pouvoir tirer le meilleur parti de leur installation.

ÖSSZEFOGLALÁS

Az eleveniszapos eljárás alapfolyamatai jól ismertek és az oxigénigény, iszapszaporulat és sok más jellemző leírására több matematikai modell áll rendelkezésre. A tervező és az üzemeltető feladatköre azonban nem csak az eleveniszapos eljárásra, hanem az egész telepre terjed ki. Az eleveniszap hányadrésze tartózkodik az ülepítőben egy adott pillanatban? Az elfolyó lebegőanyag jelentősen befolyásolja a tisztított víz minőségét, miért nem lehet ezt a lebegőanyag koncentrációt a Stokes törvény alapján számítani? Milyen körülmények között lehet iszapfelúszásra számítani? Az eleveniszapos modellek a reaktortér zónáit ideálisan kevertnek tételezik fel. Azonban az eleveniszap pehely belsejében megtelepedett mikroorganizmusok teljesen más körülmények között szaporodnak, mint szomszédaik a pehely felületén. Milyen körülmények között és hogyan befolyásolja a pH és vízkémia a telepen lezajló biológiai és kémiai folyamatokat? Az elfolyó foszforkoncentráció csökkenthető vas- és aluminium-só adagolás segítségével – mi okozza az elfolyó foszforkoncentráció jelentős ingadozását, látszólag függetlenül az alkalmazott vegyszeradagtól? Hogyan tervezzünk és üzemeltessünk egy eleveniszapos rendszert aktívszénpor adagolással kiegészítve? Hogyan befolyásolja az adszorpció és az adaptáció az elfolyó víz minőségét? A respirogramm görbék fontos, szakemberek számára "első látásra" nyilvánvaló információt hordoznak a jelenlevő komponensek koncentrációjáról és lebontási kinetikájáról – lehetséges szimuláció és numerikus optimalizálás nélkül kiértékelni ezeket a tipikus görbeformákat? Van gyakorlati haszna a parameter-érzékenység analízisnek? Mennyi az iszapkor a rendszerben négy nappal a fölösiszapelvétel leállítása után (négy napig nem lehet nullával osztani…). A befolyó szennyvíz KOI/izzítási maradék aránya gyakran változik – lehet ebből a befolyó szubsztrát összetételére következtetni, hogyan viszonyul az a szennyvíz zsír/szénhidrát/fehérje tartalmához? Milyen következtetések vonatók le különböző elemek alapján végzett anyagmérlegek segítségével az Anammox reakcióról?

Ez a disszertáció ezekre a látszólag véletlenszerűen szétszórt kérdésekre kíván választ adni, négy részre bontva: a szennyvíztisztítás fizikai, kémiai és biológiai alapfolyamatai, valamint egyéb elméleti vonatkozások területén.

Az **1. Részben, Fizikai folyamatok** címmel, egy dinamikus utóülepítő modell leírása található. A modell az ülepítőben lévő lebegőanyag és eleveniszap koncentrációjának teljes vertikális profilját képes előrejelezni, az elfolyó lebegőanyagtól kezdve az iszapfelhő helyzetén át a recirkulált iszap koncentrációjáig. A fejezetben bizonyítást nyer, hogy az elfolyó lebegőanyag részecskék ülepedési sebessége közvetetten függ a koncentrációjuktól. A módosított (dupla-exponenciális) Vesilind függvény képes leírni ezt az összefüggést, ami a koncentráció és részecskeeloszlás egyidejű változásának következménye. A Vesilind függvény további kiterjesztése két logisztikus korrekciós tényezővel olyan általános függvényt eredményez, ami a részecske-, zóna- és kompresszív-ülepedés teljes leírására

képes. Ennek az általános függvénynek az alkalmazása egy egydimenziós modellben függetleníti az eredményeket a rétegszámtól. A kompresszió modellezése hagyományosan csak kis rétegszám alkalmazásával érhető el, numerikus "diffúzióval". A Vesilind ülepedési függvény megbízhatósága az ülepedési kisérletek során nyert iszapfelhő magasság időbeli változásának helyes kiértékelésétől függ. Egy újonnan kifejlesztett automatikus módszer szükségtelenné teszi a lineáris ülepedési szakaszok kézzel való kiválasztását.

Az eleveniszapos szennyvíztisztítás matematikai modellezésének egyik legnagyobb hiányossága az, hogy a modellek nem képesek az iszap ülepedési tulajdonságainak előrejelzésére. Egy szubsztrát és oxigén profilt is figyelembevevő pehelymodell, mely fonalas baktériumok szaporodását is tartalmazza, használható erre a célra. A modell figyelembe veszi a pehely belsejében uralkodó körülményeket és a fonalas baktériumok irányított növekedését. A modellel előrejelezhetők azok az üzemelési viszonyok, amelyek alacsony oxigén koncentráció vagy alacsony F/M arány következtében iszapfelfúvódáshoz vezethetnek.

A **2. Részben, Kémiai folyamatok** címmel, egy lakossági szennyvízek esetében általánosan alkalmazható pH modell kerül bemutatásra. A pH alapvető módon befolyásolja a biológiai és kémiai folyamatokat, valamint a gázcserét is. A pH számítása és figyelembevétele az eleveniszapos, anaerob és egyéb folyamatok háttereként jelentős előrelépés a szennyvíztisztítás modellezésében. A szükséges disszociációs állandók és oldhatósági szorzatok, valamint a komplex algebrai probléma numerikus kezelése ismert a szakirodalomból. Új eredménynek számít a leggyakrabban előforduló ionok és legfontosabb csapadékok kiválasztása, és egy gyakorlatban könnyen használható számítási módszer kifejlesztése. A módszer vegyesen használt kinetikus és egyensúlyi számításokon, valamint a Túltelítettségi Indexen alapul.

A foszfor eltávolítás kémiai egyensúlyokon alapuló modelljét vizsgálva, fontos kinetikai összefüggések kerülnek napvilágra, melyeket a meglévő modell nem képes leírni. Kiterjedt kísérletek eredményeképpen egy új felületi komplexképződésen alapuló modell posztulálható, egy új kulcsparaméterrel (Aktív Reakcióhely Arány). Az Aktív Reakcióhely Arány változtatásával, ami lényegében a reakcióképes oxigénatomok és a vasatomok arányát jelzi, kinetikai összefüggések, mint pl. bekeverési energia és pehelykor hatásai is leírhatók. Az új modell konstansait nem empirikus becslések, hanem ismert vízkémiai adatbázisok alapján állítottam össze.

A **3. Részben, Biológiai folyamatok** címmel, egy korai eleveniszapos modell kiterjesztése található. A modell szénporadagolás következtében bekövetkező adszorpciós és adaptációs folyamatok leírását is tartalmazza a PACT rendszerben. Ezek a folyamatok fontos szerepet játszanak különösen ipari szennyvizek esetében. A modell több szakaszos és folyamatos, laboratóriumi és ipari méretű kisérletsorozat eredménye alapján lett kalibrálva.

Respirogrammon alapuló paraméterbecslést gyakran használunk befolyó szennyvíz koncentrációk, valamint kinetikai és sztöchiometriai paraméterek meghatározására. Egy alternatív, közvetlen paraméterbecslő módszer (DRE) a respirogramm jellegzetes alakját kihasználva, első és másodfokú deriváltak alapján határozza meg ezeket a fontos paramétereket, matematikai modell alkalmazása és optimalizálása nélkül.

A modellek komplex szerkezete miatt paramétereik gyakran kölcsönösen függnek egymástól. Egy gyakorlatban használható, egyszerű paraméter érzékenység-analízis segít a lényeges paraméterek kiválasztásában és modell összefüggéseinek könnyebb megértésében.

A **4. Részben, Elméleti megfontolások** címmel, egy közönséges differenciálegyenlet (ODE) levezetése kerül bemutatásra, amelynek alapján az eleveniszap tényleges kora számítható. Ez az életkor mérlegen alapuló egyenlet az alapja a közismert egyensúlyi iszapkor számításnak, de azzal ellentétben, dinamikus viszonyok között is használható, vagy abban az esetben is, ha egyáltalán nincs fölösiszapelvétel a rendszerben. Mindebből az a következtetés vonható le, hogy a tényleges iszapszaporulat sokkal fontosabb szerepet játszik az iszapkor meghatározásában, mint a fölösiszapelvétel.

Más elméleti megfontolások során, elemi anyagmérlegek használata alapján bebizonyítható, hogy kizárólag KOI és izzítási veszteség mérésekből is lehet a befolyó szennyvíz részletes összetételére következtetni. A befolyó szennyvíz bonthatatlan szervesanyagtartalma (X_I) alacsonyabb és állandóbb KOI/izzítási maradék aránnyal rendelkezik, mint a befolyó szubsztrát (X_S). Az ASM1 modell elemi anyagmérlege is bemutatásra kerül, N_2, CO_2 és H_2O állapotváltozók bevezetésével. Az Anammox szaporodási reakció sztöchiometriáját vizsgálva elemi anyagmérlegek alapján megállapíthatók a helyes sztöchiometriai koefficiensek. Egy általános módszer bemutatására is sor kerül, amely segítségével biokinetikai modellek koefficiensei automatikusan levezethetők.

Ezek a eredmények látszólag a szennyvíztisztítás modellezésének nagyon különböző területeit ölelik fel. Azonban közös vonásuk, hogy a telep működésének megértését segítik elő, és hozzájárulnak a tervezőmérnök vagy üzemeltető által használt számítási módszerek kiterjesztéséhez, és ezzel hatékonyabb szennyvíztelepek létrehozásához.

论文总揽

虽然活性污泥工艺的基础已经很清楚并且已经包括在一系列能够预测氧需求，污泥产量和其它工艺参数的模型中。可是对于污水处理厂设计者或运行者来说，活性污泥本身不代表污水处理厂的全部。在给定的时间内混合液的哪一部分在沉淀池中？出流的固体颗粒是如何显著地影响出流的质量以及为什么不能用 Stokes 定律计算它的浓度？在什么情况下储存在沉淀池中的污泥会导致沉淀池完全失效？活性污泥模型是否有必要把生物反应器看作理想混合-因为在活性污泥颗粒中心的微生物与其相邻的颗粒表面的微生物所处的条件相当不同。在什么条件下水化学和 pH 会对生物和化学过程产生影响以及如何在全厂模型中考虑？加入铁盐或铝盐能得到很低的出流的磷浓度-但是为什么残留的浓度变化很大而且不完全依赖加药剂量？如何设计和运行一个添加粉末活性碳的活性污泥工艺？在这样的情况下吸附和适应性是如何影响出流质量的？呼吸测量包含有组分浓度和降解动力学的重要信息-这对一个专家来说只要从曲线的形状就可知-是否有一种方法不需要详细的模拟和数值优化就可评估这些曲线的特征形状和拐点？不进行敏感性分析是否会遗漏一些实际的信息？在排泥已经停止以后的四天活性污泥反应器中固体的确切泥龄是多少(不能用零去除四)？污水中的 COD/VSS 比例变化很大 – 什么是市镇污水的基质的组分 – 这些是如何与脂/碳水化合物/蛋白质含量相联系？元素平衡能告诉我们有关缺氧氨氧化细菌(Anammox)反应的化学计量方面的什么信息？

这篇论文尝试用四个部分回答这些表面上看起来非常不同的问题: 物理的，化学的，生物的以及污水模拟理论的各方面。

第一部分, 物理过程: 这部分介绍了一个沉淀 – 浓缩过程的动力学模型。这个模型(类似模型中的第一个) 能够描述沉淀池一维上的完正的固体浓度分布，包括出流的固体浓度，泥层高度和回流固体的浓度。已经表明出流中离散颗粒的平均沉降速度可能与它们的浓度相关。修正的(双指数) Vesilind 沉降涵数利用了出流颗粒浓度和颗粒大小的分布之间存在的关系预测出流固体浓度。这个具有两个改正项的 Vesilind 涵数的进一步扩展产生了一个包括离散，区域和压缩沉降的通用沉降涵数。这样的通用函数可以在独立于泥层数的成层模型中实施。在泥层的底部通常是用来模拟通过数值模糊的压缩影响。Vesilind 沉降函数的精度取决于从沉降速度试验找到的界面与时间斜坡的合适的估计。这方面的一个进展是在拟合经验函数以后减少手工选择界面线性部分获得斜坡的自动方法。

活性污泥模拟的一个主要缺陷是不能预测活性污泥的沉降特性。这部分开发了一个能够描述活性污泥颗粒内部微观环境中基质和溶解氧梯度并且包括了丝状菌非随机生长的颗粒模型。这个模型能够预测依赖于工艺条件的导致低低溶解氧浓度(DO)和低 F/M 污泥膨胀的情况。

第二部分，化学过程: 这部分开发了一个通用的用于城市污水的 pH 模型。pH 在生物和化学反应以及气体转移中起着非常重要的作用。pH 模型作为活性污泥，厌氧

消化或者旁流工艺模型的一般的背景模型是可靠的全污水厂模型的开发向前迈出的一大步。离解和溶解常数以及解复杂的线性方程的各种数值技术已在文献中广为熟悉。这是由所选择的各种化学种类和出现在城市污水中的最主要的沉淀物所组成，并证实了所选择的离解和溶解常数，开发了使用 pH，碱度以及化学平衡动力学表达和超饱和常数混合的实际方法以便把 pH 模型达到实用的水平。

在调查一个经验的基于化学平衡的化学除磷模型时，发现了使用纯化学平衡不能描述的影响磷的残留浓度的重要动力学效应。一组广泛的实验用来支持一个具有新的关键参数(活动表面因素) 的新的表面复合模型。活动表面因素的变化(本质上是每个铁原子的活性氧原子数) 使得模型能够描述加药点的混合效应和颗粒结构，年龄对残留的磷的浓度的影响。

第三部分，生物过程：这部分描述了一个早期的带有吸附和生物适应性的 ASM1 模型的扩展。这些过程在粉末活性碳模型特别是在应用于工业污水时起到着关键的作用。这个模型已经使用一系列批次，实验室和生产规模试验进行了校准。使用了一种已经接受的用来确定污水状态变量浓度，动力学和化学计量参数的利用呼吸测量的模型参数估计方法。

这部分还描述了一种替代的称为″呼吸测量直接评价法(DRE)″。这种方法依赖于呼吸测量曲线的特征形状而不依赖数值优化技术。由于 ASM 模型结构上的相互关联性理解所有模型参数的影响有时有困难。一个强调模型结构中关键关系的敏感性分析的入门方法用来作为实践者的指南。

第四部分，理论方面：这部分开发了一个能够数值上积分的差分方程用来提供反应器中的真实泥龄。基于这个方程的泥龄形成了稳态时的 SRT （泥龄）计算的理论背景。同时可用于变化的动态条件或完全没有排泥的情况。并表明在没有排泥的情况下生物量的真实泥龄更多依赖于每天形成的新的固体。在其它的模拟方面，表明了元素平衡如何用来获得基于标准的 COD 和 VSS 测量的污水状态变量的组分的信息。

同样表明污水的惰性颗粒组分(X_I)比基质具有较低的和较少变化的 COD/VSS 比例。这部分给出了一个基于元素平衡的 ASM1 模型 （包括 N_2, CO_2 和 H_2O 的状态变量) 并建议生物动力学模型中包括元素平衡。元素平衡还用来调查缺氧氨氧化细菌(Anammox) 的生长反应和改正文献中的化学计量参数。这部分还给出了一个简单通用的方法用来开发动力学模型中的化学计量参数。

这些结果虽然表面上分散于污水处理厂模拟中非常不同的领域但是都改善了我们对一个全污水处理厂工作原理的理解，为设计工程师和操作员提供了更多的解决问题的工具和方法。

254

APPENDIX A. Solution speciation methods used

A simple system is used to demonstrate two different methods for speciation and solubility determination.

Using the iron(III) system as an example, a list of species of interest could include:

$$H^+, \ OH^-, \ H_2O, \ Fe^{3+}, \ FeOH^{2+}, Fe(OH)_2^+ \ , \text{and} \ Fe(OH)_4^-$$

There are other possible species but to keep the discussion simple these are the only ones included in this example. The species' distribution as a function of pH in solution containing 0.1 mM Fe^{3+} is shown in Figure B.1 and using log scale in Figure B.2 (this solution is supersaturated, see later).
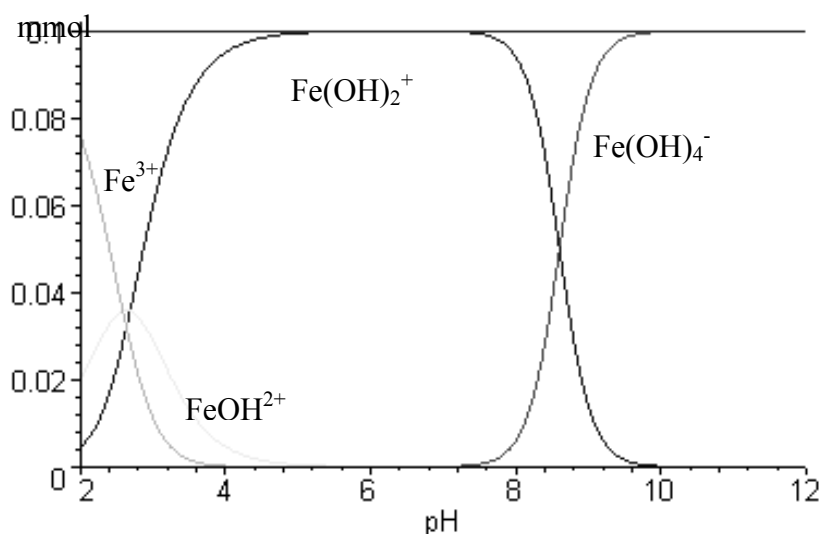

Figure B1. Species in the simple Fe-OH system
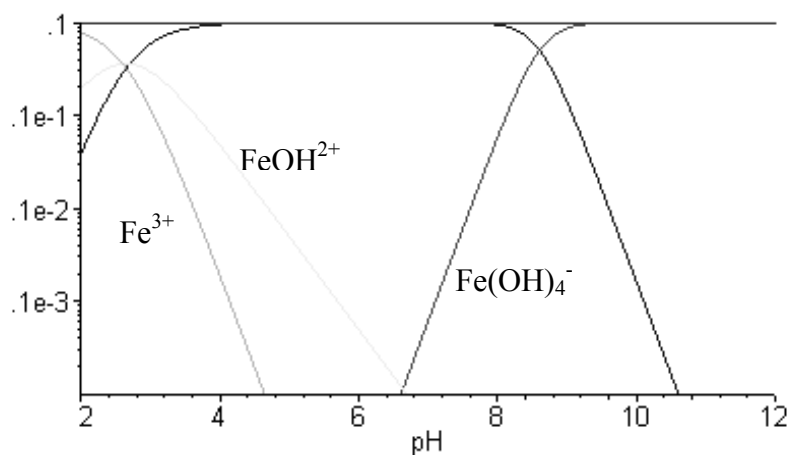
mmol

$Fe(OH)_2^+$

Figure B2. Species in the simple Fe-OH system (log scale)

The same distributions can be obtained using the Tableau or algebraic methods (Chapters 6 and 8).

The Tableau method

The mass balances and mass actions for solving chemical equilibrium problems can be represented in Tableau notation (Smith and Ferris, 2001b). For a given defined system it is desirable to determine the equilibrium concentration of all species. The example list includes seven species, so it is necessary to define seven relationships in order to solve this system. The situation can be simplified if it is realized that each of these species is not independent. Components can be selected from the list of species and used to solve the equilibrium problem. For example, if H^+ (pH) and Fe^{3+} are known the concentration of all other species can be determined from their logK values (mass action). In matrix notation pH and Fe^{3+} can be thought of as spanning the basis set.

Therefore, two equations and two unknowns are needed. The first relationship is the mass balance of iron and the second is proton balance (related to electroneutrality). We can write the Tableau:

Table B.1. Tableau for Fe–H system

H^+	Fe	logK	Species
1	0	0	$[H^+]$
0	1	0	$[Fe^{3+}]$
-1	0	-14	$[OH^-]$
-1	1	-2.19	$[FeOH^{2+}]$
-2	1	-5.67	$[Fe(OH)_2^+]$
-4	1	-21.6	$[Fe(OH)_4^-]$
[H$_T$]	[Fe$_T$]		

Table B.1 completely defines the equilibrium problem. The entries in the columns are the stoichiometric coefficients for forming each species. There is 1 H, 0 Fe in H^+ and $Fe(OH)_4^-$ is formed with one iron and removing 4 protons from water. Given the tableau, all that remains is to determine the values for $[H^+]$ and $[Fe^{3+}]$ for a specified H$_T$ and Fe$_T$. Multiplying across

256

the rows it is possible to determine species concentration and summing down the columns the total values (mass balance) are recovered. This is best understood by writing out entries for the species concentrations:

$$[H^+] = [H^+]^1 \times [Fe^{3+}]^0 \times 10^0 \tag{A.1}$$

$$[Fe^{3+}] = [H^+]^0 \times [Fe^{3+}]^1 \times 10^0 \tag{A.2}$$

$$[OH^-] = [H^+]^{-1} \times [Fe^{3+}]^0 \times 10^{-14} \tag{A.3}$$

$$[FeOH^{2+}] = [H^+]^{-1} \times [Fe^{3+}]^1 \times 10^{-2.19} \tag{A.4}$$

etc.....

It is necessary to always write the formation reactions for each species from the components. For example, to understand Equation (B.3) consider that K_w corresponds to the following reaction:

$$H_2O = H^+ + OH \qquad K_w = [H^+][OH^-] \tag{A.5}$$

If Equation (A.5) is rearranged to solve for $[OH^-]$ then Equation (A.3) is obtained. As another example, to understand Equation (A.4) consider that K for the first hydrolysis of iron(III) corresponds to the following reaction:

$$Fe^{3+} + H_2O = FeOH^{2+} + H^+ \quad K_{H1} = \frac{[FeOH^{2+}][H^+]}{[Fe^{3+}]} \tag{A.6}$$
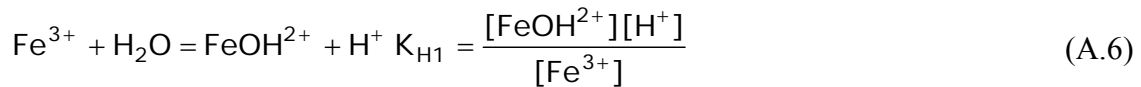
if Equation (A.6) is rearranged to solve for $[FeOH^{2+}]$ then Equation (A.4) is obtained.

To explain the summation down the columns (mass balance), consider total iron:

$$Fe_T = 0[H^+] + 1[Fe^{3+}] + 0[OH^-] + 1[FeOH^{2+}] + 1[Fe(OH)_2^+] + 1[Fe(OH)_4^-] \tag{A.7}$$

Notice that the coefficients are the entries down the iron column in the tableau.

Now the problem can easily be expressed in matrix notation. We define the 1×2 vector of unknown component concentrations as $\mathbf{X}$ so we can write $X = \big([H^+]\,[Fe^{3+}]\big)$

There is a 6×1 vector of species concentrations as well.

$$C = \begin{pmatrix} [H^+] \\ [Fe^{3+}] \\ [OH^-] \\ [FeOH^{2+}] \\ [Fe(OH)^{2+}] \\ [Fe(OH)_2^+] \\ [Fe(OH)_4^-] \end{pmatrix} \tag{A.8}$$

Total concentrations are in a 2×1 vector $T = \begin{pmatrix} [H_T] \\ [Fe_T] \end{pmatrix}$. The logK values are summarized in the 6×1 vector

$$K = \begin{pmatrix} 0 \\ 0 \\ \log K_w \\ \log K_{H1} \\ \log K_{H2} \\ \log K_{H4} \end{pmatrix} \tag{A.9}$$

Finally, a 6×2 matrix of the stoichiometric coefficients is needed:

$$A = \begin{pmatrix} 1 & 0 \\ 0 & 1 \\ -1 & 0 \\ -1 & 1 \\ -2 & 1 \\ -4 & 1 \end{pmatrix} \tag{A.10}$$

Now the minimization problem is to determine **X** that minimizes the residuals in the mass balance. This calculation is performed as follows:

minimize **R** as a function of **X** where $\qquad$ **R** = **A** x ($10^{\mathbf{C}}$) - **T** $\qquad$ (A.11)

and $\quad$ $\mathbf{C} = 10^{(\mathbf{K}+\mathbf{A}\times\mathbf{X'})}$ $\qquad\qquad\qquad\qquad\qquad$ (A.12)

The minimization can be performed using all elements of **R,** using a Newton-Raphson method for example or using other nonlinear optimization methods on some summation of R, such as the sum of squares or the sum of absolute values of residuals.

For this system with a total iron of 0.1 mM and pH 2 to 12 the results are shown in Figure A.1 and on log scale, A.2. Note that this system is supersaturated and should be further processed as described in Chapter 8.

Algebraic solution

The same example system can be solved algebraically resulting in one set of linear equations as described in Chapter 7. Maple, a symbolic solver (Maplesoft, 2005) was used for this purpose to generate the equations. The Maple .mws file with comments is provided below.

The dissociation constants in this section are expressed based on the following formulation (as per NIST, 2001):

$$Fe^{3+} + OH^- = FeOH^{2+} \tag{A.13}$$

While the Tableau example above for the same reaction uses

$$Fe^{3+} + H_2O = FeOH^{2+} + H^+ \tag{A.14}$$

However, the constants are equivalent and can be converted easily because the difference is just the autohydrolysis of water $H_2O = H^+ + OH^-$. If the water autohydrolysis reaction (log of equilibrium constants) is added to B.14, the hydroxide/Fe association reactions can be expressed in the way presented in B.15, so constants are different approximately by -14, (-28, -42).

The procedure then in Maple becomes:

1)   Specify all dissociation reactions (p = positive, m = negative charge)

```
water:=H_p*OH_m=Kw;
```
$$water := H\_p\,OH\_m = Kw$$

```
fehyd1:=FeOH1_2p/(Fe_3p*OH_m)=ksFeOH1;
```
$$fehyd1 := \frac{FeOH1\_2p}{Fe\_3p\,OH\_m} = ksFeOH1$$

```
fehyd2:=FeOH2_p/(Fe_3p*OH_m^2)=ksFeOH2;
```
$$fehyd2 := \frac{FeOH2\_p}{Fe\_3p\,OH\_m^2} = ksFeOH2$$

```
fehyd4:=FeOH4_m/(Fe_3p*OH_m^4)=ksFeOH4;
```
$$fehyd4 := \frac{FeOH4\_m}{Fe\_3p\,OH\_m^4} = ksFeOH4$$

2) Set up the mass balance for total iron (Fe$_T$)

```
femb:=Fet=Fe_3p+FeOH1_2p+FeOH2_p+FeOH4_m;
```
$$femb := Fet = Fe\_3p + FeOH1\_2p + FeOH2\_p + FeOH4\_m$$

```
femb := Fet = Fe_3p+FeOH1_2p+FeOH2_p+FeOH4_m;
```

$$femb := Fet = Fe\_3p + FeOH1\_2p + FeOH2\_p + FeOH4\_m$$

3) Solve five equations for five unknowns assuming H⁺ (pH) and ionic strength are set

```
solve({water,fehyd1,fehyd2,fehyd4,femb},{OH_m,Fe_3p,FeOH1_2p,F
eOH2_p,FeOH4_m});
```

The result is five algebraic equations:

```
OH_m:= Kw/H_p; Fe_3p:=
Fet*H_p^4/(H_p^4+ksFeOH1*Kw*H_p^3+ksFeOH2*Kw^2*H_p^2+ksFeOH4*K
w^4); FeOH4_m:=
ksFeOH4*Fet/(H_p^4+ksFeOH1*Kw*H_p^3+ksFeOH2*Kw^2*H_p^2+ksFeOH4
*Kw^4)*Kw^4; FeOH2_p:=
ksFeOH2*Fet*H_p^2/(H_p^4+ksFeOH1*Kw*H_p^3+ksFeOH2*Kw^2*H_p^2+k
sFeOH4*Kw^4)*Kw^2; FeOH1_2p:=
ksFeOH1*Fet*H_p^3/(H_p^4+ksFeOH1*Kw*H_p^3+ksFeOH2*Kw^2*H_p^2+k
sFeOH4*Kw^4)*Kw;
```

$$OH\_m := \frac{Kw}{H\_p}$$

$$Fe\_3p := \frac{Fet\ H\_p^4}{H\_p^4 + ksFeOH1\ Kw\ H\_p^3 + ksFeOH2\ Kw^2\ H\_p^2 + ksFeOH4\ Kw^4}$$

$$FeOH4\_m := \frac{ksFeOH4\ Fet\ Kw^4}{H\_p^4 + ksFeOH1\ Kw\ H\_p^3 + ksFeOH2\ Kw^2\ H\_p^2 + ksFeOH4\ Kw^4}$$

$$FeOH2\_p := \frac{ksFeOH2\ Fet\ H\_p^2\ Kw^2}{H\_p^4 + ksFeOH1\ Kw\ H\_p^3 + ksFeOH2\ Kw^2\ H\_p^2 + ksFeOH4\ Kw^4}$$

$$FeOH1\_2p := \frac{ksFeOH1\ Fet\ H\_p^3\ Kw}{H\_p^4 + ksFeOH1\ Kw\ H\_p^3 + ksFeOH2\ Kw^2\ H\_p^2 + ksFeOH4\ Kw^4}$$

4) Calculate activity correction for ionic strength

```
fm:=10^(-0.5*(sqrt(mu)/(1+sqrt(mu))-0.2*mu));
```

$$fm := 10^{\left(-\frac{0.5\ \sqrt{\mu}}{1 + \sqrt{\mu}} + 0.10\ \mu\right)}$$

```
fd:=10^(-0.5*4*(sqrt(mu)/(1+sqrt(mu))-0.2*mu));
```

$$fd := 10^{\left(-\frac{2.0\ \sqrt{\mu}}{1 + \sqrt{\mu}} + 0.40\ \mu\right)}$$

```
ft:=10^(-0.5*9*(sqrt(mu)/(1+sqrt(mu))-0.2*mu));
```

$$ft := 10^{\left(-\frac{4.5\ \sqrt{\mu}}{1 + \sqrt{\mu}} + 0.90\ \mu\right)}$$

where

    fm   = activity coefficient for monovalent ions

fd   = activity coefficient for divalent ions
        ft   = activity coefficient for trivalent ions

5) Define constanst (including activity coefficients)

```
Kw:=6.867*10^(-15)/fm^2;
```

$$Kw := \frac{0.6867000000 \ 10^{-14}}{\left(10^{\left(-\frac{0.5\sqrt{\mu}}{1+\sqrt{\mu}} + 0.10\,\mu\right)}\right)^2}$$

```
ksFeOH1:=10^(11.81)/(fd/(fm*ft));ksFeOH2:=10^(23.4)/(1/(fm*ft)
);ksFeOH4:=10^(34.4)/(1/(ft*fm^3));
```

$$ksFeOH1 := \frac{0.6456542290 \ 10^{12} \ 10^{\left(-\frac{0.5\sqrt{\mu}}{1+\sqrt{\mu}} + 0.10\,\mu\right)} \ 10^{\left(-\frac{4.5\sqrt{\mu}}{1+\sqrt{\mu}} + 0.90\,\mu\right)}}{10^{\left(-\frac{2.0\sqrt{\mu}}{1+\sqrt{\mu}} + 0.40\,\mu\right)}}$$

$$ksFeOH2 := 0.2511886432 \ 10^{24} \ 10^{\left(-\frac{0.5\sqrt{\mu}}{1+\sqrt{\mu}} + 0.10\,\mu\right)} \ 10^{\left(-\frac{4.5\sqrt{\mu}}{1+\sqrt{\mu}} + 0.90\,\mu\right)}$$

$$ksFeOH4 := 0.2511886432 \ 10^{35} \ 10^{\left(-\frac{4.5\sqrt{\mu}}{1+\sqrt{\mu}} + 0.90\,\mu\right)} \left(10^{\left(-\frac{0.5\sqrt{\mu}}{1+\sqrt{\mu}} + 0.10\,\mu\right)}\right)^3$$

6) Set concentrations

```
Ionic strength mu:=0.02:
Fet:=0.0001: (0.1 mM)
```

7) Define pH

```
H_p:=10^(-pH);
```

$$H\_p := 10^{(-pH)}$$

Now the species can be calculated as plotted in Figures A.1 and A.2. This simple example can be easily calculated on the back of an envelope, but real systems containing many components require a symbolic solver. Very complex systems may not be solvable by this method. For systems that are solvable, the algebraic method is more efficient considering the calculation time than the iterative Tableau method (which is completely scalable without limitations).

Imre Takács

Personal

Born: 1956, Budapest, Hungary
Citizenship: Hungarian and Canadian
Languages: English, Hungarian: fluent; French, Russian: basic
Children: Judit (20) and Miki (24)

Education

B.Chem.Eng.,University of Budapest, 1978   Industrial Food Processing Engineering
M.Env.Eng.,University of Budapest, 1980   Environmental Bioengineering
Dr Techn., University of Budapest, 1986   Environmental Bioengineering

Employment History

2005-present   PhD student in Applied Biological Sciences, Ghent University, Belgium
2002-present   Head, R&D, EnviroSim Associates Ltd., Flamborough, Ontario, Canada
1994-2002   Part-time Professor, Geology, McMaster University, Hamilton, Ontario,
                 Canada
1991-2002   Head, R&D, Hydromantis Inc., Hamilton, Ontario, Canada
1988-1991   Research Engineer - McMaster University, Hamilton, Ontario, Canada
1983   Project Engineer - VIZITERV, Consulting Office for Water
                Management, Budapest, Hungary
1980-1988   Project Engineer - VITUKI, Research Centre for Water
                Resources Development, Budapest, Hungary

Professional Associations

- Canadian Association for Water Quality

- International Water Association
- Water Environment Federation
- Modeling Expert Group of the Americas (MEGA), Chair
- IWA Task Group Good Modelling Practice

Experience

Actively involved in environmental research and engineering for 27 years. Extensive experience in biological and physico-chemical wastewater treatment processes, as well as drinking water treatment processes. Principal developer of a wide range of modelling and software solutions, implemented in several commercial dynamic modelling packages. Project manager and chief development engineer for several projects involving full-scale implementation and commissioning of innovative technologies on wastewater and drinking water treatment plants in the above areas. Relevant activities include:

- Principal developer and team leader on the development of two major wastewater simulation software, the General Purpose Simulator (GPS-X) and BioWin
- Developed a chemical equilibrium based water chemistry model to support ASM type biokinetic modelling (pH and metal salt precipitation reactions)
- Developed elemental balancing methodology and applied it for ASM and sidestream models
- Developed a dynamic process model for the thickening-clarification process which is able to predict underflow and effluent suspended solids concentrations as well as sludge blanket height in primary and secondary clarifiers on a dynamic basis. The model is widely used and cited worldwide. The publication in Water Research was selected as one of the ten most influential papers in the 40 years history of Water Research
- Manager of applied research projects for the largest advanced wastewater treatment plant in the US (Blue Plains, 1400MLd). Researched topics include:
  - Optimization of denitrification using various external carbon sources
  - Investigation into the mechanism of chemical phosphorus removal using iron salts
  - Development of an evaluation method of pretreatment processes and development of influent characterization methods for modelling of anaerobic digestion.
- Delivered expert training on dynamic modelling, the use of GPS-X, BioWin and various advanced wastewater process modelling techniques to the following companies (selected list):
  - US and Canada: Metro Toronto, Camp Dresser McKee, CH2MHill, M.M. Dillon, Malcolm Pirnie, Metcalf and Eddy, Union Carbide, HDR, Chevron, General Electric, Wastewater Technology International, Zenon Environmental, etc.
  - Europe: Bechtel Water, Anglian Water, Wessex Water, Yorkshire Water, Severn Trent Water, Degrémont, Générale des Eaux, Lyonnaise des Eaux, Kaldnes Miljoteknologi, Purac, Vertis bv., MWH, etc.
  - Japan: Kurita Water Industries, Nishihara Environmental Sanitation Research Corp. etc.
  - Australia – New Zealand: Brisbane Water, Beca Carter Hollings & Ferner Ltd., etc.
  - and many other companies, municipalities and universities worldwide.
- Developed critical modules of the Integrated Computer Control System (IC^2S), a comprehensive on-line package for more efficient control of wastewater treatment plants and process and sensor fault detection, including automatic respirometric data extraction
- Developed a dynamic model for the Moving Bed Bioreactor process, an innovative hybrid system technology using suspended and fixed biomass in the aeration tanks. The model is

used on numerous full-scale plants to optimize process performance, and contains one of the first mechanistic, detailed mathematical descriptions of the biofilm involved

- Co-supervisor for undergraduate and graduate students at the Geology department, McMaster University, in environmental modelling activities (Global Carbon Cycle, CO_2 Balance for the Equatorial Pacific, Flexible Pesticide Modelling System, Risk Analysis for Managers using Modelling Tools)
- Developed a simulator-based Operator Interface for optimization of effluent treatment of a plastics manufacturing site of General Electric
- Project manager on the implementation of an advanced control system for the City of San Jose, California
- Project manager in the Operational Evaluation of the Main Treatment Plant, Toronto, Ontario, including a comprehensive evaluation and modelling of this large plant (818 MLD)
- Project manager for the evaluation of the Goldbar Plant, Edmonton, Alberta, in the process evaluation subcomponent of a hydraulic gradeline and process evaluation study
- Project manager for modelling support for the Development of a Facility Plan for the Woodward Avenue STP in Hamilton, Ontario
- Directed the operations of the Balatonfűzfő Wastewater Treatment Plant (Hungary), while the municipal plant was commissioned for industrial wastewater treatment. The traditional activated sludge technology was converted to an innovative two-stage carbon-enhanced process enabling the plant to treat organic loading which increased threefold, with minor upgrade cost.
- Project manager of the full-scale evaluation program at the Budapest Water Treatment Works (largest in Hungary), implementing the carbon activated flocculation process for more efficient removal of organic pollutants from the Danube River as source water
- Project manager on the process evaluation of the Burlington Skyway, Port Colborne Seaway, and Hamilton Woodward Avenue treatment plants calibrating ASM models to typical Canadian conditions
- Project manager and project engineer on many wastewater and drinking water projects while at the Water Quality Institute, VITUKI, Hungary

List of selected publications

Szabó, A., **Takács, I.,** Murthy, S., Daigger, G., Licskó, I., Smith, S. (2008) The significance of design and operational variables in chemical phosphorus removal. Water Environment Research (accepted for publication)

Smith, S., **Takács, I.,** Murthy, S., Daigger, G. and Szabó, A. (2008) Phosphate Complexation Model and its Implications for Chemical Phosphorus Removal. Water Environment Research (accepted for publication).

Takács, I., Vanrolleghem, P.A., Wett, B., Murthy, S. (2007) Elemental balance based methodology to establish reaction stoichiometry in environmental modelling. Water Science & Technology 56. 9.

Wett, B., Murthy, S., **Takács, I.,** Hell, M., Bowden, G., Deur, A., O'Shaughnessy, M. (2007) Key Parameters for Control of DEMON Deammonification Process. Water Practice, Volume 1, Number 5, November 2007, pp. 1-11(11) online at
http://www.ingentaconnect.com/content/wef/wp/2007/00000001/00000005/art00011

Dold, P., **Takács, I.,** Mokhayeri, Y., Nichols, A., Hinojosa, J., Riffat, R., Bailey, W., Bott, C., Murthy, S. (2008) Denitrification with carbon addition – kinetic considerations. Water Environment Research, 80.

Takács, I., Dudley, J., Snowling, S. (2007) A closer look at the dangers of uncalibrated simulators. Proceedings of the WEFTEC 2007, San Diego

Stricker, A-E., **Takács, I.,** Marquot, A. (2007) Hindered and Compression Settling: Parameter Measurement and Modelling. Proceedings of the IWA Particle Separation Conference, 2007, Toulouse

Takács, I. and Vanrolleghem, P.A. (2006) Elemental balances in activated sludge modelling. In: Proceedings of the IWA World Water Congress, 10-14 September 2006, Beijing, China.

Takács, I., Murthy, S., Smith, S., McGrath, M. (2006) Chemical phosphorus removal to extremely low levels: experience of two plants in the Washington D.C. area. Water Science and Technology, 53, 21-28.

Takács, I., Fairlamb, M., Dold, P. L., Bye, C., Jones, R. and Murthy, S. (2004) pH in Wastewater Treatment Plant Modelling Proceedings of IWA 2004, Marrakech.

Takács, I., Murthy, S., Fairlamb, P. M. (2004) Chemical Phosphorus Removal Model Based On Equilibrium Chemistry. Proceedings of IWA 2004, Marrakech.

Münch, E. v., Ky, C., **Takács, I.** (2002) Modeling Approaches For Prefermentation In Conjunction With Enhanced Biological Phosphorus Removal. Proceedings of WEFTEC 2002, Chicago

Takács, I., Patry, G.G. (2002) The Dynamic Solids Residence Time. Proceedings of IWA 2002, Melbourne, Australia

Ky, R.C., Comeau, Y., Perrier, M., **Takács, I.** (2001) Modelling Biological Phosphorus Removal From a Cheese Factory Effluent by an SBR. Water Science & Technology 43:3 pp. 257-264.

Spanjers, H., **Takács, I.,** Brouwer, H. (1999) Direct parameter extraction from respirograms for wastewater and biomass characterization. Water Science and Technology 39:4 pp. 137-145.

Vanrolleghem, P.A., Spanjers, H., Petersen, B., Ginestet, P. and **Takács, I.** (1999) Estimating (combinations of) activated sludge model no. 1 parameters and components by respirometry Water Science and Technology 39:1 pp. 195-214.

Westlund, Å.D., **Takács, I.** (1999) Extracting SVI From On-Line Flow And Solids Data. Proceedings of the 8th Conference of the IAWQ on Design, Operation and Economics of Large WWTPs – Budapest Sept 6-9, 1999

Takács, I., Lockwood, S., Caplis, J.R. (1998) Simulation model helps manufacturing facility maintain regulatory compliance, optimize treatment processes, and train operators. Industrial Wastewater, May/June 1998 pp 44-46

Giroux, É. Y. Spanjers, H., Patry, G.G. and **Takács, I.** (1996) Dynamic modelling for operational design of a respirometer. Water Science and Technology 33:1 pp. 297-309.

Takács, I., Newbigging M., Romano, L., Stephenson, J. (1996) Optimizing the TF/SC Process for West Windsor Using a Comprehensive Modelling Technique. Proceedings of WEFTEC '96, Dallas, Oct. 7-9

Gall, B., **Takács, I.,** Patry, G. (1995) The effect of organic reactions in a collection system on wastewater treatment plant performance. Water Science and Technology 31:7, pp. 25-31

Ketchen, S., **Takács, I.,** Lockwood, S. (1995) Model Helps Operators With Process Decisions at the GEP-Selkirk Plant. WEFTEC 1995

Takács, I., Fleit, E. (1995) Modelling of the Micromorphology of the Activated Sludge Floc: Low DO, low F/M bulking. Water Science and Technology, 31, pp. 235-243.

Watson, B., Rupke, M., **Takács, I.,** Patry, G.G (1994) Modelling of Full-scale Wastewater Treatment Plants: How Detailed Should It Be? Water Science and Technology, 30, pp. 141-147.

Patry, G.G., **Takács, I.** (1994) GPS-X, A Wastewater Treatment Plant Simulator. Proceedings of the IMACS Symposium on Mathematical Modelling during February 2-4, 1994 at Technical University of Vienna, Austria, 3, pp. 456-459.

Takács, I., Patry, G.G., Watson, B., Gall, B. (1994) Case studies in Dynamic Modelling of Large-Scale Wastewater Treatment Plants. Proceedings of the IMACS Symposium on Mathematical Modelling during February 2-4, 1994 at Technical University of Vienna, Austria, 3, pp. 417-423.

Stokes, L., **Takács, I.,** Watson, B., Watts, J.B. (1993) Dynamic Modelling of an ASP Sewage Works - A Case Study. Water Science and Technology, 28, pp. 151-161.

Patry, G.G., **Takács, I**. (1992) Settling of Flocculent Suspensions in Secondary Clarifiers. Water Research, 26, No 4., pp. 473-479.

Takács, I., Patry, G.G., Nolasco, D. (1991) A Dynamic Model of the Clarification/Thickening Process. Water Research, 25, No 10., pp 1263-1271.

Kramer, J.R., Brassard, P., Patry G., **Takács, I.** (1990) Sensitivity of terrestrial carbon cycle on atmospheric carbon dioxide. Chemical Geology, 54, July 1990, pp. 166-168.

Patry, G.G., **Takács, I.** (1990) Modular/Multi-Purpose Modelling System for the Simulation and Control of Wastewater Treatment Plants: An Innovative Approach. Proceedings of the 45th IAWPRC Workshop on Instrumentation, Control and Automation of Water and Wastewater Treatment and Transport Systems, Yokohama/Kyoto, 26 July - 3 Aug 1990.

Takács, I., Patry, G.G. (1990) A Generalized Dynamic Model of the Thickening/Clarification Process. Proceedings of the 45th IAWPRC Workshop on Instrumentation, Control and Automation of Water and Wastewater Treatment and Transport Systems, Yokohama/Kyoto, 26 July - 3 Aug 1990.

Takács, I., Homonnay, A. (1986) Ergebnisse mit der Kombinierten A-Kohle-Pulver Belebt-schlamm-Technologie in Ungarn. Wiener Mitteilungen - Wasser, Abwasser, Gewasser, 65, M1-M25.

Takács, I. (1986) Application of a mathematical model for the activated sludge treatment. Water Science and Technology, 18. pp. 163-174.

Benedek, P., **Takács, I.** and Vallai, I. (1986) Upgrading of a wastewater treatment plant in a chemical factory. Water Science and Technology, 18, pp. 75-82.

Benedek P., Major, V. and **Takács, I.** (1985) Mathematical model suggested for carbon - activated sludge system. Water Research, 19, No. 4., pp. 407-413.

Contribution to Books:

Biological and Chemical Systems for Nutrient Removal, Chapter 11, Structured Process Models for Nutrient Removal. Editor in Chief: B. Johnson. Water Environment Federation, 2008 (in preparation)

I-learning Course on Process Design and Engineering of Biological Wastewater Treatment, Chapter 12, Final Settling. Editors: M. Henze, M.v. Loosdrecht, D. Brdjanovic, UNESCO-IHE, Delft, Netherlands, 2008 (in preparation).

Methods for Wastewater Characterization in Activated Sludge Modeling, Chapter 20, Sensitivity Analysis in Practice and Chapter 21, Guidance for Model Calibration. WERF (Water Environment Research Foundation). Alexandria, Virginia. 2003. Project 99-WWF-3, ISBN 1-893664-71-6.

Biotechnológia a Környezetvédelemben (Biotechnology in Environmental Protection), Chapter 2, Biokémiai és mikrobiológiai alapok (Biochemical and microbiological fundamentals); Chapter 3, Reakciókinetikai alapok (Fundamentals of reaction kinetics); Chapter 4.1.2, Az eleveniszapos szennyvíztisztítás általános modellje (A general model for activated sludge treatment); Chapter 4.1.6 Integrált adszorpciós-eleveniszapos eljárás (Integrated adsorption – activated sludge process) and Chapter 8.2 Ülepítés (Settling). Editor: Dr. Pál Benedek. Műszaki Könyvkiadó, Budapest, 1990. ISBN 963 10 8224 5